8-15-2011 12:00 AM

Structural Role of S100 Proteins in Membrane Repair

Atoosa Rezvanpour, *The University of Western Ontario*

Supervisor: Dr. Gary S. Shaw, *The University of Western Ontario*

A thesis submitted in partial fulfillment of the requirements for the Doctor of Philosophy degree in Biochemistry

Structural Role of S100 Proteins in Membrane Repair

(Thesis Format: Integrated-Article)

by

Atoosa Rezvanpour

Graduate Program
in
Biochemistry

A thesis submitted in partial fulfillment
of the requirements for the degree of
Doctor of Philosophy

The School of Graduate and Postdoctoral Studies
The University of Western Ontario
London, Ontario, Canada

THE UNIVERSITY OF WESTERN ONTARIO
FACULTY OF GRADUATE STUDIES

CERTIFICATE OF EXAMINATION

Chief Advisor	Examining Board
Dr. Gary S. Shaw	Dr. Hans Vogel
Advisory Committee	Dr. Peter Chidiac
Dr. Christopher Brandl	Dr. Brian Shilton
Dr. James Choy	Dr. Christopher Brandl

The thesis by

Atoosa Rezvanpour

Entitled:

Structural Role of S100 Proteins in Membrane Repair

is accepted in partial fulfillment of the
requirements for the degree of
Doctor of Philosophy

Date _____

_____
Chair of the Thesis Examination Board

ABSTRACT

Membrane repair can be modulated by the association of an S100A10 dimer with the calcium- and phospholipid-binding protein annexin A2. This heterotetrameric complex has the ability to form larger multiprotein assemblies such as those with the enlargeosome protein AHNAK and members of the transmembrane ferlin family. The main goals of this thesis were to design, synthesize and characterize a molecule that would facilitate assembly of larger S100 multiprotein complexes, investigate the arrangement of the proteins, stoichiometry and affinity of AHNAK for the S100A10-annexin A2 complex and identify structural details of the ternary complex formed between S100A10, annexin A2 and AHNAK.

Successful expression, purification and characterization of two S100-target peptide hybrid proteins comprised of S100A10 and S100B linked in tandem to annexin A2 (residues 1-15) (referred to as A10A2) and CapZ (TRTK12) (referred to as BT12), respectively, was achieved. Different protease cleavage sites were incorporated into the linkers of the hybrid proteins. Since *in situ* proteolytic cleavage showed the linker did not perturb the structures of the S100A10-annexin A2 or S100B-TRTK12 complexes, this approach was used as a scaffold for larger S100 complexes.

Peptide array experiments identified the regions of interaction within the C-terminus of AHNAK. Of the eight consensus regions observed, one of the sequences of AHNAK (AHNAK5) which showed the strongest interaction was used as a synthetic peptide to identify the binding region(s), stoichiometry and affinity with the A10A2 complex. Using NMR, fluorescence and non-denaturing electrospray mass

spectrometries, a novel asymmetric arrangement between a single AHNAK5 peptide and the A10A2 dimer having an affinity near 3 nM was identified.

The binding region of AHNAK5 on A10A2 was determined by NMR spectroscopy and X-ray crystallography. X-ray crystallography of the A10A2-AHNAK5 complex showed that the backbone structure of A10A2-AHNAK5 is similar to that of S100A10 bound to the N-terminal peptide of annexin A2 (Rety et al. 1999). From the structure, it was clear that only one AHNAK5 was bound to a dimeric A10A2 through helix IV in S100A10 and the C-terminal portion from the annexin A2 peptide. These results provide a novel mode of interaction for AHNAK5 in an S100-target complex.

Keywords: S100; Annexin A2; AHNAK; membrane repair; hybrid protein; protein interactions; NMR spectroscopy; peptide array; non-denaturing electrospray mass spectrometry; fluorescence spectroscopy; X-ray crystallography; stoichiometry.

CO-AUTHORSHIP

Chapter 1

This chapter contains an expanded version of the published manuscript Anne C. Rintala-Dempsey, Atoosa Rezvanpour, and Gary S. Shaw *FEBS J*. (2008) 275, 4956-4966. Figures 1.6 and 1.8 were produced by A.C. Rintala-Dempsey and G.S. Shaw, respectively. The manuscript was written by all three authors and final revisions were made by Dr. G.S. Shaw. This chapter also contains sections from the published manuscript Atoosa Rezvanpour, and Gary S. Shaw *Gen. Physiol. Biophys.* (2009) 28, F39-46. The remainder of the figures and written portions in this chapter were done by A. Rezvanpour.

Chapter 2

This chapter contains an expanded version of the published manuscript Atoosa Rezvanpour, Jeremy M. Phillips and Gary S. Shaw *Protein Sci.* (2009) 18, 2528-2536. The pGEX-6P-1-derived S100A10 construct was generated at Dr. Michael Walsh's laboratory (University of Calgary). The pSAF2 vector was generated by Dr. Susan Safadi (Dr. Gary S. Shaw's Laboratory, University of Western Ontario). All other experiments and analysis were carried out by A. Rezvanpour. The initial version of the manuscript was written by A. Rezvanpour, followed by revisions suggested by Dr. G.S. Shaw.

Chapter 3

Sections of this chapter come from the submitted manuscript Atoosa Rezvanpour and Gary S. Shaw *J. Biol. Chem* (2010). The High Throughput Biology Laboratory (Dr. Shawn Li, University of Western Ontario) synthesized the peptide arrays. Dr. Suya Liu (Dr. Gilles A. Lajoie's Laboratory, University of Western Ontario) performed the mass spectrometry analysis. All other experiments and analysis were carried out by A. Rezvanpour. The initial manuscript was written by A. Rezvanpour, and was revised by Dr. G.S. Shaw. The remainder of the figures and written sections in this chapter were done by A. Rezvanpour.

Chapter 4

Three-dimensional NMR experiments (HNCACB, CBCA(CO)NH and HNCA) data collection and analysis was performed by Atoosa Rezvanpour. The X-ray crystallography diffraction data were collected and analyzed by Dr. Ting W. Lee (Dr. Murray Junop's Laboratory, McMaster University). Figures 4.11-4.14 were made by A. Rezvanpour and T.W. Lee. The remainder of the figures and written sections in this chapter were done by A. Rezvanpour.

DEDICATION

For my parents, Issa and Shirin Rezvanpour, who have always shown endless love, encouragement and support.

ACKNOWLEDGEMENTS

First and foremost, I would like to thank my supervisor, Dr. Gary Shaw for taking a chance on me as a graduate research student and for all of his encouragements, support and insightful comments throughout the years. I truly couldn't have asked for a better supervisor.

To my advisory committee, Dr. Christopher Brandl and Dr. James Choy, thank you for your constructive discussions regarding my research project.

Thank you to all of the past and present Shaw lab members. You have made this lab a great place to work. Thanks for the laughter and priceless memories! I consider myself lucky for making so many lifelong friends.

To my family, thank you from the bottom of my heart for all of your love and support. To my sisters Azita and Sahar, my brother Soheil, and my dearest nephew Dion, thank you for making me smile and always being there for me. I certainly could not achieve my dreams without your help. To my parents, Issa and Shirin, I owe you every thing that I have accomplished over the years. I am forever grateful and blessed to have such wonderful parents. I love you dearly.

And last but not the least, Manuel - I thank you for being so loving and supportive. You are the best friend and husband I could've asked for. I would not be here without your encouragement through the difficult times. I love you with all my heart.

TABLE OF CONTENTS

LIST OF FIGURES

LIST OF TABLES

LIST OF ABBREVIATIONS, SYMBOLS AND NOMENCLATURE

δ	chemical shift
φ	psi angle
ψ	phi angle
ATP	adenosine triphosphate
$^{13}C_6$-glucose	^{13}C-labeled glucose
Ca^{2+}	calcium
Ca^{2+}-CaM	calcium-bound calmodulin
Ca^{2+}-S100A1	calcium-bound S100A1
Ca^{2+}-S100A6	calcium-bound S100A6
Ca^{2+}-S100A11	calcium-bound S100A11
Ca^{2+}-S100B	calcium-bound S100B
CaBP	calcium-binding protein
CacyBP/SIP	calcyclin-binding protein/Siah-1-interacting protein
$CaCl_2$	calcium chloride
CapZ	actin capping protein
CaM	calmodulin
CSI	chemical shift index
D_2O	deuterium oxide
Da	daltons
DAG	diacylglycerol
DSS	2,2'-dimethyl-2-silapentane-5-sulfonate
DTT	dithiothreitol
E. coli	Escherichia coli
EDTA	ethylenediaminetetraacetic acid
EGTA	ethylene glycol bis(2-aminoethyl ether)-N,N,N'N'-tetraacetic acid
ER	endoplasmic reticulum

ESI	electrospray ionization
GB1	B1 immunoglobulin binding domain of streptococcal protein G
GST	glutathione S-transferase
HPLC	high performance liquid chromatography
HSQC	heteronuclear single quantum coherence
Hz	hertz
ICP	inductively coupled plasma atomic emission spectrometry
IP_3	inositol-1,4,5-trisphosphate
IP_3R	inositol-1,4,5-trisphosphate receptor
IPTG	isopropyl β-D-thiogalactopyranoside
KCl	potassium chloride
K_d	dissociation constant
kDa	kilodaltons
KH_2PO_4	potassium dihydrogen phosphate
MES	2-(*N*-morpholino) ethanesulfonic acid
$MgCl_2$	magnesium chloride
MOPS	3-(N-morpholino)-propanesulfonic acid
MW	molecular weight
Na^+	sodium
NaCl	sodium chloride
Na_2HPO_4	disodium hydrogen phosphate
Na_v	voltage-gated sodium channel
NDR	nuclear Dbf2-related protein kinase
NH_4Cl	ammonium chloride
NH_4Ac	ammonium acetate
NMR	nuclear magnetic resonance
PAGE	polyacrylamide gel electrophoresis
PCR	polymerase chain reaction
PIP_2	phosphatidylinositol 4,5-bisphosphate

PLC	phospholipase C
PMCA	plasma membrane calcium ATPase
ppm	parts per million
psi	pounds per square inch
RMSD	root mean square deviation
RyR	ryanodine receptor
SDS	sodium dodecyl sulfate
SERCA	sarco-endoplasmic reticulum calcium ATPase
SR	sarcoplasmic reticulum
TASK-1	tandem-pore acid-sensing potassium channel-1
TBS	tris buffered saline
TEV	tobacco etch virus
TnC	troponin-C
Tris	tris(hydroxymethyl) aminomethane
TRTK-12	12-residue S100B-binding peptide
TRPV	transient receptor potential cation channel protein
VADAR	volume area dihedral angle reporter
WT	wild type

Ala (A)	alanine
Arg (R)	arginine
Asn (N)	asparagine
Asp (D)	aspartic acid
Cys (C)	cysteine
Gln (Q)	glutamine
Glu (E)	glutamic acid
Gly (G)	glycine
His (H)	histidine

Ile (I)	isoleucine
Leu (L)	leucine
Lys (K)	lysine
Met (M)	methionine
Phe (F)	phenylalanine
Pro (P)	proline
Ser (S)	serine
Thr (T)	threonine
Trp (W)	tryptophan
Tyr (Y)	tyrosine
Val (V)	valine

Chapter 1

Introduction

1.1 Role of Calcium in the Cell

There are at least 1,400 grams of calcium inside the human body (Carafoli 2003). While the majority of calcium resides in the skeleton and teeth, less than 1% of the ion circulates in the body cells (Carafoli 2002; 2003). The importance of calcium ions in the cell was first noted by Ringer (Ringer 1883) 128 years ago, when the heart muscle continued contracting in the presence of calcium in saline medium. Since then, the implication of calcium ion in many biological processes such as cell growth and proliferation, fertilization, neurotransmitter release, and memory have been identified (Berridge et al. 2000).

In a resting cell, the cytosolic concentration of free calcium ions is approximately 100-300 nM (Tsien 1981), which is approximately 10,000 fold lower than the concentration of the ion in the extracellular space (1 mM). This calcium concentration is also about 1,000 fold lower than that found within intracellular storage compartments such as the sarcoplasmic reticulum (SR), endoplasmic reticulum (ER), the golgi apparatus and mitochondria (Pozzan et al. 1994; Pinton et al. 1998) (Figure 1.1A). Maintaining this

Parts of this chapter have been taken from the published articles: Rezvanpour, A., and Shaw, G. S. 2009. Unique S100-target protein interactions. *Gen. Physiol. Biophys.* **28:** F39-46.

Rintala-Dempsey, A. C., Rezvanpour, A., and Shaw, G. S. 2008. S100-annexin complexes—structural insights. *FEBS J.* **275:** 4956-4966.

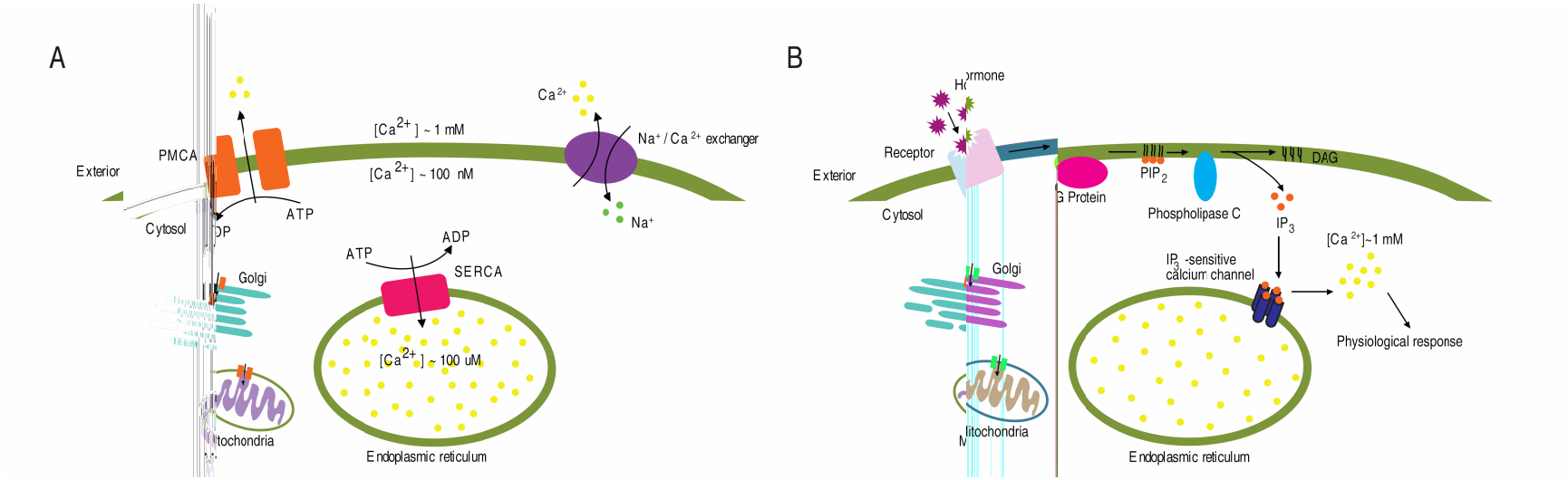

Figure 1.1. Generation of calcium signal through the inositol-lipid pathway.

Calcium homeostasis in a resting cell is illustrated in **(A)**. To maintain the low level calcium concentration of approximately 100 nM within the cell, calcium ions must be actively transported out of the cell or into intracellular organelles (ER, SR, mitochondria, golgi apparatus). Various calcium pumps such as plasma membrane calcium ATPase (PMCA) and sarco-endoplasmic reticulum calcium ATPase pumps transfer the calcium ions to the exterior of the cell or to the intracellular organelles, respectively. In addition to the pumps, Na^+/Ca^{2+} exchangers, transport calcium ions while sodium ions are entering the cell. An excitable cell **(B)** can become stimulated by a first messenger such as hormones. This results in the activation of the G protein coupled receptor and subseqently phospholipase C (PLC) which cleaves phosphatidylinositol 4,5-bisphosphate (PIP2) into 1,4,5-triphosphate (IP3) and 1,2-diacylglycerol (DAG). IP3 binding to the IP3-sensitive calcium channels (IP3R) on intracellular storage compartments leads to the opening of the channel and release of calcium into the cytosol. A local increase in the calcium concentration in the cytosol triggers a physiological response through interaction with a large number of calcium-binding proteins. (This figure was adapted and modified from Missiaen et. al. 2000 and Molecular Cell Biology 3rd Edition by Lodish et al. 1995).

tight regulation of calcium concentration is essential for sustaining life, as calcium ions act as "second messengers" in various signaling pathways.

The type of a cell designates the type of receptors located on the plasma membrane. In an excitable cell, *first messengers* such as neurotransmitters, nerve impulses or ligands stimulate these receptors, resulting in the release and increase of the local calcium ion concentration (~1 μM) in the cytoplasm. Figure 1.1B illustrates a signal transduction cascade initiated by an agonist binding to the cell-surface G protein-linked receptor. This results in the activation of phospholipase C (PLC) by the G protein and subsequent cleavage of phosphatidylinositol 4,5-bisphosphate (PIP_2) into inositol 1,4,5-triphosphate (IP_3) and 1,2-diacylglycerol (DAG) (Clapham 2007). IP_3 splits off from PIP_2 and diffuses through the cytoplasm to bind to the IP_3-sensitive calcium channels (IP_3R) on the intracellular storage compartments. This leads to the opening of the channel and release of calcium into the cytosol (Figure 1.1B). At this point calcium acts as a *second messenger* and triggers a physiological response through interaction with a large number of calcium-binding proteins (CaBP) such as the EF-hand calcium-binding family of proteins.

In order to prepare for the next signal, the cell must actively remove the calcium ions. Calcium is taken up through calcium pumps to the extracellular space or intracellular compartments through plasma membrane calcium-ATPase (PMCA) and sarco-endoplasmic reticulum ATPase (SERCA) pumps (Pozzan et al. 1994; Pinton et al. 1998), respectively (Figure 1.1A). Na^+/Ca^{2+} exchangers also remove calcium ions to the exterior of the cell.

1.2 The EF-Hand Calcium-Binding Motif

With at least 600 identified members in the human genome, the EF-hand calcium-binding family of proteins comprises the largest subfamily of CaBP (Kawasaki et al. 1998). The name EF-hand was first introduced by Kretsinger and Nockolds over 30 years ago with the atomic resolution structure of the crab calcium-buffering protein parvalbumin (Kretsinger and Nockolds 1973). As shown in Figure 1.2, an EF-hand motif consists of two α-helices that are connected by a calcium-binding loop. The term EF-hand is used as the shape of this domain resembles a right hand with an extended index finger and thumb, depicting the N-terminal helix (helix E) and the C-terminal helix (helix F), respectively (Tufty and Kretsinger 1975). The remaining curled fingers represent the 10-12 amino acid calcium-binding loop. A CaBP may contain between 2-12 EF-hand loops to maximize the calcium capacity (Carafoli 2002).

The classical, *canonical EF-hand* loop is characterized by a sequence of 12 amino acids with the pattern X * Y * Z * -Y * -X * * -Z, where the letters are the residues that participate in metal coordination and the asterisks are the intervening residues (Strynadka and James 1989). The amino acids at positions 1, 3, 5, 9 (via water) and 12 of this sequence provide the oxygen ligand to the calcium ion by sidechain carboxyl groups, and position 7 coordinates the ion through the main chain carbonyl group. Consequently, the calcium ion is coordinated in a pentagonal bipyramidal arrangement with preferences for aspartate, glycine and glutamate in positions 1, 6, and 12, respectively (Marsden et al. 1989).

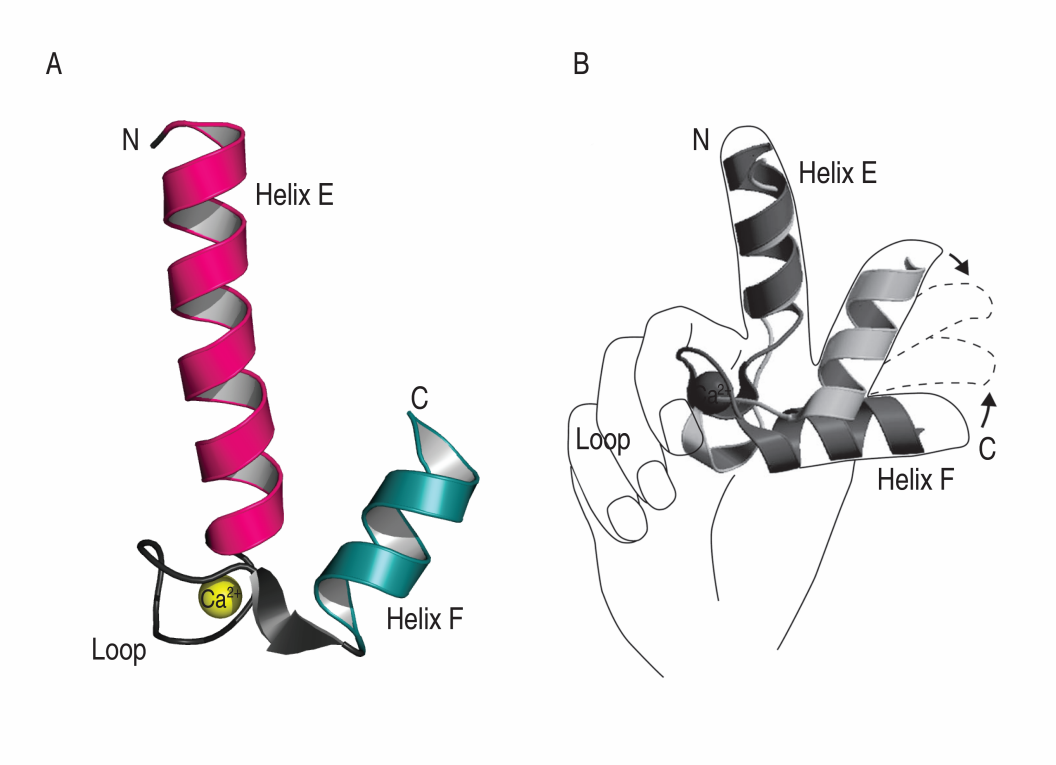

Figure 1.2. The structure of an EF-hand motif.

(A) The EF-hand calcium-binding motif is comprised of an entering helix (pink) and an exiting helix (aqua) that are connected by the calcium binding loop (grey). **(B)** The motif was called an EF-hand as the N-terminal helix E corresponds to the index finger and the C-terminal helix F represents the extended thumb. The remaining flexed fingers form the calcium binding loop. The movements of the C-terminal helix (helix F) in the closed conformation (light grey) before binding to calcium and after calcium-binding in the open conformation (dark grey) are also presented. (Figure adapted and modified from Lewit-Bentley et al. 2000).

Another type of EF-hand motif contains 14 amino acids within the calcium-binding loop and has the X * * Y * Z * * -Y * -X * * -Z pattern (Strynadka and James 1989). In this case, extra residues are introduced between the X and Y, as well as the Z and –Y positions and the calcium coordination occurs with the main chain carbonyl groups at positions X, Y, and Z. The EF-hand motif with this type of calcium coordination is referred to as a *pseudo EF-hand* loop (Strynadka and James 1989).

1.3 Overview of EF-Hand Calcium Binding Proteins

CaBPs can be divided into two distinct classes: 1) calcium buffers (or calcium signal modulators) and 2) calcium sensors (da Silva and Reinach 1991). Calcium buffers are acidic proteins that can be found in the cytosol, organelles or integrated in membranes (Carafoli 2003). They have a high affinity for calcium and can store large amounts of calcium. By doing so, these proteins can regulate the intracellular calcium concentration or transport the calcium throughout the cell. Members of the calcium buffering proteins include calbindin D_{9K} found in the cytosol and calsequestrin found in the SR. Calbindin D_{9K} is a small protein of 75 residues and is composed of a pair of EF-hand loops connected by a linker. While calcium binding occurs with positive cooperativity (Linse et al. 1987), it does not result in major conformational changes, therefore the calcium-bound protein maintains a “closed” conformation (Skelton et al. 1994; Gifford et al. 2007). Consequently, with no identified binding partner, calbindin D_{9K} functions as a transporter for calcium ions within the cell.

Calcium sensors, on the other hand, have moderate affinities in the range of 1 to 10 μM for calcium (Schaub and Heizmann 2008), and exist in the calcium-free (apo) state at resting concentrations of the ion. A local increase in calcium concentration beyond the resting level results in the calcium-binding by the calcium-sensor proteins. This leads to a significant calcium-induced conformational change and thus the exposure of previously buried hydrophobic surface for interaction with biological targets. Some members of the calcium-sensor family include calmodulin (Han and Campbell 2007), troponin-C (TnC) and the S100 protein family.

Calmodulin is a small (148 amino acids), highly conserved protein found ubiquitously in eukaryotes. This protein binds to a large number of targets (more than 350) such as myosin light chain kinase and calcineurin in a calcium-dependent manner (Yap et al. 2000) and regulates a vast number of cellular activities such as cell growth, muscle contraction, and secretion. Calmodulin is comprised of two lobes of EF-hand pairs that are connected through a flexible linker (Kuboniwa et al. 1995; Shao et al. 2006), giving it a "dumbbell-like" overall shape (Babu et al. 1988) (Figure 1.3). The two N- and C-terminal EF-hand loops in each lobe are arranged in a four-helix bundle. Consequently, calmodulin is able to bind a total of four calcium ions ($K_d^{calcium}$ ~ 1-10 μM) in response to an increase in intracellular calcium concentration (Teo and Wang 1973). Upon calcium-binding, the α-helices of each EF-hand motif modify their interhelical angle such that the position of each helix pair changes from an anti-parallel arrangement (130-140º) to an almost perpendicular conformation (89º) (Shao et al. 2006). These structural changes allow the "closed" helical bundles of the two lobes to obtain an

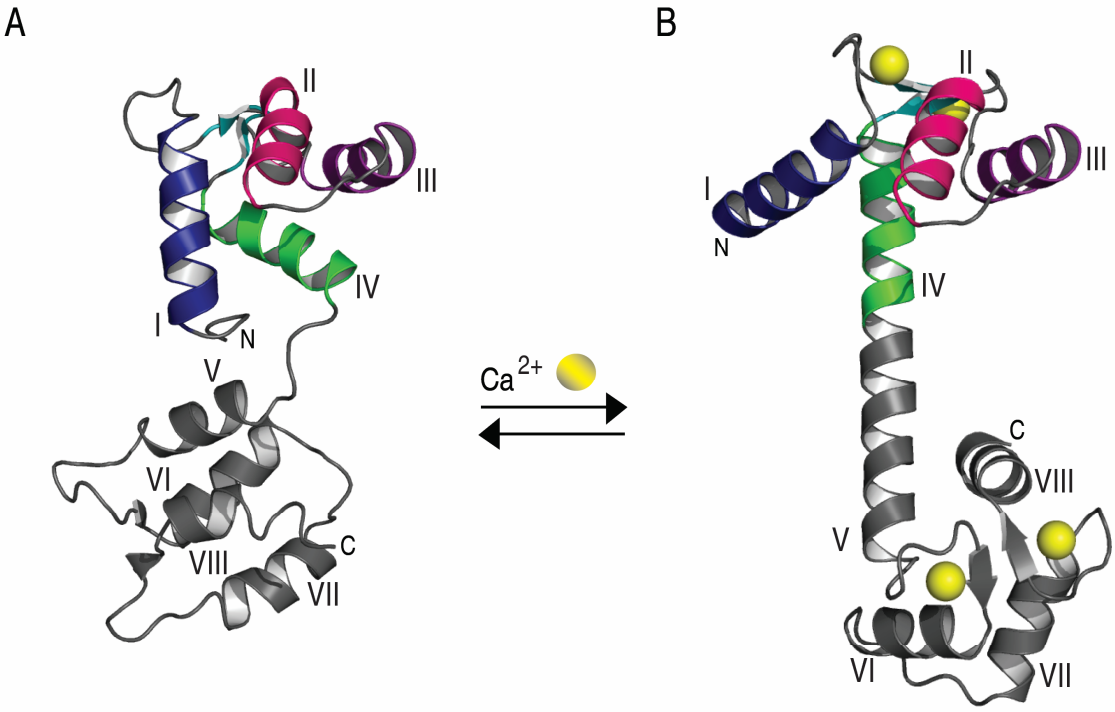

Figure 1.3. Calcium-induced conformational changes of calmodulin.

Ribbon diagrams of **(A)** apo-calmodulin (1DMO) (Zhang et al. 1995), and **(B)** calcium-bound calmodulin (3CLN) (Babu, et al. 1988) showing calcium induced conformational changes in the two lobes of EF-hand pairs. Calmodulin has an overall "dumbbell-like" appearance (Kuboniwa et al. 1995). Upon calcium-binding, the α-helices of each EF-hand motif modify their interhelical angle such that the position of each helix pair changes from an anti-parallel arrangement (130-140º) to an almost perpendicular conformation (89º) (Zhang et al. 1995). Increased exposure of the hydrophobic surface allows for interaction with target protein. In both diagrams, the helices in the N-terminal lobes are coloured, while the helices in the C-terminal lobes are in grey.

"open" conformation with an exposed hydrophobic surface for interaction with target proteins.

1.4 Structures of S100 Proteins

The S100 protein family is a group of 25 members, found solely in vertebrates. These proteins undergo a calcium-induced structural change during signalling events. As a result, the calcium-bound forms of S100 proteins are able to interact with target molecules, giving rise to a variety of biological responses including protein phosphorylation, cell growth, motility and gene transcription (Rintala-Dempsey et al. 2006). The structures of several S100 proteins have been determined using NMR spectroscopy and x-ray crystallography and show the details of the calcium-binding sites, dimerization motif and structural changes upon calcium binding. Unlike the dumbbell shapes of well-studied EF-hand calcium-binding proteins such as calmodulin (Babu et al. 1988) and troponin-C (Herzberg and James 1985), the S100 proteins have a more compact, globular structure. As shown for S100A11 (Figure 1.4) each S100 protomer is comprised of two helix-loop-helix motifs, or EF-hands, connected by a flexible linker. The N-terminal calcium-binding site (site I) is a "pseudo" EF-hand, while the tighter binding C-terminal site (site II) is a canonical EF-hand. The majority of S100 proteins form symmetric non-covalent homodimers, a feature that is unique to these proteins within the EF-hand family of calcium-binding proteins. S100 proteins have also shown the formation of heterodimers, such as that formed between S100A8 and S100A9 (Korndorfer et al. 2007). The dimer interface is composed of the antiparallel arrangement

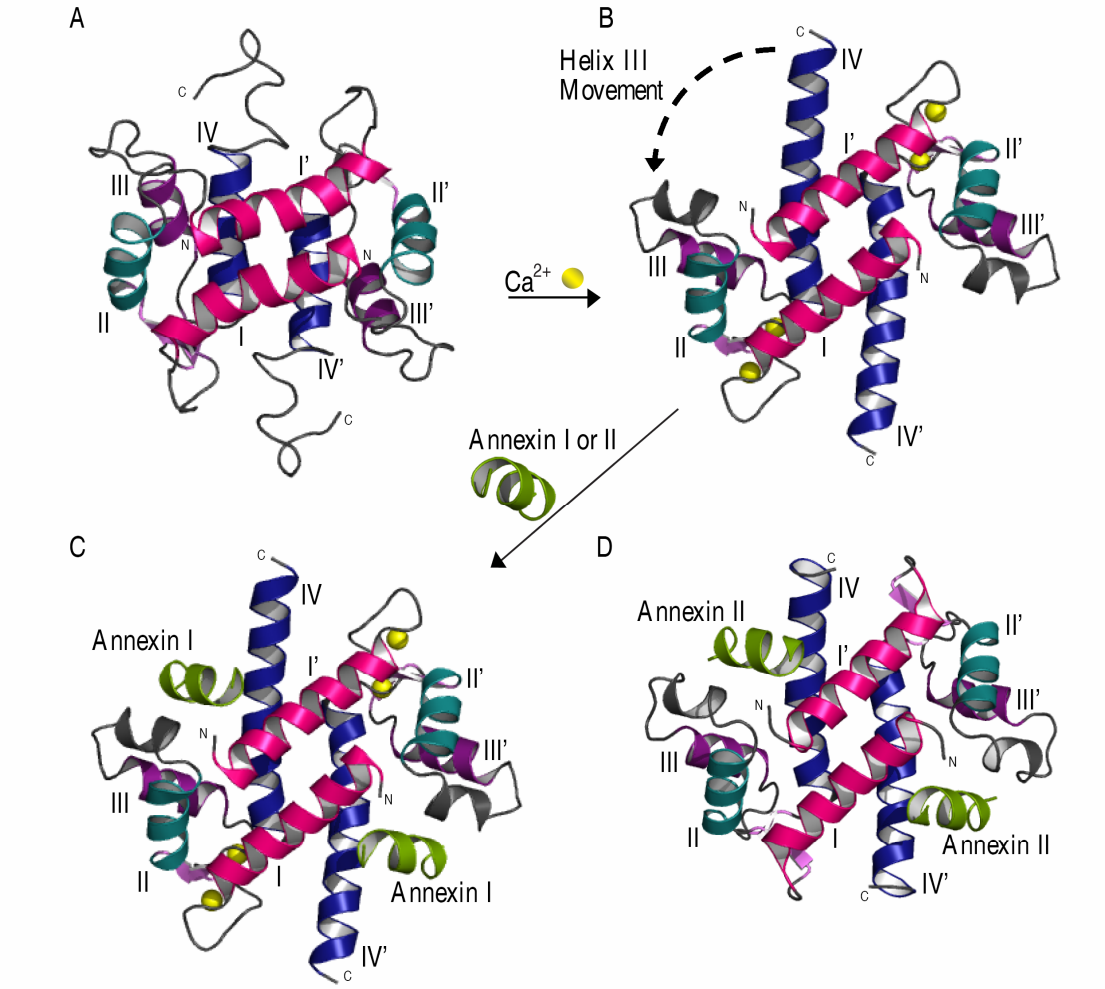

Figure 1.4. Calcium-induced conformational changes of S100 proteins.

Ribbon diagrams of **(A)** apo-S100A11 (1NSH) (Dempsey et al. 2003) and **(B)** Ca^{2+}-S100A11 (1QLS) (Rety et al. 2000) are shown in similar orientations to demonstrate the conformational changes that occur upon calcium-binding. The helices are numbered I-IV for one monomer and I'-IV' for the other. Helix I is shown in pink, helix II in aqua, helix III in purple and helix IV in blue. The β-sheets in the calcium-binding loops are shown in light purple and the calcium ions as yellow spheres. When calcium binds to S100A11 the largest conformational changes occur in the C-terminal EF-hand. Helix III moves ~ 40º with respect to helix IV, exposing a hydrophobic cleft between helix IV and the linker of one monomer and helix I' of the second monomer. **(C)** Binding of the N-terminal region of annexin A1 (green) is mediated by hydrophobic residues of the binding cleft on either side of S100A11 dimer (1QLS) (Rety et al. 2000) making contacts with helices III and IV from one monomer and helix I' of the partner monomer simultaneously. **(D)** The structure of S100A10 bound to the N-terminal region of annexin A2 (1BT6) (Rety et al. 1999) is shown to illustrate the similarity to the Ca^{2+}-S100A11-annexin A1 structure. When the two S100-annexin structures are superimposed, the backbone RMSD is 0.85.

of helices I and IV of each protomer. The two calcium-binding loops are held in close proximity via a short antiparallel β-sheet and are on the opposite side of the molecule relative to the N- and C-termini.

In the calcium-free (apo) structures of several S100 proteins, including apo-S100A11, helices III and IV are nearly parallel to one another, resulting in a number of residues at their interface that are inaccessible to solvent and giving the protein a more "closed" structure (Dempsey et al. 2003). Upon calcium-binding, the N-terminus of helix III moves by almost 40° relative to helix IV and becomes nearly perpendicular to helix IV, exposing hydrophobic residues on both helices (V57, M61, L85, A88, F93 in S100A11), as well as on helix I (I12, I16) and the linker region (L45, A47, F48), that were previously buried in the apo state (Figure 1.4). In S100A11 it has also been noted that helix IV becomes elongated upon calcium binding. The large conformational change of helix III and exposure of hydrophobic residues, first shown for S100B (Drohat et al. 1998; Matsumura et al. 1998; Smith and Shaw 1998) and S100A6 (Otterbein and Dominguez 2002) has become a trademark of the S100 calcium-binding event and is responsible for the interactions of these proteins with a diverse array of target proteins (Rintala-Dempsey et al. 2006). One member of the S100 family, S100A10, differs from others as it is unable to bind calcium ions due to a three-residue deletion in site I (N28, N29, T30 of S100A11 are absent in S100A10) and mutations of acidic calcium-coordinating residues in site II (D68 and E77 of S100A11 are substituted with C61 and S70 in S100A10) (see sequences in Figure 1.6A). Remarkably, the structure of calcium-free S100A10 (Rety et al. 1999) is nearly identical (rmsd 0.85 Å) in structure to that of

calcium-bound S100A11 (Ca^{2+}-S100A11) (Rety et al. 2000) despite the presence (or absence) of calcium ions in their calcium-binding loops (Figure 1.4).

In S100A10 and Ca^{2+}-S100A11, helices I and IV comprise the dimer interface as in the other S100 structures, however helix IV is markedly longer in apo-S100A11, extending nearly to the C-terminus. Helix III has a similar orientation in both S100A10 and in Ca^{2+}-S100A11, thus exposing very similar hydrophobic regions and residue composition (Figure 1.4).

1.5 Structures of the Annexin Proteins

In humans there are 12 different annexin proteins, annexins A1-A11 and A13 that have orthologs in most vertebrates (Fernandez and Morgan 2003). As of April 2011, there were 69 three-dimensional structures of annexin proteins, most from x-ray crystallographic methods, deposited to the Protein Data Bank (www.rcsb.org). These structures include full-length, truncated and mutant forms of the annexins (particularly annexin A5), as well as annexin-protein complexes. In particular, vertebrate structures of human annexins A1, A2, A3, A5, A8 and bovine annexins A4 and A6 have been determined, some in both the calcium-free and calcium-bound forms.

Consistent with the first annexin structure determined, annexin A5 (Huber et al. 1990a; Huber et al. 1990b; Concha et al. 1993; Sopkova et al. 1993), all annexins except annexin A6, form a core domain consisting of four conserved structural repeat sequences (I-IV), each about 70-75 residues in length. Annexin A6 is a unique member of the annexin family possessing two four-repeat core domains connected by a linker region

(Avila-Sakar et al. 1998), a result of a gene duplication event. As shown in Figure 1.5 for annexin A1 (Rosengarth et al. 2001), each repeat unit is formed from five α-helices (A-E) arranged such that helices A, B, D and E are roughly anti-parallel to each other while helix C is nearly perpendicular to these helices. The repeats pack into two distinct arrangements within the core domain. The repeat pairs I/IV and II/III pack together mostly due to hydrophobic interactions between helices B and E in each repeat, arranged in a near antiparallel fashion (Weng et al. 1993; Rosengarth et al. 2001). For example, in annexin A2 (Shao et al. 2006) residues in helices B and E from repeat I (V54, V57 and V98, L102) and repeat IV (I289, V293 and A330, Y333, L334) form a tight non-polar network between these two repeat units. In general the hydrophobic nature of these residues in the annexin sequences is highly conserved.

Calcium binding to the annexins promotes their binding to phospholipid-containing membranes. Most structures of annexins show that coordination of calcium ions by the annexins occurs via three residues in the A/B loop that ligate the calcium ion using their backbone carbonyl atoms and the bidentate side chain of either an aspartic or glutamic acid 38 residues downstream in the D/E loop (Figure 1.5) (Seaton 1996). Water molecules satisfy the remaining two coordination sites for each calcium ion. In this manner, each annexin protein coordinates one calcium ion per repeat giving rise to the trademark annexin sequence pattern GXGT-(38)-D/E (Geisow et al. 1986). In addition, secondary coordination of calcium ions with lower affinity have also been noted within the D/E loops of repeats I and III as in annexin A1 (Rosengarth and Luecke 2003) and A2 (Shao et al. 2006) or in the A/B loop near the primary calcium site in this region. In

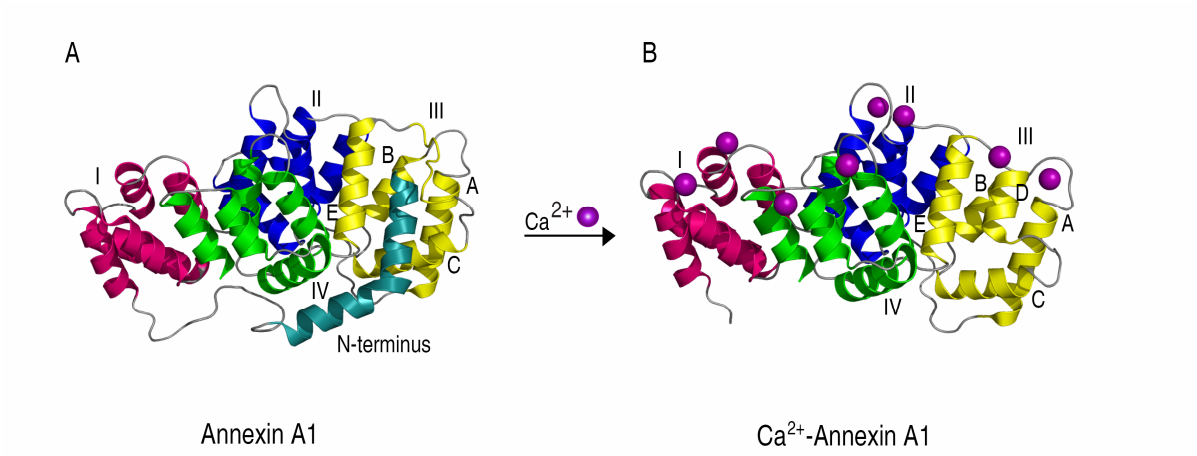

Figure 1.5. Extrusion of the N-terminal helix in annexin A1 upon calcium binding.

Ribbon representations of **(A)** apo-annexin A1 (1HM6) (Rosengarth et al. 2001) and **(B)** Ca^{2+}-annexin A1 (1MCX) (Rosengarth et al. 2003). The core domain repeats are colored pink for repeat I, blue for repeat II, yellow for repeat III and green for repeat IV. The helices of repeat III are labeled A-E. The N-terminus of apo-annexin A1 was resolved in the calcium-free crystal structure and is shown in teal. The extreme N-terminal helix of annexin A1 is associated with repeat III in the absence of calcium and essentially takes the place of helix D. In the presence of calcium the N-terminal helix is not visible in the structure and is presumed to be expelled from the core domain. The calcium ions are shown as orange spheres.

both these cases a greater number of water molecules are used to satisfy the calcium coordination. Further, these sites appear to have a greater variability within the annexin structures, likely due to differences in crystallization conditions. Remarkably, the calcium ions all lie on the same curved side of the annexin structures (Swairjo et al. 1995) forming a convex surface proposed to interact with phospholipids (Figure 1.5).

Unlike the structures of EF-hand signalling proteins such as troponin-C (Herzberg and James 1985) or members of the S100 protein family (Nelson and Chazin 1998; Maler et al. 2002), the annexins do not appear to undergo a significant structural change within their core domains upon calcium binding. For example, a comparison of the calcium-free and calcium-bound forms of annexins A1 and A2 show only 1.56 and 0.72 Å differences between the backbone arrangements of these structures. The most significant difference between these structures is a disruption of the packing of the helices in repeat III of calcium-free annexin A1 due to the presence of an N-terminal helix. The N-terminal extension ranges between eleven (annexin A6) and more than 50 residues (annexin A7, A11) and is only found in some annexins (A1, A2, A6, A7, A9, A11). However, annexin A1 is the only member of the group where the intact N-terminal sequence is visible in the x-ray structure (Rosengarth et al. 2001). In the calcium-free state this structure shows that the N-terminus of annexin A1 forms a kinked α-helix where residues A2-A11 from this helix are buried against helix E (D259-A271) of repeat III and backing on to helix C. The unique feature of this N-terminal helix is that it has essentially replaced helix D from the helical packing arrangement in repeat III found in the calcium-bound form of annexin A2 or in other annexin structures. In the presence of calcium, the

N-terminal helix is absent from the annexin A1 structure suggesting it has been extruded from the core structure (Rosengarth and Luecke 2003). This calcium-sensitive extrusion is reminiscent of that exhibited by the EF-hand protein recoverin which releases an N-terminal myristoyl group upon calcium binding (Ames et al. 1995a; Ames et al. 1995b). Studies of peptides derived from the N-terminus of annexin A1 reveal that an extruded N-terminus likely has little regular secondary structure but undergoes a coil-helix transition upon protein or membrane binding (Yoon et al. 2000; Hu et al. 2008).

1.6 Structures of S100 Proteins in Complex with the Annexins

The first structure of an S100 protein in complex with an annexin protein was solved by Rety et al. (Rety et al. 1999) and comprised S100A10 bound to the first 13 residues of the N-terminus of annexin A2. One year later, the structure of Ca^{2+}-S100A11 bound to the 14 N-terminal residues of annexin A1 was determined (Rety et al. 2000). These two structures (Figure 1.4) provide valuable information regarding how these two protein families physically interact with one another, and how these interactions give rise to the biological functions that have been observed in the cell. S100s have long been known to interact with members of the annexin family and that these interactions play a role in membrane fusion events (Harder and Gerke 1993; Mayorga et al. 1994; Jost et al. 1997). In particular, the structures reveal a common mode of interaction among these two protein families as well as key elements for target specificity.

Early studies showed that the binding of annexins A1 and A2 to Ca^{2+}-S100A11 and S100A10 respectively was strongly dependent on the unique N-terminal regions of

the annexin proteins (Johnsson et al. 1986; Johnsson et al. 1988; Mailliard et al. 1996; Jost et al. 1997). This was confirmed from crystal structures of Ca^{2+}-S100A11 and S100A10 (Rety et al. 1999) in the presence of N-terminal annexin peptides. Despite the differences between the sequences of the S100 proteins (Figure 1.6), their calcium-bound state and the sources of the two annexin peptides, both structures show two annexin peptides per S100 dimer, located in near-identical binding sites on either side of the S100 molecule (Figure 1.4). Each peptide makes contacts with both S100 protomers resulting in the bridging together of the two protomers by the annexin protein. In each case, the peptides form α-helical structures when bound to their S100 binding partners, as had been previously predicted based on their sequences (Acetyl-AMVSEFLKQAWFID and Acetyl-STVHEILSKLSLEG for annexin A1 and A2, respectively) (Johnsson et al. 1988; Becker et al. 1990; Mailliard et al. 1996) and the structure of this region in the calcium-free form of annexin A1 (Rosengarth et al. 2001). Furthermore, N-acetylation of the peptides is a requirement for the S100-annexin interactions (Johnsson et al. 1988; Becker et al. 1990; Rety et al. 2000) since removal of the acetyl group in annexin A2 results in a 2700-fold decrease in binding affinity to S100A10 (Becker et al. 1990). Although no direct contacts are made between the acetyl groups and the S100 proteins, it has been suggested that the acetyl group aids in stabilizing the helix dipole of the annexin N-terminus and therefore the required helical conformation of the peptide. The backbone RMSD for the entire Ca^{2+}-S100A11-annexin A1 and S100A10-annexin A2 complexes is 0.85 Å. This is a clear indication of a common mode of interaction between these members of the S100 and annexin families.

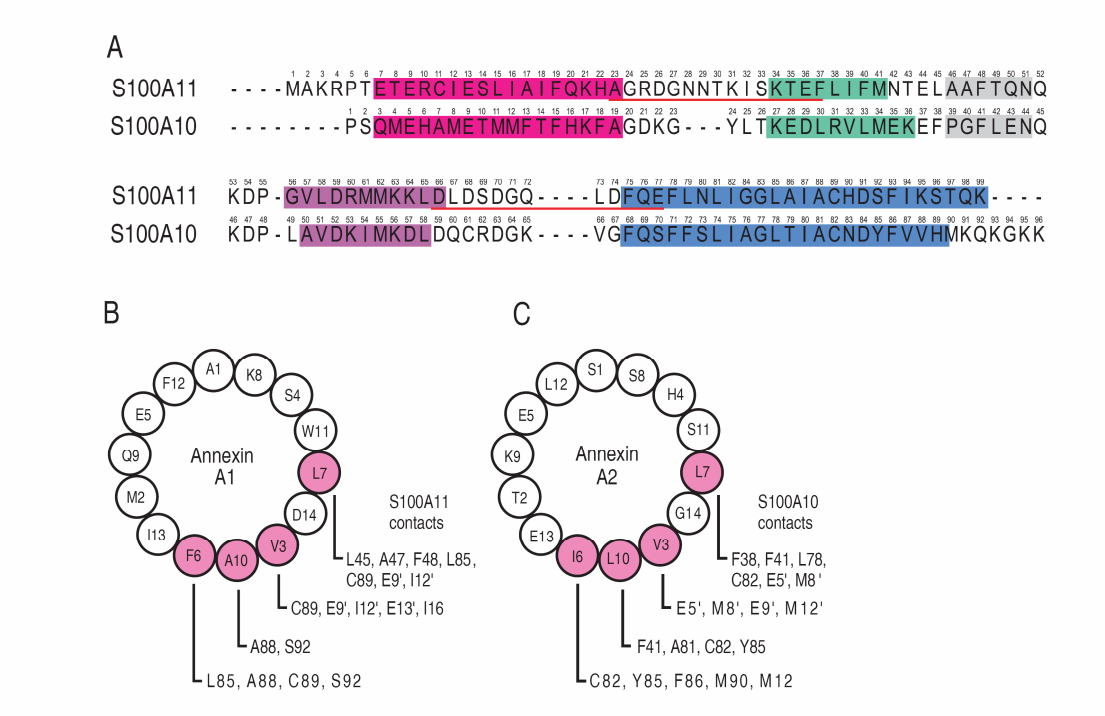

Figure 1.6. Similarity of sequences and protein-protein contacts in S100-annexin structures.

(A) A sequence alignment of S100A11 (pig) and S100A10 (human) is shown to allow comparison of the residues involved in interactions with the annexin peptides. The helices are shaded in similar colours to those used in Figure 1.4 and the calcium-binding loop residues are underlined. Schematic representations of the contacts between S100A11 and the annexin A1 peptide **(B)** and between S100A10 and annexin A2 **(C)** are shown to illustrate the similarities in the two complexes. The annexin peptides are shown as helical wheels to show the relative positions of the amino acids in the helices, with the key hydrophobic residues shaded in light purple forming a XOOXXOOX motif. The residues of the respective S100 binding partners that make contacts (< 6 Å) with each of the hydrophobic residues are labeled. For example, the side chain of L7 of annexin A1 is within 6 Å of the side chains of L45, A47, F48 within the linker of S100A11, L85 and C89 of helix IV and E9' and I12' of helix I' of the other monomer. L7 of annexin A2 makes nearly identical contacts with F38, F41, L78, C82, E5' and M8' of S100A10 as can be seen when the residues are compared in the sequence alignment of the two proteins.

Hydrophobic surface plays a major role in the interactions between the annexin N-termini and the S100 proteins. The amphipathic nature of the annexin sequences presents a series of hydrophobic residues on one face of the α-helix that interact with S100A10 or Ca^{2+}-S100A11. In annexin A1, the hydrophobic surface is made up of V3, F6, L7 and A10 and in annexin A2 it is made up of residues V3, I6, L7 and L10 (Figure 1.6). This representation clearly indicates a strong conservation of hydrophobic residues at these positions (XOOXXOOX; X=hydrophobic residue, O=polar residue) that make the largest number of contacts with the S100 proteins. In the S100A10-annexin A2 structure, V3 of the annexin A2 peptide interacts with a large number of residues in helix I' (E5', M8', E9', M12'). Similarly, E9', I12', E13' and I16' of S100A11 are in close proximity to V3 of annexin A1 (Figure 1.6B). The importance of this residue was further illustrated by its substitution with a polar amino acid, that lead to a complete loss of binding between annexin A2 and S100A10 (Becker et al. 1990). However, the Ca^{2+}-S100A11-annexin A1 complex formation seems less sensitive to substitution since replacement of V3 with alanine results in little change in binding affinity (Rintala-Dempsey et al. 2006). The residue at position 6 (I or F) makes numerous contacts with helix IV (C82, Y85, F86, M90 in S100A10 and L85, A88, C89, S92 in S100A11). The sidechain of L7 makes the largest number of contacts with the S100 proteins by interacting with residues in the linker (F38, F41 in S100A10 and L45, A47, F48 in S100A11), helix IV (L78, C82 in S100A10 and L85, C89 in S100A11) and helix I' (E5', M8' in S100A10 and E9', I12' in S100A11). Reduction of the size of the hydrophobic sidechain at positions 6 and 7 by substitution with either an alanine or valine in both

annexins A1 and A2 dramatically reduces binding, indicating the close packing of the S100-annexin interaction (Becker et al. 1990; Rintala-Dempsey et al. 2006). The residue at position 10 (A or L) is near helix IV (A81, C82, Y85 in S100A10 and A88, S92 in S100A11). Several hydrogen bonds between the peptides and the S100 proteins stabilize the interaction.

The structures of the S100A10-annexin A2 and Ca^{2+}-S100A11–annexin A1 heterotetramers show how a single S100 protein might interact with two annexin proteins (Rety et al. 1999; Lewit-Bentley et al. 2000; Rety et al. 2000). As proposed by Gerke and Moss (Gerke and Moss 2002) this would provide an elegant mechanism whereby calcium-binding by an annexin protein not only promotes its association with a phospholipid membrane but also facilitates interaction with either S100A10 or Ca^{2+}-S100A11 allowing two membrane surfaces to be brought within close proximity for a fusion or vesiculation event.

1.7 Insights into other S100-Annexin Interactions

Other interactions between the S100 and annexin families have been reported. Consistent with the calcium-induced conformational change observed in S100A11, most of these complexes require the calcium form of the S100 protein although there are a few calcium-independent interactions, including S100A4 and annexin A2 (Semov et al. 2005). Some annexins, such as annexin A6, have many possible S100 binding partners: S100A1 (Garbuglia et al. 2000), S100A6 (Zeng et al. 1993), S100A11 (Chang et al. 2007) and S100B (Garbuglia et al. 2000), while other S100 proteins can interact with several

different annexins. For example, S100A6 has been shown to bind annexins A2 (Filipek et al. 1995), A6 (Zeng et al. 1993) and A11 (Tokumitsu et al. 1992). The S100A6-annexin A11 interaction appears to involve a similar pattern of hydrophobic residues (XOOXXOOX) from the N-terminal extension of annexin A11 (L52, M55, A56 and M59) (Sudo and Hidaka 1999) as observed for annexins A1 and A2 and this region is predicted to adopt an amphipathic helix. Similar to the S100A10-annexin A2 complex, S100A4 also interacts with the N-terminus of annexin A2 in a calcium-independent manner (Semov et al. 2005). Alternatively, the interaction between S100A11 and annexin A6 involves residues within each of the two core domains of annexin A6 (Chang et al. 2007). A similar conclusion has been reached for the interaction of S100A1 and S100B with annexin A6 (Garbuglia et al. 2000). In this latter case, and for the S100A12-annexin A5 interaction (Hatakeyama et al. 2004) it has also been observed that the extreme C-terminus of the S100 protein is not involved in the annexin interaction. This is in contrast to observations for the S100A10-annexin A2 and Ca^{2+}-S100A11-annexin A1 complexes (Figures 1.4 and 1.6) where the C-termini of the S100 proteins are indispensable, likely due to the elongated nature of helix IV which extends nearly to last residue in each protein. Together, these results indicate that multiple modes of binding between S100 proteins and annexins are possible.

Uncovering the potential binding sites in the core domains of annexins A1, A2 and A5 for S100 proteins have not yet been attempted. Other than the calcium-sensitive extrusion of the N-terminal helix from annexin A1 and A2, the most significant structural change observed in the annexins is the exposure of Trp187 in annexin A5 at high calcium

ion concentrations (Huber et al. 1992; Concha et al. 1993; Sopkova et al. 1993). The exposure of this residue facilitates binding to the phospholipid membrane so is unlikely to also be used for interactions with an S100 protein. In addition, this residue is not conserved in annexins A1 and A2 where lysine residues exist. Rather, the most obvious choice for S100 protein binding with the annexins is the opposite "side" of the core domain from the membrane-binding region. An attractive site might be helix C from domain IV as this helix sits near the bottom of the structure (Figure 1.4). In the absence of calcium, helix C is protected by the N-terminal helix in annexins A1 and A2. Upon calcium binding to the annexin protein, several residues near helix C become mostly exposed (E305, N309, D310, A313, K317 in annexin A1). Several of the analogous residues are also exposed in annexin A5. However, analysis of this helix does not reveal the XOOXXOOX motif used in the N-terminal helix, suggesting a different mode of interaction may be occurring. It is also interesting that residues V287-V298 in annexin A2 match the TRTK-12 consensus motif observed for peptide binding to S100B (McClintock and Shaw 2000). However, most of these residues appear to be buried in annexin A2. Further experiments will be needed to confirm whether this or some alternative site on the annexin proteins is used to interact with other S100 proteins.

While the structures of Ca^{2+}-S100A11 and S100A10 clearly show the surfaces used to interact with annexins A1 and A2 respectively, models of other S100-annexin complexes such as Ca^{2+}-S100A11 with annexin A6 are not available. However, some information about potential binding sites can be gleaned by examination of S100 protein structures in the apo- and calcium-bound states. For example, S100A11 utilizes several

residues in helices I (E9, I12, I13, I16), the linker (L45, A47, F48) and the extreme C-terminus of helix IV (L85, A88, C89, S92) to interact with annexin A1 (Figure 1.6). Many of these residues are inaccessible in the calcium-free state and would be expected to provide an interactive surface not only for annexin A1 but for other annexin proteins. It will be important to complete site directed mutagenesis experiments on S100 proteins such as S100A11 to understand the roles of these residues on the affinities for different annexin proteins.

1.8 Different Modes of Recognition for S100 Target Protein Complexes

The three-dimensional structures of several S100 proteins have been determined in complex with a variety of peptides derived from their parent proteins. These include calcium- bound S100B (Ca^{2+}-S100B) in complex with peptides from the C-terminal region of p53 (Rustandi et al. 2000), the N-terminal regulatory domain from Ndr kinase (Bhattacharya et al. 2003) and the actin-capping protein CapZ (TRTK12) (Inman et al. 2002; McClintock and Shaw 2003; Charpentier et al. 2010); calcium-bound S100A1 (Ca^{2+}-S100A1) in complex with peptides from CapZ (Wright et al. 2009) and the cytosolic region of the ryanodine receptor (RyR) (Wright et al. 2008); calcium-bound S100A6 (Ca^{2+}-S100A6) in complex with a C-terminal region from the Siah-1 interacting Protein (SIP) (Lee et al. 2008) and, Ca^{2+}-S100A11 in complex with the N-terminus of the phospholipid-binding protein annexin A1 (Rety et al. 2000). In addition, the structure of S100A10, an S100 protein unable to bind calcium due to substitutions in both calcium-binding loops, is available in complex with the N-terminal region from annexin A2 (Rety

et al. 1999). In general these structures show there are at least three distinct modes a target protein adopts when binding to an S100 protein (Figure 1.7), all showing a symmetric relationship and 1:1 stoichiometry for the target:S100 protomer.

The first mode of binding involves the interaction between the target protein and the hydrophobic surface exposed between helices III and IV due to calcium binding to the S100 protein. In this case, all interactions between the target and the S100 protein occur at the S100 protomer level. This type of interaction is exhibited in the Ca^{2+}-S100B structures with TRTK12 (Protein Data Bank accession codes - 1MWN, 1MQ1, 3IQO), Ndr kinase (1PSB, Figure 1.7A) and p53 (1DT7), and the Ca^{2+}-S100A1 structures with TRTK12 (2KBM, Figure 1.7A) and the ryanodine receptor (2KF2). In the p53 (Rustandi et al., 2000) and Ndr kinase (Bhattacharya et al. 2003) structures, each bound peptide forms a three-turn α-helix such that its N-terminus lies near the N-terminus of helix III and its C-terminus has key interactions with the C-terminus of helix IV of Ca^{2+}-S100B. In contrast, the TRTK12 structures with Ca^{2+}-S100A1 (Wright et al., 2009) and Ca^{2+}-S100B (Inman et al., 2002) form 1.5 turn α-helices and are aligned nearly perpendicular to the orientations of the p53 and Ndr peptides such that the C-terminus of TRTK12 is closer to the middle of helix IV (Figure 1.7A). Even though the TRTK12 peptide binds within the helix III-IV cleft in both structures the presentation of the peptide is different when bound to Ca^{2+}-S100A1 compared to Ca^{2+}-S100B. In Ca^{2+}-S100A1 the anchoring tryptophan (W7) of TRTK12 interacts with residues towards the C-terminus of helix IV (L81, A84, C85, F88) whereas in Ca^{2+}-S100B, this same tryptophan interacts with residues in the linker (L44, E45, I47) and helix III (V53, V56). These differences have the

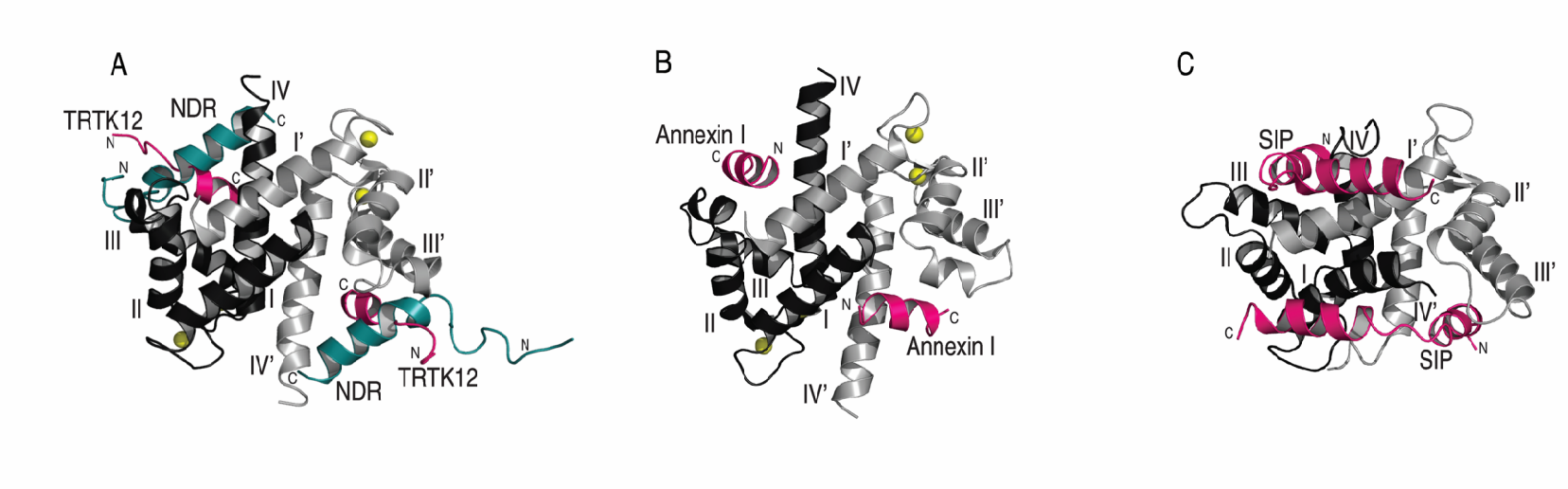

Figure 1.7. Different modes for target protein interaction with S100 proteins.

(A) Binding to the helix III-IV hydrophobic displayed by TRTK12 (pink) bound to Ca^{2+}-S100A1 (2KBM) (Wright et al. 2009) and NDR kinase (cyan) bound to Ca^{2+}-S100B (1PSB) (Bhattacharya et al. 2003). **(B)** Binding near helix I' at the dimer interface displayed by the N-terminal region of annexin A1 (pink) and Ca^{2+}-S100A11 (1QLS) (Rety et al. 2000). **(C)** Two- site surface mode displayed by the C-terminal region of SIP bound to Ca^{2+}-S100A6 (2JTT) (Lee et al. 2008). Ribbon diagrams of the calcium-saturated S100 proteins are presented with one of the protomers shaded in black (helices labeled as I-IV) and the other protomer shown in light grey (helices labeled as I'-IV'). Calcium ions are illustrated in yellow spheres.

effect of rotating the entire TRTK12 peptide by about 60˚ and "tipping" the peptide by about 20˚ towards helix III in the Ca^{2+}-S100B structure. Pictorially the binding of a peptide representing the cytosolic region from the ryanodine receptor to Ca^{2+}-S100A1 (Wright et al. 2008) appears to be quite similar to that described for TRTK12. However, major differences exist as the RyR peptide forms a three-turn α-helix and is oriented nearly 180˚ with respect to TRTK12 such that its C-terminus is proximal to the N-terminus of helix III in Ca^{2+}-S100A1. An anchoring tryptophan (W5) in the RyR peptide interacts with residues near the middle of helix IV (L77, A80, L81) but also with I57 in helix III. The diversity of the interactions exhibited by these five S100-target peptide structures can be attributed to the binding surfaces in S100A1 and S100B that are broader and flatter than other calcium-sensor proteins (i.e. calmodulin) and have different distributions of hydrophobic and charged residues (Lee et al. 2008). This observation likely accounts for the broad spectrum of target proteins that interact with the S100 proteins and makes prediction of target binding based on protein sequence somewhat problematic.

The second mode of interaction utilized by the S100 proteins is displayed by structures of Ca^{2+}-S100A11 (1QLS, Figure 1.7B) and S100A10 (1BT6) in complexes with the N-terminal peptides from annexins A1 and A2 respectively (Rety et al. 1999; Rety et al. 2000). Unlike the diversity displayed by Ca^{2+}-S100A1 and Ca^{2+}-S100B, these structures show nearly identical locations and orientations for peptide binding such that < 1 Å rmsd exists between structures. In both structures the annexin peptide bridges the two S100 protomers such that its C-terminus interacts with the linker and helix IV of one

protomer while the annexin N-terminus has contacts near the N-terminus of helix I' of the partner protomer. The similarity of these S100-annexin structures is not surprising given the conservation of hydrophobic residues in both annexin peptides. The interacting residues correspond to V3, F6, L7 and L10 in annexin A1 and V3, I6, L7 and L10 in annexin A2 forming a XOOXXOOX interaction motif (X=hydrophobic residue, O=variable). This level of conservation does not exist between the TRTK12, RyR, p53 and Ndr sequences described earlier in complex with Ca^{2+}-S100A1 or Ca^{2+}-S100B proteins. Some similarity also exists in the annexins contacting residues in S100A10 and Ca^{2+}-S100A11, especially in helix I' and helix IV.

Although it has been shown that N-terminal peptides from annexins A1 and A2 both interact with Ca^{2+}-S100A11 (Rintala-Dempsey et al. 2006), it is interesting to note that annexin A1 does not form a tight complex with S100A10 (Streicher et al. 2009). Further, a strong level of specificity has been shown for S100 recognition of annexins A1 and A2. Other than S100A10 and Ca^{2+}-S100A11, the only other S100 protein that displays a tight calcium-dependent interaction with annexin A1 is S100A6 (Streicher et al. 2009).

Whereas both the previous modes of target peptide binding with S100 proteins utilized different albeit contiguous surfaces, the recent structure (Lee et al. 2008) of the C-terminal domain from the Siah-1 Interacting Protein (2JTT) shows a hybrid two-site surface (Figure 1.7C). In this structure the SIP peptide forms two distinct three-turn α-helices oriented nearly perpendicular to each other upon binding to Ca^{2+}-S100A6. The first helix (Helix A) occupies a position and orientation similar to that observed for the

RyR peptide utilizing the hydrophobic groove between helices III and IV. Helix A of SIP lies diagonally across helix III in Ca^{2+}-S100A6 with L196 and I199 anchoring the peptide through interactions with residues in helix IV and the C-terminus of helix III respectively. The second helix in SIP (helix B) lies across helix I' of the adjacent protomer, in effect bridging the two S100A6 subunits analogous to the S100-annexin complexes. Whereas the annexin structures only contact the N-terminus of helix I' in either S100A10 or Ca^{2+}-S100A11, helix B in SIP has interactions towards the more central portion of helix I' (I9', I13' and K18'). This results in helix B of SIP and helix I of Ca^{2+}-S100A6 running along opposite faces of helix I' forming a near mirror image of each other, albeit helices I and B are oriented in opposite directions. The two binding regions for SIP to Ca^{2+}-S100A6 could in part be due to the length of the SIP fragment (189-219; 30 residues) that is significantly longer than any of the other target peptides for which structures are available. Lee and co-workers show that the two helices in SIP are not equivalent in their abilities to coordinate S100A6 with helix A having a much tighter binding, while the less hydrophobic helix B enhances the affinity by about 4-fold.

The three modes of target binding to the S100 proteins utilize two distinct binding regions – the helix III-IV hydrophobic groove and the dimer interface near helix I' on the partner protomer. It has been suggested that the combination of these two regions might represent the full interaction surface for single or multiple protein interactions with the S100 proteins. Otterbein proposed this idea by superimposing the peptide binding regions for annexins A1 or A2, and p53 on the surface of Ca^{2+}-S100A6 showing these peptides occupied distinct regions of the surface with no observable steric

clashes between the peptides (Otterbein et al. 2002). Subsequently, it was shown for TRTK12 binding to Ca^{2+}-S100B that a region similar to the annexin binding site was left exposed, and that a larger target protein might be accommodated (McClintock and Shaw 2003). The structure of SIP bound to Ca^{2+}-S100A6 (~1100 Å) provides the first structural evidence for a target protein that occupies both the helix III-IV groove and helix I' interface, a binding surface that is nearly twice the size of other S100 target protein surfaces (500-700 Å). Amongst the questions raised by this important structure and earlier hypotheses are – is there evidence for other S100 protein complexes that might utilize this larger target protein binding surface or can this surface possibly accommodate simultaneous binding for two distinct target proteins?

1.9 Evidence for Multiprotein S100 Complexes Involving Annexin Proteins

A variety of S100 protein interactions have been shown to be more complicated than a single target interacting per S100 protomer molecule. For example multiprotein complexes between S100A10 and annexin A2 and either AHNAK (Benaud et al. 2004; De Seranno et al. 2006), TRPV5/6 (van de Graaf et al. 2003; Borthwick et al. 2008) or plasminogen (MacLeod et al. 2003) have been identified from two- and three-hybrid or direct binding experiments. The S100A10-annexin A2 complex is thought to be necessary to recruit an additional target, or allow both targets to bind simultaneously indicating that the binding sites for AHNAK, TRPV5/6 and plasminogen on S100A10 are likely distinct from those of annexin A2. The complexes described here focus on those for S100A10, largely because it functions well in yeast two-hybrid experiments. Other S100 proteins

(S100B, S100A1, S100A6) do not respond well in this method due to the calcium-sensitivity of their protein interactions, although homo- and heterodimeric S100 complexes can be identified using two-hybrid experiments (Deloulme et al. 2000; Deloulme et al. 2003).

The interaction between the transient receptor potential cation channel proteins TRPV5 and TRPV6 with S100A10 has been shown using two-hybrid and co-immunoprecipitation experiments (Figure 1.8A) (van de Graaf et al. 2003; Borthwick et al. 2008). In this role, the S100A10-annexin A2 complex is thought to mediate trafficking of the TRPV5 and TRPV6 proteins to the plasma membrane where they act as calcium-selective channels. The site of interaction on TRPV5 and TRPV6 for S100A10 has been localized to its intracellular C-terminal tail. Using a series of truncated and substituted proteins this has been refined to contain residues 598-603 (VATTV), a highly conserved region in both channel proteins. Although S100A10 forms a ternary complex with annexin A2 and either TRPV5 or TRPV6, there does not appear to be a direct interaction between the annexin and TRPV proteins based on negative results from immunoprecipitation experiments. Rather, S100A10 seems to bridge the two proteins indicative of different binding sites for annexin A2 and TRPV5/TRPV6, although this has not been demonstrated yet. Since S100A10 and annexin A2 co-localize with TRPV5/TRPV6, the S100A10-annexin A2 complex has been proposed to traffic these calcium channels to the plasma membrane.

S100A10 has been shown to interact with the potassium channel TASK-1 using two-hybrid, GST pull-down and co-immunoprecipitation experiments, and has a role in

the trafficking of TASK-1 to the plasma membrane (Girard et al. 2002; Renigunta et al. 2006). TASK-1 is an important regulator of membrane potential that can be affected by a variety of factors including pH, hormone and neurotransmitter binding. Two studies show binding of S100A10 to the C-terminus of TASK-1 albeit to different regions of the channel protein. In one study, S100A10 was observed to interact with the extreme C-terminal sequence (SSV) of TASK-1 previously established as a site for 14-3-3 binding (Girard et al. 2002). In more recent work, the S100A10 site was localized to a more central region in the C-terminus (residues 292-331) of TASK-1 (Renigunta et al. 2006). A portion of this sequence is highly conserved in TASK-1 orthologs, but not in TASK-3, which exhibits little binding to S100A10. Further, a segment of this sequence (FRNVYAEML) bears a strong similarity to the interaction motif (XOOXXOOX) used by annexins A1 and A2 upon binding to S100A11 and S100A10, respectively (Mailliard et al. 1996; Rintala-Dempsey et al. 2008). An interaction between S100A10 and annexin A2 in the presence of TASK-1 can not be shown suggesting the S100A10 binding regions for TASK-1 and annexin A2 at least partly overlap. It has further been shown that the S100A10 interaction promotes retention of TASK-1 in the endoplasmic reticulum due to the presence of a retention signal at the extreme C-terminus of S100A10 (KQKGKK) (Renigunta et al. 2006). Alternatively, binding of S100A10 to TASK-1 has been suggested to mask an endoplasmic retention signal near the C-terminus of TASK-1 (KRR) and promote trafficking of the potassium channel to the plasma membrane (Girard et al. 2002).

S100A10 interacts with the bluetongue virus protein NS3 (Beaton et al. 2002), a

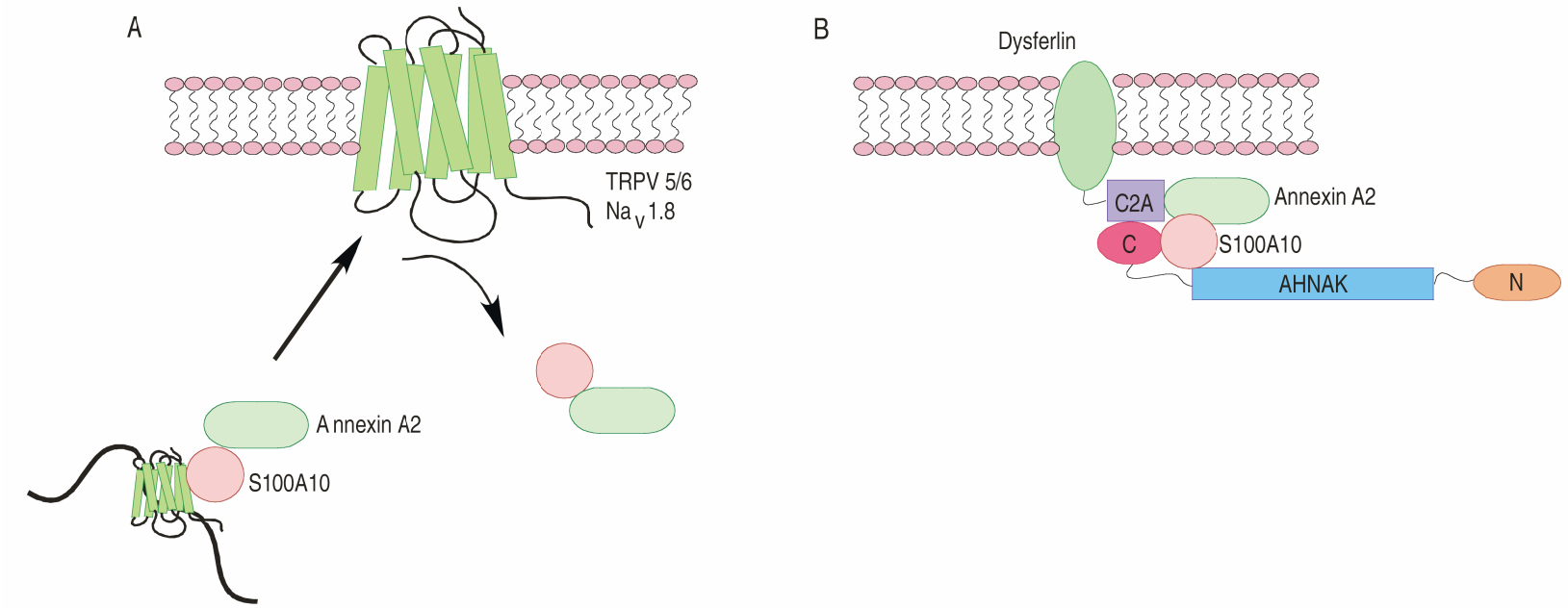

Figure 1.8. Possible involvement of S100A10 in multiprotein complexes.

(A) Possible complexes formed by membrane channel proteins such as TRPV5, TRPV6 or Nav1.8 and S100A10-annexin A2 for trafficking to the plasma membrane. Once inserted into the membrane, the S100A10-annexin A2 could dissociate or become associated with phospholipids in the membrane. **(B)** Proposed interactions in the dysferlin complex are based on multiple biochemical experiments. The C-terminus of AHNAK is shown to interact with S100A10 and annexin A2, while the dysferlin C2A domain is near annexin A2 (adapted from Huang et al. 2007). In all cases, dimeric S100A10 could coordinate two annexin A2 proteins although for simplicity only one is shown.

membrane spanning protein thought to have a role in the export of virus particles from infected cells. Two-hybrid and affinity experiments show that residues at the N-terminus of NS3 (1-13) are most important for its interaction with S100A10. This region has the potential for α-helix formation and possesses a sequence (LSGLIQRF) corresponding to the annexin binding motif (XOOXXOOX) suggesting these two proteins likely share the same binding region on S100A10 (Figure 1.7B). Using synthetic peptides corresponding to the N-terminus of NS3, it was shown that a peptide comprising residues 1-14 could compete with annexin A2 for S100A10 binding. Whereas annexin A2 could displace NS3 from an S100A10-NS3 complex, NS3 could only partially displace annexin A2 from an S100A10-annexin A2 complex indicating annexin A2 has a tighter binding to S100A10 than does NS3. It was suggested that NS3 might play a role in localizing a virus particle to the interior of the plasma membrane by bridging S100A10 and the virus particle providing an efficient route for extrusion from the cell.

The voltage-gated sodium channel $Na_v1.8$ has been observed, using two-hybrid experiments, to interact with S100A10 (Figure 1.8A) (Okuse et al. 2002; Poon et al. 2004). Further, this interaction facilitates trafficking of the channel protein to the plasma membrane resulting in functional Na^+ currents. Other voltage-gated channels such as $Na_v1.2$, $Na_v1.5$, $Na_v1.7$ and $Na_v1.9$ have much poorer affinity for S100A10 providing evidence that some degree of specificity for the voltage-gated sodium channel $Na_v1.8$ exists. The site of interaction with S100A10 has been localized to the N-terminus of the sodium channel. In particular residues 74-103 of the voltage-gated sodium channel $Na_v1.8$ are sufficient to bind to S100A10 in GST pull-down assays. Reciprocal

experiments using segments of S100A10 show that a region spanning much of the C-terminal half of the protein is able to interact with the N-terminal region of the voltage-gated sodium channel. This region does not include the extreme N- or C-termini of S100A10, known to interact with the annexin proteins so would appear to be a unique binding surface. However, it has not been shown whether annexin A2 can also bind to S100A10 in the presence of the sodium channel, an event that could facilitate association with the plasma membrane.

A multiprotein complex has been identified between S100A10, annexin A2 and AHNAK (Figure 1.8B) (Benaud et al. 2004; De Seranno et al. 2006), a protein found in the lumen of enlargeosome and trafficked to the plasma membrane in response to calcium flux. Recruitment of AHNAK to the plasma membrane by S100A10 in complex with annexin A2 is also proposed to maintain the proper cytoarchitecture of epithelial cells (Benaud et al. 2004). AHNAK is an important protein for cell membrane differentiation and membrane repair (Kouno et al. 2004), is expressed in epithelial cells and localizes near the plasma membrane. The protein contains three main structural domains; an amino terminus (251 aa), a central region containing thirty-six repeats and a C-terminus (1002 aa) (Shtivelman and Bishop 1993). The interaction between S100A10 and annexin A2 utilizes the N-terminus of annexin A2 similar to that observed in the S100A10-annexin A2 tetramer crystal structure (Rety et al. 1999). In the absence of annexin A2, a weak interaction between S100A10 and the C-terminal portion of AHNAK is present. However, the strength of this interaction was increased more than 150-fold in the presence of annexin A2. Further, *in vitro* binding assays showed no detectable

interactions between annexin A2 and the C-terminus of AHNAK, in the absence of S100A10, or S100A10 with AHNAK in the absence of annexin A2. These observations suggest that S100A10-annexin A2 tetramer formation is likely a prerequisite for the interaction with AHNAK. Using a series of GST pull-down assays, a 20-residue region in AHNAK corresponding to residues 5654-5673 was found to be sufficient to bind to S100A10-annexin A2 and can compete for binding to the complex with the entire AHNAK C-terminus having a K_d of about 30 nM (De Seranno et al. 2006). The AHNAK interaction appears to be specific for annexin A2 since other annexins (A4, A11) are not recovered from immunoprecipitation experiments. However, given the similarity of the binding surfaces and interacting residues for annexins A1 and A2 (Rintala-Dempsey et al. 2008), it is possible that an S100A10-annexin A1 or Ca^{2+}-S100A11-annexin A1/A2 may also participate in the AHNAK complex. Interestingly, Ca^{2+}-S100B is able to compete with S100A10-annexin A2 for binding to the AHNAK C-terminus. Further, it has been observed that Zn^{2+} binding to S100B enhance its association with AHNAK (Gentil et al. 2001). Unlike the S100A10-annexin A2 interaction that utilizes only the C-terminus of AHNAK, several regions in AHNAK are able to interact with Ca^{2+}-S100B. These include sequences in the repeat regions in the central portion of AHNAK (820-1330, 2589-3059, 3730-4188) as well as its C-terminus.

1.10 Role for S100 Proteins in Membrane Repair

The fusion of cellular phospholipid membranes is an important step during membrane repair, vesicular trafficking and exocytosis. A requisite for plasma membrane

repair is calcium-regulated exocytosis, controlled by a number of proteins that coordinate resealing of the membrane. One exocytotic compartment implicated in membrane fusion is the enlargeosome, characterized by the large scaffolding protein AHNAK, that relocates to the plasma membrane immediately following membrane damage (Zhang, et al. 2004). In addition to AHNAK, calcium-sensors such as members from the synaptotagmin, ferlin (dysferlin) and annexin protein families are involved in membrane repair. Upon membrane rupture, these sensor proteins respond to the calcium influx by localizing near the inner membrane surface. Recent proteomic analyses have identified approximately 115 proteins in the dysferlin complex including calpain 3, annexin A2 and AHNAK (de Morree et al. 2010; Cacciottolo et al. 2011) that might be responsible for the repair process. These studies indicate that large protein complexes are likely needed to orchestrate the repair process and restore the integrity of the membrane.

S100A10, AHNAK and the annexins have been shown to be constituent proteins in the dysferlin membrane repair complex (Huang et al. 2007). This multiprotein complex is thought to form at the site of muscle, epithelial and auditory cell damage to facilitate wound repair. The mechanism of cell membrane repair involves the aggregation of vesicles containing dysferlin, a type II membrane spanning protein, near the wound.

In vivo and *in vitro* studies show that annexin A2 is a central protein involved in membrane transport events such as endo/exocytosis (Sarafian et al. 1991; Emans et al. 1993; Harder and Gerke 1993; Diakonova et al. 1997; Harder et al. 1997; Jost et al. 1997; Merrifield et al. 2001; Knop et al. 2004; Ayala-Sanmartin et al. 2008; Zibouche et al. 2008; Illien et al. 2010). Calcium-binding to the annexins promotes their localization and

association with phospholipid-containing membranes through the convex surface of the core domain (Swairjo et al. 1995). In the case of annexins A1 and A2, calcium binding is proposed to lead to the release of the previously buried N-terminus to an exposed position available for interaction with S100A10 protein (Gerke and Moss 2002). Thus, an S100A10 dimer can coordinate a pair of annexin A2 proteins, potentially bridging adjacent phospholipid membranes into close proximity during a membrane fusion event (Gerke and Moss 2002). This leads to the aggregation of vesicles and formation of an endomembrane patch (Figure 1.9). As with S100A10 and annexin A2, the AHNAK protein gets located on the plasma membrane (Kouno et al. 2004), where the interaction between dysferlin and this complex can mediate the docking and fusion of the patch and sealing of the membrane. For instance, a high calcium concentration (extracellular, via the wound) causes annexin A1 and A2 association with a dysferlin-containing vesicle and damaged plasma membranes. The central protein in this process, dysferlin (Doherty and McNally 2003; Shao et al. 2006; Glover and Brown 2007), has been shown to co-localize and co-immunoprecipitate with annexins A1 and A2 (Lennon et al. 2003). Recent three-hybrid and co-immunoprecipitation experiments have also provided some details of the dysferlin repair complex. Using a series of truncated AHNAK constructs it has been shown that the extreme C-terminal domain of AHNAK is responsible for dysferlin binding. Although dysferlin possesses six ~130-residue C2 domains, the AHNAK interaction is localized to only the N-terminal C2A domain of dysferlin, a region that typically coordinates calcium as a prerequisite for phospholipid binding. Calcium binding to the dysferlin C2A domain is not a requirement for its interaction with AHNAK.

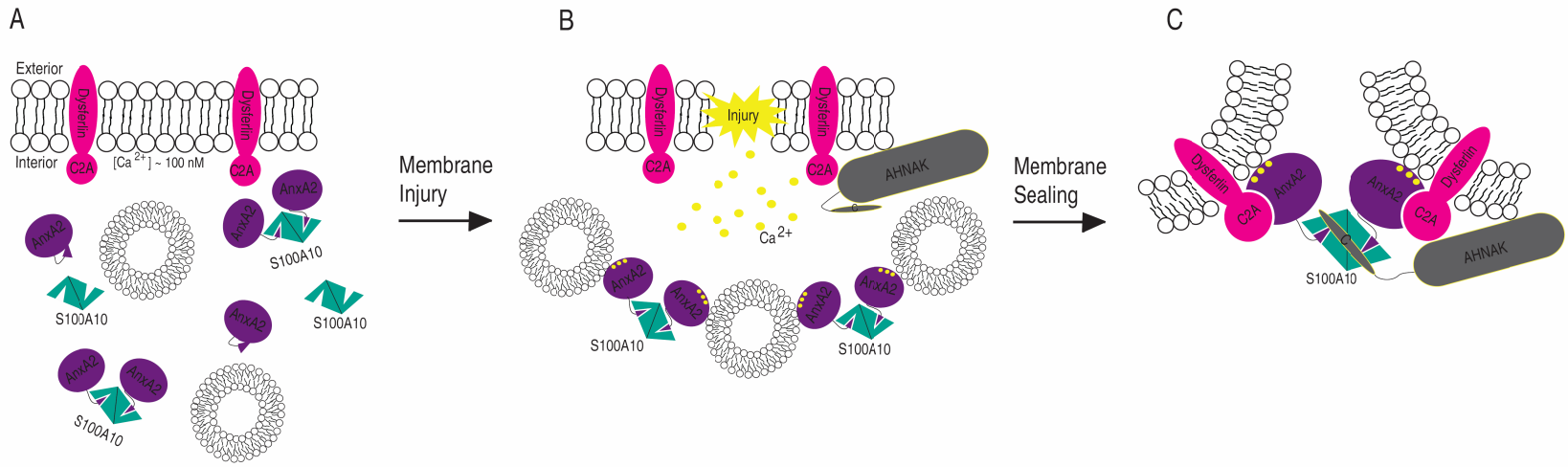

Figure 1.9. Hypothetical diagram illustrating possible interactions of the dysferlin complex important in membrane repair.

(A) Under resting calcium levels (100 nM), apo-S100A10 interacts with the N-terminal region of annexin A2. **(B)** In the case of a lesion in the membrane, calcium influx raises the intracellular calcium concentration locally, triggering the patch repair response. Intracellular vesicles get aggregated by calcium-bound annexin A2 that is in complex with the S100A10 to form an endo-membrane patch. **(C)** This complex is trafficked to the site of disruption. Dysferlin and AHNAK molecules present on the plasma membrane mediate docking and fusion of the patch and sealing of the membrane. Proposed interactions in the dysferlin complex are based on multiple biochemical experiments. The C-terminus of AHNAK is shown to interact with S100A10-annexin A2 complex, while the dysferlin C2A domain is near annexin A2.

Although the exact mechanisms whereby AHNAK is recruited for plasma membrane repair are not clear, annexin A2 and S100A10 co-localize with AHNAK at the plasma membrane along with dysferlin providing some evidence this multiprotein complex functions in the repair process.

1.11 Scope of Thesis

The multiple binding modes used by the S100 proteins to interact with a diverse array of target proteins suggest a great deal of flexibility in the manner an S100 protein recognizes a partner protein. This may prove useful to simultaneously coordinate more than a single target protein by some S100 proteins. Recent *in vivo* and *in vitro* experiments suggest that S100A10-annexin A2 can form multiprotein complexes with other proteins such as AHNAK and dysferlin that are important in plasma membrane repair.

Lack of structural information on the arrangement, affinities and structures of these proteins in the complex does not allow understanding the mechanisms of membrane repair. Consequently, further biochemical and structural experiments will be needed to ascertain the general role of S100 proteins in larger multiprotein complexes.

The main goals of this thesis were 1) design, synthesize and characterize a molecule that would facilitate assembly of larger S100 multiprotein complexes, 2) investigate the arrangement of the proteins, stoichiometry and affinity of AHNAK for the S100A10-annexin A2 complex and 3) identify structural details of the ternary complex formed between S100A10, annexin A2 and AHNAK complex.

The first objective was achieved by designing a hybrid protein in which S100A10 was linked in tandem to the N-terminus of annexin A2 (residues 1-15). The generality of this method was demonstrated by synthesizing a similar hybrid molecule between S100B and the central region of CapZ (TRTK12; residues 1-12). Using NMR spectroscopy, it was shown that the spectra for the S100A10-annexin A2 and S100B-TRTK12 hybrid proteins are nearly identical to those obtained for the complexes formed between the individual S100 proteins and synthetic peptides. The hybrid S100A10-annexin A2 protein was used in the peptide array experiments to uncover the binding region of this protein on AHNAK. The identified 20-residue C-terminal region of AHNAK with the strongest interaction to the S100A10-annexin A2 complex was then used in the remaining experiments. NMR spectrometry, non-denaturing electro-spray mass spectrometry (ES-MS) and fluorescence spectroscopy provided the evidence for a novel 1:1 interaction between an S100A10-annexin A2 dimer and an AHNAK peptide. The dissociation constant of the interaction between the AHNAK peptide and S100A10-annexin A2 was determined by fluorescence spectroscopy. Finally, NMR spectroscopy and X-ray crystallography confirmed that the interaction of AHNAK to the S100A10-annexin A2 complex utilizes residues from both, the S100A10 protein and annexin A2 peptide. Chemical shift mapping produced a binding surface for the S100A10-annexin A2-AHNAK complex. These results provided a novel model of a larger protein assembly required during the membrane repair process.

1.12 References

Ames, J.B., Porumb, T., Tanaka, T., Ikura, M., and Stryer, L. 1995a. Amino-terminal myristoylation induces cooperative calcium binding to recoverin. *J. Biol. Chem.* **270:** 4526-4533.

Ames, J.B., Tanaka, T., Ikura, M., and Stryer, L. 1995b. Nuclear magnetic resonance evidence for Ca^{2+}-induced extrusion of the myristoyl group of recoverin. *J. Biol. Chem.* **270:** 30909-30913.

Avila-Sakar, A.J., Creutz, C.E., and Kretsinger, R.H. 1998. Crystal structure of bovine annexin VI in a calcium-bound state. *Biochim. Biophys. Acta* **1387:** 103-116.

Ayala-Sanmartin, J., Zibouche, M., Illien, F., Vincent, M., and Gallay, J. 2008. Insight into the location and dynamics of the annexin A2 N-terminal domain during Ca(2+)-induced membrane bridging. *Biochim Biophys Acta* **1778:** 472-482.

Babu, Y.S., Bugg, C.E., and Cook, W.J. 1988. Structure of calmodulin refined at 2.2 Å resolution. *J. Mol. Biol* . **203:** 191-204.

Beaton, A.R., Rodriguez, J., Reddy, Y.K., and Roy, P. 2002. The membrane trafficking protein calpactin forms a complex with bluetongue virus protein NS3 and mediates virus release. *Proc Natl Acad Sci U S A* **99:** 13154-13159.

Becker, T., Weber, K., and Johnsson, N. 1990. Protein-protein recognition via short amphiphilic helices; a mutational analysis of the binding site of annexin II for p11. *EMBO J.* **9:** 4207-4213.

Benaud, C., Gentil, B.J., Assard, N., Court, M., Garin, J., Delphin, C., and Baudier, J. 2004. AHNAK interaction with the annexin 2/S100A10 complex regulates cell membrane cytoarchitecture. *J Cell Biol* **164:** 133-144.

Berridge, M.J., Lipp, P., and Bootman, M.D. 2000. The versatility and universality of calcium signalling. *Nat. Rev. Mol. Cell. Biol.* **1:** 11-21.

Bhattacharya, S., Large, E., Heizmann, C. W., Hemmings, B., Chazin, W. J. 2003. Structure of the Ca^{2+}/S100B/NDR kinase peptide complex: insights into S100 target specificity and activation of the kinase. *Biochemistry* **42:** 14416-14426.

Borthwick, L.A., Neal, A., Hobson, L., Gerke, V., Robson, L., and Muimo, R. 2008. The annexin 2-S100A10 complex and its association with TRPV6 is regulated by cAMP/PKA/CnA in airway and gut epithelia. *Cell Calcium* **44:** 147-157.

Cacciottolo, M., Belcastro, V., Laval, S., Bushby, K., di Bernardo, D., and Nigro, V. 2011. Reverse Engineering Gene Network Identifies New Dysferlin-interacting Proteins. *J Biol Chem* **286:** 5404-5413.

Carafoli, E. 2002. Calcium signaling: a tale for all seasons. *Proc Natl Acad Sci U S A* **99:** 1115-1122.

Carafoli, E. 2003. The calcium-signalling saga: tap water and protein crystals. *Nat Rev Mol Cell Biol* **4:** 326-332.

Chang, N., Sutherland, C., Hesse, E., Winkfein, R., Wiehler, W.B., Pho, M., Veillette, C., Li, S., Wilson, D.P., Kiss, E., et al. 2007. Identification of a novel interaction between the Ca(2+)-binding protein S100A11 and the Ca(2+)- and phospholipid-binding protein annexin A6. *Am J Physiol Cell Physiol* **292:** C1417-1430.

Charpentier, T.H., Thompson, L.E., Liriano, M.A., Varney, K.M., Wilder, P.T., Pozharski, E., Toth, E.A., and Weber, D.J. 2010. The effects of CapZ peptide (TRTK-12) binding to S100B-Ca2+ as examined by NMR and X-ray crystallography. *J Mol Biol* **396:** 1227-1243.

Clapham, D.E. 2007. Calcium signaling. *Cell* **131:** 1047-1058.

Concha, N.O., Head, J.F., Kaetzel, M.A., Dedman, J.R., and Seaton, B.A. 1993. Rat annexin V crystal structure: Ca(2+)-induced conformational changes. *Science* **261:** 1321-1324.

da Silva, A.C.R., and Reinach, F.C. 1991. Calcium binding induces conformational changes in muscle regulatory proteins. *Trends Biochem. Sci.* **16:** 53-57.

De Morree, A., Hensbergen, P.J., van Haagen, H.H., Dragan, I., Deelder, A.M., t Hoen, P.A., Frants, R.R., and van der Maarel, S.M. 2010. Proteomic analysis of the dysferlin protein complex unveils its importance for sarcolemmal maintenance and integrity. *PLoS One* **5:** e13854.

De Seranno, S., Benaud, C., Assard, N., Khediri, S., Gerke, V., Baudier, J., and Delphin, C. 2006. Identification of an AHNAK binding motif specific for the Annexin2/S100A10 tetramer. *J Biol Chem* **281:** 35030-35038.

Deloulme, J.C., Assard, N., Mbele, G.O., Mangin, C., Kuwano, R., and Baudier, J. 2000. S100A6 and S100A11 are specific targets of the calcium- and zinc-binding S100B protein in vivo. *J. Biol. Chem.* **275:** 35302-35310.

Deloulme, J.C., Gentil, B.J., and Baudier, J. 2003. Monitoring of S100 homodimerization and heterodimeric interactions by the yeast two-hybrid system. *Microsc Res Tech* **60:** 560-568.

Dempsey, A.C., Walsh, M.P., and Shaw, G.S. 2003. Unmasking the annexin I interaction from the structure of Apo-S100A11. *Structure* **11:** 887-897.

Diakonova, M., Gerke, V., Ernst, J., Liautard, J.P., van der Vusse, G., and Griffiths, G. 1997. Localization of five annexins in J774 macrophages and on isolated phagosomes. *J Cell Sci* **110 (Pt 10):** 1199-1213.

Doherty, K.R., and McNally, E.M. 2003. Repairing the tears: dysferlin in muscle membrane repair. *Trends Mol Med* **9:** 327-330.

Drohat, A.C., Baldisseri, D.M., Rustandi, R.R., and Weber, D.J. 1998. Solution structure of calcium-bound rat S100B (bb) as determined by nuclear magnetic resonance spectroscopy. *Biochemistry* **37:** 2729-2740.

Emans, N., Gorvel, J.P., Walter, C., Gerke, V., Kellner, R., Griffiths, G., and Gruenberg, J. 1993. Annexin II is a major component of fusogenic endosomal vesicles. *J Cell Biol* **120:** 1357-1369.

Fernandez, M.P., and Morgan, R.O. 2003. Structure, function and evolution of the annexin gene superfamily. In *Annexins : biological importance and annexin-related pathologies*. (ed. J. Bandorowicz-Pikula), pp. 21-37. Landes Bioscience/Eurekah.com ; Kluwer Academic/Plenum, Georgetown, Tex. New York.

Filipek, A., Wojda, U., and Lesniak, W. 1995. Interaction of calcyclin and its cyanogen bromide fragments with annexin II and glyceraldehyde 3-phosphate dehydrogenase. *Int J Biochem Cell Biol* **27:** 1123-1131.

Garbuglia, M., Verzini, M., Hofmann, A., Huber, R., and Donato, R. 2000. S100A1 and S100B interactions with annexins. *Biochim Biophys Acta.* **1498:** 192-206.

Geisow, M.J., Fritsche, U., Hexham, J.M., Dash, B., and Johnson, T. 1986. A consensus amino-acid sequence repeat in Torpedo and mammalian Ca2+-dependent membrane-binding proteins. *Nature* **320:** 636-638.

Gentil, B.J., Delphin, C., Mbele, G.O., Deloulme, J.C., Ferro, M., Garin, J., and Baudier, J. 2001. The giant protein AHNAK is a specific target for the calcium- and zinc-binding S100B protein: potential implications for Ca2+ homeostasis regulation by S100B. *J Biol Chem* **276:** 23253-23261.

Gerke, V., and Moss, S.E. 2002. Annexins: from structure to function. *Physiol Rev* **82:** 331-371.

Gifford, J.L., Walsh, M.P., and Vogel, H.J. 2007. Structures and metal-ion-binding properties of the Ca2+-binding helix-loop-helix EF-hand motifs. *Biochem J* **405:** 199-221.

Girard, C., Tinel, N., Terrenoire, C., Romey, G., Lazdunski, M., and Borsotto, M. 2002. p11, an annexin II subunit, an auxiliary protein associated with the background K+ channel, TASK-1. *Embo J* **21:** 4439-4448.

Glover, L., and Brown, R.H., Jr. 2007. Dysferlin in membrane trafficking and patch repair. *Traffic* **8:** 785-794.

Han, R., and Campbell, K.P. 2007. Dysferlin and muscle membrane repair. *Curr Opin Cell Biol* **19:** 409-416.

Harder, T., and Gerke, V. 1993. The subcellular distribution of early endosomes is affected by the annexin II2p11(2) complex. *J Cell Biol* **123:** 1119-1132.

Harder, T., Kellner, R., Parton, R.G., and Gruenberg, J. 1997. Specific release of membrane-bound annexin II and cortical cytoskeletal elements by sequestration of membrane cholesterol. *Mol Biol Cell* **8:** 533-545.

Hatakeyama, T., Okada, M., Shimamoto, S., Kubota, Y., and Kobayashi, R. 2004. Identification of intracellular target proteins of the calcium-signaling protein S100A12. *Eur J Biochem* **271:** 3765-3775.

Herzberg, O., and James, M.N.G. 1985. Structure of the calcium regulatory muscle protein troponin C at 2.8 A resolution. *Nature* **313:** 653-659.

Hu, N.J., Bradshaw, J., Lauter, H., Buckingham, J., Solito, E., and Hofmann, A. 2008. Membrane-induced folding and structure of membrane-bound annexin A1 N-terminal peptides: implications for annexin-induced membrane aggregation. *Biophys J* **94:** 1773-1781.

Huang, Y., Laval, S.H., van Remoortere, A., Baudier, J., Benaud, C., Anderson, L.V., Straub, V., Deelder, A., Frants, R.R., den Dunnen, J.T., et al. 2007. AHNAK, a novel component of the dysferlin protein complex, redistributes to the cytoplasm with dysferlin during skeletal muscle regeneration. *Faseb J* **21:** 732-742.

Huber, R., Berendes, R., Burger, A., Schneider, M., Karshikov, A., Luecke, H., Romisch, J., and Paques, E. 1992. Crystal and molecular structure of human annexin V after refinement. Implications for structure, membrane binding and ion channel formation of the annexin family of proteins. *J Mol Biol* **223:** 683-704.

Huber, R., Romisch, J., and Paques, E.P. 1990a. The crystal and molecular structure of human annexin V, an anticoagulant protein that binds to calcium and membranes. *Embo J* **9:** 3867-3874.

Huber, R., Schneider, M., Mayr, I., Romisch, J., and Paques, E.P. 1990b. The calcium binding sites in human annexin V by crystal structure analysis at 2.0 A resolution. Implications for membrane binding and calcium channel activity. *FEBS Lett* **275:** 15-21.

Illien, F., Finet, S., Lambert, O., and Ayala-Sanmartin, J. 2010. Different molecular arrangements of the tetrameric annexin 2 modulate the size and dynamics of membrane aggregation. *Biochim Biophys Acta* **1798:** 1790-1796.

Inman, K.G., Yang, R., Rustandi, R.R., Miller, K.E., Baldisseri, D.M., and Weber, D.J. 2002. Solution NMR structure of S100B bound to the high-affinity target peptide TRTK-12. *J. Mol. Biol.* **324:** 1003-1014.

Johnsson, N., Marriott, G., and Weber, K. 1988. p36, the major cytoplasmic substrate of src tyrosine protein kinase, binds to its p11 regulatory subunit via a short amino-terminal amphiphatic helix. *EMBO J.* **7:** 2435-2442.

Johnsson, N., Vandekerckhove, J., Van Damme, J., and Weber, K. 1986. Binding sites for calcium, lipid and p11 on p36, the substrate of retroviral tyrosine-specific protein kinases. *FEBS Lett* **198:** 361-364.

Jost, M., Zeuschner, D., Seemann, J., Weber, K., and Gerke, V. 1997. Identification and characterization of a novel type of annexin-membrane interaction: Ca2+ is not required for the association of annexin II with early endosomes. *J Cell Sci* **110 (Pt 2):** 221-228.

Kawasaki, H., Nakayama, S., and Kretsinger, R.H. 1998. Classification and evolution of EF-hand proteins. *Biometals* **11:** 277-295.

Knop, M., Aareskjold, E., Bode, G., and Gerke, V. 2004. Rab3D and annexin A2 play a role in regulated secretion of vWF, but not tPA, from endothelial cells. *Embo J* **23:** 2982-2992.

Korndorfer, I.P., Brueckner, F., and Skerra, A. 2007. The crystal structure of the human (S100A8/S100A9)2 heterotetramer, calprotectin, illustrates how conformational changes of interacting alpha-helices can determine specific association of two EF-hand proteins. *J Mol Biol* **370:** 887-898.

Kouno, M., Kondoh, G., Horie, K., Komazawa, N., Ishii, N., Takahashi, Y., Takeda, J., and Hashimoto, T. 2004. AHNAK/Desmoyokin is dispensable for proliferation,

differentiation, and maintenance of integrity in mouse epidermis. *J Invest Dermatol* **123:** 700-707.

Kretsinger, R.H., and Nockolds, C.E. 1973. Carp muscle calcium-binding protein. II. Structure determination and general description. *J. Biol. Chem.* **248:** 3313-3326.

Kuboniwa, H., Tjandra, N., Grzesiek, S., Ren, H., Klee, C.B., and Bax, A. 1995. Solution structure of calcium-free calmodulin. *Nature Struct. Biol.* **2:** 768-776.

Lee, Y.T., Dimitrova, Y.N., Schneider, G., Ridenour, W.B., Bhattacharya, S., Soss, S.E., Caprioli, R.M., Filipek, A., and Chazin, W.J. 2008. Structure of the S100A6 complex with a fragment from the C-terminal domain of Siah-1 interacting protein: a novel mode for S100 protein target recognition. *Biochemistry* **47:** 10921-10932.

Lennon, N.J., Kho, A., Bacskai, B.J., Perlmutter, S.L., Hyman, B.T., and Brown, R.H., Jr. 2003. Dysferlin interacts with annexins A1 and A2 and mediates sarcolemmal wound-healing. *J Biol Chem* **278:** 50466-50473.

Lewit-Bentley, A., Rety, S., Sopkova-De OliveiraSantos, J., and Gerke, V. 2000. S100-Annexin complexes: some insights from structural studies. *Cell Biol Int.* **24:** 799-802.

Lewit-Bentley, A., Rety, S. 2000. EF-hand calcium-binding proteins. *Curr Opin Struct Biol* **10:** 637-643.

Linse, S., Brodin, P., Drakenberg, T., Thulin, E., Sellers, P., Elmden, K., Grundstrom, T., and Forsén, S. 1987. Structure-function relationships in EF-hand Ca^{2+}-binding proteins. Protein engineering and biophysical studies of calbindin D_{9k}. *Biochemistry* **26:** 6723-6735.

MacLeod, T.J., Kwon, M., Filipenko, N.R., and Waisman, D.M. 2003. Phospholipid-associated annexin A2-S100A10 heterotetramer and its subunits: characterization of the interaction with tissue plasminogen activator, plasminogen, and plasmin. *J Biol Chem* **278:** 25577-25584.

Mailliard, W.S., Haigler, H.T., and Schlaepfer, D.D. 1996. Calcium-dependent binding of S100C to the N-terminal domain of annexin I. *J. Biol. Chem.* **271:** 719-725.

Maler, L., Sastry, M., and Chazin, W.J. 2002. A structural basis for S100 protein specificity derived from comparative analysis of apo and Ca^{2+}-calcyclin. *J. Mol. Biol.* **317:** 279-290.

Marsden, B.J., Shaw, G.S., and Sykes, B.D. 1989. Calcium binding proteins. Elucidating the contributions to calcium affinity from analysis of species variants and peptide fragments. *Biochem. Cell Biol.* **68:** 587-601.

Matsumura, H., Shiba, T., Inoue, T., Harada, S., and Kai, Y. 1998. A novel mode of target recognition suggested by the 2.0 A structure of holo S100B from bovine brain. *Structure* **6:** 233-241.

Mayorga, L.S., Beron, W., Sarrouf, M.N., Colombo, M.I., Creutz, C., and Stahl, P.D. 1994. Calcium-dependent fusion among endosomes. *J Biol Chem* **269:** 30927-30934.

McClintock, K.A., and Shaw, G.S. 2000. A logical sequence search for S100B target proteins. *Protein Sci.* **9:** 2043-2046.

McClintock, K.A., and Shaw, G.S. 2003. A novel S100 target conformation is revealed by the solution structure of the Ca2+-S100B-TRTK-12 complex. *J Biol Chem* **278:** 6251-6257.

Merrifield, C.J., Rescher, U., Almers, W., Proust, J., Gerke, V., Sechi, A.S., and Moss, S.E. 2001. Annexin 2 has an essential role in actin-based macropinocytic rocketing. *Curr Biol* **11:** 1136-1141.

Missiaen, L., Robberecht, W., van den Bosch, L., Callewaert, G., Parys, J. B., Wuytack, F., Raeymaekers, L., Nilius, B., Eggermont, J., and De Smedt, H. 2000. Abnormal intracellular Ca^{2+} homeostasis and disease. *Cell Calcium* **28:** 1-21.

Nelson, M.R., and Chazin, W.J. 1998. Structures of EF-hand Ca^{2+} -binding proteins: Diversity in the organization, packing and response to Ca^{2+} binding. *Biometals* **11:** 297-318.

Okuse, K., Malik-Hall, M., Baker, M.D., Poon, W.Y., Kong, H., Chao, M.V., and Wood, J.N. 2002. Annexin II light chain regulates sensory neuron-specific sodium channel expression. *Nature* **417:** 653-656.

Otterbein, L.R., Kordowska, J., Witte-Hoffmann, C., Wang, C.L., and Dominguez, R. 2002. Crystal structures of S100A6 in the Ca(2+)-free and Ca(2+)-bound states: the calcium sensor mechanism of S100 proteins revealed at atomic resolution. *Structure (Camb)* **10:** 557-567.

Pinton, P., Pozzan, T., and Rizzuto, R. 1998. The Golgi apparatus is an inositol 1,4,5-trisphosphate-sensitive Ca2+ store, with functional properties distinct from those of the endoplasmic reticulum. *Embo J* **17:** 5298-5308.

Poon, W.Y., Malik-Hall, M., Wood, J.N., and Okuse, K. 2004. Identification of binding domains in the sodium channel Na(V)1.8 intracellular N-terminal region and annexin II light chain p11. *FEBS Lett* **558:** 114-118.

Pozzan, T., Rizzuto, R., Volpe, P., and Meldolesi, J. 1994. Molecular and cellular physiology of intracellular calcium stores. *Physiol Rev* **74:** 595-636.

Renigunta, V., Yuan, H., Zuzarte, M., Rinne, S., Koch, A., Wischmeyer, E., Schlichthorl, G., Gao, Y., Karschin, A., Jacob, R., et al. 2006. The retention factor p11 confers an endoplasmic reticulum-localization signal to the potassium channel TASK-1. *Traffic* **7:** 168-181.

Rety, S., Osterloh, D., Arie, J.P., Tabaries, S., Seeman, J., Russo-Marie, F., Gerke, V., and Lewit-Bentley, A. 2000. Structural basis of the Ca(2+)-dependent association between S100C (S100A11) and its target, the N-terminal part of annexin I. *Structure Fold Des* **8:** 175-184.

Rety, S., Sopkova, J., Renouard, M., Osterloh, D., Gerke, V., Tabaries, S., Russo-Marie, F., and Lewit-Bentley, A. 1999. The crystal structure of a complex of p11 with the annexin II N-terminal peptide. *Nat Struct Biol* **6:** 89-95.

Ringer, S. 1883. A further Contribution regarding the influence of the different Constituents of the Blood on the Contraction of the Heart. *J Physiol* **4:** 29-42 23.

Rintala-Dempsey, A.C., Rezvanpour, A., and Shaw, G.S. 2008. S100-annexin complexes--structural insights. *Febs J* **275:** 4956-4966.

Rintala-Dempsey, A.C., Santamaria-Kisiel, L., Liao, Y., Lajoie, G., and Shaw, G.S. 2006. Insights into S100 target specificity examined by a new interaction between S100A11 and annexin A2. *Biochemistry* **45:** 14695-14705.

Rosengarth, A., Gerke, V., and Luecke, H. 2001. X-ray structure of full-length annexin 1 and implications for membrane aggregation. *J Mol Biol* **306:** 489-498.

Rosengarth, A., and Luecke, H. 2003. A calcium-driven conformational switch of the N-terminal and core domains of annexin A1. *J Mol Biol* **326:** 1317-1325.

Rustandi, R.R., Baldisseri, D.M., and Weber, D.J. 2000. Structure of the negative regulatory domain of p53 bound to S100B(bb). *Nat. Struct. Biol.* **7:** 570-574.

Sarafian, T., Pradel, L.A., Henry, J.P., Aunis, D., and Bader, M.F. 1991. The participation of annexin II (calpactin I) in calcium-evoked exocytosis requires protein kinase C. *J Cell Biol* **114:** 1135-1147.

Schaub, M.C., and Heizmann, C.W. 2008. Calcium, troponin, calmodulin, S100 proteins: from myocardial basics to new therapeutic strategies. *Biochem Biophys Res Commun* **369:** 247-264.

Seaton, B.A. 1996. *Annexin V molecular structure, ligand binding and biological function*, R.G.Landes:Georgetown, TX, pp. 15-29.

Semov, A., Moreno, M.J., Onichtchenko, A., Abulrob, A., Ball, M., Ekiel, I., Pietrzynski, G., Stanimirovic, D., and Alakhov, V. 2005. Metastasis-associated protein S100A4 induces angiogenesis through interaction with Annexin II and accelerated plasmin formation. *J Biol Chem* **280:** 20833-20841.

Shao, C., Zhang, F., Kemp, M.M., Linhardt, R.J., Waisman, D.M., Head, J.F., and Seaton, B.A. 2006. Crystallographic analysis of calcium-dependent heparin binding to annexin A2. *J Biol Chem* **281:** 31689-31695.

Shtivelman, E., and Bishop, J.M. 1993. The human gene AHNAK encodes a large phosphoprotein located primarily in the nucleus. *J Cell Biol* **120:** 625-630.

Skelton, N.J., Kordel, J., Akke, M., Forsen, S., and Chazin, W.J. 1994. Signal transduction versus buffering activity in Ca^{2+}-binding proteins. *Struct. Biol.* **1:** 239-245.

Smith, S.P., and Shaw, G.S. 1998. A novel calcium-sensitive switch revealed by the structure of human S100B in the calcium-bound form. *Structure* **6:** 211-222.

Sopkova, J., Renouard, M., and Lewit-Bentley, A. 1993. The crystal structure of a new high-calcium form of annexin V. *J Mol Biol* **234:** 816-825.

Streicher, W.W., Lopez, M.M., and Makhatadze, G.I. 2009. Annexin I and annexin II N-terminal peptides binding to S100 protein family members: specificity and thermodynamic characterization. *Biochemistry* **48:** 2788-2798.

Strynadka, N.C.J., and James, M.N.G. 1989. Crystal structures of the helix-loop-helix calcium-binding proteins. *Ann. Rev. Biochem.* **58:** 951-998.

Sudo, T., and Hidaka, H. 1999. Characterization of the calcyclin (S100A6) binding site of annexin XI-A by site-directed mutagenesis. *FEBS Lett* **444:** 11-14.

Swairjo, M.A., Concha, N.O., Kaetzel, M.A., Dedman, J.R., and Seaton, B.A. 1995. Ca(2+)-bridging mechanism and phospholipid head group recognition in the membrane-binding protein annexin V. *Nat Struct Biol* **2:** 968-974.

Teo, T.S., and Wang, J.H. 1973. Mechanism of activation of a cyclic adenosine 3':5'-monophosphate phosphodiesterase from bovine heart by calcium ions.

Identification of the protein activator as a Ca2+ binding protein. *J Biol Chem* **248:** 5950-5955.

Tokumitsu, H., Mizutani, A., Minami, H., Kobayashi, R., and Hidaka, H. 1992. A calcyclin-associated protein is a newly identified member of the Ca2+/phospholipid-binding proteins, annexin family. *J Biol Chem* **267:** 8919-8924.

Tsien, R.Y. 1981. A non-disruptive technique for loading calcium buffers and indicators into cells. *Nature* **290:** 527-528.

Tufty, R.M., and Kretsinger, R.H. 1975. Troponin and parvalbumin calcium binding regions predicted in myosin light chain and T4 lysozyme. *Science* **187:** 167-169.

van de Graaf, S.F., Hoenderop, J.G., Gkika, D., Lamers, D., Prenen, J., Rescher, U., Gerke, V., Staub, O., Nilius, B., and Bindels, R.J. 2003. Functional expression of the epithelial Ca(2+) channels (TRPV5 and TRPV6) requires association of the S100A10-annexin 2 complex. *Embo J* **22:** 1478-1487.

Weng, X., Luecke, H., Song, I.S., Kang, D.S., Kim, S.H., and Huber, R. 1993. Crystal structure of human annexin I at 2.5 A resolution. *Protein Sci* **2:** 448-458.

Wright, N.T., Cannon, B.R., Wilder, P.T., Morgan, M.T., Varney, K.M., Zimmer, D.B., and Weber, D.J. 2009. Solution structure of S100A1 bound to the CapZ peptide (TRTK12). *J Mol Biol* **386:** 1265-1277.

Wright, N.T., Prosser, B.L., Varney, K.M., Zimmer, D.B., Schneider, M.F., and Weber, D.J. 2008. S100A1 and calmodulin compete for the same binding site on ryanodine receptor. *J Biol Chem* **283:** 26676-26683.

Yap, K.L., Kim, J., Truong, K., Sherman, M., Yuan, T., and Ikura, M. 2000. Calmodulin target database. *J Struct Funct Genomics* **1:** 8-14.

Yoon, M.K., Park, S.H., Won, H.S., Na, D.S., and Lee, B.J. 2000. Solution structure and membrane-binding property of the N-terminal tail domain of human annexin I. *FEBS Lett* **484:** 241-245.

Zeng, F.Y., Gerke, V., and Gabius, H.J. 1993. Identification of annexin II, annexin VI and glyceraldehyde-3-phosphate dehydrogenase as calcyclin-binding proteins in bovine heart. *Int J Biochem* **25:** 1019-1027.

Zhang, M., Tanaka, T., Ikura, M. 1995. Calcium-induced conformational transition revealed by the solution structure of apo calmodulin. *Nat Struct Biol* **2:** 758-767.

Zhang, Z. Q., Wietgrefe, S. W., Li, Q., Shore, M. D., Duan, L., Reilly, C., Lifson, J. D., and Haase, A. T. 2004. Roles of substrate availability and infection of resting and activated CD4+ T cells in transmission and acute simian immunodeficiency virus infection. *Proc Natl Acad Sci U S A* **101**(15), 5640-5645.

Zibouche, M., Vincent, M., Illien, F., Gallay, J., and Ayala-Sanmartin, J. 2008. The N-terminal domain of annexin 2 serves as a secondary binding site during membrane bridging. *J Biol Chem* **283:** 22121-22127.

Chapter 2

Design of High-Affinity S100-Target Hybrid Proteins

2.1 Introduction

Although some structures of different S100 proteins bound to target peptides have been determined, only three crystal structures are available (S100A10-annexin A2, Ca^{2+}-S100A11-annexin A1, Ca^{2+}-S100B-TRTK12) (Rety et al. 1999; Rety et al. 2000; Charpentier et al. 2010). This is likely due to the difficulties associated with crystal formation of the S100-target complexes. Better progress has been made for S100-target complexes by NMR spectroscopy where structures such as calcium-bound S100B (Ca^{2+}-S100B) with peptide binding regions from p53 (Rustandi et al. 2000), Ndr kinase (Bhattacharya et al. 2003) and CapZ (Inman et al. 2002; McClintock and Shaw 2003) have been determined. However, some of these structures suffer from imprecision of the side chains, especially at the protein-peptide interface making details of the interaction difficult to characterize. This could be improved by ^{15}N, ^{13}C-labeling of the target peptide although this is very costly for a synthetic peptide and can suffer from low yields and proteolysis when expressed as a fusion protein. Only one example of a biosynthetic, isotopically-labeled peptide exists for the 30-residue Siah-1 interacting region for Ca^{2+}-S100A6 (Lee et al. 2008).

Parts of this chapter have been taken from the published article: Rezvanpour, A., Phillips, J. M., and Shaw, G. S. 2009. Design of high-affinity S100-target hybrid proteins. *Protein Sci.* **18:** 2528-2536.

In this chapter, a method is described in which S100B and S100A10 are used as the carrier proteins for target peptides from CapZ and annexin A2, respectively. The premise is that the S100 protein will protect the target peptide from degradation during biosynthesis and purification. S100A10 and S100B proteins were linked to the N-terminal region of annexin A2 (residues 1-15) and the central region of CapZ (TRTK12; residues 1-12) using linkers containing different protease cleavage sites to facilitate isolation of the target peptides. NMR spectroscopy has been used to show that the spectra for the S100A10-annexin A2 (A10A2) and S100B-TRTK12 (BT12) hybrid proteins are nearly identical to those obtained for the complexes formed between the individual S100 proteins and synthetic peptides.

2.2 Materials and Methods

2.2.1 Source of Materials

The expression vector for human S100A10 (pGEX-6P-1-derived vector, GE Healthcare) was generously provided by Dr. Michael Walsh (University of Calgary, Alberta, Canada). For expression vectors with an in-frame N-terminal GB1 fusion of TRTK12, annexin A2 and AHNAK, pSAF2 vector was obtained from Dr. Susan Safadi (University of Western Ontario). All forward and reverse oligonucleotides described within this chapter were synthesized by Sigma-Genosys (Mississauga, ON, Canada). T4 DNA ligase was purchased from Fermentas Life Sciences (Burlington, ON, Canada). Pfu Turbo DNA polymerase was purchased from Stratagene (La Jolla, CA, USA). All other chemicals used in cloning were purchased from BioShop Canada (Burlington, ON,

Canada). PreScission protease was obtained from GE Healthcare (Buckinghamshire, UK). All DNA sequencing were performed at Robarts Research Institute Sequencing Facility (London, ON, Canada).

$^{15}NH_4Cl$ and $^{13}C_6$-glucose were obtained from Cambridge Isotope Laboratories, Inc. (Andover, MA). Puratronic grade $CaCl_2$ (99.9995% purity) was purchased from Johnson-Matthey (Ward Hill, MA). Annexin A2 (STVHEILSKLSLEG) and TRTK12 (TRTKIDWNKILSLE) peptides were synthesized as previously described (McClintock and Shaw 2003; Rintala-Dempsey et al. 2006). All other reagents used in the following experiments were of the highest purity commercially available.

2.2.2 Construction of GB1-TRTK12, -annexin A2, and –AHNAK in E. coli Expression Vectors

pSAF2 plasmid, a derivative of the pGEV1 expression vector, containing an in-frame N-terminal GB1 gene was used to construct the GB1-TRTK12 (residues 1-12), -annexin A2 (residues 1-15), and –AHNAK (residues 5654-5673) genes. The genes were under control of a T7 RNA polymerase promoter and were used for inducible expression of them in *E. coli*. In these vectors the N-terminal GB1 gene was linked to the TRTK12, annexin A2, and AHNAK through a linker containing a thrombin protease cleavage site. Five glycine residues were added to enhance the accessibility of the protease cut site, which would be used to remove the GB1 tag following purification. There was also a His_6 tag at the C-terminus which was separated from TRTK12, annexin A2, and AHNAK by a tobacco etch virus (TEV) cleavage site.

The entire DNA sequences coding for TRTK12, annexin A2, and AHNAK were created using 5'-phosphorylated, one forward and one reverse single-stranded (ss), complementary primers (Table 2.1). The forward and reverse primers were designed such that following annealing, the double-stranded (ds) DNA fragment would have *Bam*HI and *Xho*I over-hangs at the N- and C-terminus, respectively. 1 µL of 1 µg/µL stock solutions of the forward and reverse primers were mixed with 2 µL of Buffer 3 (50 mM Tris-HCl, 100 mM NaCl, 10 mM $MgCl_2$, 1 mM DTT, pH 7.9) and the total volume was adjusted to 20 µL with ddH_2O. The mixture was heated to 100 ºC for 2 minutes in a water bath to eliminate the secondary structure of the single-stranded oligonucleotides and slowly cooled down to room temperature to facilitate the proper annealing of the complementary oligonucleotides. The annealed reaction (5 µL) was mixed with 1 µL of Bromophenol blue and run on a 8 % native polyacrylamide gel in TBE (Tris-borate-EDTA) buffer. The gel was then stained in TBE buffer with ethidium bromide. The double-stranded DNA fragment was ligated with the *Bam*HI and *Xho*I digested pSAF2 vector (Safadi and Shaw 2007) using T4 DNA ligase and then transformed into *E. coli* strain JM-109. Single colonies were selected and the correct constructs were confirmed by DNA sequencing.

2.2.3 Expression and Purification of GB1-TRTK12, -annexin A2, and -AHNAK

The GB1-TRTK12, -annexin A2 and -AHNAK vectors were transformed into *E. coli* strain BL21 (DE3)-RIL expression cells (Invitrogen), which contain extra copies of the *argU*, *ileY*, and *leuW* tRNA genes to recognize AGA, AGG, AUA, and CUA codons. Overnight cultures (25 mL) were used to inoculate 1 L of pre-warmed LB

Table 2.1. Oligonucleotides used in synthesis of GB1-TRTK12, -annexin A2 and AHNAK expression vectors.

Parental Vector	Oligonucleotide Name	Oligonucleotide Sequence (5'-3')	Length
pSAF1	TRTK (F2)	GATCCATGACTCGTACTAAGATAGATTGGAACA AGATACTGTCTC	45
	TRTK (R2)	TCGAGAGACAGTATCTTGTTCCAATCTATCTTAG TACGAGTCATG	45
	AnnexinII (F2)	GATCCATGAGCACCGTACACGAAATCTTGAGCA AACTGTCCCTGGAAGGGC	51
	AnnexinII (R2)	TCGAGCCCTTCCAGGGACAGTTTGCTCAAGATTT CGTGTACGGTGCTCATG	51
	AHNAK (F2)	GATCCATGGGCAAAGTCACGTTCCCCAAAATGAA GATCCCTAAATTCACGTTCTCCGGCAGAGAGTTAC	69
	AHNAK (F2)	TCGAGTAACTCTCTGCCGGAGAACGTGAATTTAG GGATCTTCATTTTGGGGAACGTGACTTTGCCCATG	69

medium supplemented with 50 µg/mL ampicillin. The cultures were grown at 37 ºC to a density of (A_{600}) 0.8 AU, when they were induced with 1 mM IPTG. Induction continued for another 4 h with constant shaking at 37 ºC. Cells were harvested by centrifugation at 6,000 rpm for 15 min at 4 ºC. Following addition of one complete-mini protease inhibitor tablet and PMSF (1 mM final concentration), the cells were lysed by French Pressure at 20,000 psi. Ultracentrifugation of the lysed cells was performed to remove cell debris on a Beckman ultracentrifuge at 38,000 rpm for 90 min. All fractionation steps were performed at 4 °C. The supernatant was filtered through 0.45 micron low protein binding Millipore syringe filters (Millipore) to remove the particulate matter. The protein was subsequently applied to a 5 mL Ni-NTA column pre-equilibrated in 20 mM Tris-HCl, 10 mM imidazole, 300 mM NaCl, pH 8.0. The column was washed with the same buffer containing 20 mM imidazole until the OD_{280} returned to baseline. Bound protein was then eluted with a 30 mL, 20-250 mM imidazole gradient in the elution buffer. Fractions containing the protein were pooled and extensively dialyzed against TEV protease cleavage buffer (20 mM Tris-HCl, 150 mM NaCl, 10 mM imidazole, 1 mM DTT, pH 7.5) for 6 h with multiple buffer exchange. GB1-peptide was cleaved from the His_6 tag using 250 units of TEV protease in 24 h with gentle agitation. Cleaved protein was purified on a 20 mL IgG Sepharose fast flow column (Amersham) in binding buffer to remove the His_6 tag. Bound protein was eluted with 0.5 M acetic acid, pH 3.4. Protein fractions were pooled, dialyzed against thrombin cleavage buffer (20 mM Tris-HCl, 150 mM NaCl, 2.5 mM $CaCl_2$, pH 8.4) and cleaved with a 1:2000 wt:wt ratio of thrombin to protein for 14 h at 20 ºC. Cleaved GB1 was then isolated from the

peptides utilizing an IgG Sepharose column as described above. The integrity of all proteins was verified on 16.6% SDS-PAGE gel and electrospray ionization mass spectrometry (Biological Mass Spectrometry Laboratory, University of Western Ontario).

2.2.4 Molecular Modeling of Hybrid S100 Proteins

The lengths of the linker connecting S100A10 to annexin A2 or S100B to TRTK12 were determined using Swiss-PDB Viewer (Guex and Peitsch 1997). The coordinates for S100A10 bound to annexin A2 (PDB code: 1BT6) (Rety et al. 1999) and Ca^{2+}-S100B complexed with TRTK12 (PDB codes: 1MQ1, 1MWN) (Inman et al. 2002; McClintock and Shaw 2003) were obtained from the Protein Data Bank (Berman et al. 2000). The last four residues at the C-terminus of S100A10 were disordered and not visible in the structure. Initial linkers were built using glycine spacers with moderate rotations of φ,ψ angles. A total of nine glycine residues was required to connect the observed C-terminus of S100A10 (K91) to the N-terminus of the annexin A2 peptide (STVHEILSKLSLEG). Eleven glycine residues were added in the S100B-TRTK12 (BT12) hybrid from the C-terminus of the S100B (E91) to the N-terminus of the TRTK12 peptide (TRTKIDWNKILS). Each structure was energy minimized using steepest descent minimization. Upon completion, glycine residues were swapped to those corresponding to the TEV (S100A10) or PreScission (S100B) cleavage sites. Subsequent energy minimization and visualization was used to insure the absence of bad contacts between the linker residues and the corresponding S100 protein.

2.2.5 Construction of the S100A10-annexin A2 Hybrid Gene

A derivative of the pGEX-6P-1 expression vector containing the human homologue of S100A10 was used to construct the A10A2 hybrid gene. The QuikChange method (Stratagene, La Jolla, CA) was used in three consecutive steps to a) substitute the last four amino acid residues of S100A10; K93E, G94N, K95L, K96Y, b) insert a TEV protease cleave site, and c) generate the annexin A2 hybrid DNA fragment. Forward and reverse primers used in these procedures are shown in Table 2.2. The resulting vectors at each step of the cloning were confirmed by DNA sequencing.

2.2.6 Expression and Purification of S100A10 and S100A10-Annexin A2

Uniformly ^{15}N, ^{13}C-labeled GST-S100A10 and GST-S100A10-annexin A2 (A10A2) were over-expressed in the BL21 (DE3) Codon Plus *E. coli* strain using M9 minimal medium supplemented with 1 g $^{15}NH_4Cl$ and 2 g $^{13}C_6$-glucose as the sole nitrogen and carbon sources, respectively. The cultures were grown at 37 ºC in the presence of ampicillin (50 μg/mL) to a density of (A_{600}) 0.8 AU, then induced by adding 1 mM IPTG. Induction continued for another 8 h with constant shaking at 37 ºC. Cells were harvested by centrifugation at 6,000 rpm for 15 min and lysed by French Pressure at 20,000 psi. Cell debris was removed by centrifugation at 38,000 rpm for 90 min. All fractionation steps were performed at 4 °C. The supernatant was applied to a 5 mL glutathione-linked Sepharose column equilibrated in PBS buffer (140 mM NaCl, 2.7 mM KCl, 10 mM Na_2HPO_4, 1.8 mM KH_2PO_4, pH 7.3). The ^{15}N, ^{13}C-labeled GST-S100A10 or GST-A10A2 were eluted in elution buffer (50 mM Tris-HCl, 20 mM reduced glutathione,

Table 2.2. Oligonucleotides used in synthesis of A10A2 expression vector.

Parental Vector	Oligonucleotide Name	Oligonucleotide Sequence (5'-3')	Length
S100A10	S100A10-AnX(F1)	GTGCACATGAAGCAGGAGAACCTGTACTGACTCGAGCGGCCG	42
	S100A10-AnX(R1)	CGGCCGCTCGAGTCAGTACAGGTTCTCCTGCTTCATGTGCAC	42
	S100A10-AnX(F2)	CAGGAGAACCTGTACTTTCAAGGGGATTCCACAGTTTGACTCGAGCGGCCG	51
	S100A10-AnX(R2)	CGGCCGCTCGAGTCAAACTGTGGAATCCCCTTGAAAGTACAGGTTCTCCTG	51
	S100A10-AnX(F3)	GGGGATTCCACAGTTCACGAGATTCTGTCGAAATGACTCGAGCGGCCG	48
	S100A10-AnX(R3)	CGGCCGCTCGAGTCATTTCGACAGAATCTCGTGAACTGTGGAATCCCC	48
	S100A10-AnX(F4)	CACGAGATTCTGTCGAAACTATCTCTAGAAGGGGACTGACTCGAGCGGCCG	51
	S100A10-AnX(R4)	CGGCCGCTCGAGTCAGTCCCCTTCTAGAGATAGTTTCGACAGAATCTCGTG	51

pH 8.0). Fractions containing the protein were pooled and extensively dialyzed against PreScission protease cleavage buffer (50 mM Tris-HCl, 150 mM NaCl, 1 mM EDTA, 1 mM DTT, pH 7.0) overnight. S100A10 or A10A2 were cleaved from the glutathione S-transferase protein using 150 units of PreScission protease in 48 h. The cleaved protein was applied to a GST column in binding buffer and the flow-through fractions were collected. MALDI-TOF mass data for A10A2 (MW_{calc} = 14517.9 Da; MW_{obs} = 14507.2 Da for ^{15}N, ^{13}C-labeled protein) confirmed the protein identities.

2.2.7 Construction of the S100B-TRTK12 Hybrid Gene

The pSS2 expression vector containing human S100B was utilized to construct the S100B-TRTK12 (BT12) hybrid gene (Smith et al. 1996). In the first step, a unique *Xho*I reporter cut site (5' C↓TCGAG 3') was generated directly adjacent to the stop codon of the S100B coding sequence using the QuikChange kit (Stratagene, La Jolla, CA). The primers used are shown in Table 2.3. The PCR reaction was conducted using Pfu Turbo DNA polymerase (Stratagene, La Jolla, CA) and the parental DNA was digested with *Dpn*I endonuclease (Bostrom et al.). The amplified, nicked PCR product was then transformed into the competent *E. coli* strain JM109 to repair the nick of the mutant DNA fragment. Single colonies were selected and the correct constructs were confirmed by DNA sequencing. The vector was then cleaved with *Xho*I restriction enzyme and dephosphorylated with 1 μL of alkaline phosphatase (Amersham Pharmacia Biotech) to prevent religation of the cut vector. The digestion reaction was run on a 1% agarose gel and the corresponding band was extracted using QIAquick Gel Extraction Kit (Qiagen).

Forward and reverse primers (5'-phosphorylated, Sigma-Aldrich) corresponding to residues from the linker region, the entire TRTK12 peptide and appropriate *Xho*I site over-hangs (Table 2.3) were annealed together as described in Section 1.2.2. The double-stranded DNA fragment was ligated with the unique *Xho*I site of the dephosphorylated vector containing the S100B gene using T_4 DNA ligase and then transformed into *E. coli* strain JM-109. Single colonies were selected and the correct orientation and a single insertion of the annealed primers in the resulting vectors were confirmed by DNA sequencing.

2.2.8 Expression and Purification of S100B and S100B-TRTK12

Expression and purification of uniformly ^{15}N, ^{13}C-labeled BT12 in *Escherichia coli* strain N99 were conducted as described for human S100B (Smith et al. 1996). The protocol was modified by reducing the $(NH_4)_2SO_4$ concentration to 50% saturation due to the decreased solubility of BT12 compared to S100B. Following dialysis (25 mM Tris-HCl, 100 mM NaCl, 1 mM DTT, and 5 mM $CaCl_2$, pH 7.5), BT12 was applied to a phenyl-Sepharose (Amersham Biosciences) column equilibrated in the same buffer. The column was washed (25 mM Tris-HCl, 100 mM NaCl, 1 mM DTT, 1 mM $CaCl_2$, pH 7.5) and BT12 was eluted with EGTA buffer (25 mM Tris-HCl, 100 mM NaCl, 1 mM DTT, and 1 mM EGTA, pH 7.5). MALDI-TOF mass data for ^{15}N-labeled BT12 (desformylmethionine MW_{calc} = 13430.2 Da; MW_{obs} = 13427.3 Da, desformyl MW_{calc} = 13563.2 Da; MW_{obs} = 13559.5 Da, and formylmethionine MW_{calc} = 13591.2 Da; MW_{obs} = 13587.6 Da) confirmed the presence of the three chemically different forms of BT12 at

Table 2.3. Oligonucleotides used in synthesis of BT12 expression vector.

Parental Vector	Oligonucleotide Name	Oligonucleotide Sequence (5'-3')	Length
S100B	XhoIfor	GGCTGCTTTCTAATCTCACTCGAGCTCATGTTCAAA GAACTCG	43
	XhoIrev	CGAGTTCTTTGAACATGAGCTCGAGTGAGATTAGAA AGCAGCC	43
S100B-XhoI	Linker TRTK-for	TCGACCTCTTCCAAGGCCCAGGCGGCGGCGGCACTC GTACTAAAATAGATTGGAACAAGATACTCTCTC	69
	Linker TRTK-rev	TCGAGAGAGAGTATCTTGTTCCAATCTATTTTAGTA CGAGTGCCGCCGCCGCCTGGGCCTTGGAAGAGG	69

its N-terminus similar to those previously characterized for S100B (Smith et al. 1997).

2.2.9 NMR Spectroscopy

All NMR experiments were acquired at 35 ºC on a Varian INOVA 600 MHz spectrometer equipped with a ^{13}C-enhanced triple resonance cold probe. NMR samples of 0.5 mM (monomer) uniformly ^{15}N, ^{13}C-labeled S100A10 and A10A2 were prepared in 10% D_2O, 20 mM MOPS, 1 mM EDTA, 1 mM DTT, 50 mM arginine, 50 mM glutamic acid, and 100 mM NaCl buffer at pH 7.0, and 100 μM DSS as an internal standard. Uniformly ^{15}N, ^{13}C-labeled NMR samples of 0.7 mM S100B and BT12 were prepared in a similar buffer using either 20 mM $CaCl_2$ or 1 mM EDTA. Sequential ^{1}H, ^{13}C, and ^{15}N resonance assignments of A10A2 and calcium saturated BT12 were completed using HNCACB (Wittekind and Mueller 1993), CBCA(CO)NH (Grzesiek and Bax 1992a), HNCO (Kay et al. 1990), HNCA (Grzesiek and Bax 1992b), and C(CO)NH experiments (Kay 1993). Sensitivity-enhanced ^{1}H-^{15}N HSQC spectra (Kay et al. 1992) for A10A2 were acquired using carrier frequencies of 4.705 (^{1}H) and 114.0 ppm (^{15}N) and spectral widths of 8000.0 and 1700.0 Hz, respectively. Similar spectra were generated for Ca^{2+}-BT12 using carrier frequencies of 4.702 (^{1}H) and 120.0 ppm (^{15}N) and spectral widths of 8000.0 and 2000.0 Hz, respectively. All data were processed using NMRPipe and NMRDraw (Delaglio et al. 1995) and spectra were analyzed by NMRView (Johnson and Belvins 1994). The ^{1}H-^{15}N HSQC spectra of the ^{15}N, ^{13}C-labeled A10A2, and BT12 hybrid proteins cleaved with TEV and PreScission proteases were acquired 48 h

following the addition of 16 units of each of the enzymes respectively. The presence of the fully cleaved product in the NMR sample was verified by SDS-PAGE.

2.2.10 NMR Titration Experiments

The ^{15}N, ^{13C}-labeled S100A10 in complex with annexin A2 peptide was prepared by the titration of 0.5 mM (monomer) S100A10 with a 20 mM stock solution of annexin A2 peptide under constant buffer conditions. A final peptide concentration of 0.8 mM was used. The pH of the sample remained at 7.0 throughout the titration. The sample was mixed after each addition and equilibrated for 15 minutes. The total volume increase of the NMR sample was 24 μL (4%). ^{1}H-^{15}N HSQC spectra were recorded at each point to monitor the titration. A sample of 0.7 mM (monomer) apo-S100B was prepared in 12 mM $CaCl_2$ and titrated with a 20 mM stock solution of TRTK12 peptide in the same buffer (above) to a final peptide concentration of 0.9 mM. The pH of the sample remained at 7.0 throughout the titration.

2.3 Results

2.3.1 Cloning of GB1-TRTK12, -annexin A2, and -AHNAK in Expression Vectors

In order to obtain pure bacterially expressed peptides, the peptide sequence was fused to a larger, stable and soluble protein which would not only protect it from proteolysis in the cell but also improve its solubility. Previous attempts to biosynthetically prepare annexin A1 and A2 peptides using GST-tagged constructs lead to <1 mg peptide/L culture and the isolated peptide was prone to proteolysis (Rintala-Dempsey,

unpublished results). The approach opted here involved expression of TRTK12 (TRTKIDWNKILS), annexin A2 (STVHEILSKLSLEG), and AHNAK (GKVTFPKMKIPKFTFSGREL) peptides as GB1 fusion proteins. The B1 immunoglobulin binding domain of streptococcal protein G (GB1) is a smaller, N-terminal protein of about 56 residues (Huth et al. 1997; Safadi and Shaw 2007), which was linked to the peptides through 5 glycine residues and a thrombin cleavage site (LVPR/GS) as outlined in Figure 2.1. To further protect the C-terminus of the peptides from degradation by proteases and to facilitate the isolation of untagged peptides, the peptides were linked to a C-terminal His_6 tag through a TEV cleavage site (ENLYFQ/S).

The insert for each cloning reaction was designed as single-stranded primers (forward and reverse) encoding the entire sequence of each one of the peptides with a minimum of 41 complementary bases (Figure 2.1). Proper annealing of the two primers would generate a double-stranded DNA fragment containing over-hangs compatible with those created by *Bam* HI and *Xho* I endonucleases at the N- and C-terminus, respectively. The double-stranded DNA fragments were readily inserted with the correct orientation into the *Bam* HI and *Xho* I endonucleases cut sites of digested pSAF2 vector (Figure 2.2).

2.3.2 Expression and Purification of GB1-TRTK12, -annexin A2, and -AHNAK

In order to obtain unlabeled, ^{15}N-labeled and ^{15}N, ^{13}C-labeled TRTK12, annexin A2 and AHNAK peptides, bacterial overexpression of GB1 fusion peptides was examined in 1 L of LB. High levels of expression of unlabeled GB1-TRTK12 after induction with 1 mM IPTG are illustrated in Figure 2.3. Similar results were observed

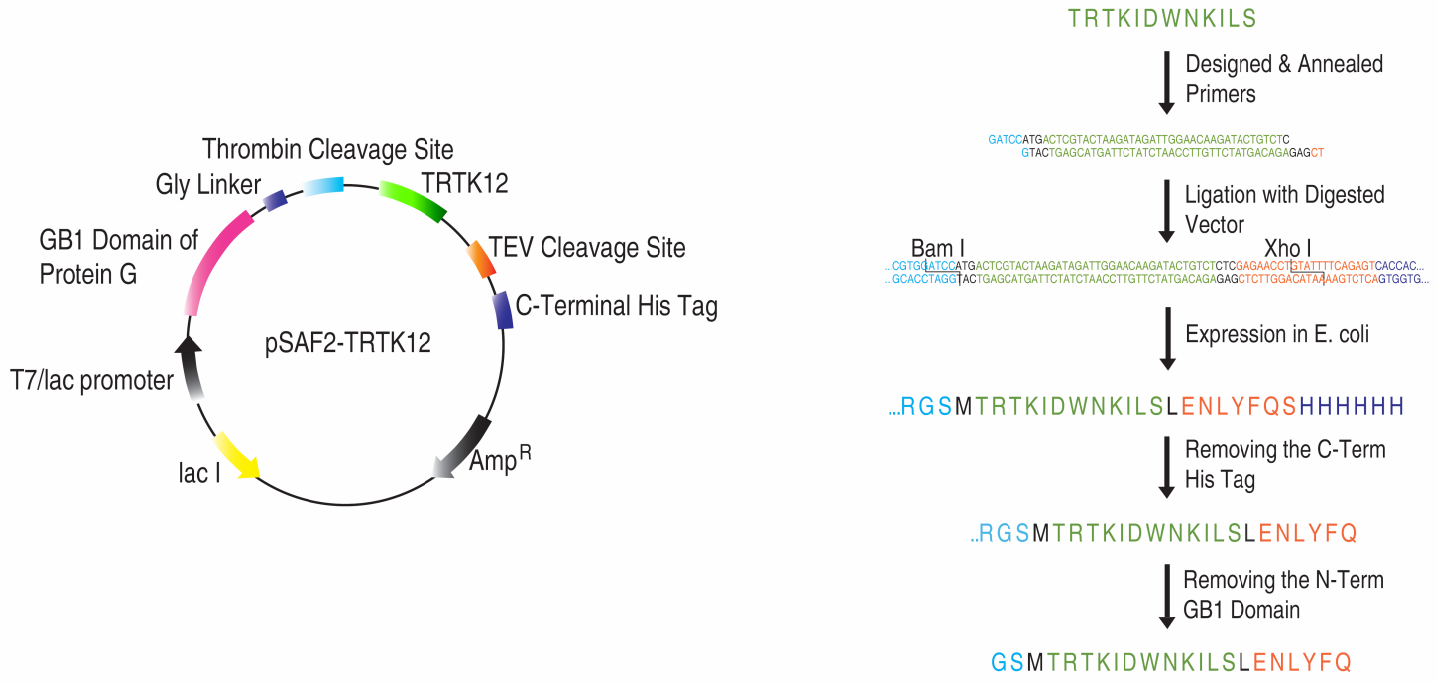

Figure 2.1. Development of cloning and purification procedures for a GB1-TRTK12 fusion protein.

N-terminal GB1 was linked to TRTK12 through 5 glycine residues and a thrombin cleavage site. A C-terminal His-tag was also connected to the peptide by a TEV cleavage site. The forward and reverse single-stranded oligonucleotides were designed encoding the entire amino acid sequence of the TRTK12 peptide with 41 complementary bases. Annealed primers would generate a double-stranded DNA fragment containing *Bam* HI and *Xho* I sticky ends at the N- and C-terminus, respectively. The DNA fragment was then inserted into pSAF2 vector. Expression of pSAF2-TRTK12 in *E. coli* is followed by purification using the Ni-NTA and IgG-Sepharose fast flow columns.

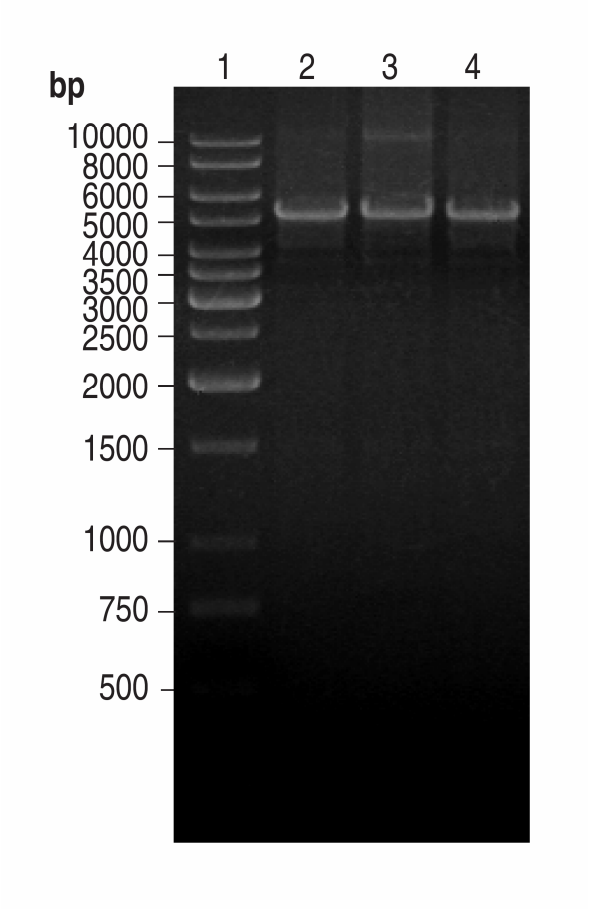

Figure 2.2. Cloning of GB1-TRTK12, -annexin A2 and -AHNAK.

The DNA samples (5 uL) are run on a 1% agarose gel stained with ethidium bromide. The sizes for the molecular standard bands are indicated on the left. Lane 1 contains the molecular weight DNA ladder. Lanes 2, 3 and 4 contain the DNA for GB1-TRTK12, -annexin A2 and -AHNAK, respectively.

for the GB1-annexin A2 and -AHNAK fusion proteins. Following cell lysis, the supernatant was loaded onto a Ni-NTA column. Bound protein was then eluted by increasing the level of imidazole in the elution buffer. After dialysis of GB1-TRTK12, the protein was cleaved from the His_6 tag using TEV protease and purified on an IgG Sepharose fast flow column that binds to the GB1 domain of the protein. Bound protein was eluted at low pH with 0.5 M acetic acid (pH 3.4). A Coomassie-stained SDS-PAGE gel of the fractions is presented in Figure 2.4 showing 3 major bands: the first and second ones are slightly below and above 10 kDa molecular standard marks respectively, and the third one around 15 kDa. To identify the band corresponding to GB1-TRTK12, a sample from one of the fractions was sent for electrospray ionization mass spectrometry. Figure 2.5 shows a mass spectrum of three species in the sample with molecular weights of 15667.11, 7598.55, and 9294.42 Da. The peak at 9294.42 Da was in good agreement with the calculated molecular weight of intact GB1-TRTK12 (MWcal = 9296.2 Da) and appeared as the middle band on the SDS-PAGE gel. This band ran slightly above 10 kDa molecular standard mark, which is a characteristic of GB1 bound proteins (Safadi and Shaw 2007). The peak with molecular weight of 7598.55 Da represents the proteolytic product of GB1-TRTK12 (MWcal = 7600.2 Da), where the entire sequence of TRTK12 peptide as well as two residues from the linker (S and M) are cleaved from the GB1 fusion protein. Finally, the contaminating protein at 15667.11 Da is the light chain of the IgG protein that is bound to the Sepharose beads of the column and breaks down due to the low pH of the elution buffer.

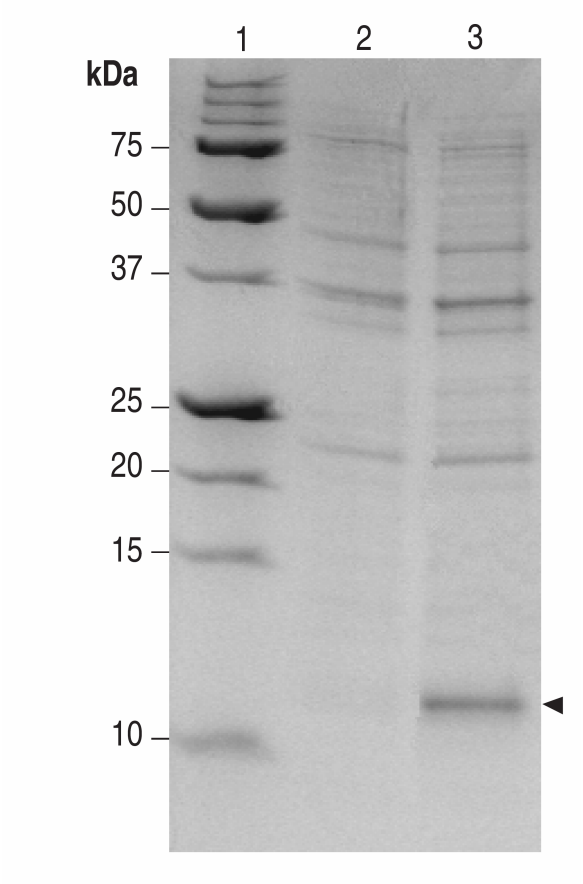

Figure 2.3. SDS-PAGE analysis of the overexpression of unlabeled GB1-TRTK12 fusion protein.

GB1-TRTK12 was expressed as described in Chapter 2 (Section 2.2.3). An aliquot of the cells before and after induction with IPTG were suspended in SDS sample buffer, heated to 90ºC for 5 min and then subjected to electrophoresis on 16.5% SDS-polyacrylamide gels and protein bands were visualized with Coomassie Brilliant Blue stain. Lane 1 contains the molecular weight standards. The positions and sizes of molecular weight standards are indicated on the left. Lane 2 shows total cellular protein prior to induction with IPTG of the 1 L culture batch. Lanes 3 contains total cellular protein 5 hours after induction of 1 L culture at 37 °C. The arrowhead indicates a high level of expression for the GB1-TRTK12 (9.3 kDa) fusion protein.

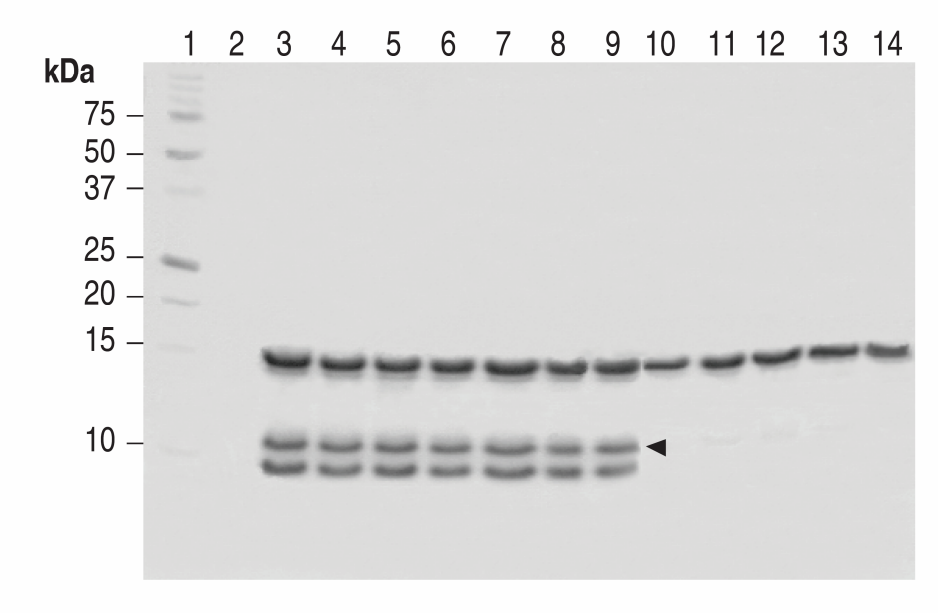

Figure 2.4. Purification of GB1-TRTK12 on IgG Sepharose fast flow column.

The protein was expressed in *E. coli* strain Bl21 (DE3)-RIL and lysed cells were purified as described in Chapter 2 (Section 2.2.3). Following the first purification step on the Ni-NTA column, fractions containing the protein were dialyzed against TEV protease cleavage buffer. GB1-TRTK12 was cleaved from the His_6 tag using TEV protease and applied to IgG Sepharose fast flow column. Bound protein was eluted with 0.5 M acetic acid, pH 3.4. Only lanes of fractions in which GB1-TRTK12 eluted are shown here. Lane 1 contains the molecular weight standards. The positions and sizes of molecular weight standards are indicated to the left of each gel. Lanes 2-13 contain elution profile of every fraction. The arrowhead indicates the band for GB1-TRTK12 (9.3 kDa) fusion protein.

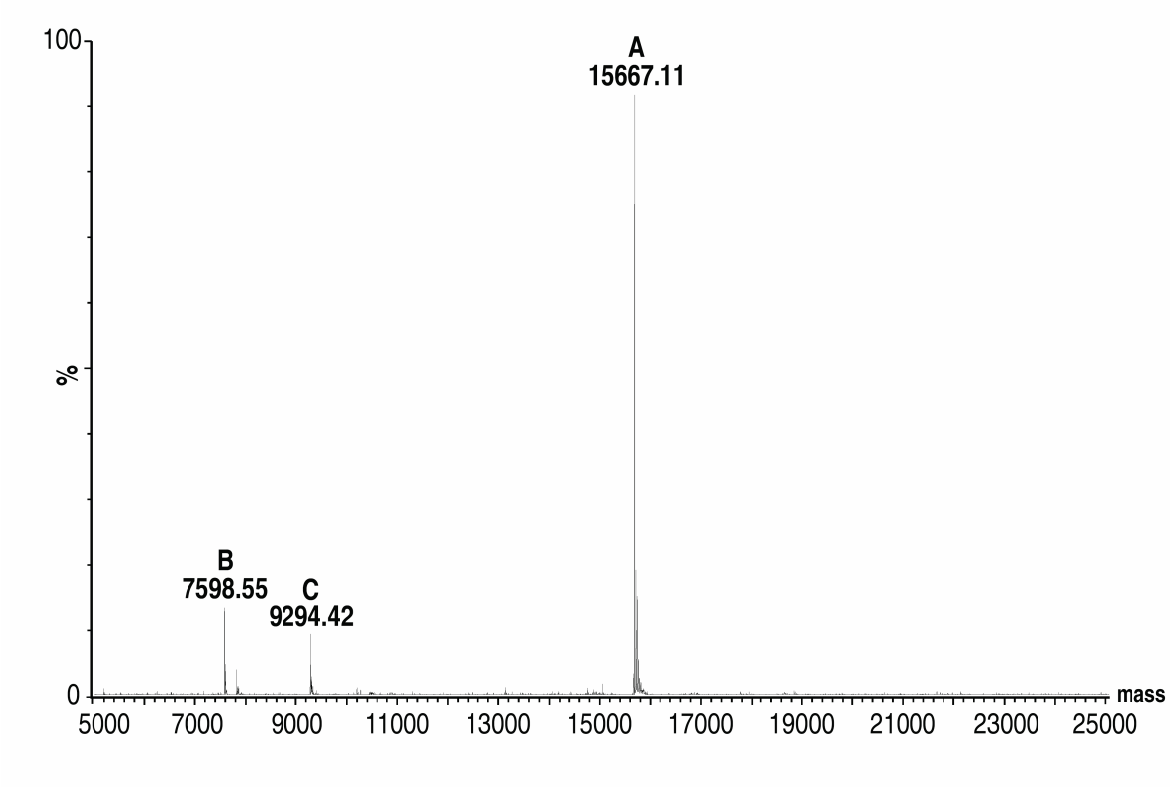

Figure 2.5. Mass spectrum of unlabeled GB1-TRTK12.

Following purification of the protein, excess salt was removed. The sample was then subjected to mass spectrometric analysis. The analysis resulted in three peaks at molecular masses of 7598.55, 9294.42, and 15667.11 Da. The peak at 9294.42 agrees with the calculated mass of GB1-TRTK12.

Changing the order of columns or addition of protease inhibitors did not improve the yield, as the TRTK12 peptide was degraded very quickly in solution. Since similar results were observed for the GB1-annexin A2 and –AHNAK fusion proteins, a different approach was taken to bacterially express the peptides.

2.3.3 Design of Hybrid S100-Target Proteins

In order to generate hybrid S100-target protein complexes, two systems that have been well characterized by structural methods were chosen. The approach taken was to analyze the relative positions of the S100 proteins and their target peptides in the structures and then incorporate a linker between the two components to create a hybrid protein. The first structure employed S100A10 in complex with the N-terminus of annexin A2 (1BT6) (Rety et al. 1999), and a second structure utilized Ca^{2+}-S100B complexed to a portion of the alpha-1 subunit of F-actin capping protein (TRTK12), CapZ (1MWN, 1MQ1) (Inman et al. 2002; McClintock and Shaw 2003). In both these structures (Figure 2.6), the C-termini of helix IV in the S100 protein are proximal to the N-terminus of the binding peptide. Although S100A10 and Ca^{2+}-S100B are structurally similar, the orientations and distances of the annexin A2 and TRTK12 peptides with respect to the S100 protein are quite different. Further, in the A10A2 complex the distance from the C-terminal carboxyl carbon of S100A10 (K91) to the N-terminal nitrogen of annexin A2 is about 16 Å. For the Ca^{2+}-S100B complexed with TRTK12 the distance ranges from about 14 - 26 Å in the families of NMR structures. The choice of these two proteins allowed for testing this approach with one protein (S100B) that

undergoes a calcium-induced conformational change in order to interact with a target, and one protein (S100A10) that is calcium-insensitive. Further, the structures of the target peptides in both structures are quite different. The annexin A2 peptide adopts an α-helical conformation for most of its sequence while the TRTK12 peptide is unstructured at its N-terminus followed by a single turn of α-helix.

The A10A2 is comprised of a linker spanning the measured protein-peptide distance (16 Å) in the S100A10-annexin A2 complex connecting the two proteins. Although this distance is sufficient to accommodate about five amino acid residues linked in a linear fashion, modeling showed that a further four residues were required in A10A2 hybrid protein to allow favorable φ,ψ angles in the linker. Within the nine-residue linker, a TEV protease cleavage site (ENLYFQ/G) was introduced. Finally, an aspartic acid at the N-terminus of the annexin A2 sequence was added to stabilize its α-helical structure (Figure 2.6A) in lieu of the acetyl group found in the native protein (Johnsson et al. 1988). For the BT12 the maximum linker length observed in the NMR structures (~26 Å) allowed approximately 11 residues to bridge the protein and target. Within this region a PreScission protease cut site (LFQ/GP) and four glycine residues were included (Figure 2.6B). The PreScission protease site allowed testing a different protease for the BT12 hybrid compared to the TEV site in the A10A2 hybrid protein. Since the Ca^{2+}-S100B complexes with TRTK12 are ensembles of NMR structures, the N-terminus of TRTK12 exhibits a wide range of positions with respect to Ca^{2+}-S100B. This may be due to the flexibility of this region in TRTK12 not observed for annexin A2 in the S100A10 complex. The glycine residues were added in BT12 to maintain backbone flexibility of

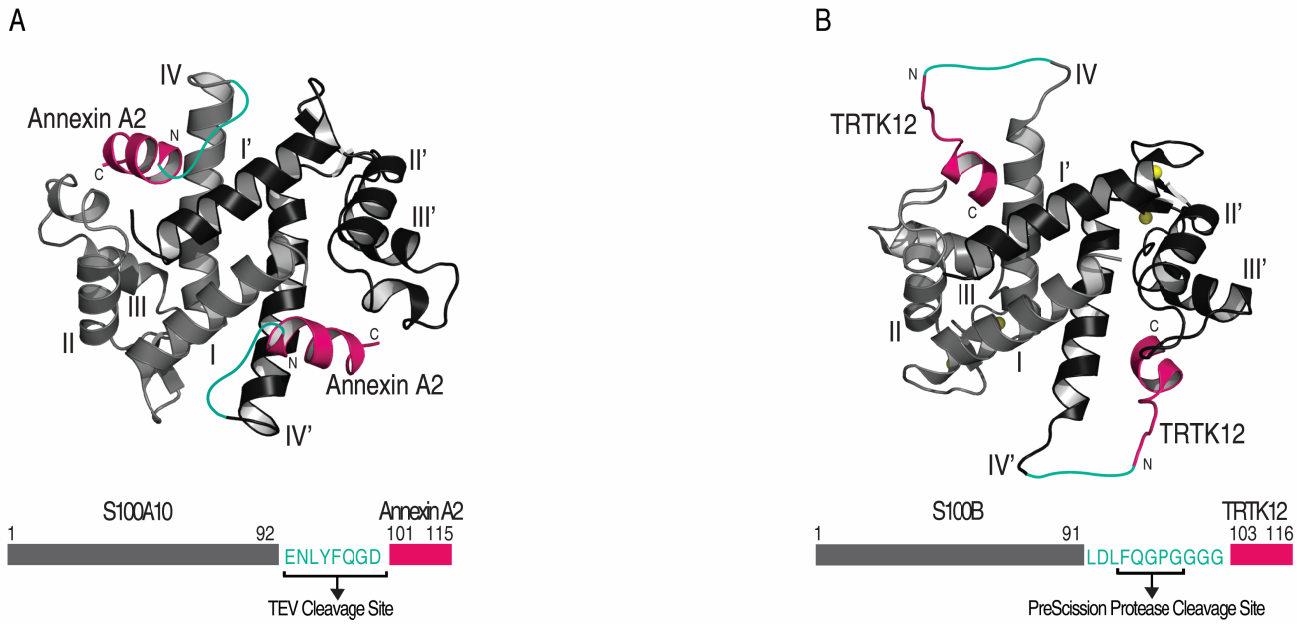

Figure 2.6. Models of the S100A10-annexin A2 (A10A2) and Ca^{2+}-S100B-TRTK12 (BT12) hybrid constructs.

Ribbon representations of S100A10 in complex with **(A)** annexin A2 (1BT6) (Rety et al. 1999) and **(B)** Ca^{2+}-S100B bound to TRTK12 (1MWN) (Inman et al. 2002) are shown in similar orientations to demonstrate how the annexin A2 and TRTK12 peptides (magenta) are joined to the S100 proteins through a linker (cyan). In each model one of the protomers is presented in light gray (helices labeled as I-IV) and the other protomer shaded in black (helices labeled as I'-IV'). Four bound calcium ions are shown as yellow spheres for Ca^{2+}-S100B. The corresponding schematics of the constructs used for A10A2 and BT12 hybrid proteins are also illustrated with S100 protein located at the N-terminus (grey), annexin A2 and TRTK12 peptides positioned at the C-terminus (magenta), and the linker (cyan) connecting the S100 proteins to the target peptides. The amino acid composition of the linker region and the corresponding protease cleavage sites are indicated. All numbering is consecutive based on the S100 protein sequences.

the linker. During the design process, the linkers for both proteins were incorporated into the existing structures by modeling. Energy minimization was used to ensure that the hybrid proteins were not constrained or distorted, or that the linker did not make any significant contacts with the S100 protein that might mask the protease cleavage sites.

2.3.4 Cloning, Expression and Purification of Hybrid S100-Target Proteins

Figure 2.7 shows the DNA product of the last cloning step for A10A2 and BT12. The DNA band for A10A2 appears higher than the 5000 bp molecular standard mark which is close to the correct molecular weight of 5334 bp. However, the BT12 DNA band ran lower (around 4500 bp) than the expected molecular weight of 6357 bp. This is most likely caused by the supercoiling of the BT12 DNA causing the DNA to run farther in the gel. Both the A10A2 and BT12 hybrid proteins were expressed using a BL21 (DE3) codon-plus *E. coli* strain. Following purification, the typical yield was 15-25 mg of ^{15}N, ^{13}C-labeled A10A2 or BT12 protein from 1L M9 minimal media cultures for heteronuclear NMR spectroscopy experiments. Based on the molecular weights of the peptides, proceeding with the cleavage of the hybrid proteins would approximately yield 2-4 mg of the isolated peptides. SDS-PAGE (Figure 2.8) and MALDI-TOF mass spectroscopy analyses showed that the proteins were homogeneous and free of degradation products, similar to the parent S100B and S100A10 proteins. In both A10A2 and BT12, the accessibility of the protease cleavage sites was tested by proteolysis using TEV and PreScission proteases, respectively. In both cases cleavage proceeded to completion allowing separation of the S100 protein and peptide partner (Figure 2.8).

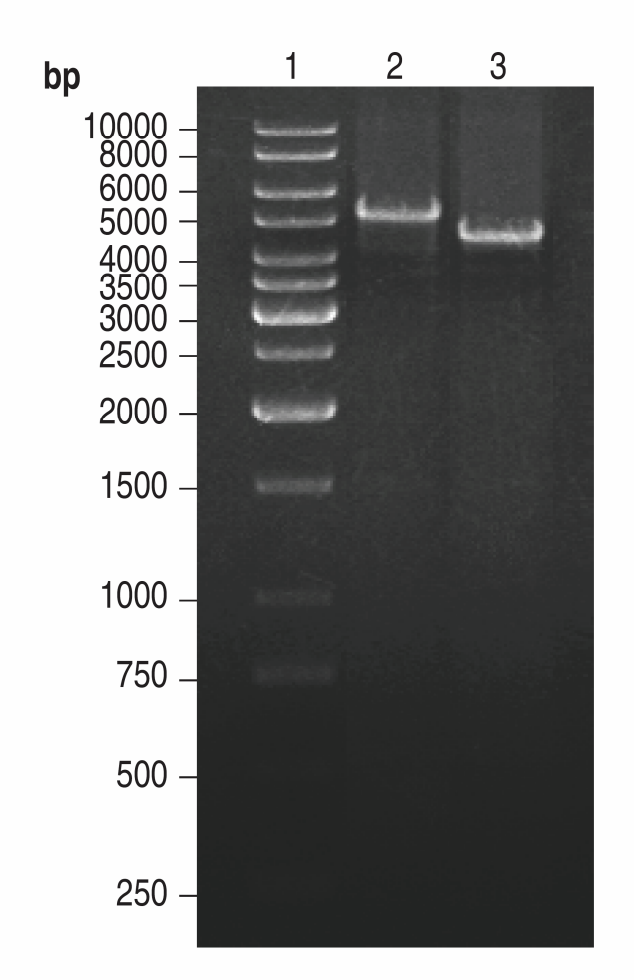

Figure 2.7. Cloning of A10A2 and BT12.

The DNA samples (5 uL) are run on a 1% agarose gel stained with ethidium bromide. The sizes for the molecular standard bands are indicated on the left. Lane 1 contains the molecular weight DNA ladder. Lanes 2 and 3 contain the DNA for A10A2 and BT12, respectively.

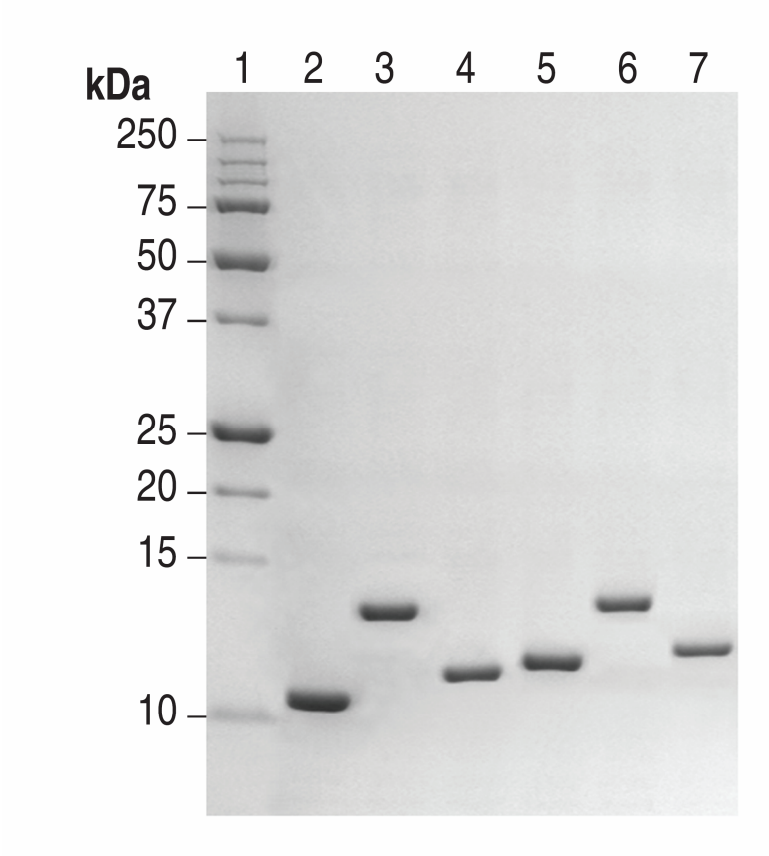

Figure 2.8. Coomassie-stained SDS-PAGE gel (16.5%) depicting the purification of A10A2 and BT12 constructs.

Lane 1 contains the protein molecular weight markers, with molecular weights labeled on the left of the gel. Lanes 2 and 5 contain S100B and S100A10, while BT12 and A10A2 hybrid constructs are presented in lanes 3 and 6, respectively. Lanes 4 and 7 show S100B and S100A10 following cleavage of BT12 and A10A2 by PreScission and TEV proteases, respectively. Each of these proteins run at a higher molecular weight than the parent due to the presence of the linker that remains appended to the C-terminus of the S100 protein. The TRTK12 and annexin A2 peptides are not observed.

2.3.5 The S100A10-Annexin A2 Hybrid Protein Adopts an Active Configuration

The A10A2 hybrid protein was examined by NMR spectroscopy to determine if the complex retained the similar structure observed in the crystal structure for S100A10 in combination with the N-terminal annexin A2 peptide. Using standard heteronuclear multiple dimensional NMR spectroscopy (HNCA, HNCACB, and CBCA(CO)NH), chemical shift assignments (^{1}H, ^{15}N, and ^{13}C) for A10A2 (Figures 2.9 and 2.10) (Table 2.4) and BT12 (Figures 2.11 and 2.12) (Table 2.5) proteins were completed. Figure 2.10 shows a representative ^{1}H-^{15}N HSQC spectrum of A10A2 that is well dispersed and characteristic of a folded S100 protein. The spectrum of A10A2 is remarkably similar to that of ^{15}N, ^{13}C-labeled S100A10 in complex with the unlabeled annexin A2 peptide (Figure 2.13). The ^{1}H-^{15}N correlations for all residues in the annexin A2 segment (S101-D115) and the TEV cleavage site (E93-G99) were easily identified in A10A2 (Figure 2.10). These residues are not visible in Figure 2.13 where the annexin A2 peptide is unlabeled. The resonances for residues S101-D115 are well separated ranging between 7.1 (S108) and 8.9 ppm (T102) indicating the annexin A2 portion of the hybrid is well folded. In contrast, the linker residues form a tight cluster between 7.9-8.3 ppm indicating this region of the A10A2 hybrid adopts little regular secondary structure. Backbone assignment of A10A2, and S100A10 in complex with individual annexin A2 peptide allowed the chemical shifts of each residue to be compared between the two complexes (Figure 2.14) as well as that for other Ca^{2+}-bound S100 proteins, indicating that little structural change has occurred in the S100A10 protein by incorporating the C- terminal linker and annexin A2 sequences. For BT12 a specific interaction between the S100B and

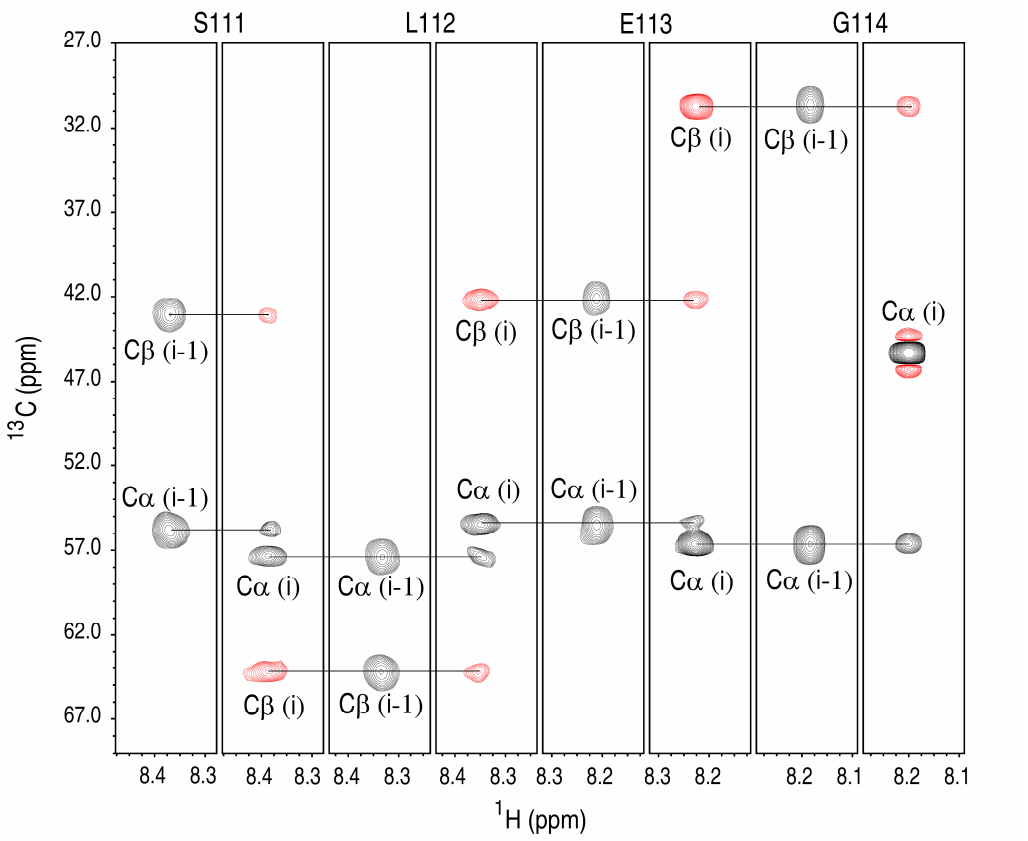

Figure 2.9. Selected regions of 600 MHz NMR spectra used for the backbone assignment of the A10A2 complex.

For each pair of planes, the CBCA(CO)NH is shown on the left and the HNCACB on the right where the x-axis is the amide proton chemical shift and the y-axis is the ^{13}C plane of the three-dimensional experiments. The Cα and Cβ for the intraresidues (indicated as i) are shown on the HNCACB spectra and the corresponding Cα and Cβ for the previous residues (i-1) are shown in the CBCA(CO)NH. The spectra illustrate ^{15}N planes for sequential assignment of residues S111-G114 of A10A2.

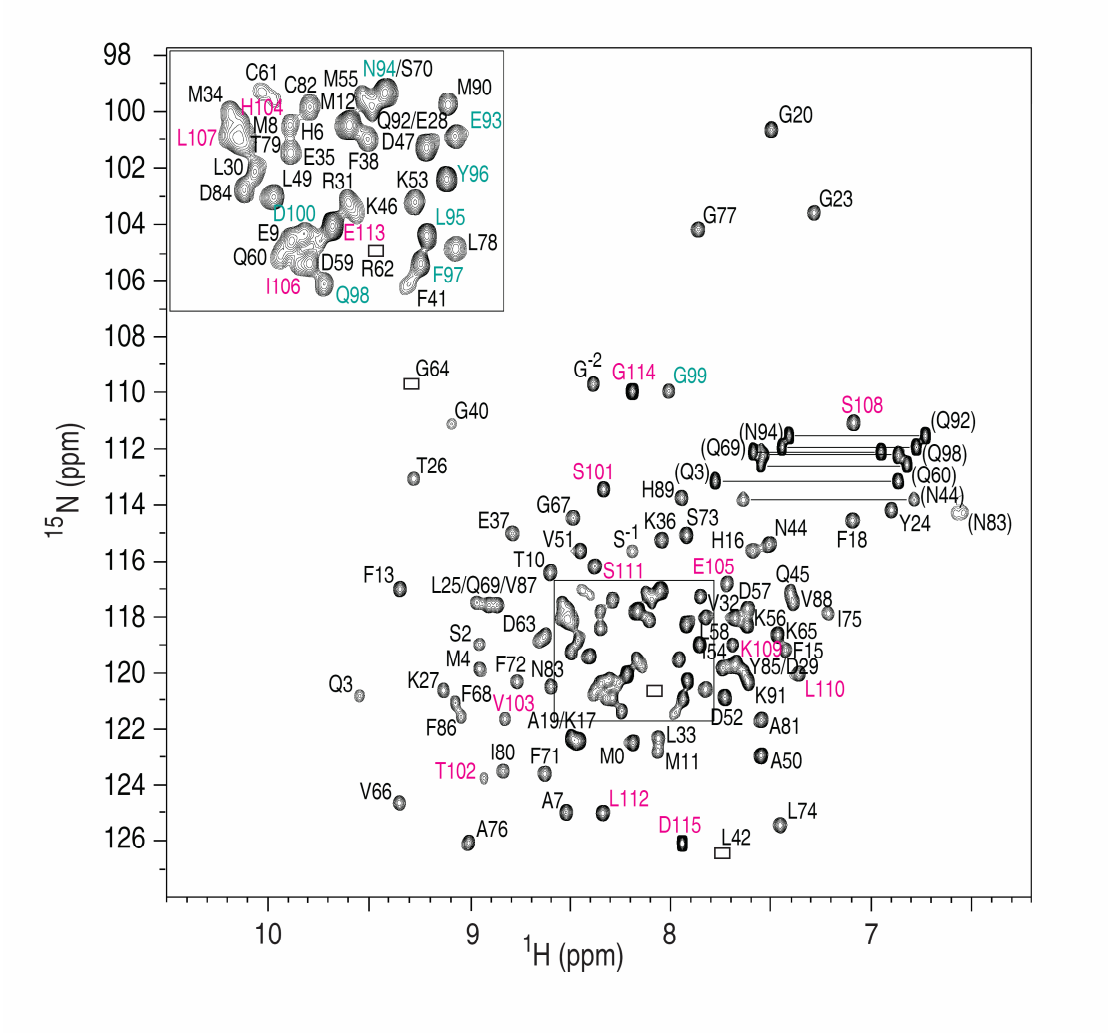

Figure 2.10. Backbone amide assignments of A10A2 hybrid protein.

^{1}H-^{15}N HSQC spectrum of 0.5 mM (monomer) uniformly ^{15}N, ^{13}C-labeled A10A2 hybrid protein acquired on a Varian INOVA 600 MHz spectrometer. The spectrum was collected in 20 mM MOPS, 1 mM EDTA, 1 mM DTT, 50 mM arginine, 50 mM glutamic acid, 100 mM NaCl, pH 7.0 at 35 ºC. Assigned backbone amide cross peaks are indicated with their one letter amino acid code and number. The residues from ^{15}N, ^{13}C-labeled annexin A2 are presented in pink and those from the linker region in cyan. Pairs of resonances for sidechain amide cross peaks are connected by horizontal lines. Peaks visible at lower contour levels are indicated by boxes.

Table 2.4. ^{15}N, ^{13}C and ^{1}H resonance assignments for human A10A2.

Residue	H^N	N	C'	C^α	C^β	Other
G^{-5}						
P^{-4}			176.09	63.30	32.14	Cγ (27.00), Cδ (49.63)
L^{-3}	8.492	122.3	178.10	55.49	42.33	Cγ (27.31), Cδ1 (24.82) Cδ2 (23.67)
G^{-2}	8.391	109.6		45.43		
S^{-1}	8.198	115.7		58.07	64.25	
M0	8.190	122.3		53.23	32.83	
P1			176.95	62.46	31.92	Cγ (27.66), Cδ (50.37)
S2	8.953	118.8	175.25	56.87	65.50	
Q3	9.552	120.6	180.37	59.63	28.19	Cγ (34.83), Cδ (180.53) Nε2 (112.78)
M4	8.960	119.7		56.81	30.84	
E5			179.49	60.18	29.43	Cγ (37.52)
H6	8.385	117.9	178.02	59.47	29.80	
A7	8.531	124.9	176.62	55.84	18.56	
M8	8.523	118.0	177.91	60.31	35.24	Cγ (30.62)
E9	8.315	120.2	177.83	60.53	29.92	Cγ (37.43)
T10	8.599	116.6	178.12	67.36	68.02	Cγ2 (21.43)
M11	8.069	122.7	177.21	61.30	32.59	
M12	8.178	117.9	177.83	59.99	35.10	Cγ (31.74)
F13	9.353	117.0		60.09	37.64	
T14			175.24	68.35		Cγ2 (21.17)
F15	7.440	119.2	176.02	62.81	38.79	
H16	7.592	115.7	178.06	61.16	31.47	
K17	8.467	122.3	177.87	59.40	32.04	Cγ (24.23), Cδ (29.33) Cε (42.01)
F18	7.111	114.5	178.06	60.78	40.39	
A19	8.482	122.3	179.07	53.87	18.72	
G20	7.505	100.9	174.06	44.96		
D21	7.948	111.8		56.04	42.48	
K22			178.38	57.80	31.04	Cγ (23.30)
G23	7.298	103.5	172.65	46.71		
Y24	6.912	114.1	171.76	55.49	40.13	
L25	8.967	117.5	178.21	52.86	43.36	Cγ (27.15), Cδ1 (23.65) Cδ2 (20.36)
T26	9.286	113.1	175.58	60.53	71.82	
K27	9.136	120.6	178.24	60.77	32.04	Cγ (24.96), Cδ (29.23) Cε (41.94)
E28	8.107	117.5	178.78	59.65	29.01	Cγ (36.65)
D29	7.635	120.1	177.83	57.02	42.75	
L30	8.465	118.8	177.76	57.77	41.71	Cγ (26.56), Cδ1 (23.99), Cδ2 (23.47)
R31	8.174	119.3	177.80	60.60	29.79	Cγ (27.15), Cδ (43.08)
V32	7.680	117.9	177.30	66.35	31.66	Cγ2 (22.33), Cγ1 (22.33)
L33	8.070	122.3	179.33	59.41	42.03	Cγ (28.07), Cδ1 (24.02) Cδ2 (24.02)
M34	8.554	117.5	178.02	59.17	31.83	Cγ (33.11)
E35	8.337	118.4	178.93	59.32	30.29	Cγ (36.97)
K36	8.057	115.3	178.72	57.82	33.37	Cγ (25.42), Cδ (28.59)

						Cε (42.66)
E37	8.804	114.9	176.65	56.45	29.93	Cγ (36.34)
F38	8.110	118.0		54.54	39.44	
P39			179.41			
G40	9.112	111.3		46.41		
F41	7.953	121.1	174.61	57.61	39.20	
L42	7.746	126.2		57.60	40.94	
E43			177.53	59.46	29.03	Cγ (36.70)
N44	7.523	115.3	175.40	53.71	39.19	Cγ (177.14), Nδ2 (113.30)
Q45	7.411	117.1	177.77	55.26	27.99	
K46	8.147	119.7	176.22	57.26	31.68	Cγ (24.76), Cδ (28.81)
						Cε (42.27)
D47	7.939	118.4		50.94	42.48	
P48			177.57	64.20	32.21	Cγ (27.09), Cδ (51.07)
L49	8.403	119.3	177.24	54.11	41.02	Cγ (27.37), Cδ1 (25.34)
						Cδ2 (22.79)
A50	7.562	122.8	179.69	56.12	18.65	
V51	8.442	115.7	176.57	66.28	31.21	Cγ2 (21.27), Cγ1 (23.56)
D52	7.744	120.6	178.96	57.57	40.45	
K53	7.964	119.3	178.92	59.73	32.38	Cγ (25.92), Cδ (29.35)
						Cε (42.14)
I54	7.746	119.7	177.94	64.50	38.26	Cγ1 (28.58), Cδ1 (13.18)
						Cγ2 (17.92)
M55	8.118	117.1	177.62	57.57	32.16	
K56	7.622	118.3	178.06	59.12	32.12	Cγ (24.64), Cδ (28.86)
						Cε (42.16)
D57	7.638	117.6	177.32	55.72	41.09	
L58	7.694	118.9	177.67	55.65	42.57	Cγ (26.09), Cδ1 (22.94)
						Cδ2 (22.94)
D59	8.293	120.9	177.24	54.26	40.41	Cγ (180.23)
Q60	8.382	120.6	176.75	57.80	28.56	Cγ (34.11), Cδ (180.24)
						Nε2 (111.97)
C61	8.435	117.1	176.54	58.96	27.21	
R62	8.079	120.6	175.82	57.15	28.47	Cγ (27.15), Cδ (43.43)
D63	8.655	118.8	176.73	53.76	41.08	
G64	9.255	109.6	173.84	46.11		
K65	7.471	118.4	175.30	55.39	34.36	Cγ (24.55), Cδ (29.12)
						Cε (42.25)
V66	9.356	124.5	176.25	62.62	32.58	Cγ2 (21.52), Cγ1 (21.52)
G67	8.485	114.4	174.08	44.29		
F68	9.076	121.0	177.10	62.93	39.42	
Q69	8.912	117.5	178.66	60.44	27.48	Cγ (34.20), Cδ (179.82)
						Nε2 (111.52)
S70	8.060	117.1	176.38	61.90	63.06	
F71	8.632	123.6	175.98	60.88	39.21	
F72	8.772	120.1	177.62	62.55	38.40	
S73	7.925	114.9	177.05	62.47	62.50	
L74	7.460	125.4	177.82	57.90	41.06	Cγ (25.76), Cδ1 (23.59)
						Cδ2 (23.59)
I75	7.222	117.9	179.51	62.71	35.56	Cγ1 (26.81), Cγ2 (17.52)
A76	9.005	125.8	178.58	55.28	18.68	
G77	7.871	104.4	177.60	47.36		
L78	7.833	120.6	178.65	57.58	42.61	Cγ (24.40), Cδ1 (22.17)

T79	8.499	118.3	176.85	68.55	68.79	
I80	8.837	123.6	177.78	66.10	38.29	Cγ1 (30.94), Cγ2 (17.29)
A81	7.555	121.5	181.47	55.41	18.14	
C82	8.296	117.5	176.43	63.74	26.78	
N83	8.595	120.5	176.29	58.05	39.63	
D84	8.497	119.2	174.47	57.80	40.48	
Y85	7.678	119.7	178.05	62.00	39.11	
F86	9.051	121.4	177.39	61.18	40.22	
V87	8.865	117.5	177.57	66.50	31.91	Cγ2 (22.11), Cγ1 (22.11)
V88	7.400	117.5	177.43	65.40	32.66	Cγ2 (20.39), Cγ1 (22.57)
H89	7.954	113.8	176.20	57.77	30.81	
M90	7.856	117.1	176.14	57.44	34.90	Cγ (32.54)
K91	7.620	120.1	177.21	58.58	32.48	Cγ (24.76), Cδ (28.82)
Q92	8.166	117.6	176.25	56.99	28.93	Cγ (34.04), Cδ (180.18) Nε2 (111.06)
E93	7.838	117.9	175.97	56.75	30.05	Cγ (36.29)
N94	8.062	117.1	174.58	53.84 (4.518)	38.38	Cγ (177.51), Nδ2 (111.87)
L95	7.922	120.1	176.30	55.28 (4.248)	42.59	Cγ (27.04), Cδ1 (24.96) Cδ2 (23.64)
Y96	7.862	118.8	175.23	57.48 (4.508)	38.93	
F97	7.946	120.9	175.24	57.71 (4.239)	39.17	
Q98	8.245	121.4	176.04	55.96 (4.293)	29.60	Cγ (33.85), Cδ (180.35) Nε2 (111.49)
G99	8.013	110.0	173.81	45.57		Hα2 (3.941), Hα3 (3.900)
D100	8.361	120.1	176.34	54.88 (4.750)	41.59	
S101	8.343	113.5		58.15 (4.796)	63.82	
T102	8.921	123.6	176.29	66.64	69.36	Cγ2 (22.14)
V103	8.823	121.5	179.81	67.84 (3.578)	31.76	Cγ1 (21.61)
H104	8.533	117.9	176.72	60.35 (3.957)	28.86	
E105	7.710	116.6	179.37	59.05 (3.953)	29.33	Cγ (36.04)
I106	8.328	121.0	178.14	66.05 (4.151)	38.95	Cγ1 (29.13), Cγ2 (18.33)
L107	8.623	118.4	178.42	58.27 (4.644)	41.59	Cγ (27.46), Cδ1 (23.97) Cδ2 (23.97)
S108	7.101	111.0	178.28	60.65 (4.164)	63.57	
K109	7.688	119.7	177.32	55.84 (4.304)	33.28	Cγ (24.33), Cδ (28.60) Cε (42.62)
L110	7.373	120.1	177.08	55.84 (4.086)	43.06	Cγ (25.91), Cδ1 (23.39) Cδ2 (23.40)
S111	8.377	116.2	174.75	57.38 (4.608)	64.27	
L112	8.347	124.9	177.21	55.45 (4.331)	42.15	Cγ (27.34), Cδ1 (25.26) Cδ2 (23.10)
E113	8.222	120.1	176.63	56.63 (4.317)	30.69	Cγ (36.34)
G114	8.195	110.1	172.88	45.31		Hα2 (3.970), Hα3 (3.900)
D115	7.947	125.8		55.86 (4.424)	42.49	

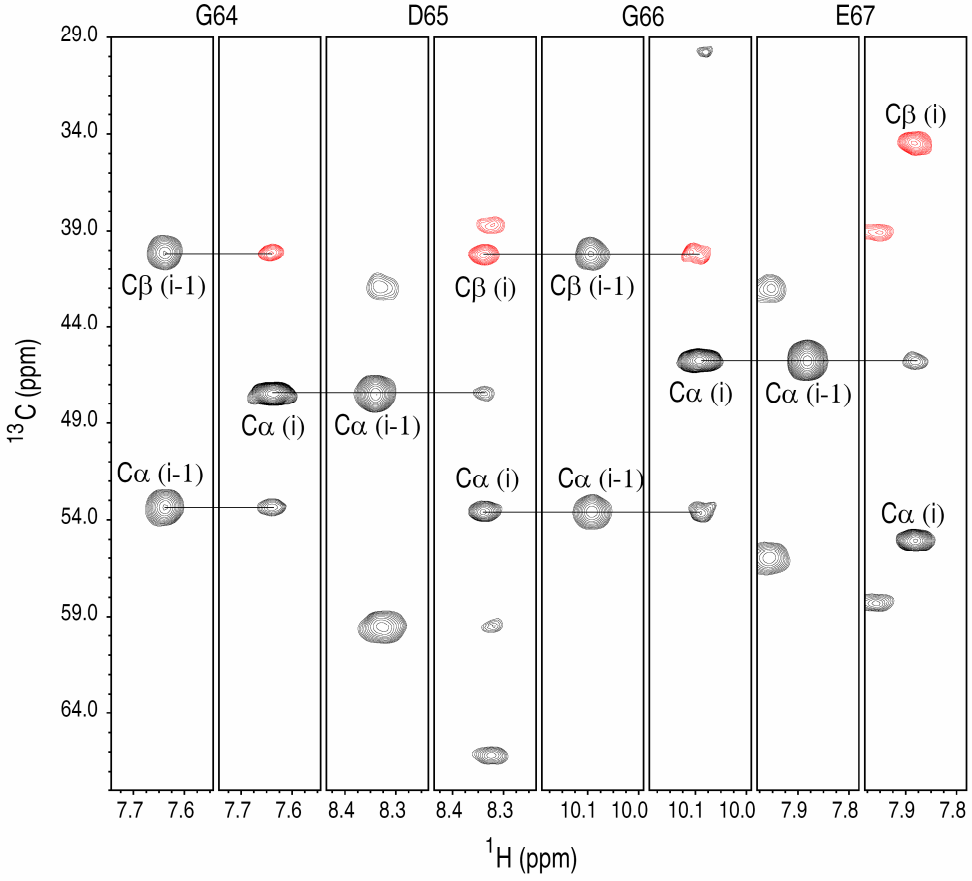

Figure 2.11. Selected regions of 600 MHz NMR spectra used for the backbone assignment of the BT12 complex.

For each pair of planes, the CBCA(CO)NH is shown on the left and the HNCACB on the right where the x-axis is the amide proton chemical shift and the y-axis is the ^{13}C plane of the three-dimensional experiments. The Cα and Cβ for the intraresidues (indicated as i) are shown on the HNCACB spectra and the corresponding Cα and Cβ for the previous residues (i-1) are shown in the CBCA(CO)NH. The spectra illustrate ^{15}N planes for sequential assignment of residues G64-E67 of the BT12.

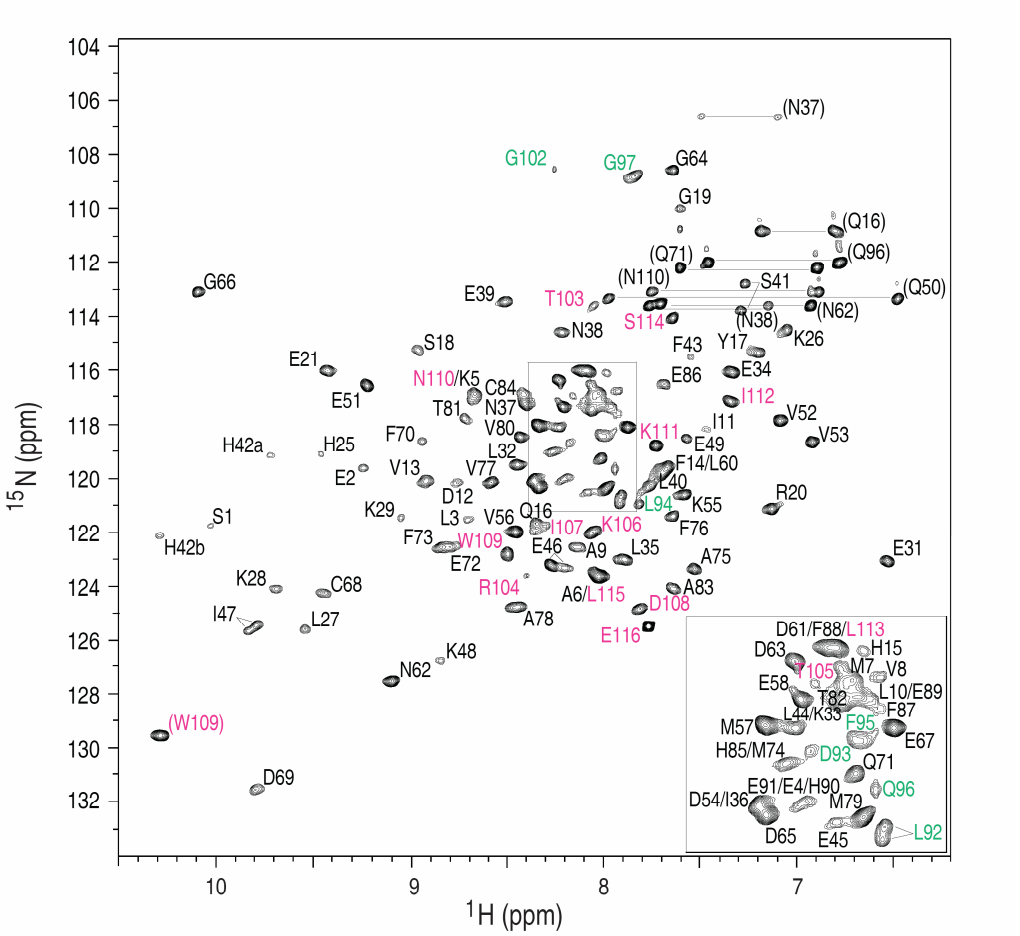

Figure 2.12. Backbone amide assignments of BT12 hybrid protein.

^{1}H-^{15}N HSQC spectrum of 0.7 mM (monomer) uniformly ^{15}N, ^{13}C-labeled BT12 hybrid protein acquired on a Varian INOVA 600 MHz spectrometer. The spectrum was collected in 20 mM MOPS, 20 mM $CaCl_2$, 1 mM DTT, 50 mM arginine, 50 mM glutamic acid, 100 mM NaCl, pH 7.0 at 35 ºC. Assigned backbone amide cross peaks are indicated with their one letter amino acid code and number. The residues from ^{15}N, ^{13}C-labeled TRTK12 are presented in pink and those from the linker region in cyan. Pairs of resonances for sidechain amide cross peaks are connected by horizontal lines.

Table 2.5. ^{15}N, ^{13}C and ^{1}H resonance assignments for human BT12.

Residue	H^N	N	C	C^α	C^β	Other
S1		121.9	174.72	57.50	65.56	
E2	9.243	119.6	179.68	59.80	29.22	
L3	8.699	121.5	177.70	58.20	42.52	
E4	8.228	120.0	178.70	59.68	29.37	
K5	8.687	117.0	179.80	60.17	32.74	
A6	8.047	123.4	178.83	55.14	18.05	
M7	8.061	116.6	178.22	60.81	33.34	
V8	8.026	116.9	177.73	67.00	31.60	
A9	8.148	122.6	179.06	55.48	18.52	
L10	8.064	117.3	178.56	58.68	42.05	
I11	7.473	118.1	178.00	66.05	38.86	
D12	8.751	120.0	179.74	57.77	41.34	
V13	8.914	120.0	177.05	66.15	31.18	
F14	7.685	119.6	177.46	62.82	38.98	
H15	7.993	116.2	178.07	58.57	29.00	
Q16	8.349	121.6	177.72	58.58	28.29	Cγ (33.57), Nε2 (110.5), Hε21 (6.81), Hε22 (7.19)
Y17	7.210	115.4	176.26	60.93	40.59	
S18	8.943	115.4	177.44	61.05		
G19	7.605	110.1	173.69	45.51		
R20	7.134	121.1	177.38	59.90	30.94	
E21	9.428	116.2		54.78	35.06	
G22						
D23						
K24			176.59	58.08	31.40	
H25	9.483	118.9	173.35	55.48	31.11	
K26	7.057	114.6	174.95	55.29	39.18	
L27	9.536	125.7	175.95	52.74	43.65	
K28	9.690	124.2	177.71	55.07	33.08	
K29	9.046	121.5	177.70	62.55	32.00	
S30	8.113	110.5	177.29	61.11	61.11	
E31	6.542	123.1	177.72	58.68	31.44	
L32	8.444	119.6		57.67	42.13	
K33	8.318	118.1	177.05	60.40	32.63	
E34	7.345	116.2	177.99	59.35	29.36	
L35	7.894	123.0	179.06	59.51	41.93	
I36	8.325	120.4	178.37	66.21	38.82	
N37	8.407	117.3	177.53	54.71	37.26	Nδ2 (106.6), Hδ21 (7.108) Hδ22 (7.501)
N38	8.219	114.7	177.13	55.03	40.53	
E39	8.511	113.5	178.13	55.34	30.90	
L40	7.717	120.0	177.31	54.41	42.04	
S41	7.272	112.8	175.80	60.01	64.27	
H42	10.254	121.9	176.15	59.28	28.69	
F43	7.543	115.5	174.68	56.85	41.09	
L44	8.237	118.1	176.36	53.13	44.33	
E45	8.130	120.7	175.61	56.67	30.78	
E46	8.270	123.4	177.32	56.67	30.86	

I47	9.832	125.7	176.23	62.20	38.31	
K48	8.861	126.8	176.07	56.39	34.60	
E49	7.580	118.5		55.35	31.51	Cδ (180.42)
Q50			177.07	58.25	28.15	Cγ (32.85), Nε2 (112.9) Hε21 (6.497), Hε22 (7.974)
E51	9.219	116.6	178.65	59.66	29.23	
V52	7.094	117.8	177.26	66.35	31.28	
V53	6.929	118.5	177.28	66.24	31.20	
D54	8.360	120.0	178.64	57.94	39.80	
K55	7.580	120.7	179.69	58.63	32.23	
V56	8.452	121.9	177.55	67.19	31.49	
M57	8.345	118.1	177.28	57.82	30.74	
E58	8.216	117.3	178.81	59.16	29.72	
T59	7.641	114.0	175.15	66.06	69.16	
L60	7.673	119.6	178.04	55.63	43.21	
D61	8.120	116.1	176.29	54.56	39.92	Cγ (176.05)
N62	9.087	127.6	176.28	54.49	40.20	Nδ2 (113.2), Hδ21 (6.934) Hδ22 (7.767)
D63	8.234	116.3	178.00	53.35	40.14	
G64	7.639	108.6	175.18	47.47		
D65	8.338	120.4	177.37	53.61	40.17	
G66	10.094	113.1	172.68	45.78		
E67	7.880	118.1	175.05	55.07	34.45	
C68	9.452	124.2	174.77	56.97	27.93	
D69	9.790	131.4	175.52	53.04	40.28	
F70	8.939	118.5	176.63	63.35	38.66	
Q71	8.016	119.2	179.79	59.61	28.30	Cγ (34.27), Nε2 (111.7), Hε21 (6.909), Hε22 (7.613)
E72	8.795	122.6	179.47	58.71	30.09	
F73	8.843	122.6	177.27	60.34	39.40	
M74	8.269	118.9	179.24	55.13	29.30	
A75	7.535	123.4	180.63	55.13	17.53	
F76	7.640	121.5	176.68	60.07	38.08	
V77	8.578	120.0	179.69	66.92	31.08	
A78	8.466	124.9	179.25	56.35	17.74	
M79	7.989	120.4	178.77	59.50	33.84	
V80	8.430	118.5	177.71	66.58	32.02	
T81	8.717	117.7	177.28	68.24	68.30	
T82	8.125	117.3	176.39	68.04	67.92	
A83	7.637	124.2	179.93	55.35	18.09	
C84	8.410	117.0	175.75	63.48	26.29	
H85	8.247	118.9	176.21	59.87	29.85	
E86	7.690	116.6	177.96	58.56	29.87	
F87	7.979	117.4	176.39	58.95	39.84	
F88	8.125	116.2	177.01	57.36	38.92	
E89	8.072	117.0	175.53	57.14	33.37	
H90	8.147	120.0	175.53	56.84	30.18	
E91	8.188	120.0	176.49	57.03	29.88	
L92	7.915	120.7	177.38	56.24 (4.139)	42.19	
D93	8.173	118.8	176.75	54.86 (4.507)	40.90	
L94	7.815	120.8	177.39	55.88 (4.073)	42.15	
F95	8.013	118.4	175.76	58.30 (4.493)	39.14	
Q96	7.946	119.6	175.86	55.79 (4.355)	29.75	Cγ (33.90), Nε2 (111.7)

						Hε21 (6.792), Hε22 (7.466)
G97	7.830	108.7		44.71		Hα2 (4.044), Hα1 (4.000)
P98			177.80	63.71	31.95	
G99	8.530	109.3		45.54		
G100			174.73	45.46		
G101						
G102	8.236	108.6	174.22	45.29		
T103	8.084	113.9	174.55	61.91	69.88	
R104	8.393	123.5	176.09	56.15 (4.486)	31.03	
T105	8.173	117.0	173.30	62.03 (4.304)	69.95	
K106	8.049	121.9	176.05	55.46 (4.415)	34.46	
I107	8.335	121.9	174.34	61.75 (3.956)	38.18	
D108	7.821	124.9	176.98	52.89 (4.502)	42.87	
W109	8.489	122.7	178.36	61.19	29.35	Cγ (176.27), Nε1 (129.5) Hε1 (10.283)
N110	8.664	116.9	177.55	56.09 (4.558)	37.73	Nδ2 (112.9), Hδ21 (6.901) Hδ22 (7.752)
K111	7.736	118.8	178.26	57.79 (4.163)	32.05	
I112	7.355	117.0	176.39	62.87 (3.808)	38.13	
L113	8.086	115.8	176.59	55.14 (4.436)	42.05	
S114	7.710	113.5	174.61	58.50 (4.445)	63.06	
L115	8.031	123.8	176.43	55.21 (4.370)	42.27	
E116	7.773	125.4		58.06 (4.110)	31.28	

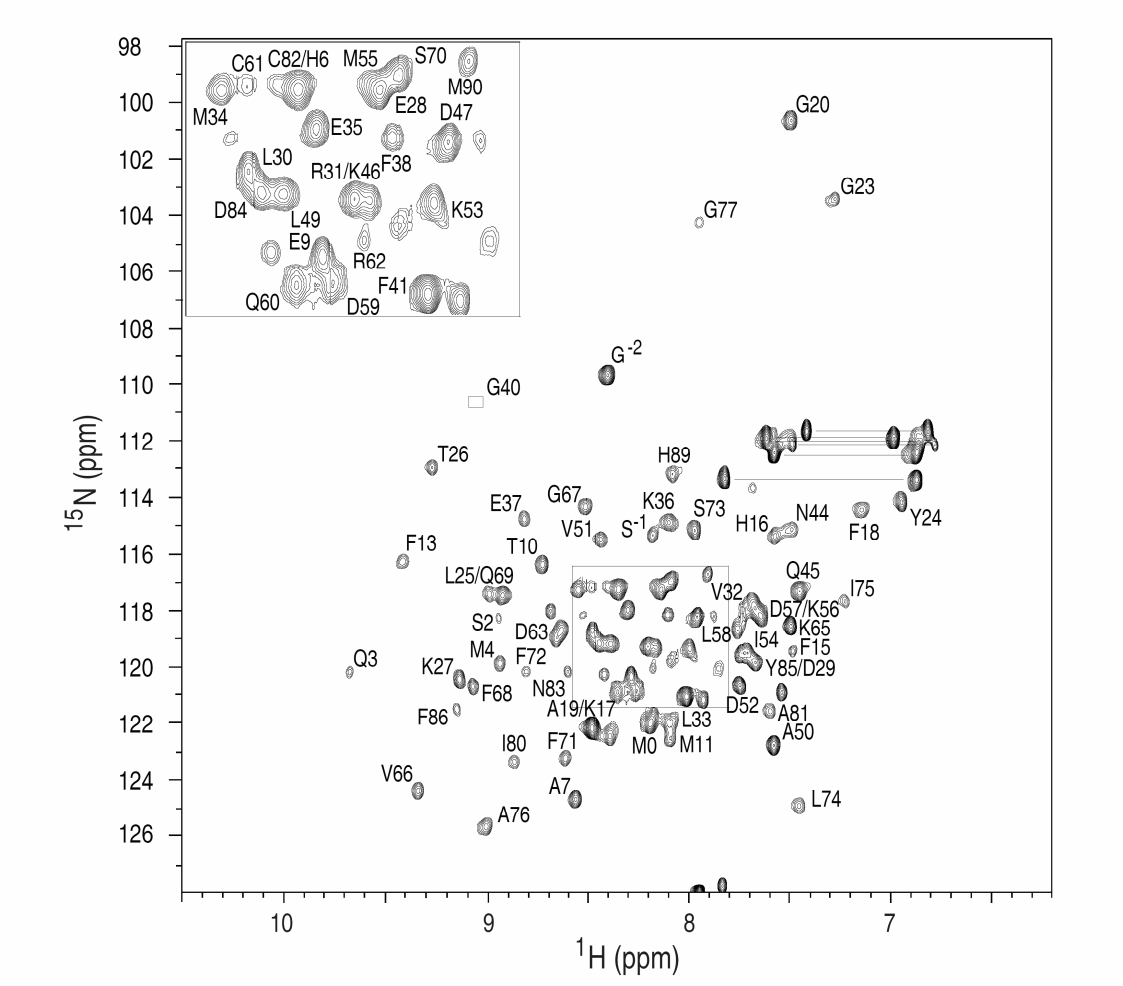

Figure 2.13. Backbone amide assignments of S100A10-annexin A2 complex.

^{1}H-^{15}N HSQC spectrum of 0.5 mM (monomer) uniformly ^{15}N, ^{13}C-labeled S100A10 protein bound to 0.5 mM annexin A2 peptide at pH 7.0 acquired on a Varian INOVA 600 MHz spectrometer at 35 ºC. Assigned backbone amide cross peaks are indicated with their one letter amino acid code and number. Pairs of resonances for sidechain amide cross peaks are connected by horizontal lines. Peaks visible at lower contour levels are indicated by boxes.

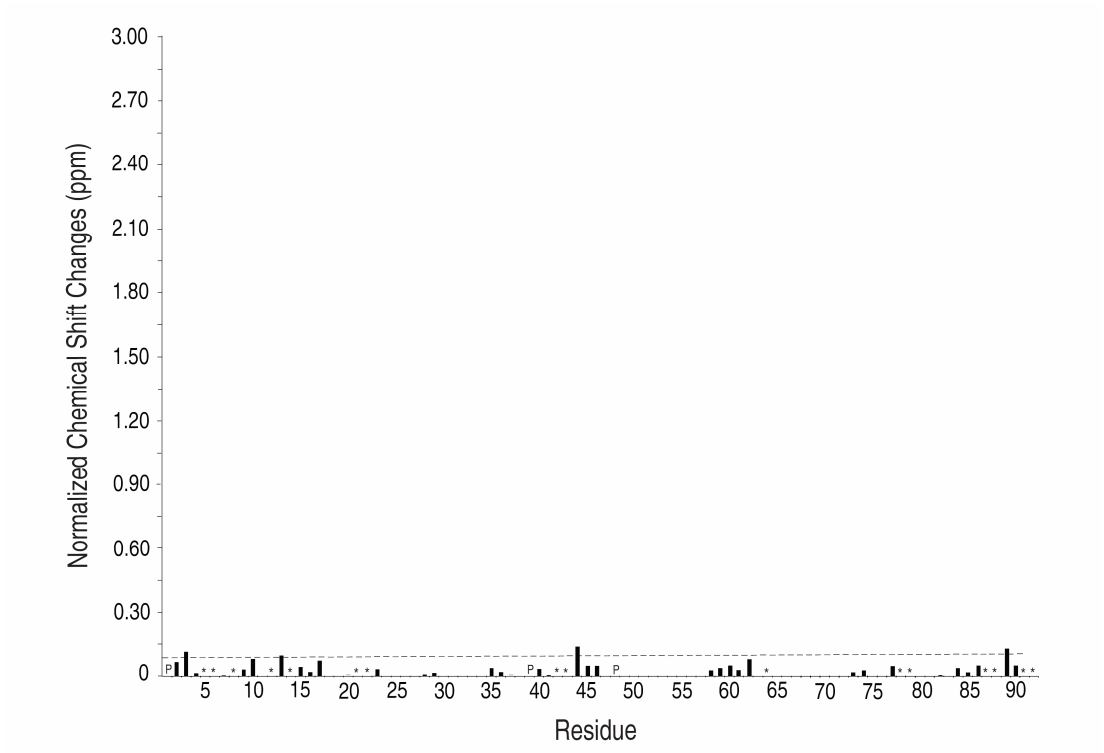

Figure 2.14. Comparison of the changes in chemical shift of the A10A2 hybrid protein and S100A10 in complex with individual annexin A2 peptide.

Chemical shift changes ($\Delta\delta$) were normalized in both ^{1}HN and ^{15}N using the formula $[\{HN^2 + (N/5)^2\}/2]^{1/2}$. The dashed line indicates the average change in chemical shift at 0.09 ppm. Proline residues are shown as "P" and asterisks indicate missing assignments in either or both proteins.

TRTK12 segments was not observed in the absence of calcium (data not shown). However, upon calcium addition to BT12, a spectrum was obtained (Figure 2.12) that was nearly identical to that for Ca^{2+}-S100B in complex with a synthetic TRTK12 peptide (Figure 2.15). As shown in Figure 2.12, for BT12 all resonances in the linker (L92-G102) and TRTK (T103-E116) sequences were identified with the exception of three glycine residues (G99-G101) in the linker that were absent from the spectra due to the fast exchange with the solvent. Once more, backbone assignment of the BT12 and S100B in complex with individual TRTK12 peptide allowed measuring the chemical shift changes of each residue between the two complexes (Figure 2.16) as well as that for other Ca^{2+}-bound S100 proteins indicating that little structural change occurred in the S100B protein as the result of incorporating the C-terminal linker and TRTK12 sequences.

One advantage of the A10A2 and BT12 hybrid proteins is that they allow *in situ* cleavage of the linker using TEV or PreScission enzymes, respectively. Figure 2.17 shows the ^{1}H-^{15}N HSQC spectrum of the A10A2 hybrid protein following TEV cleavage. The positions of the amide resonances for the S100A10 and annexin A2 components in this spectrum are nearly identical to those found in the presence of the linker (Figure 2.10). Importantly, the NMR spectrum shows a tight complex is maintained between S100A10 and annexin A2 despite the absence of N-terminal acetylation of the annexin protein. Parallel experiments for the BT12 hybrid protein following cleavage with PreScission protease yielded similar results (Figure 2.18).

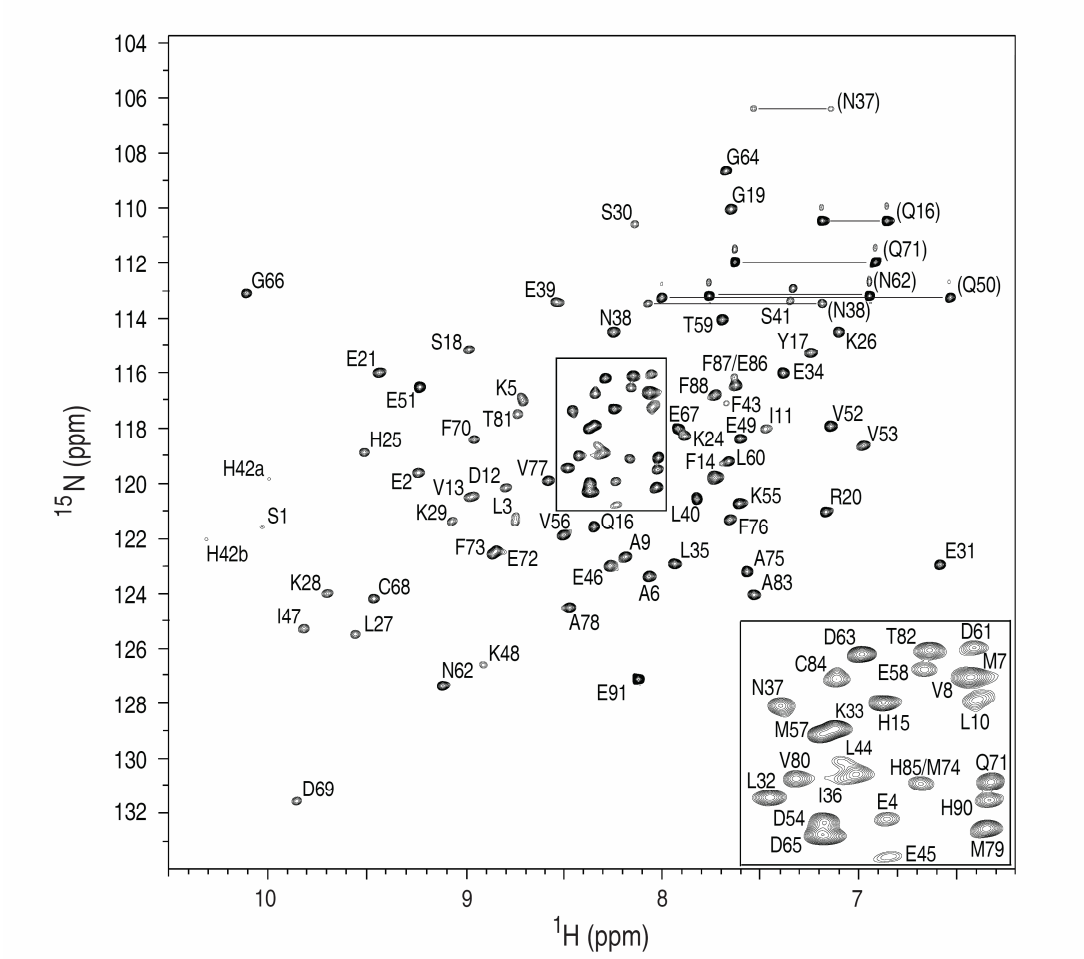

Figure 2.15. Backbone amide assignments of S100B-TRTK12 complex.

^{1}H-^{15}N HSQC spectrum of 0.7 mM (monomer) uniformly ^{15}N, ^{13}C-labeled S100B protein bound to 0.7 mM TRTK12 peptide in the presence of 6 mM $CaCl_2$ at pH 7.0 acquired on a Varian INOVA 600 MHz spectrometer at 35 ºC. Assigned backbone amide cross peaks are indicated with their one letter amino acid code and number. Pairs of resonances for sidechain amide cross peaks are connected by horizontal lines.

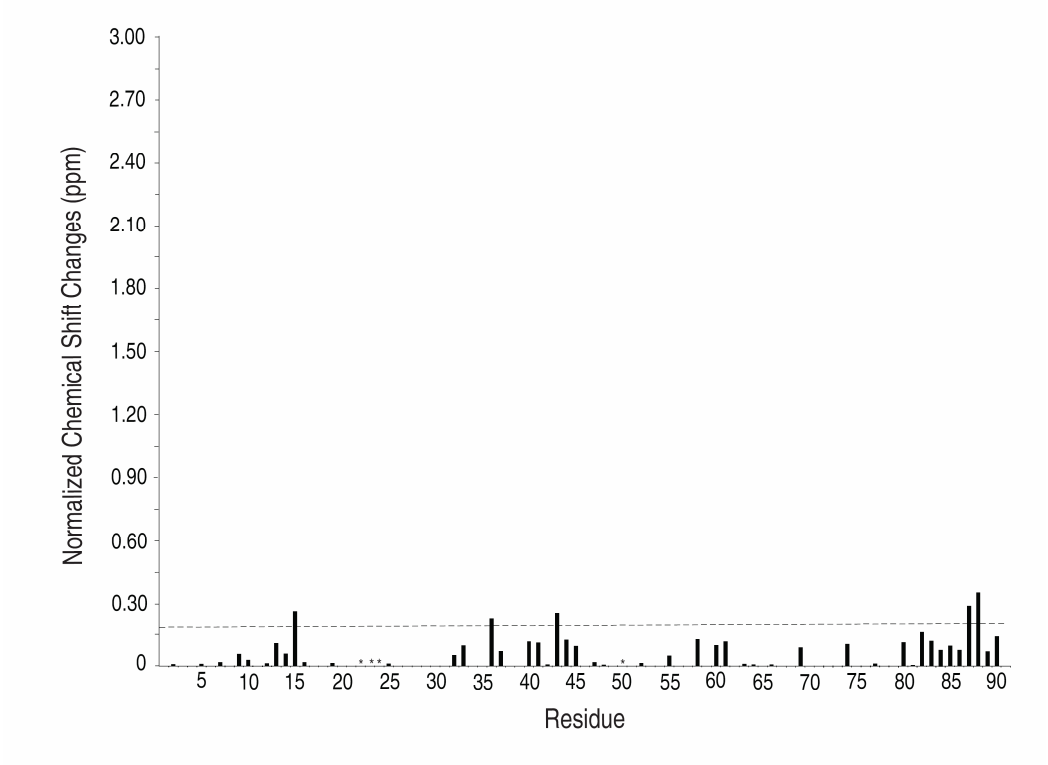

Figure 2.16. Comparison of the changes in chemical shift of the BT12 hybrid protein and S100B in complex with individual TRTK12 peptide.

Chemical shift changes ($\Delta\delta$) were normalized in both ^{1}HN and ^{15}N using the formula $[\{HN^2 + (N/5)^2\}/2]^{1/2}$. The dashed line indicates the average change in chemical shift at 0.17 ppm. The asterisks indicate missing assignments in either or both proteins.

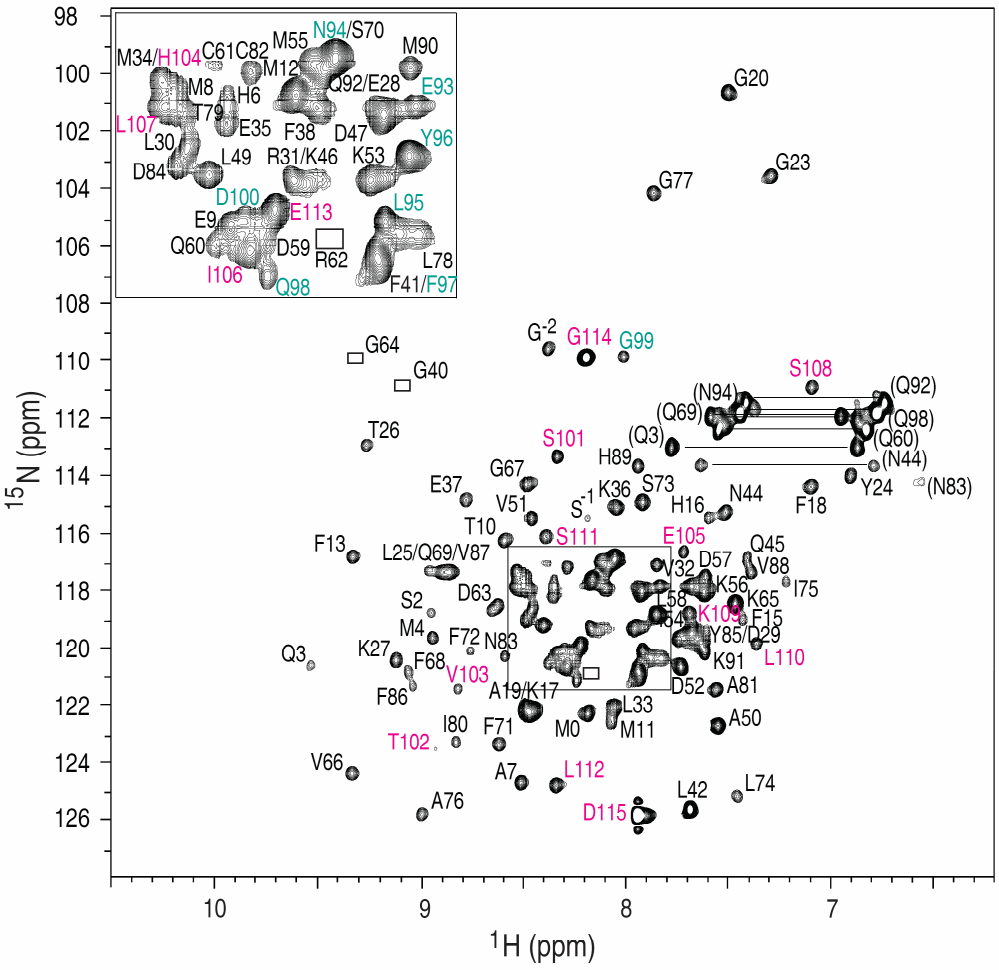

Figure 2.17. ^{1}H-^{15}N HSQC spectrum of A10A2 cleaved with TEV protease.

0.5 mM (monomer) uniformly ^{15}N, ^{13}C-labeled A10A12 protein 48 h following cleavage with TEV protease at pH 7.0 acquired on a Varian INOVA 600 MHz spectrometer at 35 ºC. Assigned backbone amide cross peaks are indicated with their one letter amino acid code and number. Pairs of resonances for sidechain amide cross peaks are connected by horizontal lines. Peaks visible at lower contour levels are indicated by boxes.

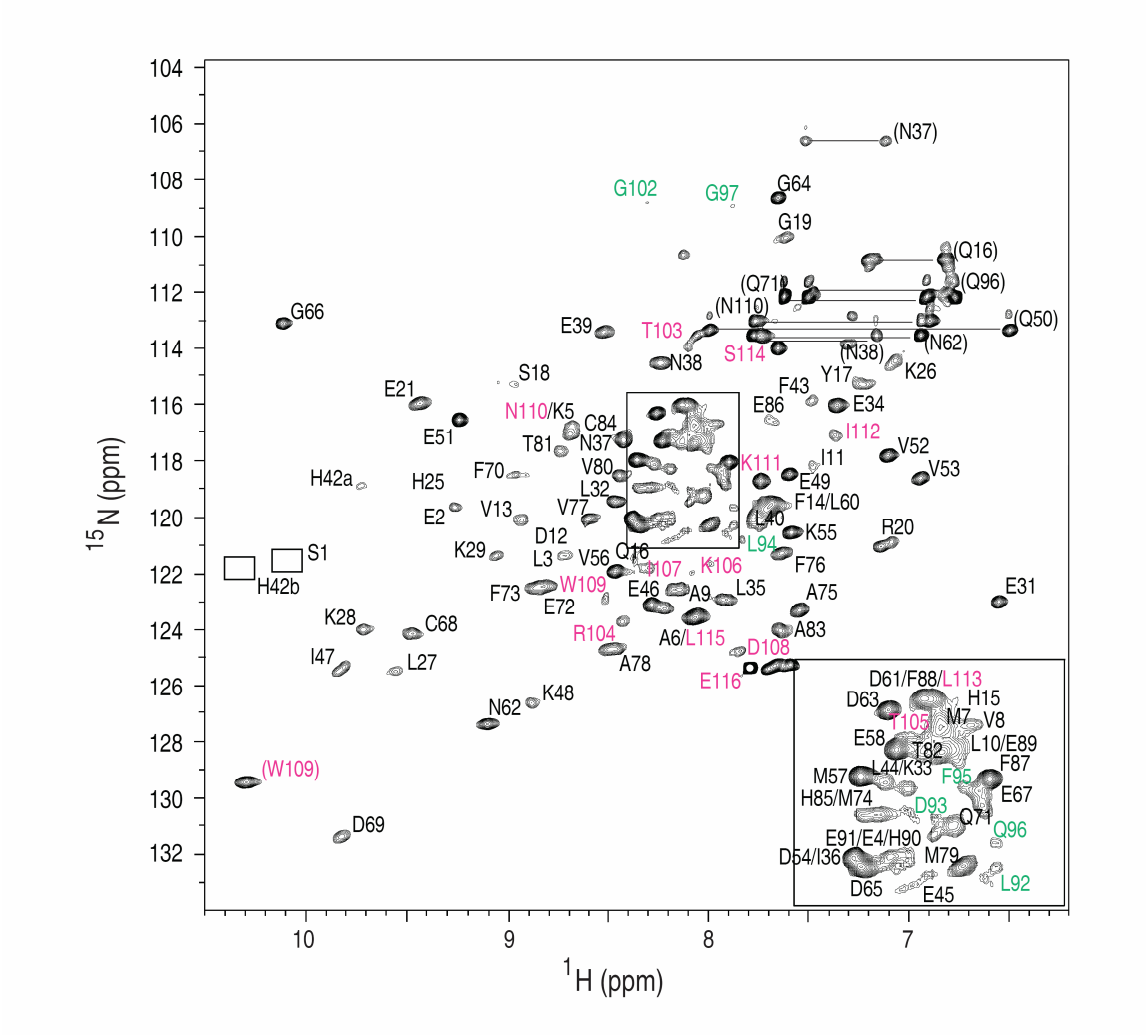

Figure 2.18. ^{1}H-^{15}N HSQC spectrum of BT12 hybrid protein cleaved with PreScission protease.

0.7 mM (monomer) uniformly ^{15}N, ^{13}C-labeled BT12 protein 48 h following cleavage with PreScission protease at pH 7.0 acquired on a Varian INOVA 600 MHz spectrometer at 35 ºC. Assigned backbone amide cross peaks are indicated with their one letter amino acid code and number. Pairs of resonances for sidechain amide cross peaks are connected by horizontal lines. Peaks visible at lower contour levels are indicated by boxes.

The assignments of Hα, Cα and C' resonances of the annexin A2 and TRTK12 regions in the A10A2 and BT12 hybrid proteins allowed their secondary structures to be determined using the chemical shift index (Wishart et al. 1992). This analysis (Figure 2.19) shows that residues T102-S108 of annexin A2 form a well-defined α-helix. This compares very well with the crystal structure of S100A10 with the N-terminal peptide from annexin A2 (1BT6) that shows residues T2-K9 (T102-K109 in A10A2) adopt an α-helical structure (Rety et al. 1999). The secondary structure of TRTK12 in the BT12 hybrid protein shows an unstructured N-terminus and a single turn of α-helix from D108-K111. The position of the α-helix in BT12 agrees well with the previously reported crystal and NMR structures of Ca^{2+}-S100B in complex with TRTK12 (1MWN and 3IQO) (Inman et al. 2002; Charpentier et al. 2010).

2.4 Discussion

2.4.1 High Yield Bacterial Expression of S100-Target Hybrid Proteins

Bacterial expression of peptides is a challenging task since unstructured peptides are prone to degradation by proteases during purification. This results in very low yields of purified peptides and can lead to inhomogeneity of the peptide due to non-specific proteolysis. Although successful methods have been developed using GB1-tagged (Lindhout et al. 2003) or His-tagged (Lee et al. 2008) peptides for S100B and S100A6 respectively, in our hands previous attempts to biosynthetically prepare annexin A1 and A2 peptides using GST- or GB1 constructs lead to <1 mg peptide/L culture and the isolated peptides were prone to proteolysis (Rintala-Dempsey, unpublished results). In

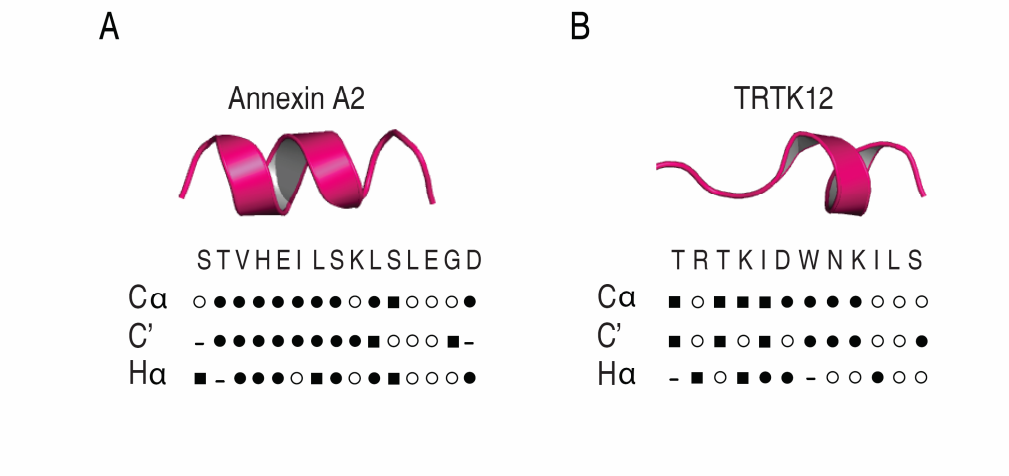

Figure 2.19. Secondary structure determinations for annexin A2 and TRTK12 peptides in the A10A2 and BT12 hybrid constructs using the chemical shift index (Wishart et al. 1992) for Cα, C' and Hα atoms.

The secondary structure identified for each atom is shown as α-helix (●), β-strand (■) or coil conformation (○).

the current work, a successful method has been developed for bacterial expression of annexin A2 and TRTK12 peptides by linking them to S100A10 and S100B, respectively. In essence the target protein is used as a carrier for the target peptide. Similar approaches have been described previously to produce hybrid molecules of calmodulin bound to the 26-residue binding region of myosin light-chain kinase (M13) (Porumb et al. 1994; Hayes et al. 2004), and peptides from the calmodulin-binding domains of calcineurin (Renigunta et al. 2006), the olfactory nucleotide-gated ion-channel (Chyan et al. 2005), tobacco MAPK phosphatase-1 (Ishida et al. 2009), and chromogranin A (Kang et al. 2007). In all of these studies, the linker was composed of only glycine residues in order to maintain flexibility in the linker connecting the carrier protein to the target peptides. Here, it was demonstrated that this is not a necessary requirement and that alternate amino acids can be used. This is particularly important for the incorporation of proteolytic cleavage sites such as TEV or PreScission protease used in this work to obtain complete digestion of the target sites. In principle, this method would allow purification of the target peptides (annexin A2 or TRTK12). For NMR studies, this would provide a rapid and facile method to obtain reasonable quantities of ^{15}N, ^{13}C-labeled peptides. Alternatively, it was chosen not to purify the cleaved peptides and examine the intact hybrid protein or the complex after *in situ* cleavage. This further simplifies the procedure and in the case of protein-peptide complexes offers the advantage of perfect 1:1 stoichiometry.

One requirement for the interaction between some S100 proteins and target peptides is the N-terminal acetylation of the peptides (Johnsson et al. 1986; Johnsson et al. 1988; McClintock and Shaw 2003). For example, both annexins A1 and A2 are

naturally acetylated. Although, crystal structures of S100A10 in complex with annexin A2 and Ca^{2+}-S100A11 bound to annexin A1 do not illustrate direct contact between the S100 protein and the peptide acetyl groups (Rety et al. 1999; Rety et al. 2000), unacetylated peptides show ~1000-fold decreased binding affinity for the respective S100 proteins (Johnsson et al. 1988). It has been suggested that the acetyl group acts to stabilize the α-helical conformation of the peptide. In the A10A2 hybrid protein acetylation of the annexin A2 moiety is not possible. However, an acidic residue was incorporated at the N-terminus of the annexin A2 sequence to neutralize the helical dipole and stabilize the helix structure. The result clarified that A10A2 hybrid maintains a tight association between the S100A10 and the annexin peptide indicating the acidic residue is sufficient to stabilize the interaction. In support of this approach, a GST-annexin A2 fusion protein also shows tight binding to S100A10 presumably because the annexin N-terminus is extended (by GST) in place of acetylation (Mailliard et al. 1996). Similarly, an interaction between TRTK12 and S100B is enhanced upon acetylation of the TRTK12 peptide (McClintock et al. 2002), even though the α-helix forms further down the peptide sequence (Inman et al. 2002). The hybrid BT12 protein would support this enhanced interaction by mimicking the neutralized TRTK12 sequence.

2.4.2 Applications and Limitations in utilizing S100-Target Hybrid Proteins

One of the limitations that could be associated with biosynthesis of hybrid proteins method is that the hybrid proteins might suffer from reduced solubility in the unbound form. This was not a problem for A10A2 because binding of annexin A2 to

S100A10 is not calcium sensitive. However, for BT12 the hybrid showed poorer solubility in the absence of calcium and exhibited NMR spectra suggestive of protein oligomerization. This is perhaps not surprising given that the TRTK12 peptide motif or accompanying linker could result in non-specific interactions in the absence of calcium. However, upon calcium binding the BT12 showed excellent solubility and provided ^{1}H-^{15}N HSQC spectra that were better compared to the individual protein peptide complexes.

In summary, the approach presented here demonstrated a successful method of high yield bacterial expression of S100 hybrid proteins. Two different protease cleavage sites were successfully incorporated into the linker regions and can be used *in situ* to form the S100-peptide complex. This method could be applied for the synthesis of S100 binding peptides for biophysical or biological characterization by X-ray crystallography or NMR. Further, the S100-target hybrid proteins may prove useful for the assembly and examination of larger S100 complexes. In the following chapters, A10A2 hybrid protein is used to study the ternary complex involving S100A10, annexin A2 and AHNAK proteins.

2.5 References

Berman, H.M., Westbrook, J., Feng, Z., Gilliland, G., Bhat, T.N., Weissig, H., Shindyalov, I.N., and Bourne, P.E. 2000. The Protein Data Bank. *Nucleic Acids Res* **28:** 235-242.

Bhattacharya, S., Large, E., Heizmann, C. W., Hemmings, B., Chazin, W. J. 2003. Structure of the Ca^{2+}/S100B/NDR kinase peptide complex: insights into S100 target specificity and activation of the kinase. *Biochemistry* **42:** 14416-14426.

Bostrom, S.L., Westerlund, C., Rochester, S., and Vogel, H.J. 1988. Binding of a dihydropyridine felodipine-analogue to calmodulin and related calcium-binding proteins. *Biochem Pharmacol* **37:** 3723-3728.

Charpentier, T.H., Thompson, L.E., Liriano, M.A., Varney, K.M., Wilder, P.T., Pozharski, E., Toth, E.A., and Weber, D.J. 2010. The effects of CapZ peptide (TRTK-12) binding to S100B-Ca2+ as examined by NMR and X-ray crystallography. *J Mol Biol* **396:** 1227-1243.

Chyan, C.L., Huang, P.C., Lin, T.H., Huang, J.W., Lin, S.S., Huang, H.B., and Chen, Y.C. 2005. Purification, crystallization and preliminary crystallographic studies of a calmodulin-OLFp hybrid molecule. *Acta Crystallogr Sect F Struct Biol Cryst Commun* **61:** 785-787.

Delaglio, F., Grzesiek, S., Vuister, G.W., Zhu, G., Pfeifer, J., and Bax, A. 1995. NMRPipe: a multidimensional spectral processing system based on UNIX pipes. *J Biomol NMR* **6:** 277-293.

Grzesiek, S., and Bax, A. 1992a. Correlating backbone amide and sidechain resonances in larger proteins by multiple relayed triple resonance NMR. *J. Am. Chem. Soc.* **114:** 6291-6293.

Grzesiek, S., and Bax, A. 1992b. An efficient experiment for sequential backbone assignment of medium-sized isotopically enriched proteins. *J. Mag. Reson.* **99:** 201-207.

Guex, N., and Peitsch, M.C. 1997. SWISS-MODEL and the Swiss-PdbViewer: an environment for comparative protein modeling. *Electrophoresis* **18:** 2714-2723.

Hayes, M.J., Merrifield, C.J., Shao, D., Ayala-Sanmartin, J., Schorey, C.D., Levine, T.P., Proust, J., Curran, J., Bailly, M., and Moss, S.E. 2004. Annexin 2 binding to phosphatidylinositol 4,5-bisphosphate on endocytic vesicles is regulated by the stress response pathway. *J Biol Chem* **279:** 14157-14164.

Huth, J.R., Bewley, C.A., Jackson, B.M., Hinnebusch, A.G., Clore, G.M., and Gronenborn, A.M. 1997. Design of an expression system for detecting folded protein domains and mapping macromolecular interactions by NMR. *Protein Sci* **6:** 2359-2364.

Inman, K.G., Yang, R., Rustandi, R.R., Miller, K.E., Baldisseri, D.M., and Weber, D.J. 2002. Solution NMR structure of S100B bound to the high-affinity target peptide TRTK-12. *J. Mol. Biol.* **324:** 1003-1014.

Ishida, H., Rainaldi, M., and Vogel, H.J. 2009. Structural studies of soybean calmodulin isoform 4 bound to the calmodulin-binding domain of tobacco mitogen-activated protein kinase phosphatase-1 provide insights into a sequential target binding mode. *J Biol Chem* **284:** 28292-28305.

Johnson, B.A., and Belvins, R.A. 1994. NMRView: A computer program for the visualization and analysis of NMR data. *J Biomol NMR* **4:** 603-614.

Johnsson, N., Marriott, G., and Weber, K. 1988. p36, the major cytoplasmic substrate of src tyrosine protein kinase, binds to its p11 regulatory subunit via a short amino-terminal amphiphatic helix. *EMBO J.* **7:** 2435-2442.

Johnsson, N., Vandekerckhove, J., Van Damme, J., and Weber, K. 1986. Binding sites for calcium, lipid and p11 on p36, the substrate of retroviral tyrosine-specific protein kinases. *FEBS Lett* **198:** 361-364.

Kang, S., Kang, J., Yoo, S.H., and Park, S. 2007. Recombinant preparation and characterization of interactions for a calmodulin-binding chromogranin A peptide and calmodulin. *J Pept Sci* **13:** 237-244.

Kay, L.E. 1993. Pulse-field gradient-enriched three dimensional NMR experiment for correlating ^{13}Ca/B, ^{13}C', and ^{1}Ha chemical shifts in uniformly ^{13}C-labeled proteins dissolved in H_2O. *J. Am. Chem. Soc.* **115:** 2055-2057.

Kay, L.E., Ikura, M., Tschudin, R., and Bax, A. 1990. Three-dimentional triple-resonance NMR spectroscopy of isotopically enriched proteins. *J. Magn. Reson.* **89:** 496-514.

Kay, L.E., Keifer, P., and Saarinen, T. 1992. Pure absorption gradient enhanced heteronuclear single quantum correlation spectroscopy with improved sensitivity. *J. Am. Chem. Soc.* **114:** 10663-10665.

Lee, Y.T., Dimitrova, Y.N., Schneider, G., Ridenour, W.B., Bhattacharya, S., Soss, S.E., Caprioli, R.M., Filipek, A., and Chazin, W.J. 2008. Structure of the S100A6 complex with a fragment from the C-terminal domain of Siah-1 interacting

protein: a novel mode for S100 protein target recognition. *Biochemistry* **47:** 10921-10932.

Lindhout, D.A., Thiessen, A., Schieve, D., and Sykes, B.D. 2003. High-yield expression of isotopically labeled peptides for use in NMR studies. *Protein Sci* **12:** 1786-1791.

Mailliard, W.S., Haigler, H.T., and Schlaepfer, D.D. 1996. Calcium-dependent binding of S100C to the N-terminal domain of annexin I. *J. Biol. Chem.* **271:** 719-725.

McClintock, K.A., and Shaw, G.S. 2003. A novel S100 target conformation is revealed by the solution structure of the Ca2+-S100B-TRTK-12 complex. *J Biol Chem* **278:** 6251-6257.

McClintock, K.A., Van Eldik, L.J., and Shaw, G.S. 2002. The C-terminus and linker region of S100B exert dual control on protein-protein interactions with TRTK-12. *Biochemistry* **41:** 5421-5428.

Porumb, T., Yau, P., Harvey, T.S., and Ikura, M. 1994. A calmodulin-target peptide hybrid molecule with unique calcium-binding properties. *Prot. Eng.* **7:** 109-115.

Renigunta, V., Yuan, H., Zuzarte, M., Rinne, S., Koch, A., Wischmeyer, E., Schlichthorl, G., Gao, Y., Karschin, A., Jacob, R., et al. 2006. The retention factor p11 confers an endoplasmic reticulum-localization signal to the potassium channel TASK-1. *Traffic* **7:** 168-181.

Rety, S., Osterloh, D., Arie, J.P., Tabaries, S., Seeman, J., Russo-Marie, F., Gerke, V., and Lewit-Bentley, A. 2000. Structural basis of the Ca(2+)-dependent association between S100C (S100A11) and its target, the N-terminal part of annexin I. *Structure Fold Des* **8:** 175-184.

Rety, S., Sopkova, J., Renouard, M., Osterloh, D., Gerke, V., Tabaries, S., Russo-Marie, F., and Lewit-Bentley, A. 1999. The crystal structure of a complex of p11 with the annexin II N-terminal peptide. *Nat Struct Biol* **6:** 89-95.

Rintala-Dempsey, A.C., Santamaria-Kisiel, L., Liao, Y., Lajoie, G., and Shaw, G.S. 2006. Insights into S100 target specificity examined by a new interaction between S100A11 and annexin A2. *Biochemistry* **45:** 14695-14705.

Rustandi, R.R., Baldisseri, D.M., and Weber, D.J. 2000. Structure of the negative regulatory domain of p53 bound to S100B(ββ). *Nat. Struct. Biol.* **7:** 570-574.

Safadi, S.S., and Shaw, G.S. 2007. A disease state mutation unfolds the parkin ubiquitin-like domain. *Biochemistry* **46:** 14162-14169.

Smith, S.P., Barber, K.R., Dunn, S.D., and Shaw, G.S. 1996. Structural influence of cation binding to recombinant human brain S100b: Evidence for calcium-induced exposure of a hydrophobic surface. *Biochemistry* **35:** 8805-8814.

Smith, S.P., Barber, K.R., and Shaw, G.S. 1997. Identification and structural influence of a differentially modified N-terminal methionine in human S100b. *Protein Sci.* **6:** 1110-1113.

Wishart, D.S., Sykes, B.D., and Richards, F.M. 1992. The chemical shift index: A fast and simple method for the assignment of protein secondary structure through NMR spectroscopy. *Biochemistry* **31:** 1647-1651.

Wittekind, M., and Mueller, L. 1993. HNCACB, a high-sensitivity 3D NMR experiment to correlate amide-proton and nitrogen resonances with the alpha- and beta-carbon resonances. *J. Magn. Reson. Series B.* **101:** 171-180.

Yap, K.L., Kim, J., Truong, K., Sherman, M., Yuan, T., and Ikura, M. 2000. Calmodulin target database. *J Struct Funct Genomics* **1:** 8-14.

Yoon, M.K., Park, S.H., Won, H.S., Na, D.S., and Lee, B.J. 2000. Solution structure and membrane-binding property of the N-terminal tail domain of human annexin I. *FEBS Lett* **484:** 241-245.

Zeng, F.Y., Gerke, V., and Gabius, H.J. 1993. Identification of annexin II, annexin VI and glyceraldehyde-3-phosphate dehydrogenase as calcyclin-binding proteins in bovine heart. *Int J Biochem* **25:** 1019-1027.

Chapter 3

The S100A10-Annexin A2 Complex Provides a Novel Asymmetric Platform for AHNAK Recruitment

3.1 Introduction

A requisite for plasma membrane repair is calcium-regulated exocytosis, controlled by a number of proteins that coordinate resealing of the membrane. One exocytotic compartment implicated in membrane fusion is the enlargeosome, characterized by the large scaffolding protein AHNAK, that relocates to the plasma membrane immediately following membrane damage (Zhang et al. 2004). In addition to AHNAK, calcium-sensors such as dysferlin and annexin family members are involved in membrane repair. Upon membrane rupture, these sensor proteins respond to the calcium influx by localizing near the inner membrane surface.

Membrane repair and membrane-receptor protein trafficking can be modulated by the association of an S100A10 dimer with the calcium- and phospholipid-binding protein annexin A2. This heterotetrameric complex (Rety et al. 1999) has the ability to form larger multiprotein assemblies such as those with AHNAK and members of the transmembrane ferlin family (ie. dysferlin). *In vitro* and *in vivo* experiments have shown that the C-terminal domain of AHNAK (van de Graaf et al. 2003; Borthwick et al. 2008) interacts with S100A10 while bound to annexin A2 (Shtivelman and Bishop 1993).

Parts of this chapter have been taken from the submitted article: Rezvanpour, A., and Shaw, G. S. 2011. The S100A10-annexin A2 complex provides a novel asymmetric platform for AHNAK recruitment. *J. Biol. Chem.*

Available structural information about the arrangement and mechanisms used by multi-protein complexes such as those involved in membrane repair is very limited. In this chapter, peptide array analysis was used to uncover the binding region(s) of different proteins within the complexes formed between S100A10, annexin A2, the C-terminal region of AHNAK and the C2A domain of dysferlin proteins. For instance, the designed S100A10-annexin A2 (A10A2) hybrid protein (described in Chapter 2) in which S100A10 was linked in tandem to the N-terminal 15 residues of annexin A2, was used in peptide array experiments, to identify the regions of interaction within the C-terminus of AHNAK. Of the eight consensus regions observed, one of the sequences (referred to as AHNAK5) having a strong interaction was used as a synthetic peptide to identify the binding region(s), stoichiometry and affinity with the A10A2 complex. Using NMR spectroscopy, non-denaturing electrospray mass spectrometry and fluorescence spectroscopy a novel asymmetric ternary arrangement between a single AHNAK5 peptide, an S100A10 dimer and two annexin A2 peptides was described. These results provide the first structural model of a multi-protein assemblage necessary during the membrane repair. To examine the possibility for the formation of other ternary complexes involving S100A10 and annexin A2, the interaction between S100A10 or A10A2 with the transient receptor potential cation channel protein, TRPV5, was also investigated by peptide array analysis.

Furthermore, the interaction between other components of the membrane repair machinery was tested. For instance, to identify potential binding sites other than the 12 residue N-terminal region of annexin A2 with the S100A10 protein, peptide arrays of full

length annexin A2 were probed with S100A10 or A10A2 proteins. Finally, the interaction between the apo- and calcium-bound C2A domain of dysferlin with the S100A10 and C-terminal domain of AHNAK was examined by NMR spectroscopy.

3.2 Materials and Methods

3.2.1 Source of Materials

The expression vector for human S100A10 (pGEX-6P-1-derived vector, GE Healthcare) was a generous gift from Dr. Michael Walsh (University of Calgary, Alberta, Canada). All forward and reverse oligonucleotides described within this chapter were synthesized by Sigma-Genosys (Mississauga, ON, Canada). T4 DNA ligase was purchased from Fermentas Life Sciences (Burlington, ON, Canada). Pfu Turbo DNA polymerase was purchased from Stratagene (La Jolla, CA, USA). All other chemicals used in cloning were purchased from BioShop Canada (Burlington, ON, Canada). All DNA sequencing was performed at Robarts Research Institute Sequencing Facility (London, ON, Canada).

$^{15}NH_4Cl$ and $^{13}C_6$-glucose were obtained from Cambridge Isotope Laboratories, Inc. (Andover, MA). Puratronic grade $CaCl_2$ (99.9995% purity) was purchased from Johnson-Matthey (Ward Hill, MA). Peptide arrays were produced at Dr. Shawn Li's laboratory (University of Western Ontario, ON, Canada). All other reagents used in the following experiments were of the highest purity commercially available.

3.2.2 Construction of S100A10^{C82S} and A10A2^{C82S} in E. coli Expression Vectors

DNA fragments encoding either rabbit S100A10 or the S100A10-annexin A2 (A10A2) hybrid proteins (Rezvanpour et al. 2009) were contained in pGEX-6P-1 vectors. QuikChange site-directed mutagenesis (Wang and Malcolm 1999) was performed to convert the cysteine codon (Cys82) to a serine in both plasmids using forward (5' GCCG GCCTCACCATTGCATCCAATGACTATTTTGTAGTGC 3') and reverse (5' GCACT ACAAAATAGTCATTGGATGCAATGGTGAGGCCGGC 3') primers. PCR products were treated with DpnI (Nebgen et al.) restriction enzyme for 1 hr at 37º C to digest the methylated template DNA and transformed into *E. coli* strain JM-109. The single point mutations in the resulting vectors were confirmed by DNA sequencing.

3.2.3 Expression and Purification of the Wild-Type and C82S Substituted Forms of S100A10 and A10A2

Unlabeled and uniformly ^{15}N, ^{13}C-labeled wild-type and C82S substituted forms of human GST-S100A10 and/or GST-A10A2 were overexpressed in the BL21 (DE3)-RIL *E. coli* strain as previously described in Section 2.2.6 (Rezvanpour et al. 2009) using 1 L of 2xYT, or M9 minimal medium supplemented with 1 g $^{15}NH_4Cl$ and 2 g $^{13}C_6$-glucose as the sole nitrogen and carbon sources, respectively. MALDI-TOF mass data for unlabeled S100A10^{C82S} (MW_{calc} = 11598.6 Da; MW_{obs} = 11599.4 Da) and A10A2^{C82S} (MW_{calc} = 13733.8 Da; MW_{obs} = 13733.5 Da) confirmed the protein identities.

3.2.4 Construction of a Short C-Terminal Fragment of AHNAK Expression Vector

An expression vector containing a short C-terminal fragment of AHNAK was synthesized by DNA 2.0 (Menlo Park, CA). This vector was composed of a His_7 tag and a TEV cleavage site at the N-terminus of the AHNAK coding gene sequence (5362-5434). The DNA was extracted from the GFC filter by incubating the filter in 100 µL of 10 mM Tris-HCl at pH 7.5 for 2 min, followed by spinning the sample in a tabletop centrifuge at full speed. The integrity of the AHNAK DNA fragment was checked by Pst1 restriction enzyme digestion on a 1% agarose gel. The DNA was transformed into the JM-109 *E. coli* strain.

3.2.5 Expression and Purification of the Wild-Type C-Terminal Fragment of AHNAK

Expression vector containing the C-terminal fragment of AHNAK (5362-5434) was transformed into *E. coli* strain BL21 (DE3) Codon Plus expression cells (Invitrogen), which contain extra copies of the *argU*, *ileY*, and *leuW* tRNA genes to recognize AGA, AGG, AUA, and CUA codons. An overnight culture (25 mL) was used to inoculate 1 L of pre-warmed LB media supplemented with 30 µg/mL kanamycin. The culture was grown at 37 ºC to a density of (A_{600}) 0.8 AU, when it was induced with 1 mM IPTG. Induction continued for another 4 h with constant shaking at 37 ºC. Cells were harvested by centrifugation at 6,000 rpm for 15 min at 4 ºC. Following addition of one complete-mini protease inhibitor tablet, PMSF (1 mM final concentration) and leupeptin (1 µL of 100 µM stock per 1 mL of lysate), the cells were lysed by French Pressure at 20,000 psi. Ultracentrifugation of the lysed cells was performed using a Beckman ultracentrifuge at

38,000 rpm for 90 min. All fractionation steps were performed at 4 °C. The supernatant was filtered through 0.45 micron low protein binding Millipore syringe filters to remove the particulate matter. The protein was subsequently applied to a 5 mL Ni-NTA column pre-equilibrated in 20 mM Tris-HCl, 10 mM imidazole, 150 mM NaCl, and 5% glycerol at pH 7.5. The column was washed with the same buffer containing 20 mM imidazole until the OD_{280} returned to baseline. Bound protein was then eluted with a 30 mL, 20-500 mM imidazole gradient in the elution buffer. Fractions containing the protein were pooled and extensively dialyzed against TEV protease cleavage buffer (20 mM Tris-HCl, 150 mM NaCl, 10 mM imidazole, 1 mM DTT, and 5% glycerol at pH 7.5) for 6 h with multiple buffer exchanges. The His_7 tag was cleaved from the N-terminus of AHNAK using 250 units of TEV protease in 48 h with gentle agitation. Cleaved protein was purified on a second 5 mL Ni-NTA column as described above. Cleaved AHNAK was eluted in the flow-through fractions. The integrity of the protein was verified on 16.6% SDS-PAGE gel and electrospray ionization mass spectrometry (Biological Mass Spectrometry Laboratory, University of Western Ontario). MALDI-TOF mass data for unlabeled AHNAK (MW_{calc} = 7827.0 Da; MW_{obs} = 7827.4 Da) confirmed the protein identity.

3.2.6 Expression and Purification of Dysferlin C2A Domain

Unlabeled and uniformly ^{15}N, ^{13}C-labeled wild-type human C2A domain of dysferlin (simply referred to as dysferlin) (residues 1-138) were overexpressed in the BL21 (DE3) *E. coli* strain using 1 L of pre-warmed LB or M9 minimal medium

supplemented with 30 μg/mL kanamycin. $^{15}NH_4Cl$ (1 g) and $^{13}C_6$-glucose (2 g) were used as the sole nitrogen and carbon sources in the M9 minimal media. Briefly, the cultures were grown at 37 ºC to a density of (A_{600}) 0.7 AU. Expression was induced by the addition of 1 mM IPTG and allowed to continue for another 4 or 8 h with constant shaking at 37 ºC. Cells were harvested by centrifugation at 6,000 rpm for 15 min, lysed by French Pressure at 20,000 psi and centrifuged at 38,000 rpm for 90 min. All fractionation steps were performed at 4 °C. The supernatant was filtered through 0.45 micron low protein binding Millipore syringe filters. The protein was subsequently applied to a 5 mL Ni-NTA column pre-equilibrated in 20 mM MES, 10 mM imidazole, 150 mM NaCl, and 5% glycerol at pH 6.7. The column was washed with the same buffer containing 20 mM imidazole until the OD_{280} returned to baseline. Bound protein was then eluted with a 30 mL, 20-500 mM imidazole gradient in the elution buffer. Fractions containing the protein were pooled and extensively dialyzed against TEV protease cleavage buffer (25 mM MES, 100 mM NaCl, 1 mM DTT, pH 5.5) for 6 h with multiple buffer exchanges. The His_6 tag was cleaved from the N-terminus of dysferlin using 250 units of TEV protease in 48 h with gentle agitation. Cleaved protein was purified on a 5 mL HiTrap SP FF column (GE Healthsciences) equilibrated in the binding buffer (25 mM MES, 100 mM NaCl, 1 mM EDTA, and 1 mM DTT, at pH 5.5). Bound dysferlin was eluted with gradual increase in salt concentration over 30 min using 25 mM MES, 250 mM NaCl, 1 mM EDTA, and 1 mM DTT at pH 5.5. Fractions containing the protein were pooled and stored at -80 ºC. The protein was extensively dialyzed against appropriate

buffers to remove EDTA from the sample particularly before calcium titration experiments.

3.2.7 Fluorescent Labeling of S100A10^{C82S}, A10A2^{C82S} and Dysferlin C2A Domain

Freshly reduced S100A10^{C82S}, A10A2^{C82S} or dysferlin C2A domain was loaded onto a pre-equilibrated Sephadex G-25 PD-10 column (GE-Healthcare) in 20 mM Tris-HCl and 1 mM EDTA at pH 7.0 in order to remove excess DTT in the protein samples. Acrylodan or Alexa Fluor 680 maleimide (Invitrogen) was dissolved in acetonitrile to a concentration of 100 mM. The acrylodan or Alexa Fluor 680 solution (100 μL) was added to 1 mL of 80 μM S100A10^{C82S}, A10A2^{C82S} or dysferlin and the reactions continued for 2 hr at room temperature until quenched with the addition of 5 mM DTT. The unreacted dye was removed by chromatography through a Sephadex G-25 PD-10 column which was pre-equilibrated in TBS buffer (50 mM Tris-HCl, and 120 mM NaCl at pH 7.4). The protein samples were exhaustively dialyzed against 20 mM Tris-HCl, 120 mM NaCl, and 1 mM DTT at pH 7.4 to eliminate all noncovalently linked dye. ESI-MS indicated a single dye molecule was covalently linked to each protein.

3.2.8 Peptide Array Experiments

Peptide arrays were produced using the SPOT technology on cellulose membranes (Dr. Shawn Li, University of Western Ontario). Peptide arrays of AHNAK contained 330 spots of 18-residue peptides that shifted by 3 residues through the C-terminal sequence of AHNAK (residues 4884-5890). A similar array of annexin A2 was

also synthesized with 18-residue peptides that shifted by either 2 or 3 residues through the entire sequence of annexin A2 protein. The peptide arrays of annexin A2 were acetylated at the N-terminus of the peptides as acetylation of the N-terminus of annexin A2 has been shown to be a requirement for the interaction (Seemann et al. 1996; Rety et al. 2000). The peptide arrays of TRPV5 contained 18-residue peptides that shifted by 1 or 2 residues through the C-terminal sequence of TRPV5 (residues 577-729). $S100A10^{C82S}$ and $A10A2^{C82S}$ were both uniformly labeled at Cys61, while dysferlin was uniformly labeled at Cys23 with Alexa Fluor 680 maleimide as described in Section 3.2.7. Membranes were hydrated using anhydrous methanol and then washed three times with a buffer containing TBS + 0.05% Tween for 10 min at room temperature. Subsequently, membranes were incubated with TBS + 0.05% Tween and skim milk blocking buffer for 1 hour, followed by a final rinse for 10 min with TBS + 0.05% Tween wash buffer. Alexa-$S100A10^{C82S}$, -$A10A2^{C82S}$ or -dysferlin (0.2-2 μM of each) in TBS + 0.05% Tween and skim milk was used to probe each array for 2 hr. The arrays were then rinsed with TBS + 0.05% Tween buffer three times for 10 min each. To eliminate background fluorescence, the arrays were treated three times with a solution of 8 M urea, 1% SDS and 0.5% β-mercaptoethanol at pH 7.0 in a sonication bath at 40º C, and washed with 10% acetic acid, 50% ethanol and 40% distilled and deionized H_2O. The spots on the arrays were visualized using the Odyssey Infrared Imaging System (LI-COR Biosciences) at 700 nm.

3.2.9 Peptide Synthesis

The AHNAK (GKVTFPKMKIPKFTFSGREL) (referred to as AHNAK5) and annexin A2 (STVHEILSKLSLEGD) (Bio Basic Inc, ON, Canada) peptides were synthesized using solid-phase peptide synthesis employing the Fmoc chemistry strategy (Grant 2002). The N-termini of the peptides were acetylated while the C-termini were amidated. The synthesized peptides were purified by C18 reversed-phase HPLC, and lyophilized. The MALDI-TOF mass data for the acetylated AHNAK (MW_{calc} = 2353.8 Da; MW_{obs} = 2352.5 Da) and annexin A2 (MW_{calc} = 1669.8 Da; MW_{obs} = 1668.6 Da) confirmed the peptides identities.

3.2.10 Mass spectrometry

Mass spectrometry analyses were carried out using a quadrupole time-of-flight mass spectrometer (Q-TOF, micromass) equipped with a nano electrospray (ES) source by Dr. Suya Liu in Dr. Gilles A. Lajoie's laboratory (University of Western Ontario, ON, Canada). Samples were loaded on a gold-coated capillary (Protona) with the tip manually opened to produce an orifice of approximately 10 μm. Positive ES was performed at a capillary voltage of 1.5 to 2 kV and cone voltage of 50V. CID experiments were carried out with collision energy of 80V using argon as the collision gas. Average molecular masses were calculated using Mass Lynx 4.0 (Micromass).

3.2.11 Fluorescence Spectroscopy

A10A2^{C82S} was purified and labeled with acrylodan as described in Section 3.2.7. The concentrations of the protein stock solutions were determined using the Bradford protein assay and triplicate amino acid analysis (Advanced Protein Technology Centre, Toronto, Canada). Fluorescence experiments were conducted in duplicate using acrylodan-labeled A10A2^{C82S} (300 nM) in 20 mM Tris-HCl, 120 mM NaCl, and 1 mM DTT at pH 7.4 (3 mL). A Fluorolog-3 steady-state fluorometer (Horiba Scientific) was used for all measurements. Solutions were excited at 375 nm and emissions were monitored between 400-600 nm using an emission band-pass of 1 nm and an integration time of 1 sec.

Titrations of A10A2^{C82S} (300 nM) with the AHNAK peptide were carried out at room temperature in a stirred cell holder. A solution of AHNAK peptide was added in 3 μL increments using a calibrated 10 μL Hamilton syringe followed by three 30 μL additions to insure protein saturation. After each AHNAK addition, the sample was stirred for 2 min before scanning. Titrations were continued until a final S100 protein:AHNAK ratio of 10:1 was achieved. The dissociation constant (K_d) (Morigasaki et al.) was determined by plotting the normalized change in fluorescence (ΔF) intensity, monitored at 500 nm for acrylodan-labeled A10A2^{C82S} (P_t), as a function of AHNAK concentration (L_t). Data were fit using GraphPad Prism5 to equations 1 and 2 where ΔF_{max} is the maximum normalized change in fluorescence and PL is the concentration of the A10A2^{C82S}-AHNAK complex.

$$[PL] = [(P_t + L_t + K_d) - \{(Pt + L_t + K_d)^2 - (4P_tL_t)\}^{0.5}]/2 \quad (1)$$

$$\Delta F = [\Delta F_{max}][PL]/[P_t] \quad (2)$$

3.2.12 NMR Titration Experiments

All NMR experiments were acquired at 35 ºC on a Varian INOVA 600 MHz spectrometer equipped with a pulse field gradient triple resonance probe. A10A2^{C82S}, S100A10, the C-terminal fragment of AHNAK, the AHNAK5 peptide and dysferlin concentrations were determined by triplicate amino acid analysis (Advanced Protein Technology Centre, Toronto, Canada). The concentration of the $CaCl_2$ stock solution was determined by ICP (University of Western Ontario, ON, Canada). NMR samples of uniformly ^{15}N, ^{13}C-labeled A10A2^{C82S} (143 ± 6 μM) were prepared in 10% D_2O, 20 mM MOPS, 1 mM EDTA, 1 mM DTT, 50 mM arginine, 50 mM glutamic acid, and 100 mM NaCl buffer at pH 7.0, using DSS as an internal standard. AHNAK peptide (3320 ± 16.4 μM) was added from a stock solution to give a final AHNAK concentration of 584.6 μM. Samples were equilibrated for 15 min after each peptide addition. ^1H-^{15}N HSQC spectra were collected using carrier frequencies of 4.699 (^1H) and 114.0 ppm (^{15}N) and spectral widths of 8000.0 and 1700.0 Hz, respectively. Intensities of peaks undergoing slow exchange were measured after each addition and fit to Equation 1 using the software Prism 5.

For the NMR samples of uniformly ^{15}N-labeled dysferlin C2A domain (200 ± 7 μM), the protein was prepared in 10% D_2O, 10 mM HEPES, 1 mM DTT, and 150 mM NaCl buffer at pH 7.5, using DSS as an internal standard. $CaCl_2$ (37 mM) was titrated

from a stock solution in 1.2 μL increments for 7 additions to a calcium concentration of 1296 μM. The NMR sample of apo-dysferlin and AHNAK (5362-5434) proteins contained ~138 μM ^{15}N-labeled apo-dysferlin and ~200 μM unlabeled AHNAK. After collecting a ^{1}H-^{15}N HSQC spectrum of this sample, calcium (37 mM) was titrated in 1.2 μL increments for 7 additions to a calcium concentration of 850 μM. Samples were equilibrated for 15 min after each addition. ^{1}H-^{15}N HSQC spectra were collected using carrier frequencies of 4.772 (^{1}H) and 117.0 ppm (^{15}N) and spectral widths of 6982.6 and 1940.0 Hz, respectively.

An NMR sample of uniformly ^{15}N, ^{13}C-labeled S100A10 (350 ± 7 μM dimer) was prepared in 10% D_2O, 20 mM MOPS, 1 mM DTT, 50 mM arginine, 50 mM glutamic acid, and 100 mM NaCl buffer at pH 7.0, using DSS as an internal standard. ^{1}H-^{15}N HSQC spectra were collected using carrier frequencies of 4.750 (^{1}H) and 114.0 (^{15}N) ppm. Sequential assignment of the polypeptide backbone resonances for S100A10 was achieved by the HNCACB (Wittekind and Mueller 1993), CBCA(CO)NH (Grzesiek and Bax 1992), HNCA (Kay et al. 1990), and HNCO (Kay et al. 1990) experiments. The number of complex data points and the spectral widths were set to 512 and 8000.0 Hz for the ^{1}H (F3) dimension, and 64 and 2100.0 Hz for the ^{15}N (F2) dimension, respectively. For the HNCACB and CBCA(CO)NH experiments, 32 increments and a spectral width of 7840.0 Hz in the ^{13}C (F1) dimension were used. For the HNCA and HNCO experiments, 32 increments and a spectral width of 4524.0 Hz were used in the ^{13}C (F1) dimension.

For the NMR sample of ^{15}N, ^{13}C-labeled apo-dysferlin with unlabeled S100A10, 1:1 (200 μM of each protein) and 1:2 (200 μM:400 μM) molar ratios of

dysferlin:S100A10 were used, respectively. After collecting a ^{1}H-^{15}N HSQC spectrum of this sample, calcium (37 mM) was titrated in 3.5 μL increments for 6 additions to a calcium concentration of 1296 μM. Samples were equilibrated for 15 min after each addition. ^{1}H-^{15}N HSQC spectra were collected using carrier frequencies of 4.774 (^{1}H) and 117.0 ppm (^{15}N) and spectral widths of 6982.6 and 1940.0 Hz, respectively. All data were processed using NMRPipe and NMRDraw (Delaglio et al. 1995) and analyzed by NMRView (Johnson and Belvins 1994).

3.3 RESULTS

3.3.1 A10A2 Binds to Multiple Consensus Regions on AHNAK

To identify the AHNAK residues involved in the interaction with annexin A2-bound S100A10 complex, Alexa-A10A2^{C82S} protein was used in a separate peptide array experiment covering the C-terminus of AHNAK (residues 4884-5890). This approach identifies the sequence dependent but structurally independent interactions between A10A2^{C82S} and a series of 18-residue peptides spanning the C-terminal sequence of AHNAK. Overlapping sequences in the arrays that fluoresced upon Alexa-A10A2^{C82S} binding were used to identify the AHNAK binding sites (Figure 3.1). Blotting of the arrays with Alexa-A10A2^{C82S} revealed that A10A2^{C82S} associates with eight distinct regions within the C-terminus of AHNAK. Using the Blocks Server (blocks.fhcrc.org) to analyze these regions, a nine residue consensus sequence was identified for AHNAK that could best be represented as +X+XPKφXφ (X – variable; φ – hydrophobic residue; + – positively charged residue; P – proline; K – lysine).

Sequence

```
a           TAPDVDLHLKAPKIGFSGPKLEGG
b  DSPDINIEGPDVKIPKFKKPKFGFGPKSPKADIKSP
c  PDVDLQGPEAK*IKFPKFSMPKIGI
d      NLDTSKFAGGLHFSGPKVEGGVKGGQI
e          GSGKVTFPKMKIPKFTFSGRELVG
f          SEVKLKKSKIKMPKFNFSKPKGKGGVT
g  AEAEASSPKGKFSLFKSKKPRHRS
h            LEGGKVKGKHGKLKFGTFGGLGSKSKGHYE
Consensus              +X+XPKφXφ
```

Figure 3.1. Mapping the A10A2^{C82S} binding site on the C-terminal region of AHNAK by peptide array analysis.

A peptide array of the Asp4884-Glu5890 region of AHNAK was synthesized on a cellulose membrane. Each spot contained an 18-residue peptide shifted by 3 residues from its predecessor until the C-terminus was reached. The array was probed with Alexa Fluor 680-A10A2^{C82S} and imaged at 700 nm. The sequences of AHNAK that showed the best interaction with A10A2^{C82S} are listed beside and below the array; sequence *a* (Thr4917 - Gly4940), sequence *b* (Asp4959 - Pro4994), sequence *c* (Pro5220 - Ile5243), sequence *d* (Asn5607 - Ile5633), sequence *e* (Gly5652 - Gly5675), sequence *f* (Ser5703 - Thr5729), sequence *g* (Ala5757 - Ser5780), sequence *h* (Leu5808 - Glu5837). These sequences were used to define a consensus sequence showing positively charged (+), hydrophobic (φ) and variable (X) residues using the Blocks Server (blocks.fhcrc.org).

Examination of the sequences that interact with A10A2^{C82S} allowed for the identification of some general trends. For example, sequences *b*, *e* and *f* show the highest sequence similarity while the most intense binding at any one spot was observed within sequences *b* and *e* (4968-4985, 5652-5669). Since the residues of the conserved motif for these sequences are identical, the differences in the binding intensities for A10A2^{C82S} could indicate that the variable residues in the motif or residues on the periphery may be important for the interaction. For instance the presence of a methionine and an isoleucine with rather smaller sidechains at the respective second and fourth positions of the conserved motif of sequence *e*, instead of a phenylalanine with a ring in the sidechain at the second position or a lysine with a long, charged sidechain at the fourth position of sequence *b*, could enhance the interaction.

Sequences *a*, *d* and *g* showed weaker interactions with the A10A2^{C82S} protein likely due to one or more substitutions within the consensus region. For example, sequences *a* and *d* have a histidine at the first position instead of lysine, while sequences *d* and *g* have a small non-polar residue (G/S) at the last position in place of a larger hydrophobe. Sequence *c* is unusual due to the presence of two possible consensus sequences, the first as shown in Figure 3.1 and an alternate sequence starting at K5228, five residues prior to the indicated consensus sequence.

In general, these results agree with a previous study in which the S100A10-annexin A2 binding region within the C-terminus of AHNAK was mapped utilizing a series of GST-AHNAK deletion mutants by pull-down assays (De Seranno et al. 2006). A 20-residue region in the C-terminus of AHNAK corresponding to residues 5654-5673

(lying within sequence *e*, residues 5652-5675) was shown to be sufficient for binding to the S100A10-annexin A2 complex. Further deletions from the N- or C-terminal extremity of this 20-residue peptide abolished the interaction with the S100A10-annexin A2 complex, confirming that these residues are crucial for the interaction (De Seranno et al. 2006).

3.3.2 Unique Interactions of AHNAK with the S100A10-Annexin A2 Complex

A 20-residue AHNAK peptide (5654-5673; referred to as AHNAK5) that displayed a strong interaction with A10A2^{C82S} based on the peptide array experiments, and was consistent with GST-AHNAK pull-down assays (De Seranno et al. 2006) was synthesized and used in NMR titration experiments. Initially, the AHNAK5 peptide was titrated into ^{15}N-labeled S100A10^{C82S} in complex with an unlabeled annexin A2 peptide (residues 1-15) (Figure 3.2, black). In the absence of AHNAK5, a single resonance was observed in the ^{1}H-^{15}N HSQC spectrum for each residue in S100A10^{C82S}, consistent with the symmetric structure of the S100A10^{C82S}-annexin A2 complex where only the ^{15}N-labeled S100A10^{C82S} is visible (black spectrum). Titration of unlabeled AHNAK5 peptide to this solution led to the gradual disappearance of many of the S100A10^{C82S} resonances in the S100A10^{C82S}-annexin A2 complex and the reappearance of new peaks, indicative of a slow exchange process (Figure 3.2, pink). Remarkably, the ^{1}H-^{15}N HSQC spectrum of the ^{15}N-labeled S100A10^{C82S} in the presence of annexin A2 and AHNAK5 resulted in an increased number of peaks that did not change even in the presence of a four-fold excess of AHNAK5 peptide. In addition, many of the new resonances appeared in pairs

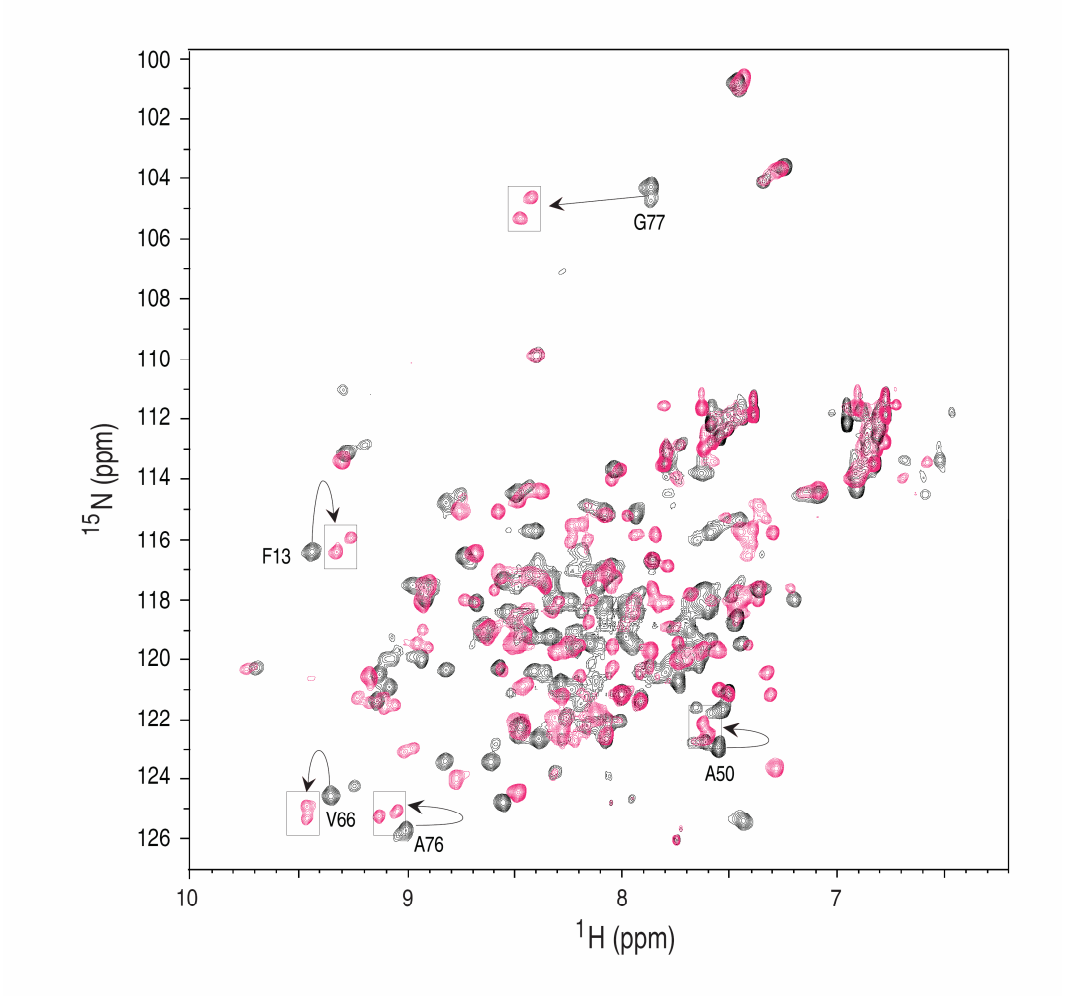

Figure 3.2. An overlay of ^{1}H-^{15}N HSQC spectrum of annexin A2-bound S100A10^{C82S} in complex with the AHNAK5 peptide.

^{1}H-^{15}N HSQC spectrum of 0.5 mM ^{15}N-labeled S100A10^{C82S} (protomer concentration) bound to 0.5 mM unlabeled annexin A2 peptide (Ac-STVHEILSLKQLEGD) (black) and in complex with 0.25 mM AHNAK5 (Ac-GKVTFPKMKIPKFTFSGREL) (pink). Peaks that exhibited obvious multiplicity in the AHNAK5 complex are labeled according to their one-letter amino acid code and residue number. Spectra were collected on a Varian Inova 600 MHz spectrometer at 35 ºC in 90% H_2O/10% D_2O at pH 7.0.

with each peak having approximately 50% of the intensity of the original peak (Figure 3.2). For example, Phe13, Val66, Ala76 and Gly77 in ^{15}N-labeled S100A10^{C82S} all appeared as two peaks in the ^{1}H-^{15}N HSQC spectrum of S100A10^{C82S}-annexin A2 in complex with AHNAK5.

To examine the effects of AHNAK5 binding on the annexin A2 portion of S100A10-annexin A2 complex, NMR titration experiments were repeated using the ^{15}N-labeled A10A2^{C82S} hybrid protein. The ^{1}H-^{15}N HSQC spectrum of A10A2^{C82S} (Figure 3.3, black) was very similar to that of the S100A10^{C82S}-annexin A2 complex (Figure 3.2) indicating the structures and interactions of the S100A10 and annexin A2 are similar in the two complexes (Rezvanpour et al. 2009). In addition, since the annexin A2 portion of A10A2^{C82S} was also ^{15}N-labeled, resonances from this segment of the hybrid protein (ie. Leu112, G114) were clearly visible in the spectrum. Similar to the S100A10^{C82S}-annexin A2 peptide complex, addition of AHNAK5 to the ^{15}N-labeled A10A2^{C82S} protein led to the disappearance of peaks from S100A10^{C82S} and annexin A2 and the appearance of new resonances on the slow exchange time scale. Upon saturation, the ^{1}H-^{15}N HSQC spectrum of ^{15}N-labeled A10A2^{C82S} bound to unlabeled AHNAK5 (Figure 3.3, cyan) bore a strong resemblance to that of ^{15}N-labeled S100A10^{C82S} in complex with both unlabeled annexin A2 and AHNAK5 peptides (Figure 3.2). This included an increased number of peaks in the A10A2^{C82S} spectrum where several resonances from the S100A10^{C82S} protein appeared as pairs (Phe13, Val66, Ala76, Gly77). Interestingly, some resonances from the annexin A2 portion of A10A2 also exhibited peak doubling upon addition of AHNAK5

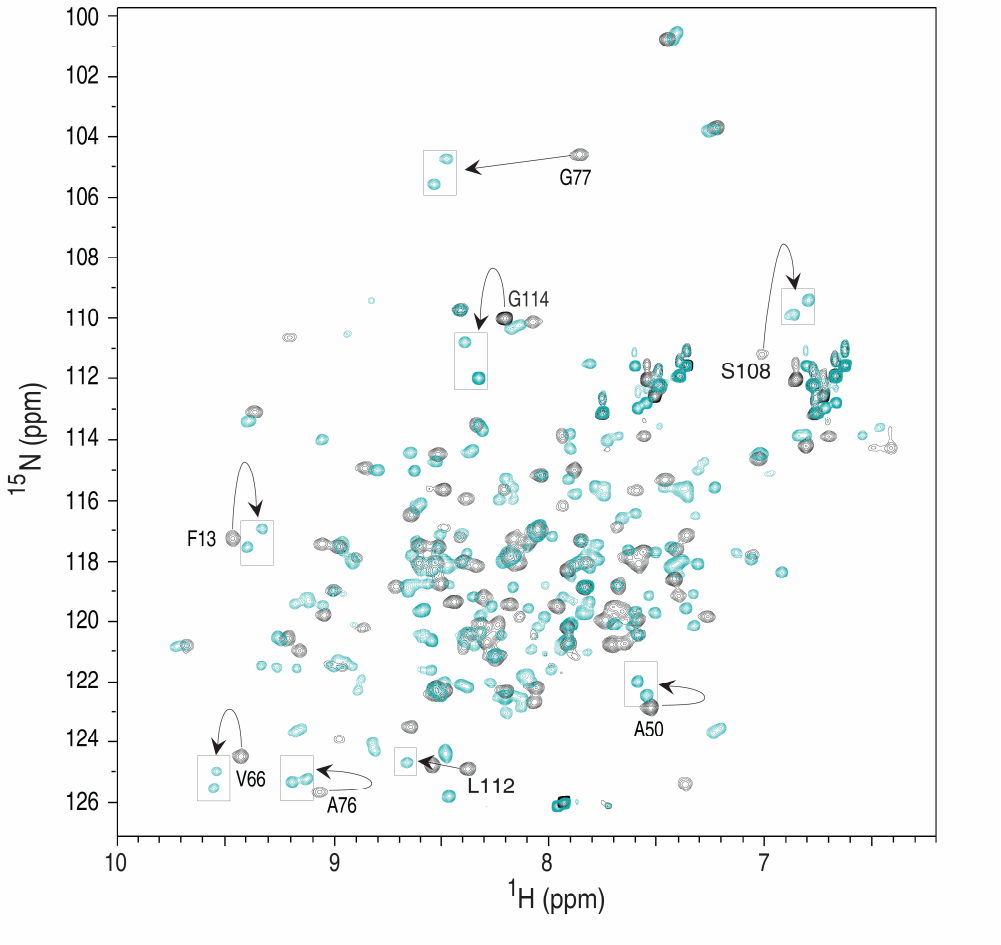

Figure 3.3. An overlay of ^{1}H-^{15}N HSQC spectrum of A10A2^{C82S} hybrid protein bound to the AHNAK5 peptide.

^{1}H-^{15}N HSQC spectrum of 0.5 mM uniformly ^{15}N-labeled A10A2^{C82S} hybrid protein (protomer) (black) and in complex with 0.25 mM AHNAK5 peptide (Ac-GKVTFPKMKI PKFTFSGREL) (cyan). Peaks that exhibited multiplicity in the AHNAK5 complex are labeled according to their one-letter amino acid code and residue number. Spectra were collected on a Varian Inova 600 MHz spectrometer at 35 ºC in 90% H_2O/10% D_2O at pH 7.0.

(L112, G114), indicating that binding of AHNAK5 affected both the S100A10^{C82S} and annexin A2 portions of the hybrid protein in a similar fashion.

The increased number of resonances and multiplicity of some peaks in both the S100A10^{C82S}-annexin A2 and A10A2^{C82S} complexes with AHNAK5 is in contrast to ^{1}H-^{15}N HSQC spectra of many other S100-target peptide complexes including Ca^{2+}-S100B with CapZ, p53 or NDR kinase, S100A6 with Siah1-interacting protein, and S100A1 in complex with CapZ or RyR (Rustandi et al. 2000; Inman et al. 2002; McClintock and Shaw 2003; Lee et al. 2008; Wright et al. 2008; Wright et al. 2009). NMR spectra from these complexes all display a similar number of resonances in the presence or absence of target, indicating a symmetric relationship in the dimer is maintained. This is borne out in three-dimensional structures of the complexes. In order to account for the unique spectral observations made for the S100A10^{C82S}-annexin A2 complex with AHNAK5 several models were considered including displacement of annexin A2 by AHNAK5, multiple orientations of AHNAK5 binding and asymmetric binding of a single AHNAK5 peptide to the S100A10^{C82S}-annexin A2 complex.

3.3.3 Asymmetric Binding of AHNAK to the A10A2 Dimer

Titrations of ^{15}N-labeled S100A10^{C82S} with AHNAK5 in the absence of annexin A2 peptide did not show an interaction between S100A10^{C82S} and AHNAK5 and resulted in precipitation of the sample. Analysis of the NMR experiments using ^{15}N-labeled A10A2^{C82S} titrated with unlabeled AHNAK5 peptide were carried out to investigate the stoichiometry and affinity of the interaction (Figure 3.4). The change in the peak

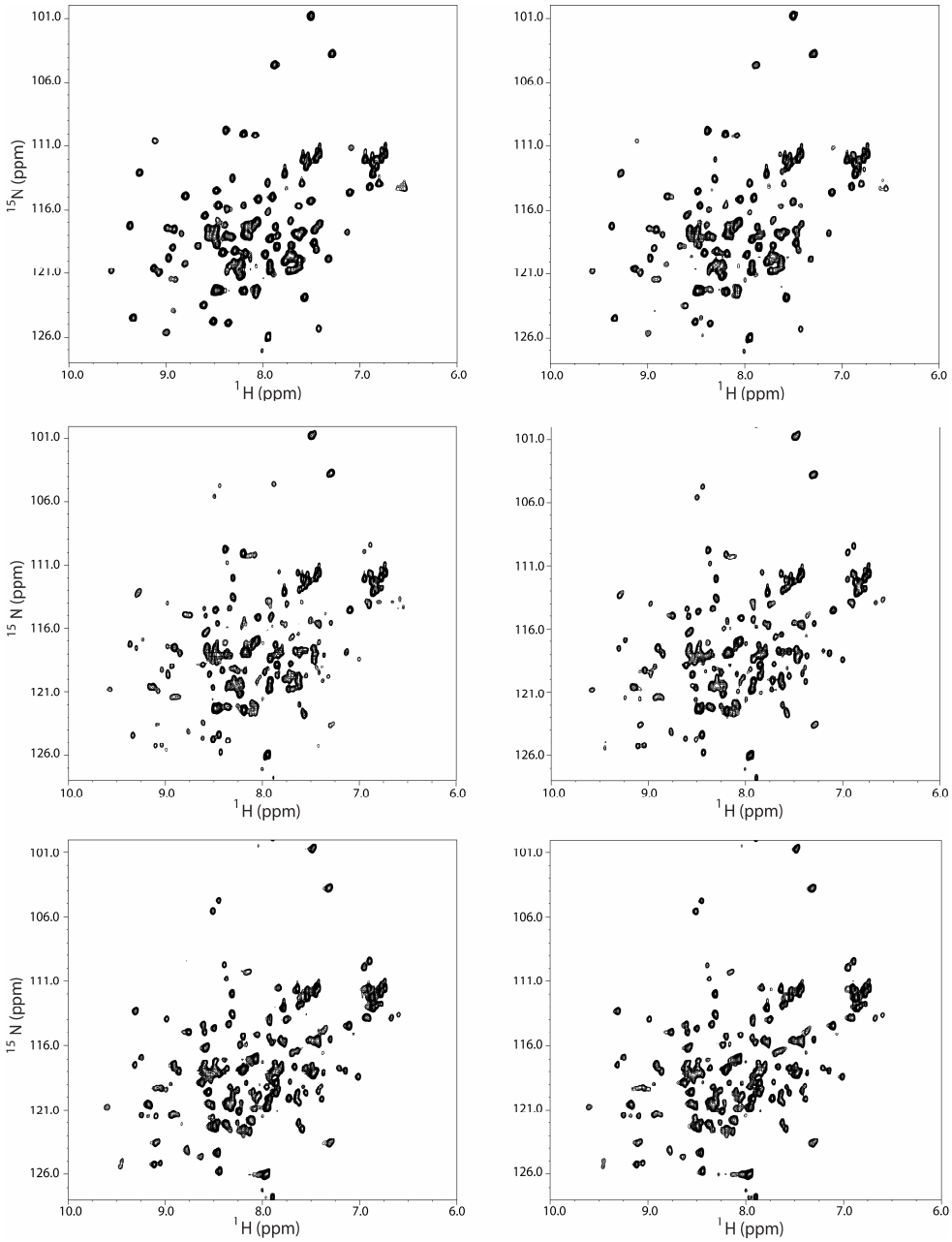

Figure 3.4. Titration of A10A2^{C82S} with the AHNAK5 peptide.

Representative ^{1}H-^{15}N HSQC spectra from the AHNAK5 titration are illustrated. Small additions of AHNAK5 peptide were made into a sample of uniformly ^{15}N, ^{13}C-labeled A10A2^{C82S} (143 μM dimer concentration). Spectra shown are at **(A)** 0 equivalents, **(B)** 0.29 eq., **(C)** 0.58 eq., **(D)** 0.78 eq., **(E)** 0.97 eq., and **(F)** 1.07 eq. of AHNAK5 peptide relative to the protein concentration. Many of the new resonances appeared in pairs with each peak having approximately 50% of the intensity of the original peak.

intensities of Gly40, Val51, Gly77 in S100A10^{C82S}, and Leu112 in annexin A2 were plotted as a function of AHNAK5 and A10A2^{C82S} concentrations (Figure 3.5). The data show near linear decreases for the peak intensities in ^{15}N-labeled A10A2^{C82S} (Figure 3.5A) and concomitant increases in the peaks intensities in the AHNAK5 complex (Figure 3.5B). The inflection point for the data sets occurs near a stoichiometry of one AHNAK5 peptide to one A10A2^{C82S} dimer. Fitting for this interaction indicated a K_d less than 1 μM although a precise determination was not possible by this method due to the high A10A2^{C82S} protein concentrations used in the NMR experiments. The data were also fit for the interaction of two AHNAK5 peptides per A10A2^{C82S} dimer, similar to other S100-target peptide complexes that display symmetric binding (Figure 3.5C). This resulted in obvious disagreement with the data, indicating the 2:1 AHNAK:A10A2^{C82S}(dimer) model was incorrect.

To provide further evidence for a 1:1 AHNAK:A10A2^{C82S}(dimer) stoichiometry and to show that both proteins are required for the recruitment of AHNAK5, a mixture of A10A2^{C82S} and AHNAK5 was subjected to non-denaturing electrospray mass spectrometry (ES-MS) (Figure 3.6) (Loo 2000). This data showed three major peaks in the spectrum corresponding to the A10A2^{C82S} protomer (MW_{obs} = 13731.8 Da, MW_{calc} = 13733.8 Da), A10A2^{C82S} dimer (MW_{obs} = 27462.4 Da, MW_{calc} = 27467.6 Da) and the A10A2^{C82S} dimer in complex with a single AHNAK5 peptide (MW_{obs} = 29815.5, MW_{calc} = 29820.4 Da). The ES-MS spectrum also showed the absence of a peak at 32173.2 Da that would be expected for the mass of the A10A2^{C82S} dimer in complex with two AHNAK5 peptides. This result corroborated the NMR titration experiments that showed

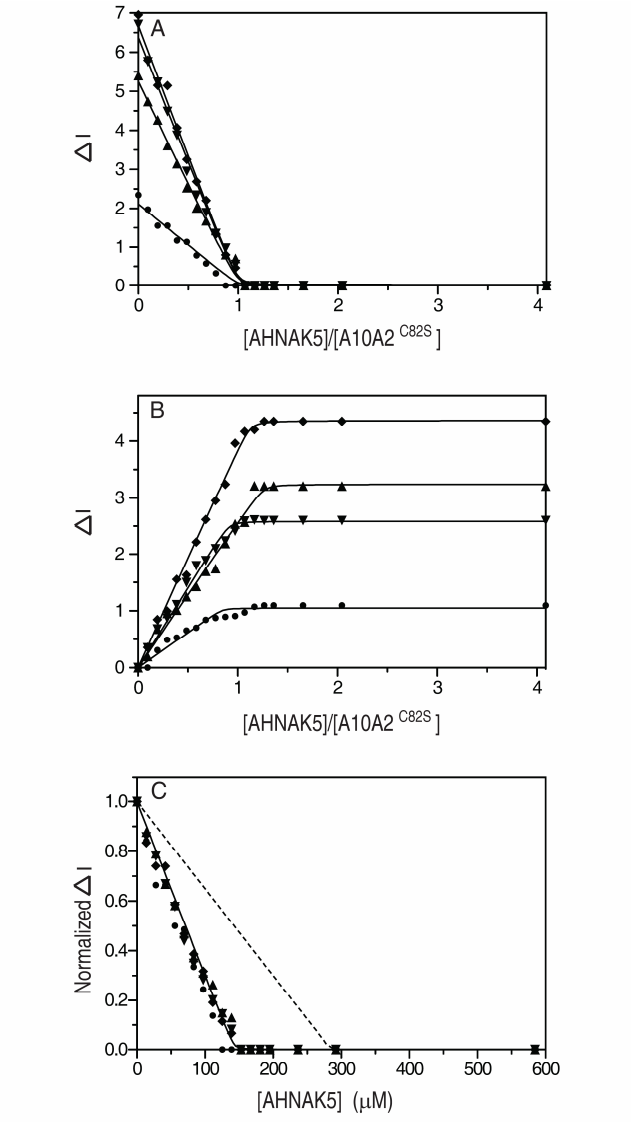

Figure 3.5. Binding plots of A10A2^{C82S} with AHNAK5 peptide measured from ^{1}H-^{15}N HSQC experiments.

Aliquots of the unlabeled AHNAK5 peptide were added to a solution of 143 μM ^{15}N, ^{13}C-labeled A10A2^{C82S} (dimer concentration) and the resulting changes in peak intensities were monitored. The binding between AHNAK5 and A10A2^{C82S} is shown as the plot of **(A)** decrease, and **(B)** increase in peak intensities for Gly40 (●), Val51 (♦) and Gly77 (▲) in S100A10^{C82S} and Leu112 (▼) in annexin A2 as a function of the AHNAK5:A10A2^{C82S} ratio. **(C)** The normalized change in peak intensities are shown as a function of AHNAK5 concentration. Data sets for Gly40 (●), Val51 (♦), Gly77 (▲), and Leu112 (▼) were globally fit for 1:1 (——) and 2:1 (-----) AHNAK5:A10A2^{C82S} stoichiometries. Data fitting is described in the Materials and Methods Section 3.2.12.

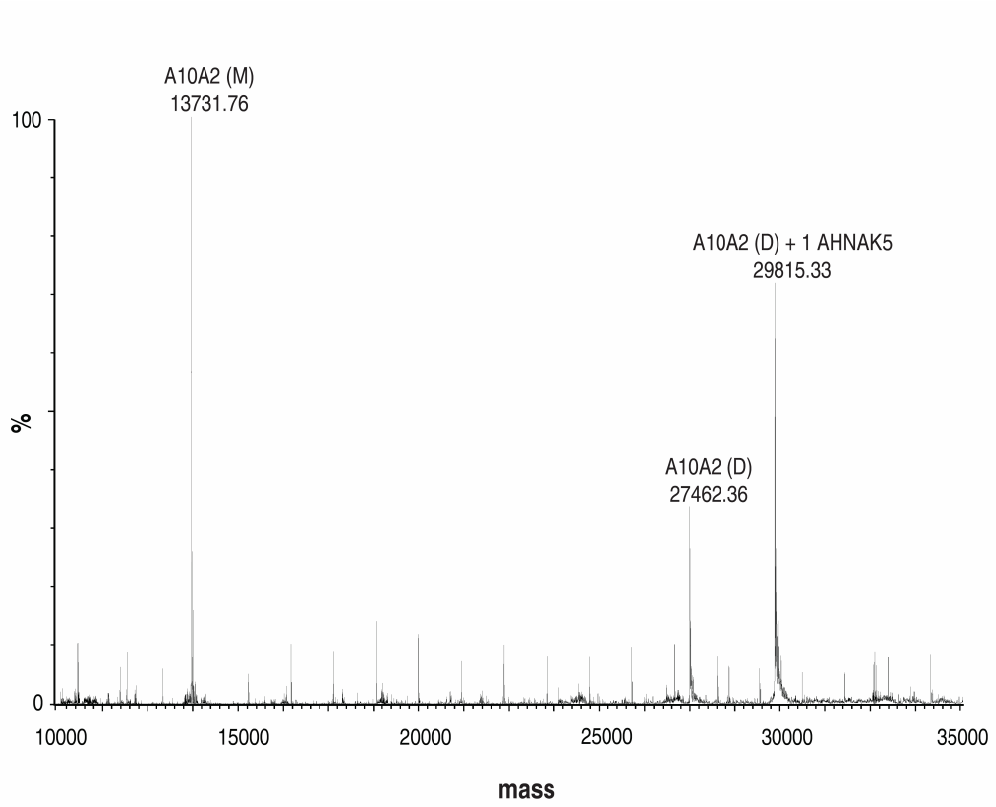

Figure 3.6. Mass spectrum showing the complex formed between A10A2^{C82S} hybrid protein and AHNAK5 peptide.

A10A2^{C82S} protein mixed with the AHNAK5 peptide illustrating masses attributed to the A10A2^{C82S} protomer (M), A10A2^{C82S} dimer (D), and A10A2^{C82S} dimer complexed with a single AHNAK5 peptide. The spectrum was obtained under non-denaturing conditions as described in the Materials and Methods Section 3.2.10.

only one AHNAK5 peptide is bound to the A10A2^{C82S} dimer. In separate experiments, S100A10^{C82S} was mixed with both the annexin A2 and AHNAK5 peptides (Figure 3.7). A representative ES-MS spectrum showed peaks representing the S100A10^{C82S} protomer (MW_{obs} = 11598.2 Da, MW_{calc} 11598.6 Da), S100A10^{C82S} dimer (MW_{obs} = 23196.3 Da, MW_{calc} = 23197.2 Da) and S100A10^{C82S} dimer bound to two annexin A2 peptides (MW_{obs} = 26530.4 Da, MW_{calc} = 26531.4). There was little evidence for a peak corresponding to an S100A10^{C82S} protomer bound to a single annexin A2 peptide (MW_{calc} = 13266.8 Da) in agreement with the crystal structure that shows the annexin A2 binding site comprises regions from both subunits of the S100A10 dimer (Rety et al. 1999). The second most intense peak in the ES-MS spectrum corresponded to the S100A10^{C82S} dimer in complex with two annexin A2 peptides and a single AHNAK5 peptide (MW_{obs} =28883.9 Da, MW_{calc} = 28884.2 Da). Repeated experiments showed no evidence of complexes with masses corresponding to the S100A10^{C82S} dimer complexed with either one or two AHNAK5 peptides (MW_{calc} = 25549.9 Da, 27901.9 Da). Similarly, a mixture of S100A10^{C82S} and AHNAK5 was subjected to non-denaturing ES-MS (Figure 3.8). This data showed three major peaks in the spectrum representing the S100A10^{C82S} protomer (MW_{obs} = 11598.7 Da, MW_{calc} = 11598.6 Da), S100A10^{C82S} dimer (MW_{obs} = 23196.5 Da, MW_{calc} = 23197.2 Da), and S100A10^{C82S} dimer in complex with a single AHNAK5 peptide (MW_{obs} = 25547.3, MW_{calc} = 25549.9 Da). In addition, a small peak corresponding to mass of the S100A10^{C82S} dimer in complex with two AHNAK5 peptides (MW_{obs} = 27899.9, MW_{calc} = 27902.7 Da) was present on the spectrum. These experiments indicate that the S100A10-annexin A2 complex has a stronger interaction

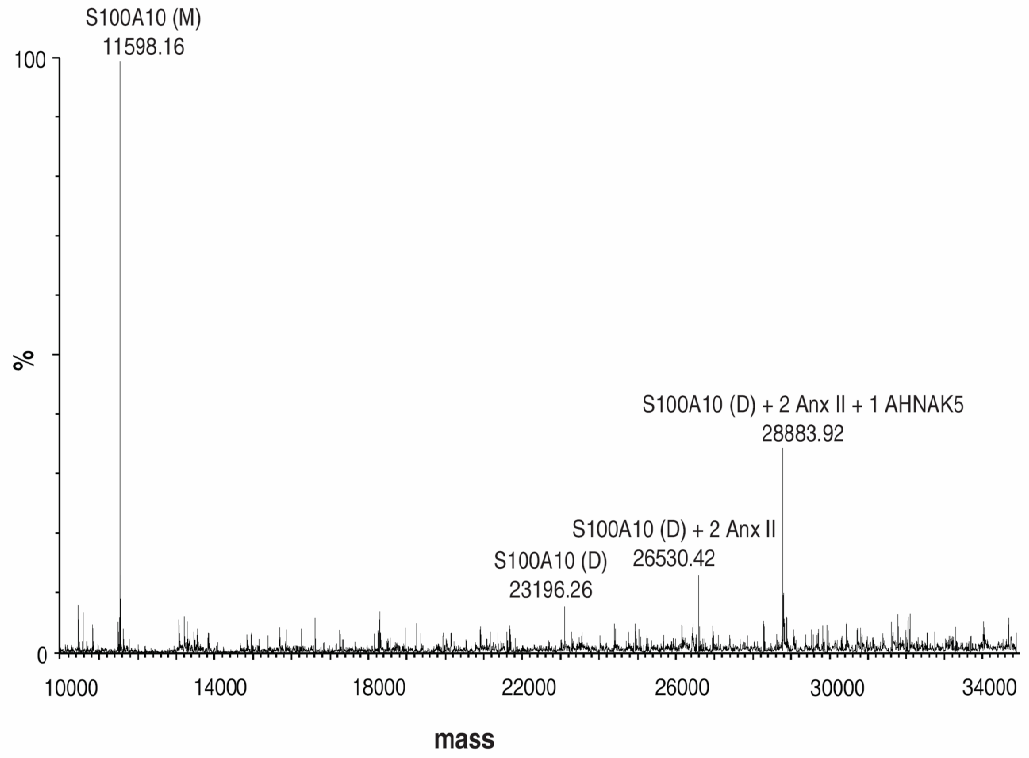

Figure 3.7. Mass spectrum depicting complexes of S100A10^{C82S}, annexin A2 and AHNAK5 peptides.

S100A10^{C82S} mixed with annexin A2 and AHNAK5 peptides showing masses corresponding to the S100A10^{C82S} protomer (M) S100A10^{C82S} dimer (D), S100A10^{C82S} dimer complexed with two annexin A2 peptides and, S100A10^{C82S} dimer complexed with two annexin A2 peptides and a single AHNAK5 peptide. The spectrum was obtained under non-denaturing conditions as described in Section 3.2.10.

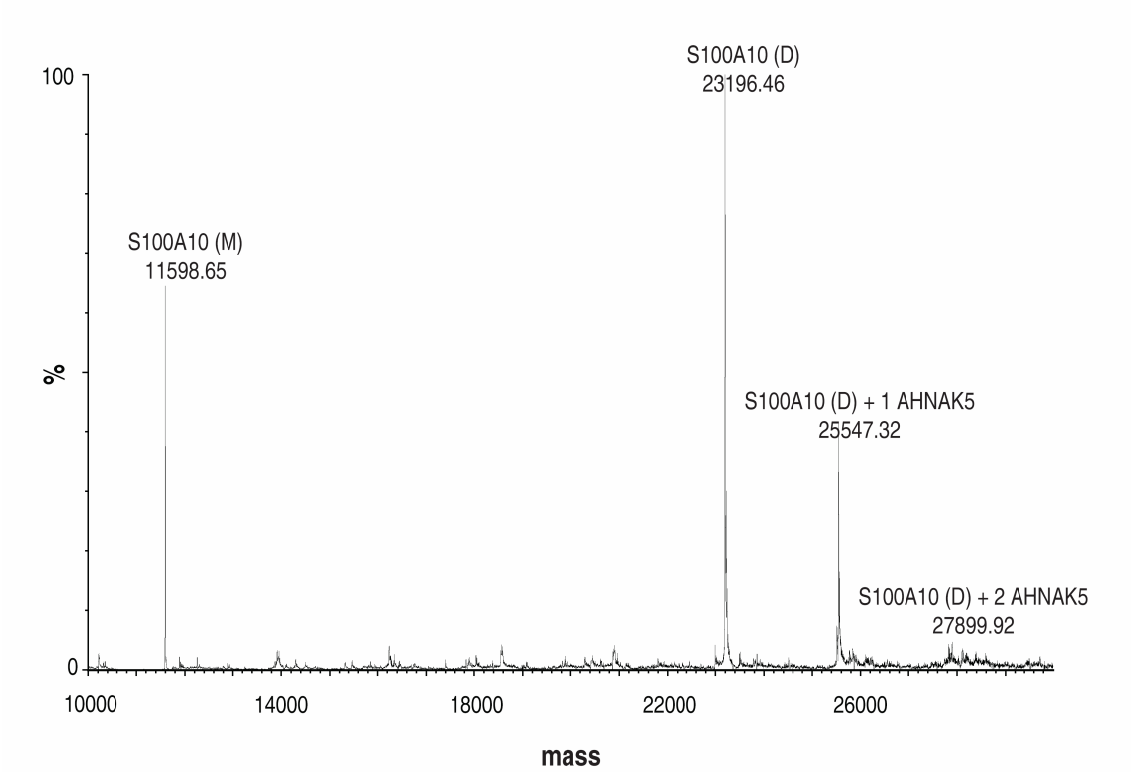

Figure 3.8. Mass spectrum depicting complexes of S100A10^{C82S}, and AHNAK5 peptide.

S100A10^{C82S} mixed with AHNAK5 peptide showing masses corresponding to the S100A10^{C82S} protomer (M), S100A10^{C82S} dimer (D), S100A10^{C82S} dimer complexed with a single AHNAK5 peptide and, S100A10^{C82S} dimer complexed with two AHNAK5 peptides. The spectrum was obtained under non-denaturing conditions as described in Section 3.2.10.

with AHNAK5, while in the absence of annexin A2, a weak interaction could exist between the S100A10^{C82S} protein and AHNAK5.

Fluorescence spectroscopy was used to calculate the binding affinity of AHNAK5 for the A10A2^{C82S} complex and S100A10^{C82S}. Since AHNAK5, A10A2^{C82S} or S100A10^{C82S} do not possess a good intrinsic fluorescence probe, S100A10^{C82S} and the A10A2^{C82S} hybrid proteins were covalently labeled with acrylodan at Cys61 in the second EF-hand loop. Initial fluorescence experiments using acrylodan-labeled S100A10^{C82S} in the absence of the annexin A2 peptide showed less than 12% change in fluorescence and little wavelength shift suggestive of a poor interaction (Figure 3.9A). The normalized change in fluorescence intensity for this titration was plotted as a function of the AHNAK5:S100A10^{C82S}(dimer) ratio (Figure 3.9B). The points were globally fit with a 1:1 ligand binding curve yielding a dissociation constant of 1.75 ± 0.2 μM. In contrast, fluorescence experiments of acrylodan-labeled A10A2^{C82S} had a fluorescence maximum near 495 nm (Figure 3.10A) that decreased in intensity and gradually shifted to 500 nm upon addition of AHNAK5, indicative of a much tighter interaction. The normalized change in fluorescence intensity for this titration was plotted as a function of the AHNAK5:A10A2^{C82S}(dimer) ratio (Figure 3.10B). Global fitting of duplicate data sets with a 1:1 ligand binding curve yielded a dissociation constant of 3.15 ± 0.6 nM. This data confirms that the interaction of AHNAK5 with the A10A2^{C82S} hybrid is markedly stronger than that with S100A10^{C82S} protein alone.

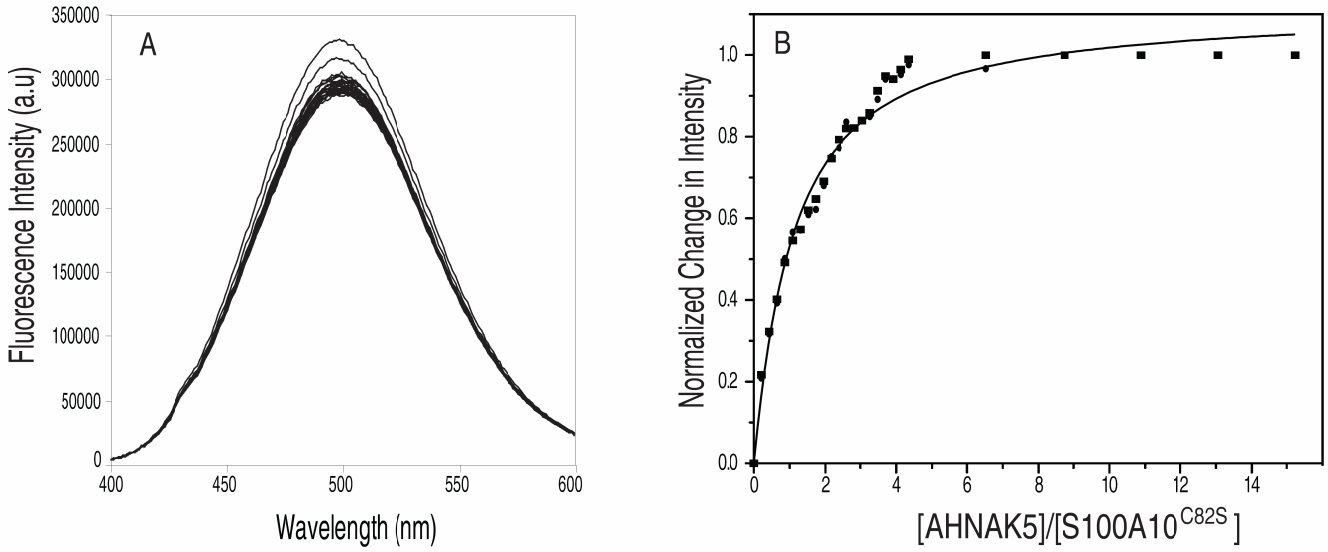

Figure 3.9. The interaction of AHNAK5 with the S100A10^{C82S} protein monitored by fluorescence spectroscopy.

(A) Fluorescence spectra of acrylodan-S100A10^{C82S} (300 nM) showing the change in acrylodan fluorescence with increasing AHNAK5 peptide concentration. **(B)** Binding curve for Acrylodan-S100A10^{C82S} titrated with the AHNAK5 peptide showing the normalized change in fluorescence measured at 500 nm as a function of AHNAK5 concentration. Data was collected from duplicate titrations and curves were fit globally with a 1:1 ligand binding function (solid line).

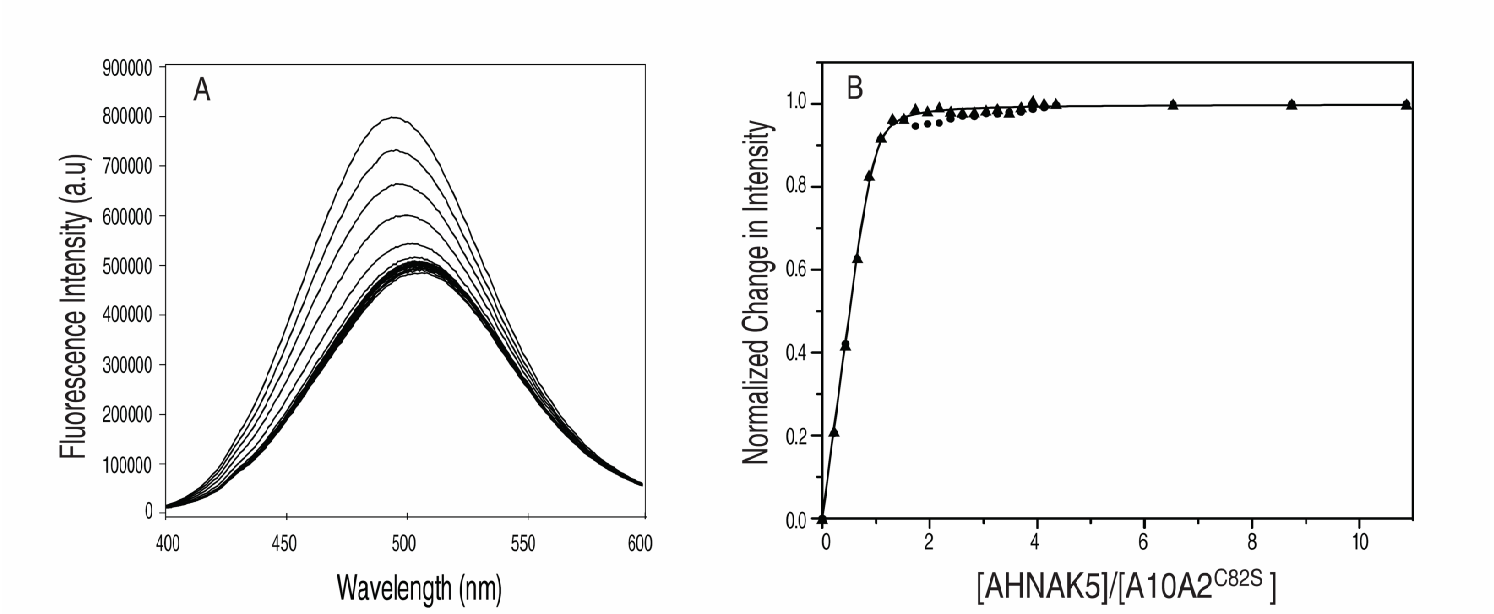

Figure 3.10. The interaction of AHNAK5 with the A10A2^{C82S} hybrid protein monitored by fluorescence spectroscopy.

(A) Fluorescence spectra of acrylodan-A10A2^{C82S} (300 nM) depicting the change in acrylodan fluorescence with increasing AHNAK5 peptide concentration. **(B)** Binding curve for Acrylodan-A10A2^{C82S} titrated with the AHNAK5 peptide showing the normalized change in fluorescence measured at 500 nm as a function of AHNAK5 concentration. Data was collected from duplicate titrations and curves were fit globally with a 1:1 ligand binding function (solid line).

3.3.4 Mapping S100A10 and A10A2 Binding Sites on C-terminal Region of TRPV5

Recent two-hybrid and co-immunoprecipitation experiments provided evidence for interaction of the transient receptor potential cation channel protein TRPV5 and TRPV6 with the S100A10 protein (van de Graaf et al. 2003; Borthwick et al. 2008). In this case, the S100A10-annexin A2 complex is thought to mediate trafficking of the TRPV5 and TRPV6 proteins to the plasma membrane where they act as calcium-selective channels. Although S100A10 forms a ternary complex with annexin A2 and either TRPV5 or TRPV6, a direct interaction between the annexin and TRPV proteins have not been observed. To examine the possible formation of a ternary complex involving S100A10 and annexin A2 proteins, the interaction between TRPV5 with S100A10 alone and the A10A2 complex was tested by peptide array analysis. Peptide arrays containing 18-residue peptides spanning the C-terminal sequence of human TRPV5 (residues 577-730) were synthesized as described in Section 3.2.8. $S100A10^{C82S}$ or $A10A2^{C82S}$ were labeled with Alexa Fluor 680 maleimide at their unique cysteine (C61) in the sequence for peptide array blotting. Cys61 is located in the second calcium-binding loop of S100A10, and is not known to be involved in target-binding. As a result, the Alexa dye should not interfere with the interaction of Alexa-$S100A10^{C82S}$ or -$A10A2^{C82S}$ with any of the peptides.

Alexa-$S100A10^{C82S}$ and -$A10A2^{C82S}$ were used for blotting the peptide arrays to determine whether the N-terminal peptide of annexin A2 in the S100A10-annexin A2 complex is required for the interaction of S100A10 with TRPV5/TRPV6. Peptide array analysis identifies the sequence dependent but structurally independent interactions

between S100A10^{C82S} or A10A2^{C82S} with the series of 18-residue peptides spanning the C-terminal sequence of human TRPV5. The binding regions on TRPV5 were identified by comparing the overlapping TRPV5 peptide sequences on the array that were fluorescent (Figure 3.11A and B). For instance, the sequences for the peptides at position 2G, 2H, and 2I on the TRPV5 18-2 array are WPRSGICGCEFGLGDRWF, RSGICGCEFGLGDRWFLR, and GICGCEFGLGDRWFLRVE, respectively. Thus, each spot on the array differs from the previous one by losing two residues from the N-terminus, while gaining two residues at the C-terminus of the peptide by moving along the protein sequence. Peptide array spots that decreased in fluorescence after a consecutive string of fluorescence spots, specify the importance of the deleted residues for the S100A10^{C82S} interaction. In all of the arrays the amino acid residues important for the interactions are shown in red (Figures 3.11-3.14).

On the TRPV5 18-1 array, S100A10^{C82S} associated with five regions of the C-terminal sequence of TRPV5 (Figure 3.11A), while the protein bound to 4 sites on the TRPV5 18-2 array (Figure 3.11B). The binding sequences for both arrays were very similar. One of the observed differences was that the two sequences spanning S669-W701 (10G-11H) and L688-E720 (12B-13G) on the TRPV5 18-1 array, appeared as one long stretch of residues covering S669-E720 (5A-6D) on the TRPV5 18-2 array. The first interaction site in TRPV5 was located at R594-G620 (2H-3G) in both arrays, which is localized to its intracellular C-terminal tail. This region contains residues 598-603 (VATTV) that is a highly conserved region in both TRPV5/TRPV6 channel proteins. These arrays uncovered specific sequences within TRPV5 that are recognized by

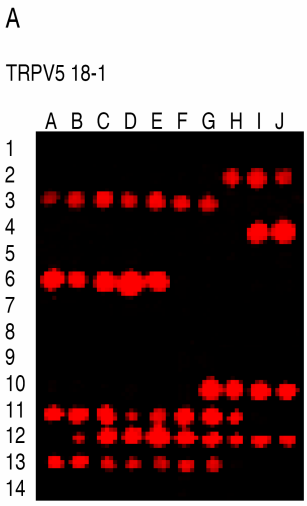

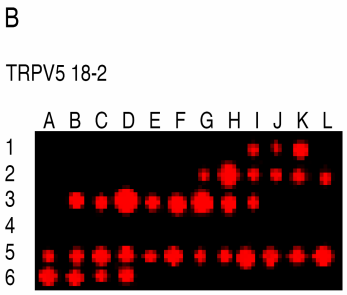

TRPV5 18-1

Position	Sequence
2H-3G	RAQVVATTVMLERKLPRCLWPRSGICG
4I-4J	RSGICGCEFGLGDRWFLRV
6A-6E	DRWFLRVENHNDQNPLRVLRYV
10G-11H	SGTLARASLALPTSSLSRTASQSSSHRGW
12B-13G	LSRTASQSSSHRGWEILRQNTLGHLNLGLNLSE

TRPV5 18-2

Position	Sequence
1I-1K	ELWRAQVVATTVMLERKLPRCL
2G-2L	WPRSGICGCEFGLGDRWFLRVENHNDQN
3B-3I	LGDRWFLRVENHNDQNPLRVLRYVEVFKNSDKED
5A-6D	SGTLARASLALPTSSLSRTASQSSSHRGWEILRQNTLGHL NLGLNLSE

Figure 3.11. Mapping the S100A10 binding site on TRPV5 protein through peptide array analysis.

A peptide array of the C-terminal sequence of human TRPV5 (577-730) was synthesized. Each spot contained an 18-residue peptide shifted by 1 **(A)** or 2 **(B)** residues from its predecessor until the C-terminus was reached. The arrays were probed with Alexa Fluor 680-S100A10^{C82S} and imaged at 700 nm. The sequences of TRPV5 corresponding to the peptides that showed the interaction with S100A10^{C82S} are listed below the array, with the residues important in the interaction in red.

S100A10^{C82S}. Furthermore, since the TRPV5 18-1 array shifted by only a single residue at each spot, it allowed to examine the importance of every residue in the protein sequence. These residues are indicated in red in Figure 3.11.

To determine whether the interaction of S100A10 with the N-terminal region of annexin A2 alters the binding of S100A10 on the TRPV5 protein, similar peptide arrays were probed with Alexa-A10A2^{C82S} (Figure 3.12A and B). A10A2^{C82S} associated with five regions on the C-terminal sequence of TRPV5 on the 18-1 array (Figure 3.12A), while the protein bound to 4 sites on the TRPV5 18-2 array (Figure 3.12B). The two sequences spanning D590-G620 (2D-3G) and R615-V633 (4I-4J) on the TRPV5 18-1 array, appeared as one extended sequence covering E591-D638 (1H-2K) on the TRPV5 18-2 array. Interestingly, the interaction sites found on the arrays blotted with Alexa-A10A2^{C82S}, were similar to those probed with Alexa-S100A10^{C82S} (Figure 3.11A and B). This suggests that association of S100A10^{C82S} with TRPV5 is not modified when S100A10^{C82S} is in complex with the N-terminal peptide of annexin A2. This shows the binding site of TRPV5 on the S100A10^{C82S} is different from that of the N-terminal peptide of annexin A2 protein. Consequently, the interaction of TRPV5 with the S100A10^{C82S}-annexin A2 complex is unlike the AHNAK protein, whereby residues from both the S100A10^{C82S} and annexin A2 are required for the strong interaction of the AHNAK with the complex.

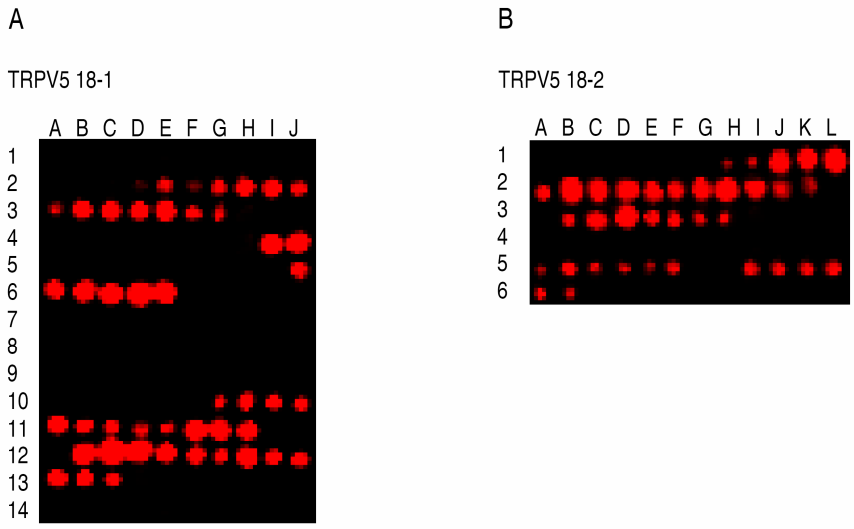

TRPV5 18-1	
Position	Sequence
2D-3G	DELWRAQVVATTVMLERKLPRCLWPRSGICG
4I-4J	RSGICGCEFGLGDRWFLRV
5J-6E	GDRWFLRVENHNDQNPLRVLRYV
10G-11H	SGTLARASLALPTSSLSRTASQSSSHRGW
12B-13C	LSRTASQSSSHRGWEILRQNTLGHLNLGL

TRPV5 18-2	
Position	Sequence
1H-2K	ELWRAQVVATTVMLERKLPRCLWPRSGICGCEF GLGDRWFLRVENHND
3B-3H	DRWFLRVENHNDQNPLRVLRYVEVFKNSDK
5A-5F	SGTLARASLALPTSSLSRTASQSSSHRG
5I-6B	SRTASQSSSHRGWEILRQNTLGHLNLGL

Figure 3.12. Identification of the A10A2^{C82S} binding region on TRPV5 protein.

A peptide array scanning the C-terminal sequence of human TRPV5 (577-730) was synthesized with each spot containing an 18-residue peptide that moves through the sequence by 1 **(A)** or 2 **(B)** residues for each spot. The arrays were blotted with Alexa Fluor 680-A10A2^{C82S} and imaged at 700 nm. The sequences of TRPV5 corresponding to the peptides that were found to interact with A10A2^{C82S} are listed below the array, with the residues important for the interaction in red.

3.3.5 S100A10 Binds to Specific Regions on Annexin A2

The crystal structure of apo-S100A10 in complex with annexin A2 is only comprised of the first twelve N-terminal residues of the annexin A2 protein (Rety et al. 1999). Consequently, this structure does not show other potential binding sites of S100A10 on the annexin A2 protein. To identify additional regions of annexin A2 that are involved in S100A10 binding, two peptide arrays containing 18-residue peptides spanning the entire sequence of human annexin A2 were synthesized as described in Section 3.2.8. The arrays were blotted with Alexa-S100A10^{C82S} or -A10A2^{C82S}, and stripped to eliminate the background fluorescence and non-specific interactions.

On the annexin A2 18-2 array, S100A10^{C82S} associated with eleven regions of annexin A2 protein (Figure 3.13A). The first interaction site (1A-1A) was found in the first 18 residues of the N-terminal tail of annexin A2 (M1-S18), which had shown a strong interaction with the S100A10 protein in the crystal structure (Rety et al. 1999). This interaction did not seem as strong compared to some other spots on the array, indicating the presence of other regions on the annexin A2 sequence that have stronger binding with S100A10^{C82S}. The second and third binding regions, L13-D34 and V51-H94, (1G-1I and 2J-3G) encompass the linker that connects the N-terminus of annexin A2 to repeat I (refer to Section 1.5, Figure 1.5) as well as helices A-D of repeat I, respectively. These two regions are located on one side of the annexin A2 protein, however, only the linker and helices A and B of repeat I are accessible to interact with residues of S100A10. A closer look at the structure of annexin A2 indicates that binding regions comprised of E125-E142 (4O-4O), I129-K148 (5A-5B), S161-A180 (6A-6B), I191-T208 (6P-6P), and

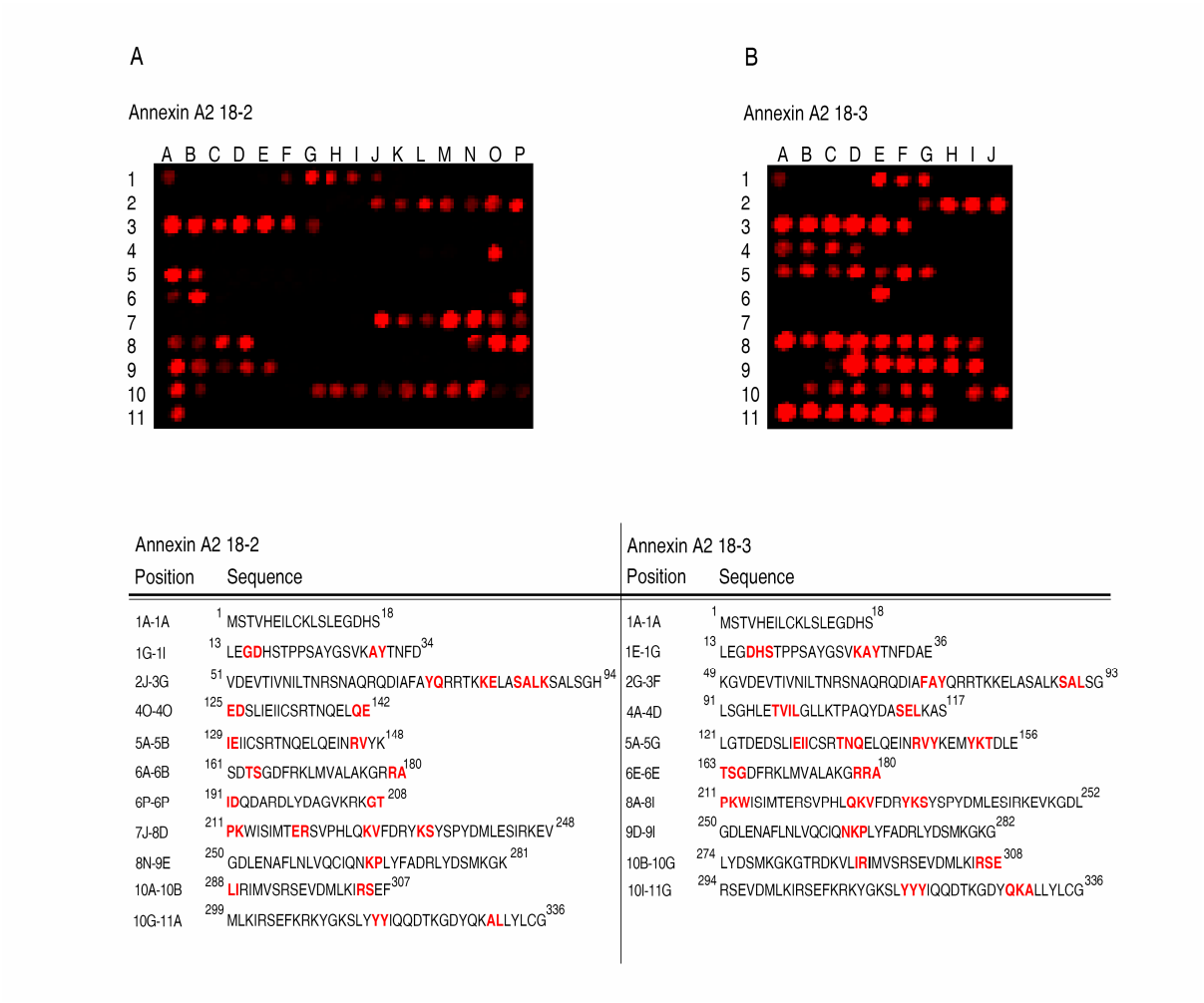

Figure 3.13. Mapping the S100A10^{C82S} binding site on annexin A2 protein through peptide array analysis.

A peptide array of the entire sequence of human annexin A2 was synthesized on a cellulose membrane. Each spot contained an 18-residue peptide shifted by 2 **(A)** or 3 **(B)** residues from its predecessor until the C-terminus was reached. The arrays were probed with Alexa Fluor 680-S100A10^{C82S} and imaged at 700 nm. The sequences of annexin A2 corresponding to the peptides that showed the best interaction with S100A10^{C82S} are listed below the array, with the residues important in the interaction in red.

G250-K281 (8N-9F) are all located at the core of annexin A2 molecule and are not available for interaction with S100A10^{C82S}. The fact that all of these regions appeared as a short or single fluorescence spot on the array is an indication for non-specific interactions of the protein to these peptides. It is noteworthy that some of the interactions observed could also be due to sequence similarity of the helices within each repeat unit of annexin A2. One of the strongest binding regions, P211-V248 (7J-8D), includes helix C of repeat III (Figure 1.5) where the N-terminal tail of annexin A2 is packed against. Therefore, it is not surprising to observe the association of S100A10^{C82S} with this region. Finally, the binding sites encompassing L288-E307 (10A-10B) and M300-K336 (10G-11A) contain the linker connecting helices B to C, as well as helices C, D, and E of repeat IV of annexin A2. These sites are located at the same side as the N-terminal tail of annexin A2, and are accessible for binding to S100A10.

Comparable results were observed for the annexin A2 18-3 array. However, S100A10^{C82S} associated with ten regions of annexin A2 protein (Figure 3.13B). Two of the interaction sites, E125-E139 (4O-4O), and I191-T208 (6P-6P), present in the annexin A2 18-2 array, were not observed on this array confirming that the single fluorescence spots were indeed non-specific. An additional weak interaction was also noted at L91-S117 (4A-4D) that is not available for interaction with S100A10.

In order to determine whether the interaction of S100A10^{C82S} with the N-terminal tail of annexin A2 alters the binding of S100A10^{C82S} to other regions of annexin A2, similar peptide arrays were probed with Alexa Fluor 680-labeled A10A2^{C82S} protein (Alexa-A10A2) (Figure 3.14A and B). In the A10A2^{C82S} hybrid protein, the S100A10^{C82S}

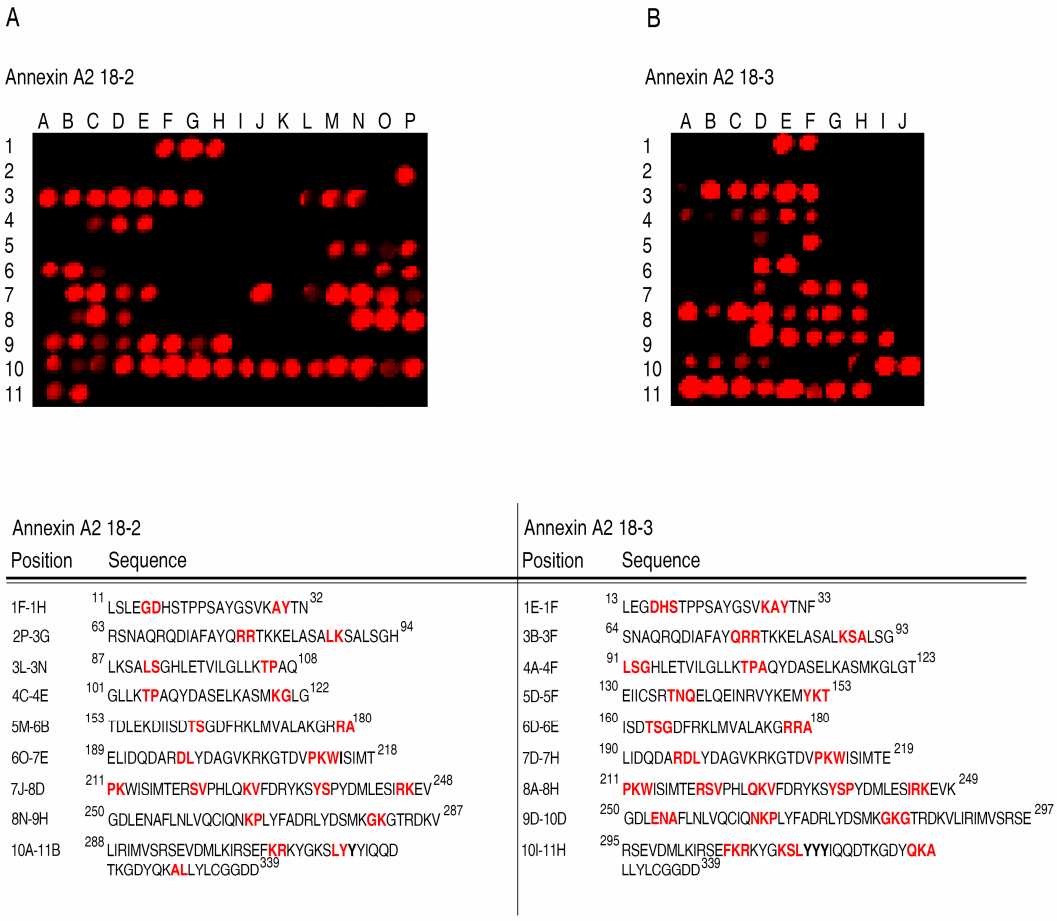

Figure 3.14. Identification of the A10A2^{C82S} binding region on annexin A2 protein.

A peptide array scanning the entire sequence of human annexin A2 was synthesized. Each spot contained an 18-residue peptide shifted by 2 **(A)** or 3 **(B)** residues from its predecessor until the C-terminus was reached. The arrays were blotted with Alexa Fluor 680-A10A2^{C82S} and imaged at 700 nm. The sequences of annexin A2 corresponding to the peptides that were found to interact with A10A2^{C82S} are listed below the array, with the residues important for the interaction in red.

is in complex with the N-terminal tail of annexin A2. As expected, Alexa-A10A2^{C82S} did not interact with the spots containing the N-terminal tail of annexin A2 on the array. In addition, some of the non-specific bindings such as E125-E139 (4O-4O), I129-K148 (5A-5B), and I186-T208 (6P-6P) observed on the arrays blotted with Alexa-S100A10^{C82S}, were absent.

Some of the interaction sites on the arrays blotted with Alexa-A10A2^{C82S} were analogous to those probed with Alexa-S100A10^{C82S} (Figure 3.13A and B), signifying that A10A2^{C82S} associates with similar sequences on the annexin A2 protein. Thus, these interactions are not modified when S100A10^{C82S} is bound to the N-terminal tail of annexin A2. Due to the high number of fluorescent spots on these arrays, it was difficult to identify the stronger binding sites.

3.3.6 Expression and Purification of the Wild-Type Dysferlin C2A Domain

Wild-type forms of human dysferlin C2A domain (simply referred to as dysferlin) (residues 1-138) were overexpressed in the BL21 (DE3) *E. coli* strain. Following the first run on the Ni-NTA column, the His_6 tag was cleaved from the N-terminus of dysferlin. The cleaved protein was not stable in buffer containing imidazole, which is used to elute the protein from Ni-NTA columns. Therefore, cleaved dysferlin was purified on a HiTrap SP FF column. Figure 3.15 shows the SDS-PAGE of the last purification step, indicating a single band at an apparent molecular weight of approximately 14.8 kDa. This roughly corresponds to the calculated molecular weight for human dysferlin (1-138) of 14805.9 Da. Since dysferlin is a calcium-binding protein,

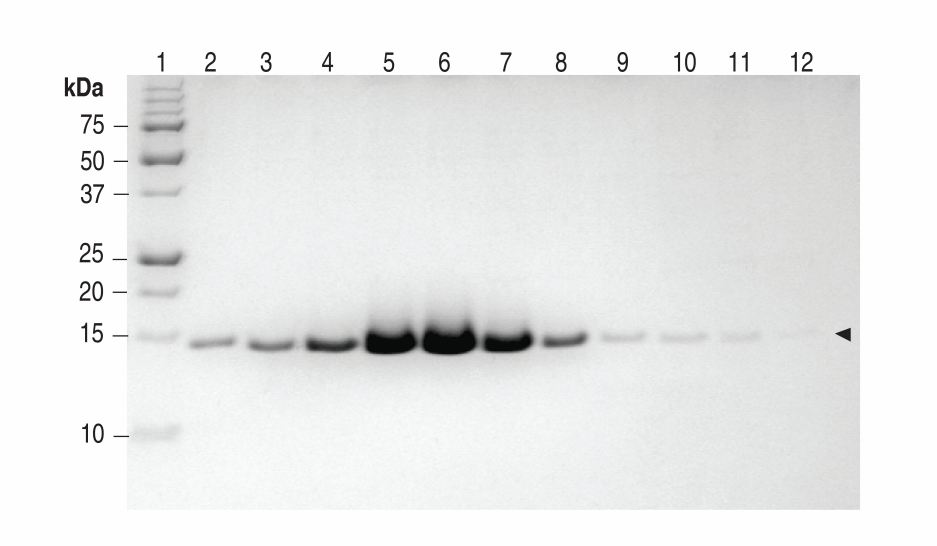

Figure 3.15. Coomassie-stained SDS-PAGE gel (16.5%) depicting the purification of wild-type C2A domain of dysferlin.

Lane 1 contains the protein molecular weight markers, with molecular weights labeled on the left of the gel. Lanes 2-12 contain elution profile of every fraction following removal of His_6 tag on the HiTrap SP FF column. The arrowhead on the right indicates dysferlin protein at molecular weight of approximately 14.8 kDa.

some of the early NMR spectra indicated that after the last purification step the protein was partially bound to calcium. To ensure that dysferlin was in the apo form, 1 mM EDTA was present in the buffers used in the second column run. Before calcium titration experiments, the protein was extensively dialyzed against EDTA-free buffers to remove excess EDTA as it could bind to calcium ions.

3.3.7 Sequential Backbone assignment of S100A10

The structure of S100A10 in the apo state and complexed with the N-terminal peptide of annexin A2 has been solved by X-ray crystallography (Rety et al. 1999). The lack of an NMR assignment of apo-S100A10 makes it difficult to determine the details of the interaction of this protein with target peptides. Thus, the NMR assignment of S100A10 was completed. Wild-type S100A10 was purified. However, concentrating this protein to a usable concentration for NMR samples resulted in rapid precipitation of S100A10. To overcome this problem, dilute S100A10 was dialyzed against a buffer containing equimolar concentrations (50 mM) of arginine and glutamic acid prior to concentration, which was previously shown to stabilize proteins during concentration (Golovanov et al. 2004). Sufficient quantities of wild-type ^{15}N, ^{13}C-labeled S100A10 for NMR samples at a concentration of 1 mM were prepared. However, the ^{1}H-^{15}N HSQC spectrum of this sample showed that the concentrated sample was too viscous which resulted in increasing the line-width of the peaks. Diluting the sample to 500 μM allowed better spectra to be collected for the resonance assignment of the protein. Chemical shift assignments (^{1}H, ^{15}N, and ^{13}C) for S100A10 were accomplished using standard

heteronuclear multiple dimensional NMR spectroscopy (HNCA, HNCACB, CBCA(CO)NH, and HNCO) (Figure 3.16 and 3.17). Figure 3.17 shows a representative ^{1}H-^{15}N HSQC spectrum of S100A10 that is well dispersed, indicating that the protein is well folded. The ^{1}H and ^{15}N backbone amide resonances of S100A10 for 78 out of 93 non-proline residues were assigned (Table 3.1). There were 5 residues on the ^{1}H-^{15}N HSQC spectrum that did not appear on any of the three-dimensional NMR spectra and thus could not be assigned. Most of the remaining residues were not visible on the spectra due to fast exchange with the solvent and could not be assigned.

3.3.8 Interaction Study of Apo- and Calcium Bound Dysferlin C2A Domain with S100A10

To further examine the arrangement of multi-protein complexes involved in membrane repair, the binding region(s) of different proteins within the complexes such as those formed between S100A10 and dysferlin must be uncovered. Sequence alignments of dysferlin with other members of the ferlin family such as synaptotagmin have proposed six potential calcium binding sites in the C2A domain of dysferlin (Britton et al. 2000). Recently, it was shown that the C2A domain of synaptotagmin (Syt1) associates with fibroblast growth factor protein (FGF) as well as one of the members of the S100 family, S100A13, in the presence of calcium (Mohan et al. 2009; Mohan et al. 2010).

The assigned spectra (^{1}H, ^{15}N, and ^{13}C) for the apo-C2A domain of dysferlin (Chantal Forristal, data not published, University of Western Ontario, ON, Canada) and S100A10 would allow the interaction of sites between dysferlin and S100A10 proteins to

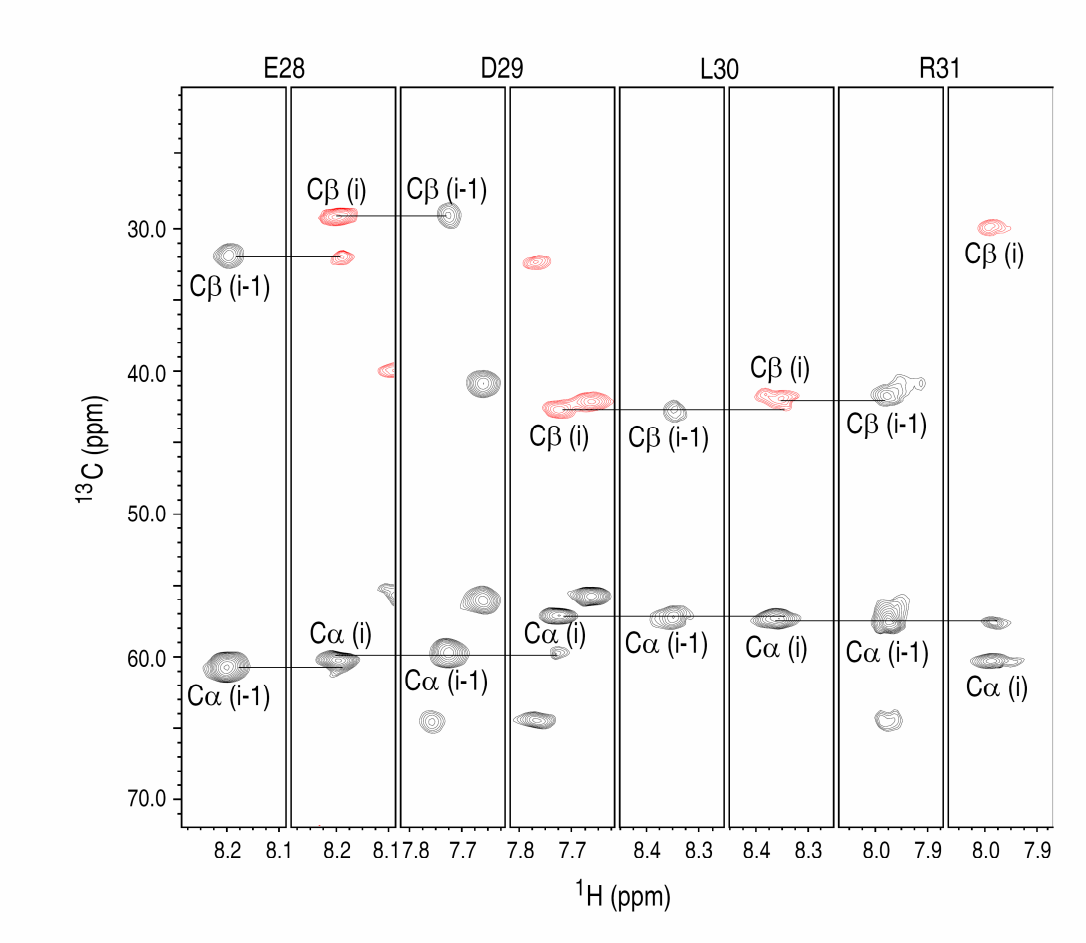

Figure 3.16. Selected regions of 600 MHz NMR spectra used for the backbone assignment of the wild-type S100A10 protein.

For each pair of planes, the CBCA(CO)NH is shown on the left and the HNCACB on the right where the x-axis is the amide proton chemical shift and the y-axis is the ^{13}C plane of the three dimensional experiments. The Cα and Cβ for the intraresidues (indicated as i) are shown on the HNCACB spectra and the corresponding Cα and Cβ for the previous residues (i-1) are shown in the CBCA(CO)NH. The spectra illustrate ^{15}N planes for sequential assignment of residues E28-E31 of the S100A10.

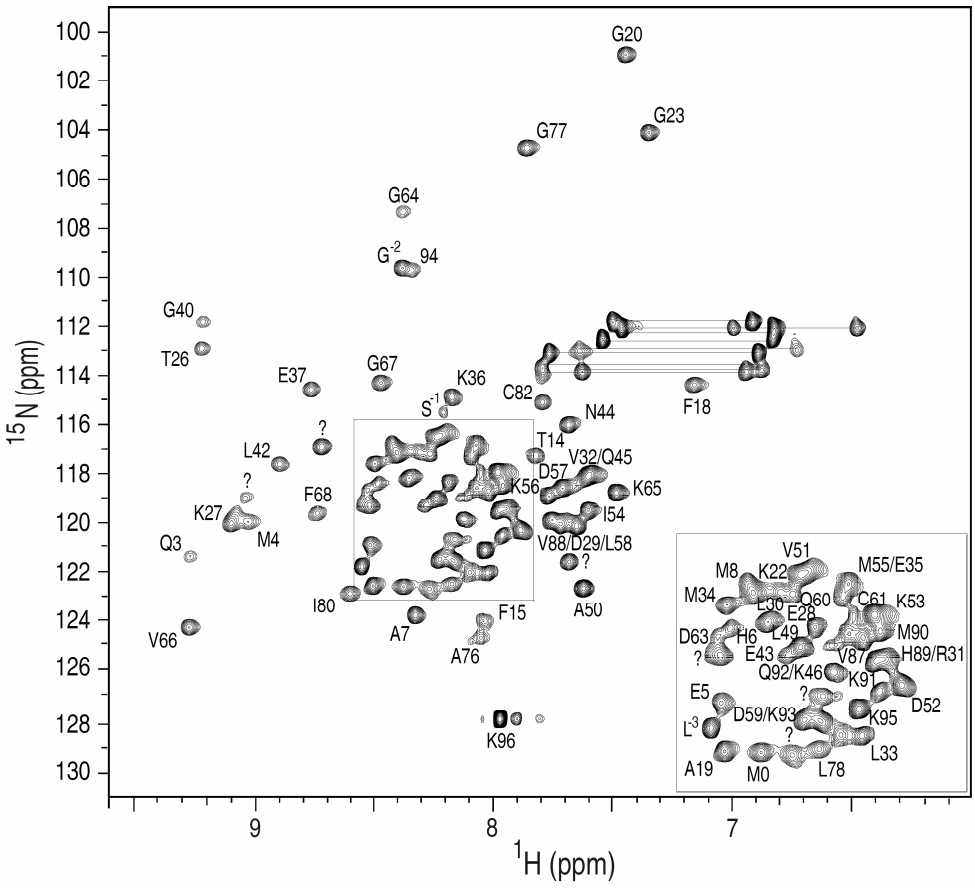

Figure 3.17. Backbone amide assignment of S100A10 protein.

^{1}H-^{15}N HSQC spectrum of 0.5 mM (monomer) uniformly ^{15}N, ^{13}C-labeled S100A10 protein acquired on a Varian INOVA 600 MHz spectrometer. The spectrum was collected in 20 mM MOPS, 1 mM DTT, 50 mM arginine, 50 mM glutamic acid, 100 mM NaCl, pH 7.0 at 35 ºC. Assigned backbone amide cross peaks are indicated with their one letter amino acid code and number. The "?" indicates the peaks that appeared on the ^{1}H-^{15}N HSQC spectrum, however, were absent on the three-dimensional NMR experiments used for assignment purposes. Pairs of resonances for side chain amide cross peaks are connected by horizontal lines.

Table 3.1. ^{15}N, ^{13}C and ^{1}H resonance assignments for human S100A10.

Residue	H^N	N	C'	C^α	C^β
P1					
S2			175.17	57.79	64.85
Q3	9.265	121.4	180.01	59.55	28.39
M4	9.023	120.1	178.81	57.92	32.02
E5	8.522	121.0	179.42	60.17	29.53
H6	8.497	118.4	178.09	59.56	29.90
A7	8.330	123.8	178.61	55.74	18.24
M8	8.410	117.1		57.83	32.02
E9				60.03	29.40
T10	8.423	116.7		66.80	68.51
M11					
M12					
F13	8.050	124.1	178.44	58.23	41.46
T14	7.840	117.2	176.98	62.70	62.55
F15	8.053	124.1		58.31	41.57
H16					
K17			177.70	59.24	32.17
F18	7.173	114.4	176.05	60.36	40.74
A19	8.506	122.7		53.92	18.77
G20	7.454	100.9		44.78	
D21			177.98	56.56	40.63
K22	8.305	117.1	178.25	57.65	31.15
G23	7.354	104.0		46.49	
Y24					
L25			178.16	53.20	43.47
T26	9.218	112.8	175.89	60.72	71.85
K27	9.098	120.1	178.46	60.70	31.95
E28	8.196	118.4	178.71	59.79	29.09
D29	7.723	120.1	177.97	57.22	42.70
L30	8.352	118.3		57.5	41.80
R31	7.980	119.7	178.16	60.26	29.78
V32	7.610	118.3	177.32	66.31	31.91
L33	8.026	122.0	179.34	59.42	42.02
M34	8.505	117.6	177.96	59.06	31.64
E35	8.084	117.3	178.76	59.26	30.11
K36	8.179	114.9	178.86	57.93	33.68
E37	8.767	114.5		56.22	30.58
F38					
P39			179.62	65.63	31.07
G40	9.256	111.8	172.46	46.46	
F41	6.882	113.6	171.81	55.60	40.14
L42	8.892	117.6	179.47	52.90	
E43	8.284	119.3	177.35	58.48	29.64
N44	7.681	116.1	175.11	53.99	39.40
Q45	7.602	118.0	177.57	55.97	28.99
K46	8.090	119.7		57.20	32.81
D47					
P48			177.77	64.28	32.44
L49	8.238	119.00	177.60	54.91	41.30
A50	7.625	122.7	178.84	55.69	18.92
V51	8.230	116.6	174.88	66.42	31.44
D52	7.896	120.2	178.81	57.61	40.75
K53	7.961	118.4	178.87	59.75	32.64
I54	7.605	119.6	178.10	64.22	38.21

M55	8.074	116.8	178.30	57.89	32.20
K56	7.771	118.9	178.17	58.88	32.26
D57	7.721	118.7	177.47	56.06	40.88
L58	7.659	120.2	177.87	55.82	42.06
D59	8.220	121.5	177.29	56.04	40.85
Q60	8.254	117.1	176.36	56.89	28.81
C61	8.050	118.0		58.95	27.54
R62			176.48	57.91	29.55
D63	8.527	118.8	176.51	54.32	40.69
G64	8.352	107.1	173.56	46.04	
K65	7.491	118.8	175.49	55.66	34.21
V66	9.271	124.4	176.08	62.43	32.73
G67	8.467	114.4	173.72	44.31	
F68	8.734	119.7		62.13	39.33
Q69					
S70					
F71					
F72					
S73					
L74					
I75			179.04	62.83	
A76	8.043	124.9	179.19	55.54	18.11
G77	7.871	104.7	176.04	47.07	
L78	8.175	122.4		59.72	39.09
T79			175.65	61.72	63.33
I80	8.605	122.8		60.86	39.06
A81			178.96	54.11	19.08
C82	7.793	115.0		59.22	28.24
N83					
D84					
Y85					
F86			176.63	60.00	39.65
V87	8.029	118.5	177.20	64.66	32.04
V88	7.761	120.0	177.14	64.50	32.30
H89	7.974	119.7	176.23	57.76	30.00
M90	8.016	118.8	176.94	56.51	32.62
K91	7.965	120.5	177.00	57.15	32.76
Q92	8.128	119.8	176.17	56.20	29.30
K93	8.166	121.8	177.07	56.79	32.94
G94	8.345	109.6	173.79	45.32	
K95	8.035	121.1		56.28	33.32
K96	7.974	128.0		57.84	33.75

be identified using chemical shift perturbations. To determine whether the interaction between S100A10 and dysferlin was dependent upon calcium binding to dysferlin, a ^{1}H-^{15}N HSQC spectrum of apo-C2A domain of dysferlin was collected (Figure 3.18A). A similar NMR sample containing excess amount of S100A10 was also prepared and a second ^{1}H-^{15}N HSQC was then obtained (Figure 3.18B). Comparison between the two spectra of C2A domain of dysferlin in the presence and absence of S100A10 showed that the peaks are in nearly identical positions. This could suggest that the interaction between C2A domain of dysferlin and S100A10 is calcium dependent.

Small additions of calcium from a stock with known concentration (determined by ICP) were made to the NMR sample of apo-C2A domain of dysferlin and ^{1}H-^{15}N HSQC spectra were collected at each point (Figure 3.19). Calcium additions resulted in the gradual disappearance of a subset of dysferlin C2A domain resonances and the reappearance of new peaks at each step of the titration. This shows the sequential association of the calcium ion to each calcium-binding loop of the protein in a slow exchange process with dissociation constants of less than 20 μM for all calcium-binding sites. The C2A domain of dysferlin was saturated when the calcium concentration was equivalent to 6 times the protein concentration (Figure 3.19F). Comparable titrations were made into the NMR sample containing the mixture of apo-C2A domain of dysferlin and S100A10 (Figure 3.20B). The ^{1}H-^{15}N HSQC of this sample was identical to the spectrum of calcium-bound dysferlin protein (Figure 3.20A), demonstrating a lack of interaction between C2A domain of dysferlin and S100A10 under the conditions used.

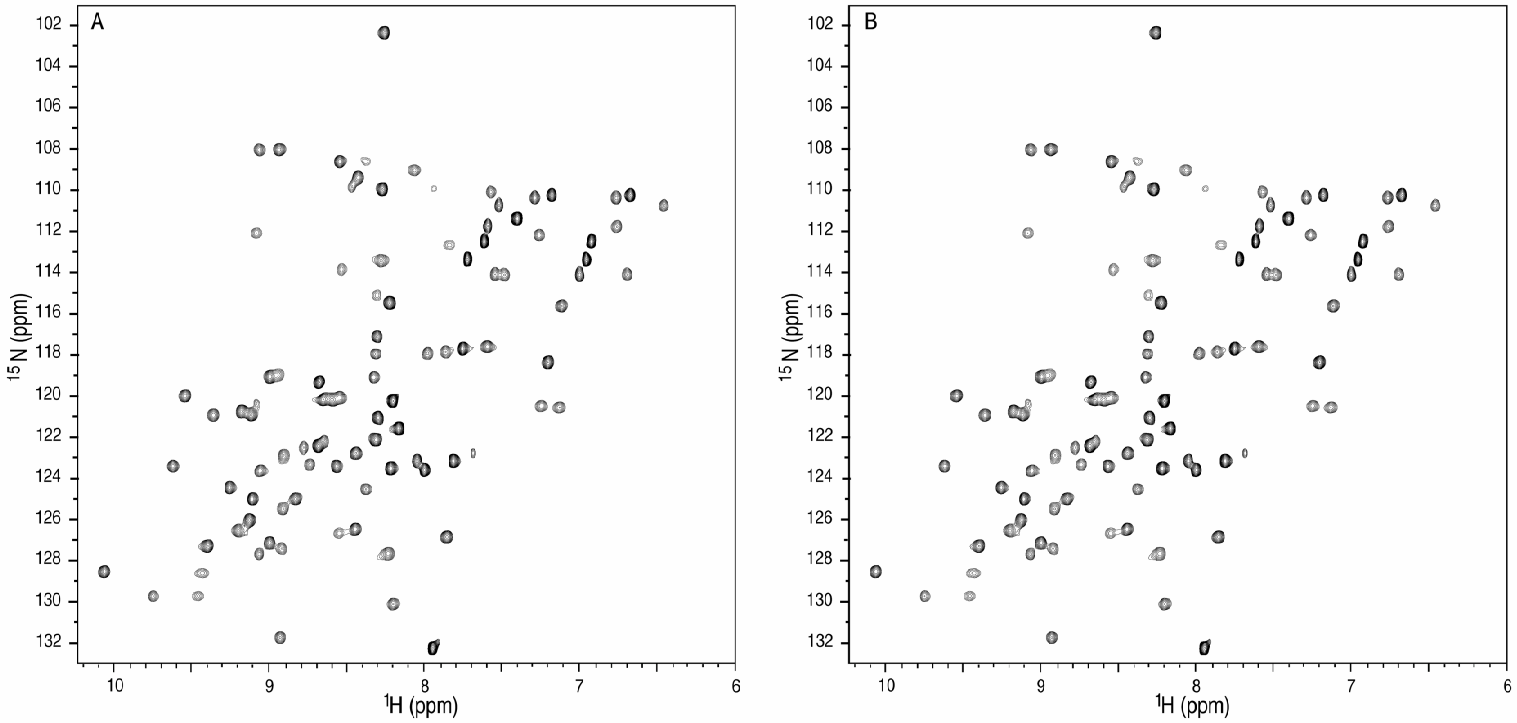

Figure 3.18. Interaction study of dysferlin C2A domain and S100A10 in the absence of calcium.

^{1}H-^{15}N HSQC spectrum of 200 mM uniformly ^{15}N, ^{13}C-labeled dysferlin C2A domain alone **(A)** and mixed with 400 mM wild-type S100A10 protein **(B)** in 10 mM HEPES, 1 mM DTT, 150 mM NaCl at pH 7.5 acquired at 35 ºC on a Varian INOVA 600 MHz spectrometer.

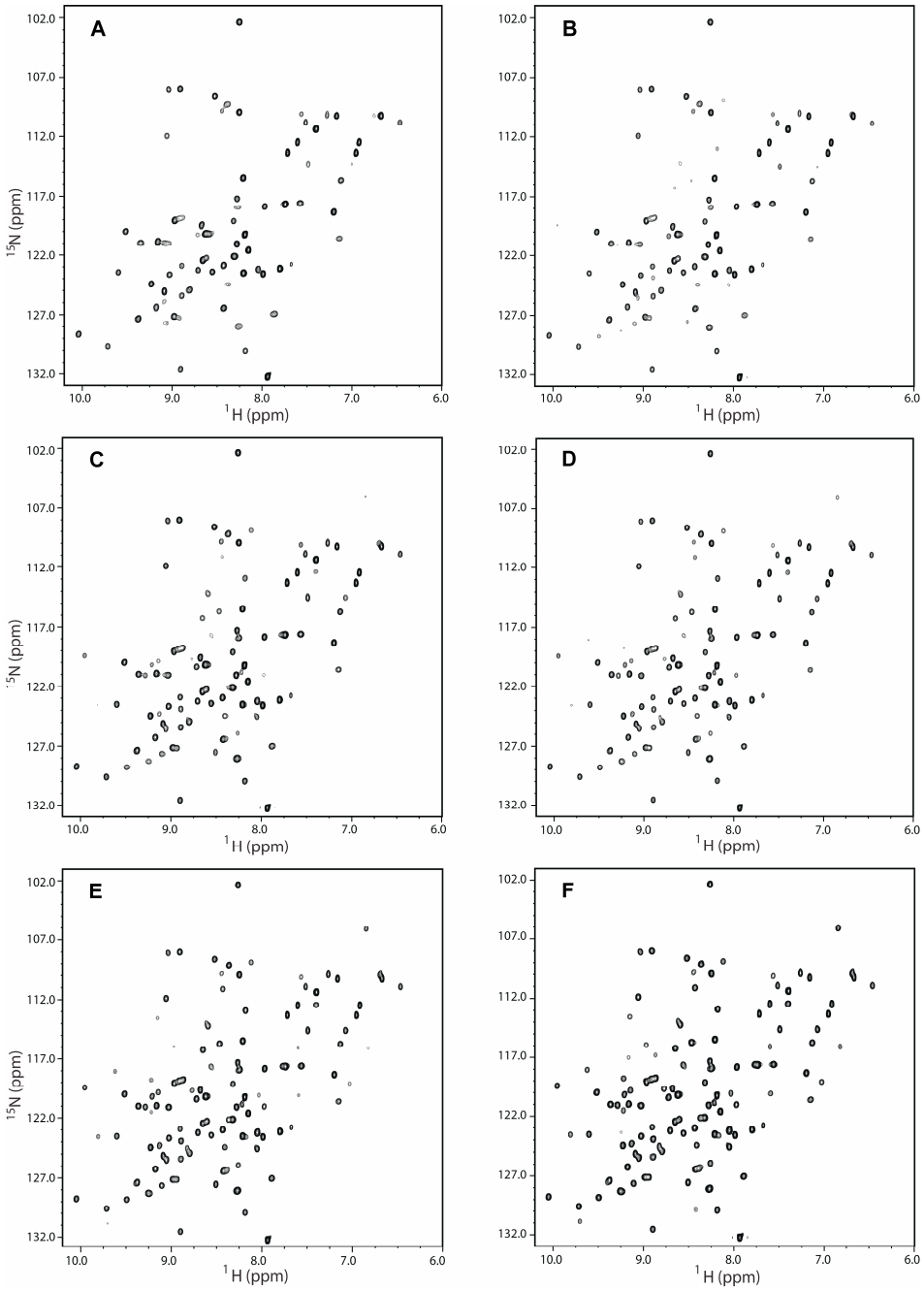

Figure 3.19. Titration of dysferlin C2A domain with calcium ions.

Representative ^{1}H-^{15}N HSQC spectra from the calcium titration are illustrated. Small additions of calcium were made into a sample of uniformly ^{15}N, ^{13}C-labeled dysferlin C2A domain (200 μM). Spectra shown are at **(A)** 1 equivalent, **(B)** 2 eq., **(C)** 3 eq., **(D)** 4 eq., **(E)** 5 eq., and **(F)** 6 eq. of calcium relative to the protein concentration. The C2A domain of dysferlin binds to 6 calcium ions.

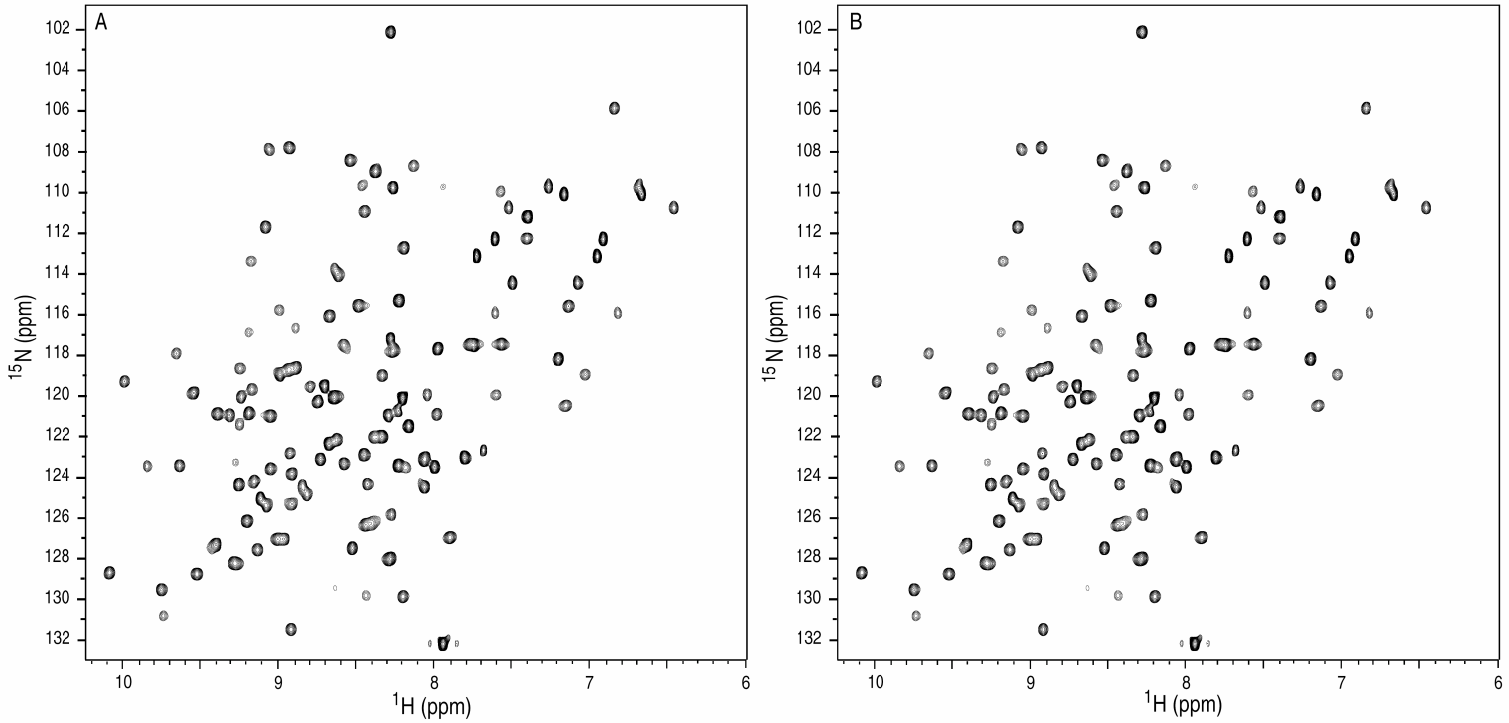

Figure 3.20. Interaction study of dysferlin C2A domain and S100A10 in the presence of calcium.

^{1}H-^{15}N HSQC spectrum of 200 mM uniformly ^{15}N, ^{13}C-labeled calcium-bound dysferlin C2A domain alone **(A)** and mixed with 400 mM wild-type S100A10 protein **(B)** in 10 mM HEPES, 1 mM DTT, 150 mM NaCl at pH 7.5 acquired at 35 ºC on a Varian INOVA 600 MHz spectrometer.

3.3.9 Expression and Purification of the C-terminal Fragment of Human AHNAK Protein

Recombinant C-terminal fragment of human AHNAK (residues 5362-5434) was expressed and purified from *E. coli* strain BL21 (DE3) Codon Plus expression cells. Since the protein degraded very quickly, purification procedures were performed at 4 °C in the presence of one complete-mini protease inhibitor tablet, PMSF and leupeptin. The protein was purified on two consecutive Ni-NTA columns. Figure 3.21 shows the SDS-PAGE of fractions from the second column run. The AHNAK protein appears as a band at approximately 9 kDa, which roughly corresponds to the calculated monomer molecular weight for the C-terminal fragment of AHNAK of 7827.0 Da. Fractions containing a single band corresponding to the mass of AHNAK were pooled and stored at -80 °C. ESI mass spectrometry was used to verify the purity, integrity and molecular weight of the protein. Figure 3.22 shows a mass spectrum of unlabeled AHNAK with two peaks. The first peak appears at 7827.4 Da, which is in agreement with the calculated mass of monomeric AHNAK. The second peak at 15652.87 Da corresponds to the molecular weight of a dimeric AHNAK protein. Fresh DTT as a reducing agent was required to prevent formation of an intermolecular disulfide bond between Cys5382 of the AHNAK.

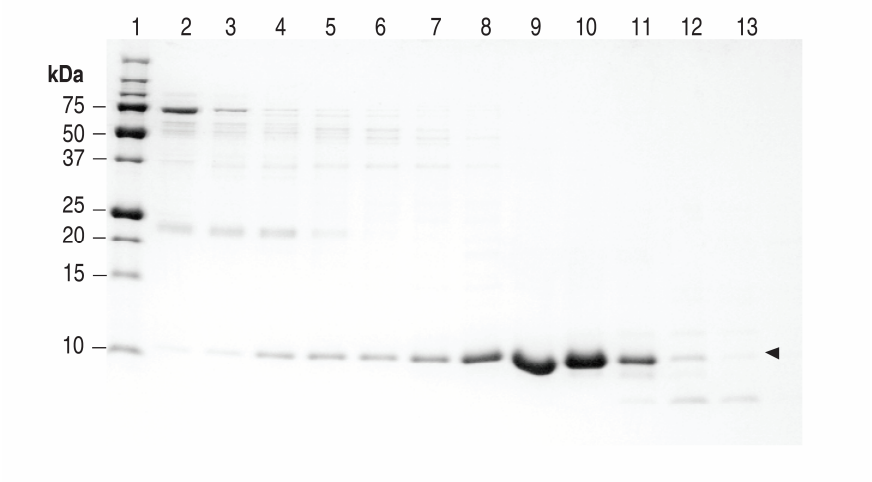

Figure 3.21. Coomassie-stained SDS-PAGE for the purification of short C-terminal fragment of AHNAK.

Lane 1 contains the protein molecular weight markers, with molecular weights labeled on the left. Lanes 2-13 contain elution profile of every fraction following removal of His_7 tag on the Ni-NTA column. The arrowhead on the right indicates monomeric AHNAK at molecular weight of approximately 9 kDa.

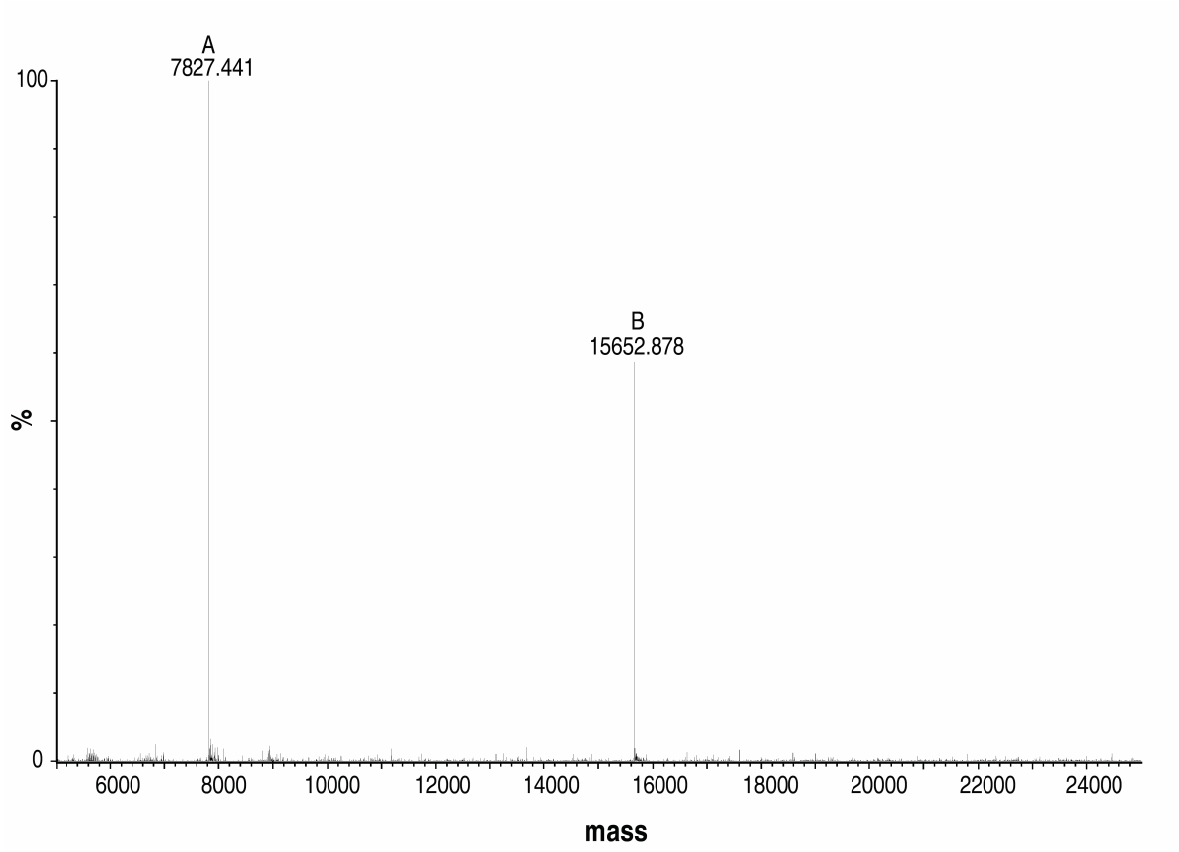

Figure 3.22. Mass spectrum of an unlabeled C-terminal domain construct of AHNAK protein.

After purification of the protein, excess salt was removed. The protein was subjected to mass spectrometric analysis to verify the molecular weight of the protein. The analysis resulted in two peaks. The peak at 7827.4 Da is in agreement with the calculated mass of monomer AHNAK (7827.0 Da). The peak at 15652.9 Da corresponds to the mass of a dimer AHNAK when a disulfide bond is formed between cysteines at position 5382.

3.3.10 Interaction Study of Apo- and Calcium Bound Dysferlin C2A Domain with the C-terminal Fragment of AHNAK

Recent three-hybrid and co-immunoprecipitation experiments have provided some evidence on the interaction between the C-terminal domain of AHNAK and the N-terminal C2A domain of dysferlin. Further, it was also shown that calcium binding to the dysferlin C2A domain is not a requirement for its interaction with AHNAK (Huang et al. 2007). To identify the residues involved in this interaction, dysferlin C2A domain was labeled with Alexa Fluor 680 maleimide at the only cysteine (Cys23) in the sequence for peptide array blotting. Alexa-dysferlin protein was used in a peptide array experiment covering the C-terminus of AHNAK (residues 4884-5890). This approach identifies the structurally independent interactions between dysferlin and a series of 18-residue peptides spanning the C-terminal sequence of AHNAK. Overlapping sequences in the arrays that fluoresced upon Alexa-dysferlin C2A domain binding were used to identify the AHNAK binding sites (Figure 3.23). Blotting of the arrays with Alexa-dysferlin revealed that the apo-dysferlin C2A domain associates with four distinct regions within the C-terminus of AHNAK. Using the Blocks Server (blocks.fhcrc.org) to analyze these regions, a six residue consensus sequence was identified for AHNAK that could best be represented as XPKφ±φ (X – variable; φ – hydrophobic residue; ± – charged residue; P – proline; K – lysine).

The most intense binding at any one spot was observed within sequences *b* (Gly5367 - Ser5393), while sequences *a* (Met5025 - Phe5042), *c* (Leu5394 - Ser5414) and *d* (Phe5619 - His5649) showed weaker interactions with the dysferlin C2A

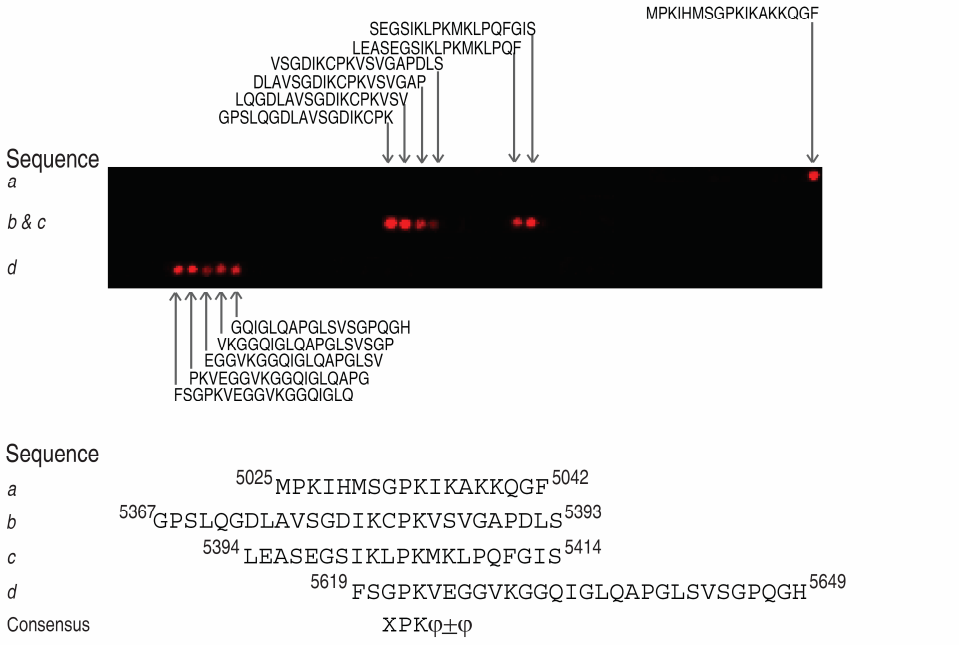

Figure 3.23. Mapping apo-dysferlin C2A domain binding site on the C-terminal region of AHNAK by peptide array analysis.

A peptide array of the Asp4884-Glu5890 region of AHNAK was synthesized. Each spot contained an 18-residue peptide shifted by 3 residues from its predecessor until the C-terminus was reached. The array was probed with Alexa Fluor 680-dysferlin and imaged at 700 nm. The sequences of AHNAK that were found to bind dysferlin C2A domain (red fluorescent spots) are listed and indicated with arrows; sequence *a* (Met5025 - Phe5042), sequence *b* (Gly5367 - Ser5393), sequence *c* (Leu5394 - Ser5414), sequence *d* (Phe5619 - His5649). These sequences were used to define a consensus sequence showing charged (±), hydrophobic (φ) and variable (X) residues using the Blocks Server (blocks.fhcrc.org).

domain. This could be due to the presence of certain residues upstream of the consensus sequence. For example, when residues L5370-G5372 were eliminated from the second fluorescent spot of sequences *b*, the fluorescent signal of the next spot was dramatically reduced.

Previous GST-pull down assays of AHNAK indicated that the binding site for dysferlin C2A domain is located between residues M5146-V5643 (Huang et al. 2007). However, the peptide array experiment identified an extra binding region, specified as sequence *a* (Met5025 - Phe5042). This interaction could be explained by sequence similarity of this region with the remaining binding sites. It would be interesting to repeat a similar array in the presence of calcium to observe whether calcium-bound dysferlin C2A domain would bind to different regions on the AHNAK.

To further examine and locate the interaction sites between dysferlin and AHNAK proteins, both the C-terminal fragment of AHNAK and the C2A domain of dysferlin proteins were purified as described in Sections 3.2.5 and 3.2.6, respectively. A ^{1}H-^{15}N HSQC spectrum of apo-C2A domain of dysferlin was collected (Figure 3.24). A similar NMR sample containing an excess amount of AHNAK was also prepared and a second ^{1}H-^{15}N HSQC was obtained (Figure 3.24). The overlay of the two ^{1}H-^{15}N HSQC spectra did not show significant changes in chemical shifts of C2A domain of dysferlin in the presence and absence of AHNAK.

To test whether this interaction is calcium dependent, small additions of calcium were made to the NMR sample of apo-C2A domain of dysferlin. Once more, the C2A domain of dysferlin was saturated when the calcium concentration was equivalent to

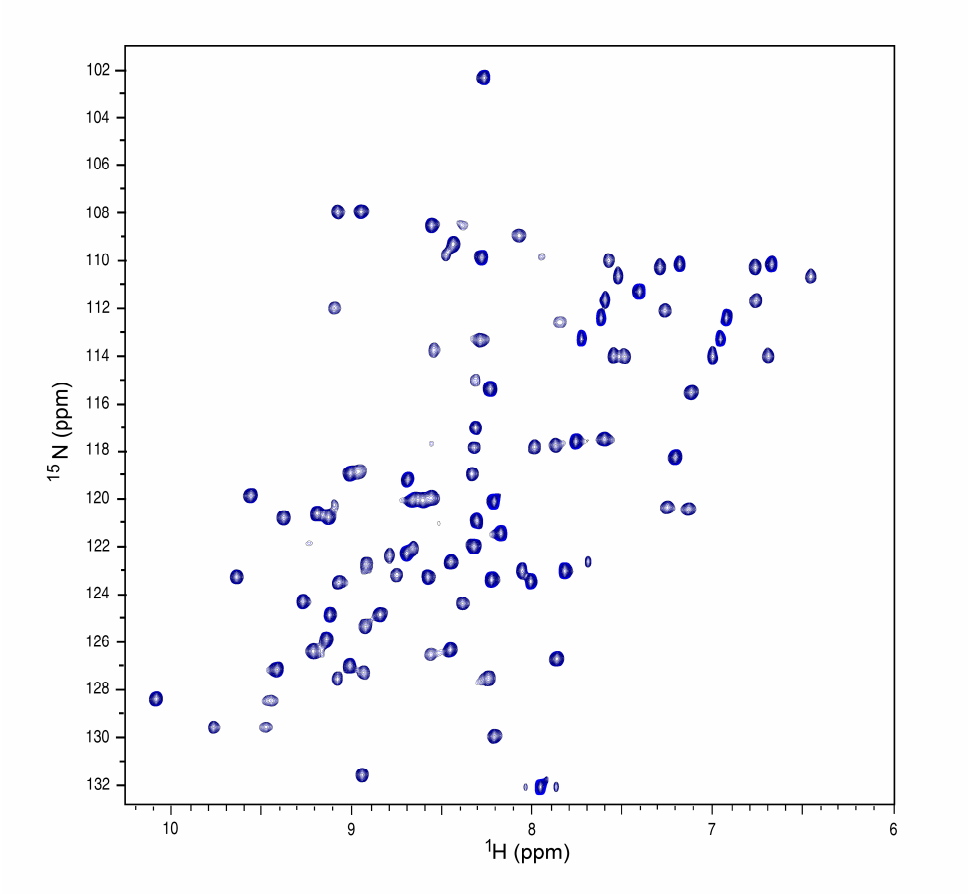

Figure 3.24. Interaction study of C2A domain of dysferlin and C-terminal fragment of AHNAK in the absence of calcium.

Overlay of ^{1}H-^{15}N HSQC spectra of apo-dysferlin (black) and apo-dysferlin mixed with C-terminal fragment of AHNAK protein (blue). Two NMR samples of 138 µM uniformly ^{15}N, ^{13}C-labeled apo-dysferlin alone and mixed with 200 µM AHNAK protein in 10 mM HEPES, 1 mM DTT, 150 mM NaCl at pH 7.5 were used to collect the respective HSQC spectra. No significant changes in chemical shifts were observed in the absence of calcium.

6 times the protein concentration (Figure 3.25). Similar titrations were made into the NMR sample containing the mixture of apo-C2A domain of dysferlin and AHNAK (Figure 3.25). The ^{1}H-^{15}N HSQC of this sample perfectly superimpose the spectrum of calcium-bound dysferlin protein. This indicates that under the conditions used, C2A domain of dysferlin does not interact with the AHNAK protein in the presence or absence of calcium. Similar results were obtained when analogous experiments in different buffer conditions (ie. 50 and 100 mM NaCl) were repeated (data not shown).

3.4 Discussion

Proteomic studies have indicated that a large number of proteins are involved in membrane repair processes (de Morree et al. 2010; Cacciottolo et al. 2011). Included in this group is the EF-hand protein S100A10, the phospholipid-binding protein annexin A2 and the enlargeosome protein AHNAK, all proposed to participate in a multi-protein complex near the plasma membrane. This chapter provides the first details of the architecture for a ternary complex between these three proteins.

3.4.1 Evidence for a Scaffolding Role of the AHNAK C-terminus

Peptide array experiments show eight potential binding regions within the C-terminal domain of AHNAK for the A10A2^{C82S} hybrid protein. Not surprisingly, these sequences all have some similarity forming a consensus sequence +X+XPKφXφ. The repeating nature of these sequences is not unique to the C-terminus of AHNAK. The central region of the protein includes 24 repeat motifs (165-residues each) suggested to

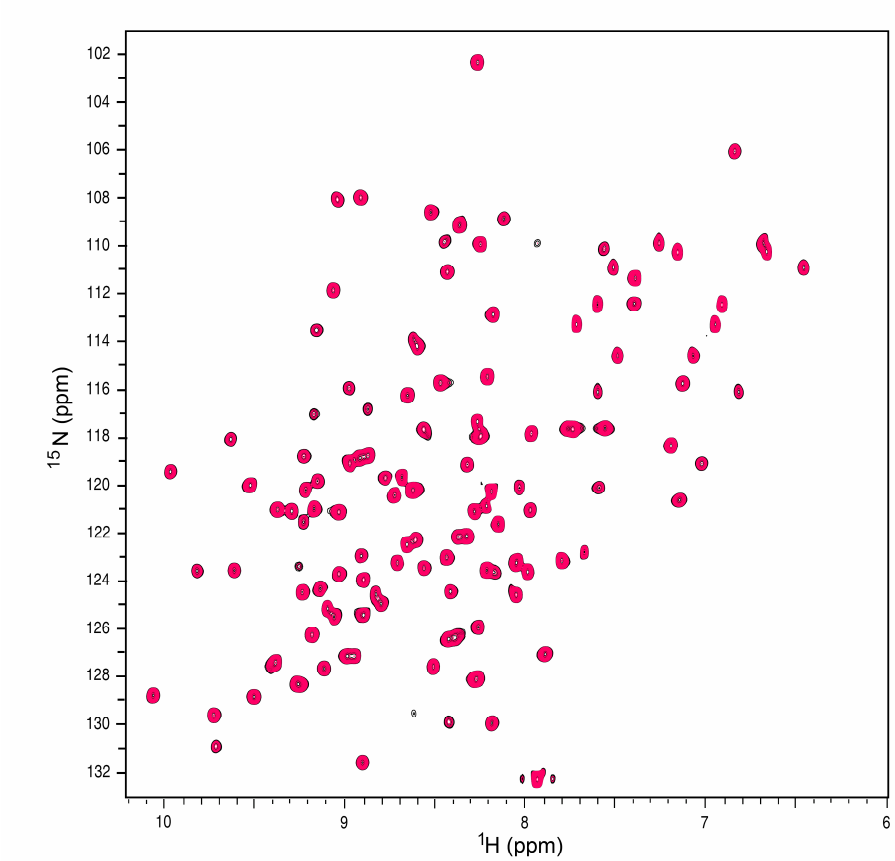

Figure 3.25. Interaction study of C2A domain of dysferlin and C-terminal fragment of AHNAK in the presence of calcium.

Overlay of ^{1}H-^{15}N HSQC spectra of calcium-bound dysferlin (black) and calcium-bound dysferlin mixed with C-terminal fragment of AHNAK protein (pink). Two NMR samples of 138 µM uniformly ^{15}N, ^{13}C-labeled apo-dysferlin alone and mixed with 200 µM AHNAK protein were titrated with 850 µM of calcium. The two samples were in 10 mM HEPES, 1 mM DTT, 150 mM NaCl at pH 7.5. ^{1}H-^{15}N HSQC spectra did not show any significant changes in chemical shifts when calcium was added.

adopt a series of β-propeller structures similar to RCC1 (Shtivelman et al. 1992; Shtivelman and Bishop 1993). The nature of the AHNAK consensus sequence differs from other S100 binding motifs such as those found in the N-terminus of annexins A1 and A2 (A/VXXφLXXφXφ) and CapZ (R/KL/IXWXXIL). The single-residue spacing of the hydrophobic residues in the AHNAK sequence suggests it does not have amphipathic character similar to the α-helical structure found in the annexin-binding sequences. In addition, a central proline residue would not favor helix formation upon binding. The possibility for eight binding regions in the C-terminus of AHNAK for the S100A10-annexin A2 complex is consistent with a scaffolding role for AHNAK. In principle, this would allow up to eight S100A10-annexin A2 heterotetramers to assemble on the C-terminus. Since binding of the complex to the phospholipid surface is governed by calcium binding to the annexin moiety, this would allow a highly cooperative association of the complex with the membrane. Despite this potential, other experiments have shown that only the Gly5654 - Gly5673 region within the C-terminus of AHNAK displays a strong interaction with the S100A10-annexin A2 (De Seranno et al. 2006). This could indicate that other sequences identified in the peptide array are masked by the AHNAK tertiary structure. Similarly, the Gly5654 - Gly5673 region had the strongest binding spot in the peptide array suggesting it could have a much stronger affinity than the other sequences.

The ability of the S100A10-annexin A2 heterotetrameric complex to participate in the assembly of other larger multiprotein complexes was also examined for transient receptor potential cation channel proteins TRPV5. Peptide array experiments uncovered

five potential binding sequences within the C-terminus of TRPV5, including residues 598-603 (VATTV) that forms a highly conserved region in both TRPV5/TRPV6 channel proteins. However, regions such as D627-V648 (ie. in Figure 3.11A, 6A-6E) showed stronger binding than that observed with the conserved VATTV sequence, to both the S100A10^{C82S} and A10A2^{C82S} proteins. The S100A10^{C82S} and A10A2^{C82S} associated to the same region on TRPV5 protein, suggesting that the N-terminal peptide of annexin A2 may not be required for the interaction of S100A10 to TRPV5. Consequently, the interaction site between TRPV5 with S100A10 or annexin A2-bound S100A10 is different from the complex formed with the AHNAK, where residues from both S100A10 and annexin A2 are required for the strong interaction of the peptide. Further experiments such as the binding affinity assays are necessary to determine whether a difference exists for the binding affinity of TRPV5 to the S100A10 or annexin A2-bound S100A10 protein, similar to that observed for the AHNAK. This experiment would indicate that although TRPV5 may use a binding mechanism different from the AHNAK protein, strong interaction of TRPV5 requires the complex formed between S100A10 and annexin A2 proteins.

3.4.2 An Asymmetric S100A10-Annexin A2-AHNAK Complex

A representative sequence (AHNAK5) identified from the peptide array was used to identify the arrangement of the S100A10-annexin A2-AHNAK5 ternary complex. Using both the A10A2^{C82S} hybrid protein and complex of S100A10^{C82S} with an N-terminal peptide of the annexin A2, a single AHNAK5 peptide was found to coordinate in

an asymmetric fashion to the S100A10-annexin A2 heterotetramer. Although it is a ternary complex, an asymmetric arrangement within an S100-target protein complex has not been observed to date. For example, multiple S100-peptide complexes such as those between S100B and CapZ (Inman et al. 2002; McClintock and Shaw 2003; Charpentier et al. 2010), p53 (Rustandi et al. 2000) or Ndr kinase (Lee et al. 2008), S100A1 with RyR (Wright et al. 2008) and CapZ (Wright et al. 2009) and S100A6 with Siah1 interacting protein (Lee et al. 2008) all display symmetric arrangements. In S100A10-annexin A2 the addition of AHNAK acts to break the symmetry of the heterotetramer. In contrast the EF-hand calcium-binding protein calmodulin (CaM) can form asymmetric complexes with the dimeric targets glutamate decarboxylase and Cdc42-WASP. In these cases, binding of calcium-activated CaM to the symmetric, dimeric arrangements of glutamate decarboxylase and Cdc42-WASP results in an overall asymmetric arrangement essential for enzyme activity (Yuan and Vogel 1998; Kim et al. 2000; Yap et al. 2003).

In the A10A2-AHNAK5 complex, significant changes in chemical shift occur mainly for residues in helix IV of the S100A10 (Gly77, Ala81) as well as the N-terminus of the annexin A2 (Leu112, G114) peptides. In the S100A10-annexin A2 structure helices IV and IV' from S100A10 form a portion of the dimer interface oriented roughly 180° from each other on one face of the protein (Rety et al. 1999). The two annexin A2 peptides in the heterotetramer are both oriented such that their C-termini lie on the same side of the complex as helices IV and IV'. Thus the interaction of AHNAK5 with the S100A10-annexin A2 is consistent with binding that utilizes one face of the dimeric protein comprising helices IV and IV' and the adjacent annexin A2 C-termini.

The tight binding between AHNAK5 and S100A10-annexin A2 (~3 nM) requires initial formation of the heterotetramer since experiments lacking the annexin A2 peptide yield a much poorer (~1000 fold) interaction. This observation is in excellent agreement with yeast triple-hybrid and *in vitro* binding assays that show both S100A10 and annexin A2 are required for strong association with the C-terminal domain of AHNAK (De Seranno et al. 2006). This requirement indicates there are two calcium-regulated steps for AHNAK delivery to the membrane surface both mediated by annexin A2. The first is the extrusion of N-terminus of annexin A2 upon calcium binding to the protein core domain allowing formation of the heterotetramer and subsequent recruitment of AHNAK. The second step is the localization of the entire complex to the phospholipid surface through calcium bridging between annexin A2 and the membrane. It is interesting that several other proteins have also shown an association with the S100A10-annexin A2 heterotetramer including TRPV5/6 (van de Graaf et al. 2003; Borthwick et al. 2008), TASK-1 (Girard et al. 2002; Renigunta et al. 2006) and NS3 (Beaton et al. 2002). While the calcium regulation of these interactions is less known, it is possible that the asymmetric interaction proposed here for AHNAK is a general feature for trafficking of these proteins to the cell membrane.

3.4.3 Interaction between Other Proteins in the Membrane Repair Complexes

In addition to the 12 residue N-terminal peptide of annexin A2, other potential binding sites for S100A10 were identified on the peptide array of full length annexin A2. In fact, interaction with the 12 residue N-terminal peptide of annexin A2 appeared as one

of the weakest binding sites for S100A10. Except for annexin A6, the remaining 11 different annexin proteins contain a core domain consisting of four conserved structural repeat sequences (I-IV) (Huber et al. 1990; Concha et al. 1993; Sopkova et al. 1993). Each repeat unit is formed from five α-helices (A-E) arranged such that helices A, B, D and E are roughly anti-parallel to each other while helix C is nearly perpendicular to these helices (Figure 1.5) (Weng et al. 1993; Rosengarth et al. 2001). Due to sequence similarity of the helices within each repeat unit of annexin A2 (Barton et al. 1991), it is not surprising to observe the binding of S100A10 to all four structural repeats on the peptide array. Peptide array analysis identifies the sequence dependent but structurally independent interactions between a protein and a series of peptides spanning a particular region of a protein. Consequently, some of the annexin A2 repeat units that showed binding with S100A10 in the peptide array will be excluded as they are buried in an intact annexin A2. In addition, the amount of protein used in probing the peptide arrays of annexin A2 with S100A10 or A10A2 was about 2 μM, which could result in non-specific interaction of the protein to these peptides particularly when the K_d of binding is low. A low dissociation constant of approximately 30 nM for the interaction of the 12 residue N-terminal peptide of annexin A2 with S100A10 was previously determined (Johnsson et al. 1988). Thus, to prevent the non-specific interactions, lower amount of proteins must be used for probing the peptide arrays.

S100A10, annexin A2 and AHNAK have been identified as binding partners of dysferlin, a central protein in the membrane repair complex (Huang et al. 2007). This multiprotein complex is proposed to facilitate wound repair of damaged epithelial,

auditory and muscle cells upon extracellular calcium influx. A better understanding of the arrangement or assembly of the proteins in the membrane repair complex allows proposing a model in which this process takes place. It has been shown that the association of annexins A1 and A2 with a dysferlin-containing vesicle and damaged plasma membranes (Doherty and McNally 2003; Glover and Brown 2007; Han and Campbell 2007) is calcium dependent. Previous GST-pull down assay (Huang et al. 2007) as well as the peptide array experiment in this work, identified the interaction of the C-terminus of AHNAK with the apo-C2A domain of dysferlin (aa 2-130), while NMR spectroscopy experiments did not indicate any interaction between the two proteins in the presence or absence of calcium. The AHNAK protein used in the NMR experiments was composed of amino acid residues 5362-5434, which is much shorter than the AHNAK protein used in the GST-pull down (5146-5643) (Huang et al. 2007) or peptide array (4884-5890) experiments. Consequently, it is possible that the binding site for AHNAK on dysferlin C2A domain is indeed located in residues 5435-5643.

NMR spectroscopy of S100A10 and the dysferlin C2A domain did not suggest a direct interaction between these two proteins in the presence or absence of calcium. In contrast, S100A13 interacts with the synaptotagmin C2A domain (Mohan et al. 2009; Mohan et al. 2010). In this case, synaptotagmin was shown to mediate the interaction between S100A10 and fibroblast growth factor (FGF1). Synaptotagmin is a synaptic vesicle protein that belongs to the fer-1 family of proteins. The Dysferlin C2A domain has the highest level of homology with the C2A domain of rat synaptotagmin (Britton et al. 2000). Furthermore, proteomic analyses identify both annexin A2 and AHNAK as

members of the dysferlin complex (de Morree et al. 2010; Cacciottolo et al. 2011). Consequently, it is possible that the interaction between S100A10, annexin A2 and dysferlin is mediated through AHNAK, the largest protein within the complex. The identification of a ternary asymmetric complex between S100A10-annexin A2 and AHNAK provides an initial framework for understanding the intricate assembly of these membrane repair proteins.

3.5 References:

Barton, G.J., Newman, R.H., Freemont, P.S., and Crumpton, M.J. 1991. Amino acid sequence analysis of the annexin super-gene family of proteins. *Eur J Biochem* **198:** 749-760.

Beaton, A.R., Rodriguez, J., Reddy, Y.K., and Roy, P. 2002. The membrane trafficking protein calpactin forms a complex with bluetongue virus protein NS3 and mediates virus release. *Proc Natl Acad Sci U S A* **99:** 13154-13159.

Borthwick, L.A., Neal, A., Hobson, L., Gerke, V., Robson, L., and Muimo, R. 2008. The annexin 2-S100A10 complex and its association with TRPV6 is regulated by cAMP/PKA/CnA in airway and gut epithelia. *Cell Calcium* **44:** 147-157.

Britton, S., Freeman, T., Vafiadaki, E., Keers, S., Harrison, R., Bushby, K., and Bashir, R. 2000. The third human FER-1-like protein is highly similar to dysferlin. *Genomics* **68:** 313-321.

Cacciottolo, M., Belcastro, V., Laval, S., Bushby, K., di Bernardo, D., and Nigro, V. 2011. Reverse Engineering Gene Network Identifies New Dysferlin-interacting Proteins. *J Biol Chem* **286:** 5404-5413.

Charpentier, T.H., Thompson, L.E., Liriano, M.A., Varney, K.M., Wilder, P.T., Pozharski, E., Toth, E.A., and Weber, D.J. 2010. The effects of CapZ peptide (TRTK-12) binding to S100B-Ca2+ as examined by NMR and X-ray crystallography. *J Mol Biol* **396:** 1227-1243.

Concha, N.O., Head, J.F., Kaetzel, M.A., Dedman, J.R., and Seaton, B.A. 1993. Rat annexin V crystal structure: Ca(2+)-induced conformational changes. *Science* **261:** 1321-1324.

de Morree, A., Hensbergen, P.J., van Haagen, H.H., Dragan, I., Deelder, A.M., t Hoen, P.A., Frants, R.R., and van der Maarel, S.M. 2010. Proteomic analysis of the dysferlin protein complex unveils its importance for sarcolemmal maintenance and integrity. *PLoS One* **5:** e13854.

De Seranno, S., Benaud, C., Assard, N., Khediri, S., Gerke, V., Baudier, J., and Delphin, C. 2006. Identification of an AHNAK binding motif specific for the Annexin2/S100A10 tetramer. *J Biol Chem* **281:** 35030-35038.

Delaglio, F., Grzesiek, S., Vuister, G.W., Zhu, G., Pfeifer, J., and Bax, A. 1995. NMRPipe: a multidimensional spectral processing system based on UNIX pipes. *J Biomol NMR* **6:** 277-293.

Doherty, K.R., and McNally, E.M. 2003. Repairing the tears: dysferlin in muscle membrane repair. *Trends Mol Med* **9:** 327-330.

Girard, C., Tinel, N., Terrenoire, C., Romey, G., Lazdunski, M., and Borsotto, M. 2002. p11, an annexin II subunit, an auxiliary protein associated with the background K+ channel, TASK-1. *Embo J* **21:** 4439-4448.

Glover, L., and Brown, R.H., Jr. 2007. Dysferlin in membrane trafficking and patch repair. *Traffic* **8:** 785-794.

Golovanov, A.P., Hautbergue, G.M., Wilson, S.A., and Lian, L.Y. 2004. A simple method for improving protein solubility and long-term stability. *J Am Chem Soc* **126:** 8933-8939.

Grant, G. 2002. *Synthetic Peptides: A User's Guide*. Oxford University Press, New York.

Grzesiek, S., and Bax, A. 1992. Correlating backbone amide and sidechain resonances in larger proteins by multiple relayed triple resonance NMR. *J. Am. Chem. Soc.* **114:** 6291-6293.

Han, R., and Campbell, K.P. 2007. Dysferlin and muscle membrane repair. *Curr Opin Cell Biol* **19:** 409-416.

Huang, Y., Laval, S.H., van Remoortere, A., Baudier, J., Benaud, C., Anderson, L.V., Straub, V., Deelder, A., Frants, R.R., den Dunnen, J.T., et al. 2007. AHNAK, a novel component of the dysferlin protein complex, redistributes to the cytoplasm with dysferlin during skeletal muscle regeneration. *Faseb J* **21:** 732-742.

Huber, R., Romisch, J., and Paques, E.P. 1990. The crystal and molecular structure of human annexin V, an anticoagulant protein that binds to calcium and membranes. *Embo J* **9:** 3867-3874.

Inman, K.G., Yang, R., Rustandi, R.R., Miller, K.E., Baldisseri, D.M., and Weber, D.J. 2002. Solution NMR structure of S100B bound to the high-affinity target peptide TRTK-12. *J. Mol. Biol.* **324:** 1003-1014.

Johnson, B.A., and Belvins, R.A. 1994. NMRView: A computer program for the visualization and analysis of NMR data. *J Biomol NMR* **4:** 603-614.

Johnsson, N., Marriott, G., and Weber, K. 1988. p36, the major cytoplasmic substrate of src tyrosine protein kinase, binds to its p11 regulatory subunit via a short amino-terminal amphiphatic helix. *EMBO J.* **7:** 2435-2442.

Kay, L.E., Ikura, M., Tschudin, R., and Bax, A. 1990. Three-dimentional triple-resonance NMR spectroscopy of isotopically enriched proteins. *J. Magn. Reson.* **89:** 496-514.

Kim, A.S., Kakalis, L.T., Abdul-Manan, N., Liu, G.A., and Rosen, M.K. 2000. Autoinhibition and activation mechanisms of the Wiskott-Aldrish syndrome protein. . *Nature* **404:** 151-158.

Lee, Y.T., Dimitrova, Y.N., Schneider, G., Ridenour, W.B., Bhattacharya, S., Soss, S.E., Caprioli, R.M., Filipek, A., and Chazin, W.J. 2008. Structure of the S100A6 complex with a fragment from the C-terminal domain of Siah-1 interacting protein: a novel mode for S100 protein target recognition. *Biochemistry* **47:** 10921-10932.

Loo, J. 2000. Electro-spray ionization mass spectrometry: a technology for studying noncovalent macromolecular complexes. *Int. J. Mass Spectrom* **200:** 175-186.

McClintock, K.A., and Shaw, G.S. 2003. A novel S100 target conformation is revealed by the solution structure of the Ca2+-S100B-TRTK-12 complex. *J Biol Chem* **278:** 6251-6257.

Mohan, S.K., Rani, S.G., Kumar, S.M., and Yu, C. 2009. S100A13-C2A binary complex structure-a key component in the acidic fibroblast growth factor for the non-classical pathway. *Biochem Biophys Res Commun* **380:** 514-519.

Mohan, S.K., Rani, S.G., and Yu, C. 2010. The heterohexameric complex structure, a component in the non-classical pathway for fibroblast growth factor 1 (FGF1) secretion. *J Biol Chem* **285:** 15464-15475.

Morigasaki, S., Li, F., Kawai, A., Yamazaki, K., Sikdar, D., Hibino, Y., and Hiraga, K. 2000. Interaction of albumin mRNA with proteins from rat liver with CCl(4)-induced injury. *Biochem Biophys Res Commun* **273:** 261-266.

Nebgen, D.R., Inoue, H., Sabsay, B., Wei, K., Ho, C.S., and Veis, A. 1999. Identification of the chondrogenic-inducing activity from bovine dentin (bCIA) as a low-molecular-mass amelogenin polypeptide. *J Dent Res* **78:** 1484-1494.

Renigunta, V., Yuan, H., Zuzarte, M., Rinne, S., Koch, A., Wischmeyer, E., Schlichthorl, G., Gao, Y., Karschin, A., Jacob, R., et al. 2006. The retention factor p11 confers an endoplasmic reticulum-localization signal to the potassium channel TASK-1. *Traffic* **7:** 168-181.

Rety, S., Osterloh, D., Arie, J.P., Tabaries, S., Seeman, J., Russo-Marie, F., Gerke, V., and Lewit-Bentley, A. 2000. Structural basis of the Ca(2+)-dependent association

between S100C (S100A11) and its target, the N-terminal part of annexin I. *Structure Fold Des* **8:** 175-184.

Rety, S., Sopkova, J., Renouard, M., Osterloh, D., Gerke, V., Tabaries, S., Russo-Marie, F., and Lewit-Bentley, A. 1999. The crystal structure of a complex of p11 with the annexin II N-terminal peptide. *Nat Struct Biol* **6:** 89-95.

Rezvanpour, A., Phillips, J.M., and Shaw, G.S. 2009. Design of high-affinity S100-target hybrid proteins. *Protein Sci* **18:** 2528-2536.

Rosengarth, A., Gerke, V., and Luecke, H. 2001. X-ray structure of full-length annexin 1 and implications for membrane aggregation. *J Mol Biol* **306:** 489-498.

Rustandi, R.R., Baldisseri, D.M., and Weber, D.J. 2000. Structure of the negative regulatory domain of p53 bound to S100B(bb). *Nat. Struct. Biol.* **7:** 570-574.

Seemann, J., Weber, K., and Gerke, V. 1996. Structural requirements for annexin I-S100C complex-formation. *Biochem J* **319 (Pt 1):** 123-129.

Shtivelman, E., and Bishop, J.M. 1993. The human gene AHNAK encodes a large phosphoprotein located primarily in the nucleus. *J Cell Biol* **120:** 625-630.

Shtivelman, E., Cohen, F.E., and Bishop, J.M. 1992. A human gene (AHNAK) encoding an unusually large protein with a 1.2-microns polyionic rod structure. *Proc Natl Acad Sci U S A* **89:** 5472-5476.

Sopkova, J., Renouard, M., and Lewit-Bentley, A. 1993. The crystal structure of a new high-calcium form of annexin V. *J Mol Biol* **234:** 816-825.

van de Graaf, S.F., Hoenderop, J.G., Gkika, D., Lamers, D., Prenen, J., Rescher, U., Gerke, V., Staub, O., Nilius, B., and Bindels, R.J. 2003. Functional expression of the epithelial Ca(2+) channels (TRPV5 and TRPV6) requires association of the S100A10-annexin 2 complex. *Embo J* **22:** 1478-1487.

Wang, W., and Malcolm, B.A. 1999. Two-stage PCR protocol allowing introduction of multiple mutations, deletions and insertions using QuikChange Site-Directed Mutagenesis. *Biotechniques* **26:** 680-682.

Weng, X., Luecke, H., Song, I.S., Kang, D.S., Kim, S.H., and Huber, R. 1993. Crystal structure of human annexin I at 2.5 A resolution. *Protein Sci* **2:** 448-458.

Wittekind, M., and Mueller, L. 1993. HNCACB, a high-sensitivity 3D NMR experiment to correlate amide-proton and nitrogen resonances with the alpha- and beta-carbon resonances. *J. Magn. Reson. Series B.* **101:** 171-180.

Wright, N.T., Cannon, B.R., Wilder, P.T., Morgan, M.T., Varney, K.M., Zimmer, D.B., and Weber, D.J. 2009. Solution structure of S100A1 bound to the CapZ peptide (TRTK12). *J Mol Biol* **386:** 1265-1277.

Wright, N.T., Prosser, B.L., Varney, K.M., Zimmer, D.B., Schneider, M.F., and Weber, D.J. 2008. S100A1 and calmodulin compete for the same binding site on ryanodine receptor. *J Biol Chem* **283:** 26676-26683.

Yap, K.L., Yuan, T., Mal, T.K., Vogel, H.J., and Ikura, M. 2003. Structural basis for simultaneous binding of two carboxy-terminal peptides of plant glutamate decarboxylase to calmodulin. *J. Mol Biol* **328:** 193-204.

Yuan, T., and Vogel, H.J. 1998. Calcium-calmodulin-induced dimerization of the carboxyl-terminal domain from petunia glutamate decarboxylase. A novel calmodulin-peptide interaction motif. *J Biol Chem* **273:** 30328-30335.

Zhang, Z.Q., Wietgrefe, S.W., Li, Q., Shore, M.D., Duan, L., Reilly, C., Lifson, J.D., and Haase, A.T. 2004. Roles of substrate availability and infection of resting and activated CD4+ T cells in transmission and acute simian immunodeficiency virus infection. *Proc Natl Acad Sci U S A* **101:** 5640-5645.

Chapter 4

Novel Structure of S100A10-Annexin A2 in Complex with the AHNAK Peptide

4.1 Introduction

The crystal structures of S100A10 and calcium-bound S100A11 in complex with the N-terminal regions of the phospholipid-binding proteins annexin A2 (Rety et al. 1999) and annexin A1 (Rety et al. 2000), respectively, illustrate the heterotetrameric nature of these complexes. The symmetric arrangement and stoichiometry of these complexes are characteristic of every S100 protein-target peptide structure examined to date, including those of Ca^{2+}-S100B in complex with peptides from the C-terminal region of p53 (Rustandi et al. 2000), the N-terminal regulatory domain of the Ndr kinase (Bhattacharya et al. 2003) and the actin-capping protein CapZ (TRTK12) (Inman et al. 2002; McClintock and Shaw 2003; Charpentier et al. 2010); Ca^{2+}-S100A1 in complex with peptides from the cytosolic regions of the ryanodine receptor (RyR) (Wright et al. 2008) and CapZ (Wright et al. 2009), and Ca^{2+}-S100A6 in complex with the C-terminus of the Siah-1 Interacting Protein (SIP) (Lee et al. 2008). These structures show that some variation in the target peptide binding-site exists (Rezvanpour and Shaw 2009), although a symmetric arrangement is always maintained comprising two S100 protomers and two target peptides. Structural information on the architecture of higher order complexes such as that involving S100A10, annexin A2 and AHNAK are unknown and would be important for understanding how this group of proteins assemble to participate in the cell membrane repair process. To examine how S100A10 and annexin A2 recruit AHNAK, a

hybrid protein complex was designed (described in Chapter 2) in which S100A10 was linked in tandem to the fifteen N-terminal residues of annexin A2 (referred to as A10A2), separated by a nine-residue spacer sequence. Previous work has shown that the linker does not perturb the structures of S100A10 or the bound annexin A2 and allows an interaction similar to the one observed with separate molecules (Rezvanpour et al. 2009). Peptide array experiments identified eight binding regions within the C-terminus of AHNAK for the interaction with the A10A2 hybrid protein (described in Chapter 3). Of the eight consensus regions observed, one of the sequences (referred to as AHNAK5) having a strong interaction was used as a synthetic peptide to identify the binding region(s), stoichiometry and affinity with the A10A2 complex. NMR spectroscopy, non-denaturing electrospray mass spectrometry and fluorescence spectroscopy identified a novel asymmetric ternary arrangement between a single AHNAK5 peptide, and an S100A10-annexin A2 heterotetramer (described in Chapter 3). In this chapter, the A10A2 hybrid protein was used to investigate the binding region of the S100A10-annexin A2 complex with the AHNAK5 peptide. Using both chemical shift mapping by NMR spectroscopy and X-ray crystallography, the three-dimensional structure of the AHNAK5 peptide on the surface of A10A2 was determined, showing that this interaction required residues from helices IV and IV' of dimeric S100A10 as well as the C-terminal portion of the N-terminal peptides of annexin A2.

4.2 Materials and Methods

4.2.1 Source of Materials

$^{15}NH_4Cl$ and $^{13}C_6$-glucose were obtained from Cambridge Isotope Laboratories, Inc. (Andover, MA). ^{15}N-methionine, ^{15}N-phenylalanine, ^{15}N-valine, ^{15}N-leucine, and ^{15}N-isoleucine were obtained from Sigma-Aldrich (St. Louis, MO). All other reagents used in the following experiments were of the highest purity commercially available.

The auxotrophic bacterial strains CT19 (*avtA::Tn5/ trpB83::Tn10/ dcm omT lon* λDE3 *ilvE12 tyrB507 aspC13*) and B834 (*F⁻ ompT hsdS$_B$(r_B^- m_B^-) gal dcm met* DE3) were kindly provided by Dr. L. Mcintosh (University of British Columbia, Canada) and Dr. H. Ling (University of Western Ontario, Canada) and were utilized in the selective ^{15}N-labeling of specific amino acids.

4.2.2 Expression and Purification of the Wild-Type and the C82S Substituted A10A2

Unlabeled wild-type and uniformly ^{15}N, ^{13}C-labeled C82S substituted ($A10A2^{C82S}$) GST-tagged human A10A2 were overexpressed in the BL21 (DE3)-RIL *E. coli* strain using 1 L of 2xYT, or 1 L of M9 minimal medium supplemented with 1 g $^{15}NH_4Cl$ and 2 g $^{13}C_6$-glucose as the sole nitrogen and carbon sources, respectively, as described in Sections 2.2.6 and 3.2.3 (Rezvanpour et al. 2009). The purification procedures were modified for the unlabeled wild-type A10A2 protein. After the last purification step, fractions containing this protein were pooled and dialyzed against a buffer containing 50 mM Tris, 100 mM NaCl at pH 7.0 and 4 ºC. This protein was concentrated and further purified by gel filtration on a HiLoad 16/60 Superdex-75 (GE

Healthcare) column using FPLC. Fractions containing wild-type A10A2 were pooled and dialyzed against 50 mM Tris, and 1 mM DTT at pH 7.5 and 4 ºC. The purity of the protein was assessed by SDS-PAGE analysis.

4.2.3 Selective ^{15}N-Labeling of A10A2^{C82S} Protein

Selectively ^{15}N-labeled A10A2^{C82S} proteins were obtained by growing *E. coli* strain CT19 (*avtA::Tn5/ trpB83::Tn10/ dcm omT lon* λDE3 *ilvE12 tyrB507 aspC13*) in M9 minimal media supplemented with either ^{15}N-phenylalanine, ^{15}N-valine, ^{15}N-leucine or ^{15}N-isoleucine in addition to the remaining 19 unlabeled amino acids. Similarly, selective ^{15}N-methionine labeling of A10A2^{C82S} protein was achieved by growing *E. coli* strain B834 (*F$^-$ ompT hsdS$_B$(r$_B^-$ m$_B^-$) gal dcm met* DE3) in M9 minimal media containing ^{15}N-methionine and the remaining 19 unlabeled amino acids. The purification of the selectively ^{15}N-labeled A10A2^{C82S} proteins followed the same protocol as described in Sections 2.2.6 and 3.2.3 (Rezvanpour et al. 2009) of the Materials and Methods.

4.2.4 Peptide Synthesis

The AHNAK5 peptide (GKVTFPKMKIPKFTFSGREL) was purchased from Bio Basic Inc (Toronto, Canada), synthesized using solid-phase peptide synthesis employing the Fmoc chemistry strategy (Grant 2002). The N-terminus of the peptide was acetylated while the C-terminus was amidated. The synthesized peptides were purified by C18 reversed-phase high performance liquid chromatography (HPLC), and lyophilized.

The MALDI-TOF mass data for the acetylated AHNAK5 (MW_{calc} = 2353.8 Da; MW_{obs} = 2352.5 Da) confirmed the identity of the peptide.

4.2.5 NMR Spectroscopy of A10A2^{C82S} and A10A2^{C82S}-AHNAK5 Complex

All NMR experiments were acquired at 35 ºC on a Varian INOVA 600 MHz spectrometer equipped with a pulsed-field gradient triple resonance probe. The concentration of A10A2^{C82S} was determined by amino acid analysis in triplicate (Advanced Protein Technology Centre, Toronto, Canada). Two NMR samples of uniformly ^{15}N, ^{13}C-labeled A10A2^{C82S} (400 ± 8 μM dimer) were prepared in 10% D_2O, 20 mM MOPS, 1 mM EDTA, 1 mM DTT, 50 mM arginine, 50 mM glutamic acid, and 100 mM NaCl buffer at pH 7.0, using DSS as an internal standard. The AHNAK5 peptide was added to one of the samples to a final concentration of 550 μM. Similarly, samples of 30-100 μM selectively ^{15}N-labeled A10A2^{C82S} proteins containing 40-110 μM unlabeled AHNAK peptide were prepared. ^{1}H-^{15}N HSQC spectra were collected using carrier frequencies of 4.691 (^{1}H) and 114.0 (^{15}N) ppm. Sequential assignment of the polypeptide backbone resonances for A10A2^{C82S} alone and A10A2^{C82S} in complex with the AHNAK5 peptide were achieved by the HNCACB (Wittekind and Mueller 1993), CBCA(CO)NH (Grzesiek and Bax 1992), and HNCA (Kay et al. 1990) experiments. The number of complex data points and the spectral widths were set to 512 and 8000.0 Hz for the ^{1}H (F3) dimension, and 32 and 1700.0 Hz for the ^{15}N (F2) dimension, respectively. For the HNCACB and CBCA(CO)NH experiments, 32 increments and a spectral width of 7840.0 Hz in the ^{13}C (F1) dimension were used. For the HNCA experiment, 32 increments and a

spectral width of 4500.0 Hz were used in the ^{13}C (F1) dimension. All data were processed using NMRPipe and NMRDraw (Delaglio et al. 1995) and analyzed by NMRView (Johnson and Belvins 1994).

4.2.6 Crystallization of the Wild-Type A10A2 in Complex with the C-Terminal Peptide of AHNAK

Prior to crystallization, an excess amount of the AHNAK5 peptide was added to a solution of purified A10A2 to ensure that all A10A2 molecules formed a complex with the AHNAK5 peptide. The excess/unbound AHNAK5 peptide was removed from the sample using a HiPrep 26/10 Desalting column (GE Healthcare) equilibrated in 50 mM Tris, and 1 mM DTT at pH 7.5. The solution of the A10A2-AHNAK5 complex was concentrated to 8 mg/mL. Screening for crystallization conditions was done using several commercial screens such as the Cryo Kit (Sigma-Aldrich), the Crystal Magic Screens I and II (BioGenova), the PEG/Ion Plus Screen (BioGenova), and the Nucleix Suite (QIAGEN). Diffraction-quality crystals were grown in five days at 20°C by the hanging-drop vapor diffusion method, with drops containing 1 μL of the solution of the A10A2-AHNAK5 complex (8 mg/mL in 50 mM Tris-HCl, 1 mM DTT at pH 7.5), 1 μL of the precipitant (QIAGEN Nucleix Suite condition #85: 100 mM sodium chloride, 200 mM magnesium chloride, 0.05 M sodium cacodylate ($(CH_3)_2AsO_2Na$), 20 % (w/v) polyethylene glycol (PEG) 1000, pH 6.5) and 0.2 μL of the crystallization additive (Hampton Research Additive Screen condition #68: 0.15 mM CYMAL-7). The reservoir contained 500 μL of 1.5 M ammonium sulfate.

4.2.7 X-ray Diffraction Data Collection and 3-D Structure Determination

X-ray diffraction data were collected at Beamline X25 (equipped with an ADSC Q315 CCD detector) of the National Synchrotron Light Source in Brookhaven National Laboratory. The data set was indexed, scaled and merged using HKL-2000 (Otwinowski and Minor 1997).

Initial phases were obtained by the molecular replacement method, using the structure of the complex of S100A10 with an N-terminal peptide from annexin A2 (molecules B and D from PDB 1BT6) as the search model (Rety et al. 1999). Molecular replacement was done, and the structural model was built and refined using PHENIX (Adams et al. 2010). During refinement, the structural model was adjusted manually when needed using Coot (Emsley et al. 2010). The stereochemical quality of the structural model was assessed using PROCHECK (Laskowski et al. 1993). Graphical representations of the structural model were prepared using PyMOL (Version 1.2r2, Schrödinger, LLC.). The interaction between A10A2 and the AHNAK5 peptide were analyzed using LIGPLOT (Wallace et al. 1995).

4.2.8 Buried Surface Area Calculation Using VADAR

The overall change in the buried surface area upon peptide binding was determined using the program VADAR (Volume Area Dihedral Angle Reporter) (Willard et al. 2003). The coordinates of the X-ray structural model of A10A2 in complex with the AHNAK5 peptide were utilized for the analysis. Further, the coordinates of the AHNAK5

peptide were removed from the A10A2-AHNAK5 complex to monitor the changes in the buried surface area of the A10A2 alone.

4.3 RESULTS

4.3.1 The C82S Substitution in the A10A2 Protein Does Not Alter Its Structure

To locate the A10A2 residues involved in the interaction with AHNAK5 peptide, backbone assignments of the protein in the absence and presence of the peptide were completed. Although the chemical shift assignment for the wild-type A10A2 was previously completed (Rezvanpour et al. 2009), to keep the experiments consistent with those performed in Chapter 3, the C82S substituted form of A10A2 was used for all NMR experiments. Due to similar properties of cysteine and serine residues, this mutation was not expected to make a dramatic conformational change in the structure of the A10A2 protein. Using standard heteronuclear multiple dimensional NMR spectroscopy (HNCA, HNCACB, and CBCA(CO)NH), chemical shift assignments (^{1}H, ^{15}N, and ^{13}C) for 90% non-proline residues of A10A2^{C82S} (Figure 4.1 and 4.2) (Table 4.1) protein was completed. Figure 4.3 compares the ^{1}H-^{15}N HSQC spectra of the wild-type and C82S substituted A10A2 proteins. Except for a few residues including I75-V88 that are adjacent to the C82S substitution site, the two spectra are superimposable, indicating that comparable geometry and chemistry are maintained in the secondary structure of both forms of A10A2 proteins.

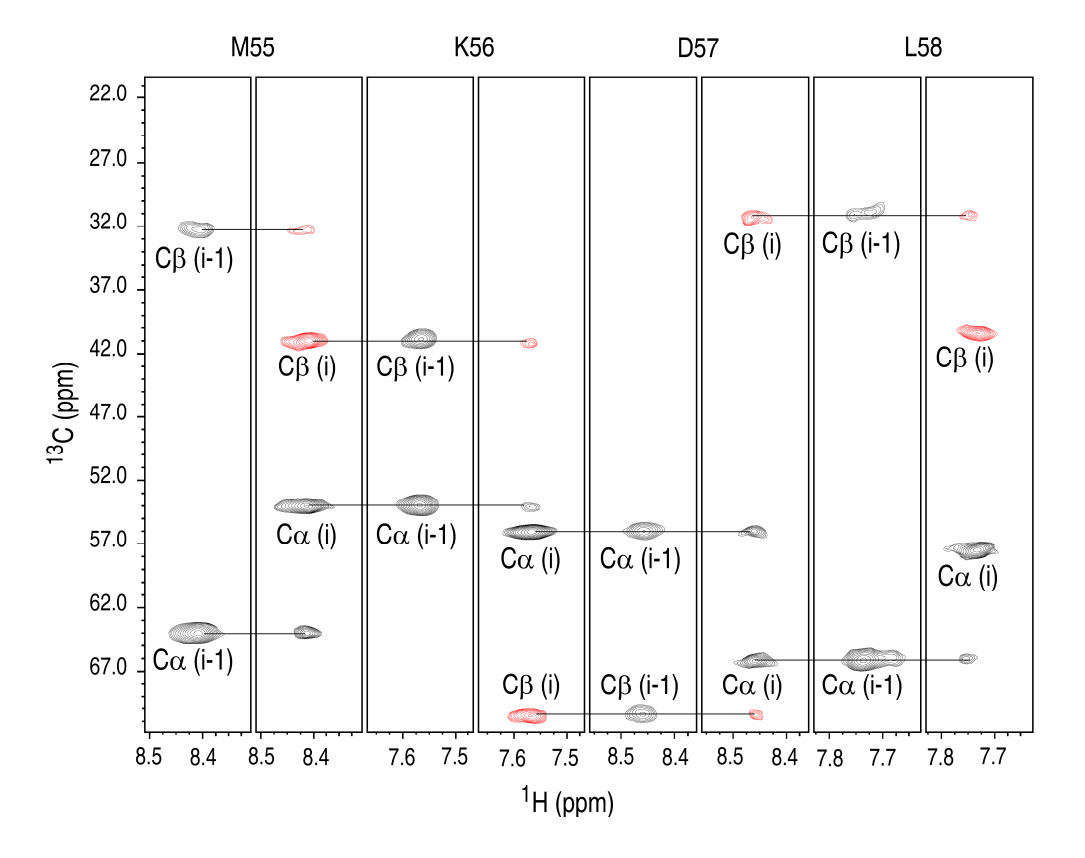

Figure 4.1. Selected regions of 600 MHz NMR spectra used for the backbone assignment of the A10A2^{C82S} protein.

For each pair of planes, the CBCA(CO)NH is shown on the left and the HNCACB on the right where the x-axis is the amide proton chemical shift and the y-axis is the ^{13}C plane of the three dimensional experiments. The Cα and Cβ for the intraresidues (indicated as i) are shown on the HNCACB spectra and the corresponding Cα and Cβ for the previous residues (i-1) are shown in the CBCA(CO)NH. The spectra illustrate ^{15}N planes for sequential assignment of residues M55-L58 of the A10A2^{C82S}.

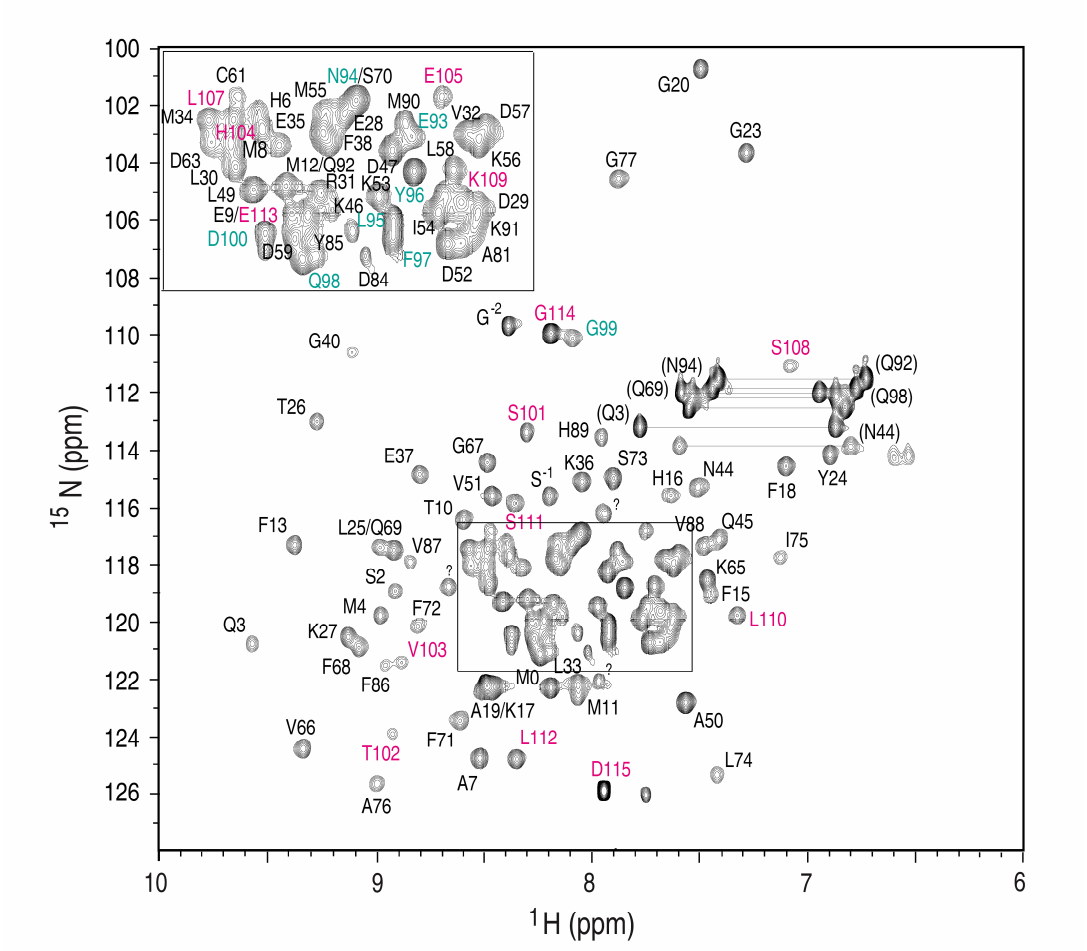

Figure 4.2. Backbone amide assignments of A10A2^{C82S} hybrid protein.

^{1}H-^{15}N HSQC spectrum of 0.4 mM (monomer) uniformly ^{15}N, ^{13}C-labeled A10A2^{C82S} hybrid protein acquired on a Varian INOVA 600 MHz spectrometer. The spectrum was collected in 20 mM MOPS, 1 mM EDTA, 1 mM DTT, 50 mM arginine, 50 mM glutamic acid, 100 mM NaCl, pH 7.0 at 35 ºC. Assigned backbone amide cross peaks are indicated with their one letter amino acid code and number. The residues from ^{15}N, ^{13}C-labeled annexin A2 are presented in pink and those from the linker region in cyan. Pairs of resonances for sidechain amide cross peaks are connected by horizontal lines.

Table 4.1. ^{15}N, ^{13}C and ^{1}H resonance assignments for human A10A2^{C82S}.

Residue	H^N	N	C^α	C^β	Other
G^{-5}			63.24	32.39	
P^{-4}	8.495	122.3	55.47	42.37	
L^{-3}					
G^{-2}	8.390	109.6	45.43		
S^{-1}	8.201	115.7	58.06	64.26	
M0	8.193	122.3	53.23	32.83	
P1			62.44	31.62	
S2	8.902	118.9	56.85	65.67	
Q3	9.566	120.9	59.54	28.19	Cγ (34.78), Nε2 (113.1), Hε21 (6.873), Hε22 (7.778)
M4	8.979	119.7	56.75	30.84	
E5			59.68	29.94	
H6	8.375	117.9	59.41	29.63	
A7	8.522	124.9	55.90	18.45	
M8	8.493	118.3	60.47	35.27	
E9	8.281	120.1	60.32	29.78	
T10	8.592	116.5	67.06	68.43	
M11	8.066	122.7	61.25	32.80	
M12	8.164	117.9	59.86	35.14	
F13	9.367	117.4	59.85	37.58	
T14					
F15	7.441	119.2	62.78	38.86	
H16	7.635	115.7	61.23	31.34	
K17	8.440	122.3	59.38	32.11	
F18	7.101	114.5	60.71	40.43	
A19	8.475	122.3	53.70	18.75	
G20	7.495	100.9	44.79		
D21					
K22			57.77	30.94	
G23	7.284	103.6	46.71		
Y24	6.900	114.1	55.61	40.53	
L25	8.976	117.5	52.85	43.53	
T26	9.270	113.1	60.58	71.90	
K27	9.125	120.6	60.59	32.06	
E28	8.091	117.5	59.51	29.08	
D29	7.629	120.0	57.14	42.88	
L30	8.472	118.8	57.59	41.78	
R31	8.172	119.3	60.55	29.67	
V32	7.660	117.9	66.31	31.78	
L33	8.066	122.3	59.32	42.11	
M34	8.566	117.5	59.41	31.87	
E35	8.318	118.3	59.33	29.93	
K36	8.040	115.3	57.77	33.38	
E37	8.792	114.9	56.44	30.34	
F38	8.131	117.9	54.54	39.53	
P39			65.27		
G40	9.115	110.6	46.48		
F41					
L42					
E43			59.29	28.96	

N44	7.509	115.3	53.82	39.29	Nδ2 (113.9), Hδ21 (6.800), Hδ22 (7.593)
Q45	7.407	117.1	55.39	28.06	
K46	8.133	119.7	57.22	31.95	
D47	7.926	118.4	50.94	42.48	
P48			64.15	32.18	
L49	8.412	119.3	54.09	40.99	
A50	7.567	122.8	56.19	18.72	
V51	8.462	115.7	66.30	31.13	
D52	7.733	120.6	57.70	40.34	
K53	7.975	119.3	59.69	32.29	
I54	7.751	120.0	64.63	38.49	
M55	8.155	117.3	57.68	32.49	
K56	7.622	118.1	59.17	32.17	
D57	7.606	117.6	55.88	41.11	
L58	7.710	118.8	55.79	42.62	
D59	8.266	120.6	54.20	40.31	
Q60			57.72	28.52	Cγ (34.09), Nε2 (111.8), Hε21 (6.839), Hε22 (7.563)
C61	8.471	117.0	59.08	27.38	
R62			57.07	28.26	
D63	8.660	118.8	53.82	41.22	
G64	9.282	109.6	45.93		
K65	7.462	118.4	55.39	34.37	
V66	9.332	124.5	62.69	32.76	
G67	8.479	114.4	44.27		
F68	9.078	121.0	62.95	39.48	
Q69	8.916	117.5	60.50	27.48	Cγ (34.13), Nε2 (112.0), Hε21 (6.823), Hε22 (7.569)
S70	8.060	117.1	61.84	63.19	
F71	8.605	123.6	60.84	39.42	
F72	8.802	120.1	62.67	38.47	
S73	7.901	114.9	61.95		
L74	7.427	125.4	57.93	41.37	
I75	7.126	117.8	62.88	40.84	
A76	8.994	125.8	55.25	18.46	
G77	7.879	104.6	47.43		
L78					
T79					
I80			66.30	38.28	
A81	7.674	120.6	55.34	18.40	
S82					
N83			54.70	40.96	
D84	8.017	121.0	55.49	42.58	
Y85	8.059	120.5	57.57	39.45	
F86	8.950	121.5	61.00		
V87	8.828	117.9	65.04		
V88	7.476	117.4	65.44	32.94	
H89	7.954	113.6	57.95	30.81	
M90	7.878	117.6	57.61	34.88	
K91	7.625	120.1	58.63	32.71	
Q92	8.169	117.9	56.92	28.96	Cγ (34.16), Nε2 (111.5), Hε21 (6.724), Hε22 (7.413)

E93	7.856	117.9	56.79	30.06	
N94	8.054	117.0	53.83	38.38	Nδ2 (111.9), Hδ21 (6.868), Hδ22 (7.538)
L95	7.918	120.1	55.29	42.63	
Y96	7.845	118.8	57.48	38.96	
F97	7.920	120.6	57.68	39.31	
Q98	8.237	121.4	55.89	29.65	Cγ (33.93), Nε2 (111.6), Hε21 (6.776), Hε22 (7.444)
G99	8.079	110.1	45.70		
D100	8.364	120.5	54.78	41.39	
S101	8.302	113.5	58.34	63.94	
T102	8.918	123.9			
V103	8.876	121.4	67.77	31.67	
H104	8.488	117.8	60.19		
E105	7.738	116.7	58.90	29.42	
I106			66.26		
L107	8.565	118.0	58.21	41.75	
S108	7.086	111.3	60.54	63.67	
K109	7.684	119.7	55.72	33.23	
L110	7.322	119.8	55.69	43.22	
S111	8.352	115.9	57.43	64.22	
L112	8.347	124.9	55.56	42.17	
E113	8.219	120.1	56.68	30.75	
G114	8.188	110.0	45.26		
D115	7.943	125.8	55.94	42.48	

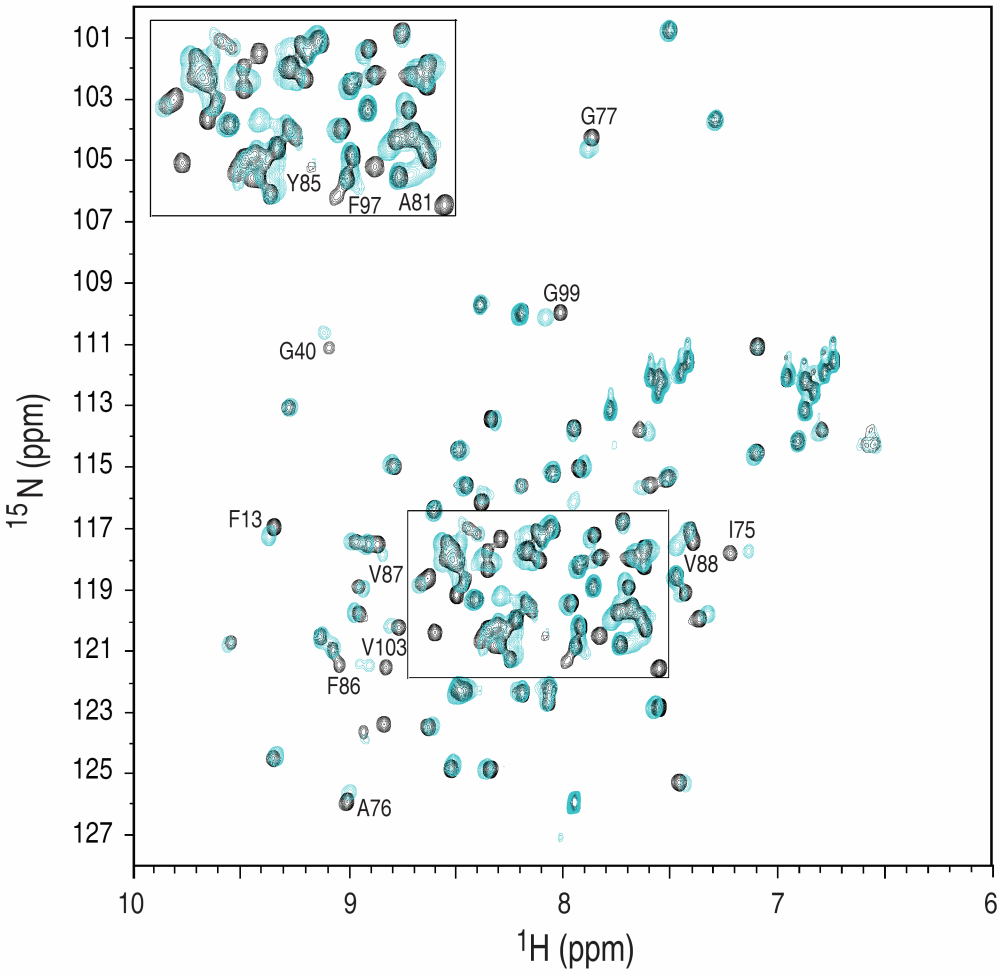

Figure 4.3. Comparison of the ^{1}H-^{15}N HSQC spectra of the wild-type and C82S substituted forms of A10A2 protein.

Overlay of ^{1}H-^{15}N HSQC spectra of wild-type (black) and C82S substituted (aqua) A10A2. NMR samples of uniformly ^{15}N, ^{13}C-labeled A10A2 (400 µM dimer) were prepared in 10% D_2O, 20 mM MOPS, 1 mM EDTA, 1 mM DTT, 50 mM arginine, 50 mM glutamic acid, and 100 mM NaCl buffer at pH 7.0. Spectra were collected on a Varian INOVA 600 MHz spectrometer at 35 ºC.

4.3.2 Backbone Assignment of A10A2^{C82S} in Complex with AHNAK5 Peptide

The 20-residue AHNAK peptide (5654-5673; AHNAK5) that displayed the strongest interaction with A10A2^{C82S} on the peptide array, was used in NMR experiments to assess structural changes that occur in A10A2^{C82S} upon formation of the complex with AHNAK5. As shown in Chapter 3 (Section 3.3.6 and Figure 4.4), titration of unlabeled AHNAK5 peptide to the solution of ^{15}N, ^{13}C-labeled A10A2^{C82S} resulted in the gradual disappearance of many of the A10A2^{C82S} resonances and the appearance of many new peaks. The large number of chemical shift changes in the amide cross peaks of the two spectra indicates that AHNAK5 peptide is indeed binding to the A10A2^{C82S} protein. Interestingly, the ^{1}H-^{15}N HSQC spectrum of the ^{15}N, ^{13}C-labeled A10A2^{C82S} in the presence of AHNAK5 resulted in an increased number of peaks in which many of the new resonances appeared in pairs with each peak having approximately 50% of the intensity of the original peak (Figure 4.4). As an initial step towards completing the assignment of the A10A2^{C82S}-AHNAK5 complex, HNCACB, CBCA(CO)NH and HNCA experiments were collected. Analyses of these spectra were quite challenging as the doubling of peaks resulted in overlapping of many peaks. Consequently, selective ^{15}N-labeling of the backbone amides of leucine, isoleucine, methionine, phenylalanine, and valine of A10A2^{C82S} in complex with AHNAK5 was performed. This accounted for 36% of the amino acid sequence of the A10A2^{C82S} protein. The simplified ^{1}H-^{15}N HSQC spectra of selective ^{15}N-labeled A10A2^{C82S}-AHNAK5 complex (Figure 4.5 and 4.6) along with the triple-resonance NMR experiments (Figure 4.7 and 4.8) contributed greatly in

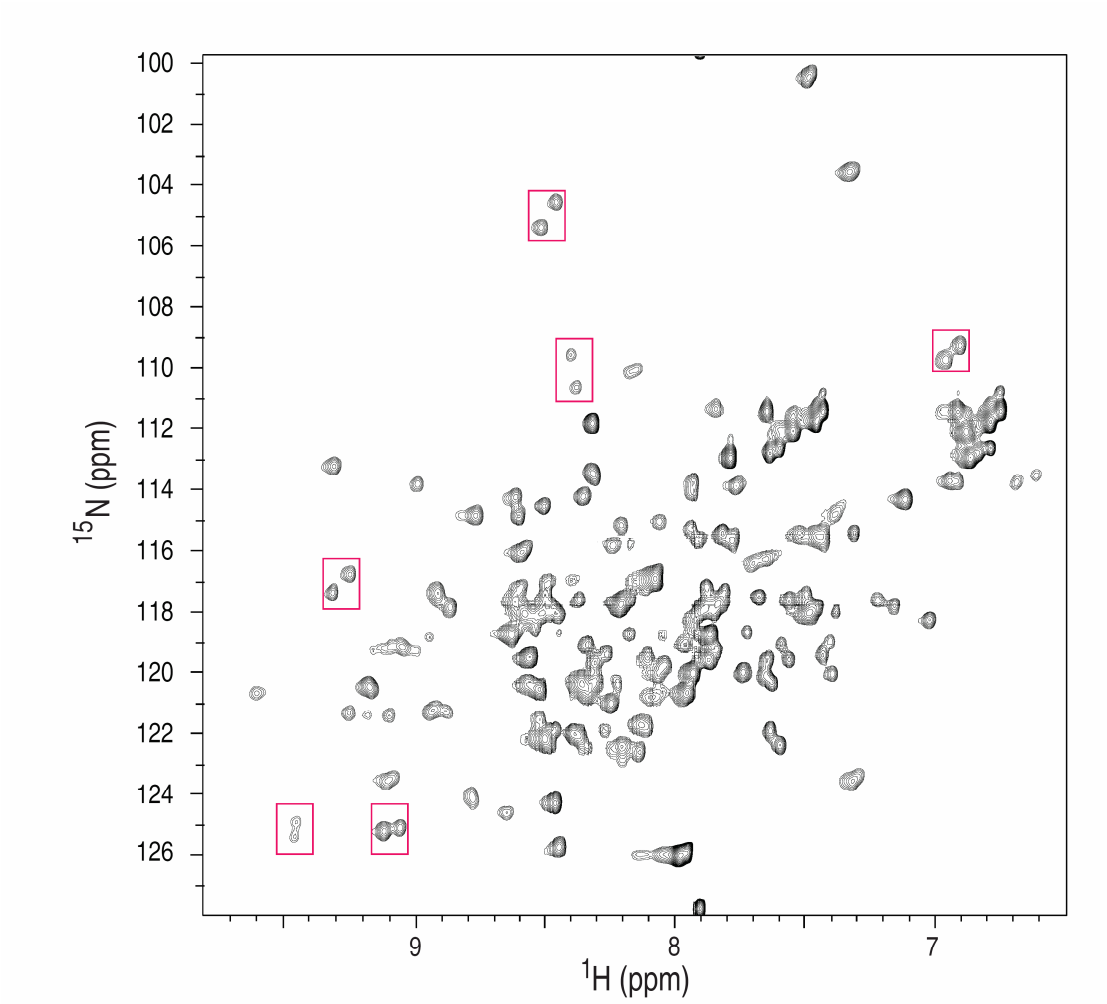

Figure 4.4. ^{1}H-^{15}N HSQC spectrum of A10A2^{C82S} hybrid protein bound to the AHNAK5 peptide.

^{1}H-^{15}N HSQC spectrum of 400 µM uniformly ^{15}N-^{13}C labeled A10A2^{C82S} hybrid protein (protomer) in complex with 550 µM AHNAK5 peptide (Ac-GKVTFPKMKIPKFTFSGR EL). Some of the peaks that exhibited multiplicity in the AHNAK5 complex are shown in boxes. Spectra were collected on a Varian INOVA 600 MHz spectrometer at 35 ºC in 90% H_2O/10% D_2O at pH 7.0.

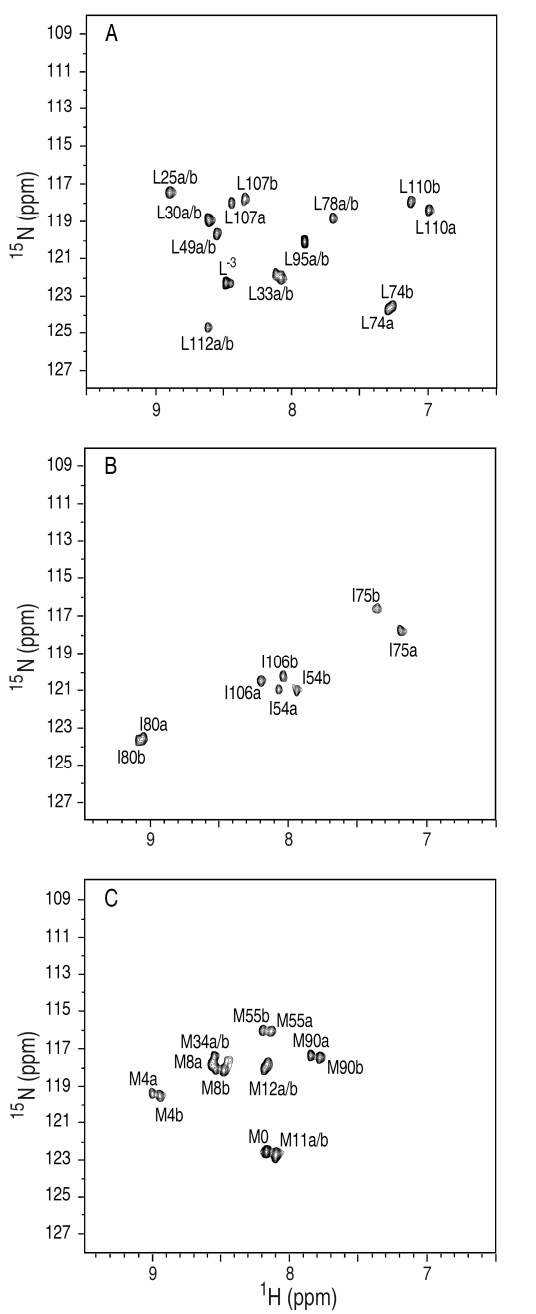

Figure 4.5. ^{1}H-^{15}N HSQC spectra of selectively ^{15}N-labeled A10A2^{C82S} in complex with the AHNAK5 peptide.

The spectra show selectively labeled **(A)** ^{15}N-leucine, **(B)** ^{15}N-isoleucine, and **(C)** ^{15}N-methionine A10A2^{C82S} in complex with AHNAK5 peptide. The residues are numbered 1-115 in both protomers. Multiple resonances from the A10A2^{C82S} protein that appeared as pairs upon addition of AHNAK5 are presented as "a" and "b" with the corresponding residue number in the first or the second protomer.

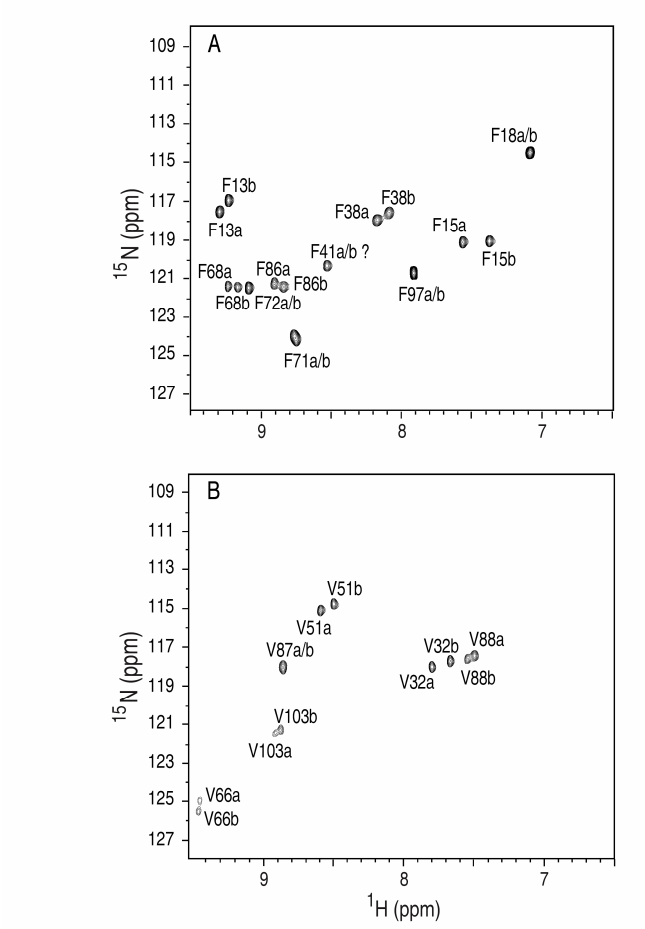

Figure 4.6. ^{1}H-^{15}N HSQC spectra of selectively ^{15}N-labeled A10A2^{C82S} in complex with the AHNAK5 peptide.

The spectra show selectively labeled **(A)** ^{15}N-phenylalanine, and **(B)** ^{15}N-valine A10A2^{C82S} in complex with AHNAK5 peptide. The residues are numbered 1-115 in both protomers. Multiple resonances from the A10A2^{C82S} protein that appeared as pairs upon addition of AHNAK5 are presented as "a" and "b" with the corresponding residue number in the first or the second protomer.

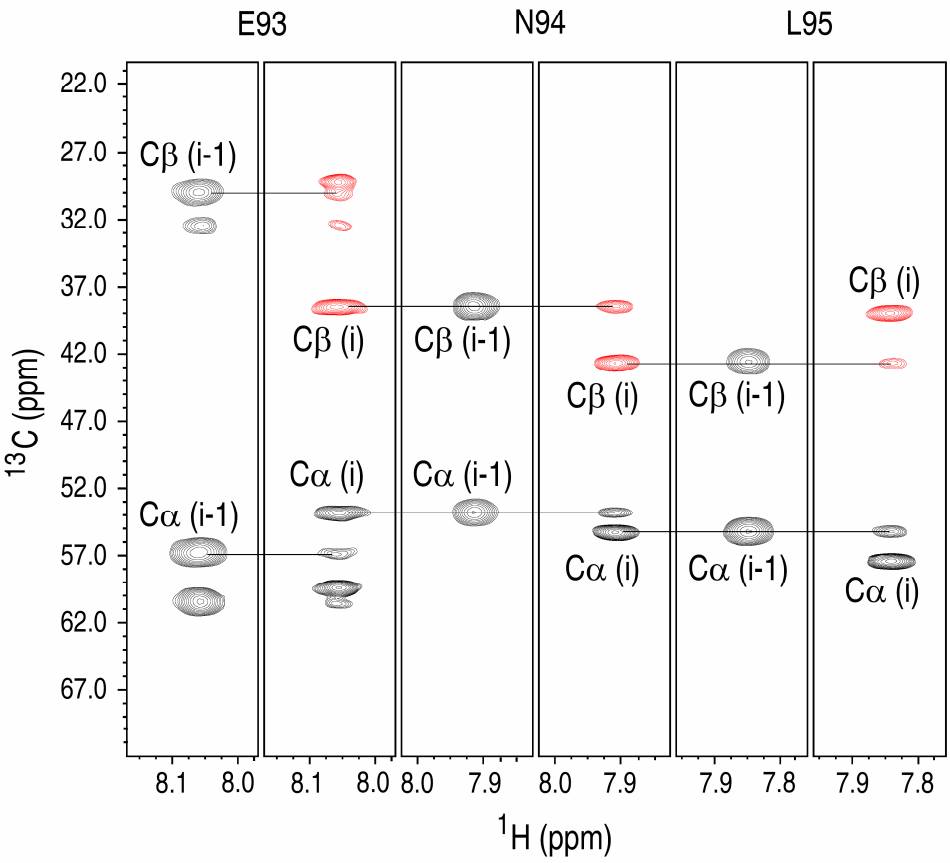

Figure 4.7. Selected regions of 600 MHz NMR spectra used for the backbone assignment of the A10A2^{C82S} in complex with the AHNAK5 peptide.

For each pair of planes, the CBCA(CO)NH is shown on the left and the HNCACB on the right where the x-axis is the amide proton chemical shift and the y-axis is the ^{13}C plane of the three dimensional experiments. The Cα and Cβ for the intraresidues (indicated as i) are shown on the HNCACB spectra and the corresponding Cα and Cβ for the previous residues (i-1) are shown in the CBCA(CO)NH. The spectra illustrate ^{15}N planes for sequential assignment of residues E93-L95 of the A10A2^{C82S} bound to the AHNAK5 peptide.

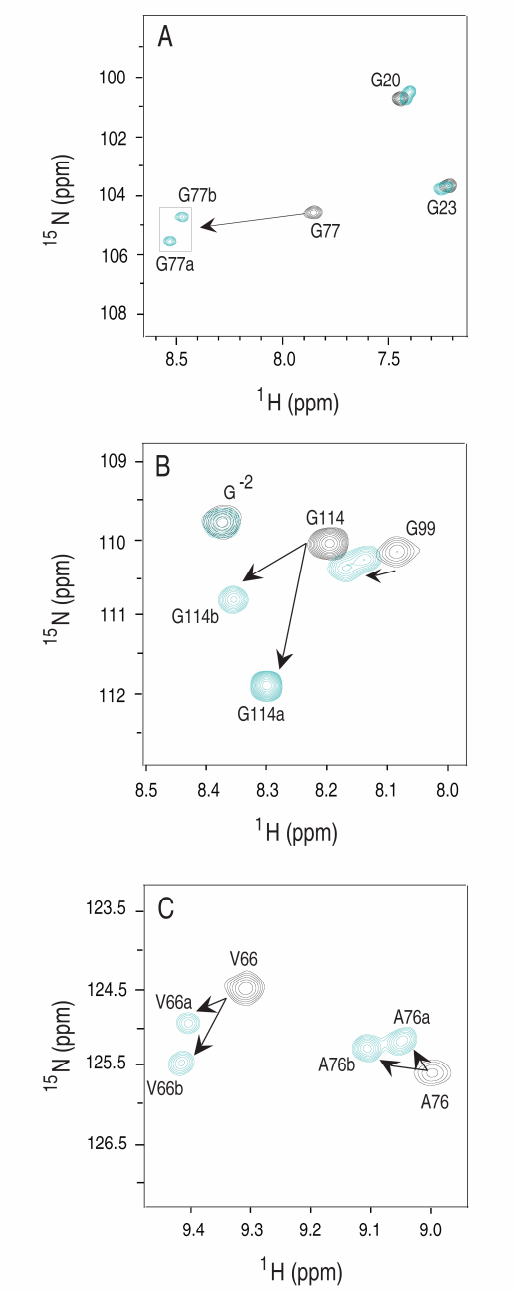

Figure 4.8. AHNAK5 peptide interacts with the A10A2^{C82S}.

Selected regions of the 600 MHz ^{1}H-^{15}N HSQC spectra showing the interaction of the AHNAK5 peptide with ^{15}N, ^{13}C-labeled **(A-C)** A10A2^{C82S} hybrid protein. In all figures, the A10A2^{C82S} alone is shown in the absence (black contours) and in the presence of 1 equivalence (aqua contours) of AHNAK5 peptide. The spectra were collected in 20 mM MOPS, 1 mM EDTA, 1 mM DTT, 50 mM arginine, 50 mM glutamic acid, 100 mM NaCl, pH 7.0 at 35 ºC. Both spectra were assigned by triple-resonance NMR experiments. Spectra are presented at the same contour levels.

identification and completion of the assignment of 107 of 112 non-proline residues in the protein (Table 4.2).

4.3.3 The Binding surface of AHNAK5 Peptide on A10A2^{C82S}

Backbone assignments of the A10A2^{C82S} alone and in complex with the AHNAK5 peptide allowed for the analysis of chemical shift changes of each residue between the two states of the protein (Figure 4.9A and B). Addition of the peptide to the A10A2^{C82S} protein resulted in different changes in the ^{1}H-^{15}N HSQC spectrum. While some peaks remained in their original positions, others shifted and appeared as single or double peak(s) in the spectrum. This suggested that the protein is affected by the peptide binding, either through direct interaction of a residue with the peptide or indirectly by a secondary effect. The most striking chemical shift perturbations occurred for residue E113 of the annexin A2 peptide region in the A10A2^{C82S} hybrid protein of both protomers a and b. Both these residues experienced an amide nitrogen chemical shift change of 1.38 ppm, which was approximately three times the average chemical shift (0.48 ppm). Several other residues also had large chemical shift perturbations including I54a, K56a/b and D59a/b in helix III, C61a/b, D63a/b and G64a/b in the second calcium binding loop, and F72a/b, I75b, G77a/b and D84a in helix IV of the S100A10^{C82S} region in both A10A2^{C82S} protomers. Furthermore, residues S108-S111 and G114 of protomer a, and L110-S111 of protomer b in the annexin A2 peptide region of A10A2^{C82S} showed significant changes in chemical shift. These observations could indicate that these residues are either directly at the protein-peptide interface or indirectly affected by

Table 4.2. ^{15}N, ^{13}C and ^{1}H resonance assignments for A10A2^{C82S}-AHNAK5 complex.

Protomer	Residue	H^N	N	C^α	C^β
	P1			62.40	32.08
	S2	9.080	119.3	56.93	65.34
	Q3	9.575	120.6	59.62	28.17
	M4	9.030	119.3	56.62	30.74
	E5			59.77	29.62
	H6	8.418	118.1	59.53	29.65
	A7	8.452	124.4	55.82	18.19
	M8	8.556	117.9	60.20	35.03
	E9	8.342	120.5	60.44	29.79
	T10	8.569	116.2	67.13	68.18
	M11	8.118	122.7	61.24	33.69
	M12	8.199	117.9	60.14	34.99
	F13	9.301	117.5	60.32	37.81
	T14				
	F15	7.580	119.2	62.77	38.90
	H16	7.508	115.7	61.15	31.42
	K17	8.362	122.2	59.33	32.00
	F18	7.098	114.4	60.59	40.50
	A19	8.483	122.3	53.79	18.74
	G20	7.474	100.8	44.78	
	D21				
	K22			57.77	30.81
	G23	7.308	103.9	46.68	
	Y24	6.918	113.9	55.59	40.05
	L25	8.897	117.5	52.88	42.95
	T26	9.298	113.4	60.68	71.87
	K27	9.162	120.6	60.58	32.28
	E28	8.059	117.1	59.44	29.03
	D29	7.633	119.7	57.06	42.70
	L30	8.616	118.8	57.52	41.46
	R31	8.246	119.4	60.67	29.97
	V32	7.789	117.9	66.51	31.81
	L33	8.111	121.8	59.19	41.76
	M34	8.582	117.5	59.53	32.23
	E35	8.528	118.8	59.22	30.06
	K36	7.928	115.3	57.69	33.37
	E37	8.750	114.9	56.36	29.91
	F38	8.182	118.0	56.83	39.31
	P39				
	G40			48.55	
	F41	8.254	121.9	57.72	40.34
	L42	7.849	119.7	57.68	40.11
	E43			59.50	28.89
	N44	7.357	114.9	53.95	39.30
	Q45	7.435	115.7	54.50	26.94
	K46			56.92	31.16
	D47	7.824	118.0	51.00	42.80
	P48			64.27	32.48
	L49	8.544	119.6	53.81	41.02

	A50	7.584	122.4	56.45	18.43
	V51	8.584	114.9	67.29	31.14
	D52	7.724	120.1	57.57	40.33
	K53			58.57	29.07
	I54	8.068	121.0	66.05	38.63
	M55	8.161	116.0	58.98	32.66
	K56	7.411	115.7	58.83	32.17
“a”	D57	7.430	118.0	55.27	42.50
	L58			56.87	40.57
	D59	8.376	117.1	57.52	40.30
	Q60	8.156	118.8	59.92	32.66
	C61	7.696	116.6	58.72	29.24
	R62			63.24	32.35
	D63	8.488	122.3	55.53	42.36
	G64	8.385	109.7	45.43	
	K65	7.445	118.0	55.45	34.60
	V66	9.438	125.0	62.28	32.30
	G67	8.342	114.4	44.42	
	F68	9.238	121.4	63.56	
	Q69			60.58	27.19
	S70	7.992	117.1	61.67	63.56
	F71	8.762	124.1	60.49	39.08
	F72	9.087	121.4	62.58	38.75
	S73			62.31	62.73
	L74	7.297	123.6	58.31	40.59
	I75	7.198	117.8	62.77	
	A76	9.045	125.1	55.00	18.53
	G77	8.497	105.6	48.44	
	L78	7.708	118.8	58.00	42.31
	T79			67.24	67.68
	I80	9.100	123.6	66.22	38.22
	A81	7.417	119.6	55.16	19.91
	C82	7.767	115.8	62.99	
	N83	8.472	121.8	57.94	39.40
	D84	8.321	119.2	57.96	40.53
	Y85				
	F86	8.925	121.3	61.19	40.41
	V87	8.842	118.0	66.45	31.97
	V88	7.478	117.5	65.47	32.77
	H89	7.911	114.0	58.00	31.56
	M90	7.856	117.4	57.54	34.89
	K91	7.636	120.1	58.43	32.62
	Q92	8.178	117.9	56.89	28.90
	E93	7.869	117.9	56.87	29.95
	N94	8.060	117.0	53.82	38.43
	L95	7.912	120.1	55.26	42.61
	Y96	7.844	118.8	57.46	38.95
	F97	7.934	120.6	57.68	39.18
	Q98	8.230	121.0	55.94	29.51
	G99	8.116	110.1	45.67	
	D100	8.348	120.5	54.74	41.47
	S101	8.297	113.6	58.27	63.84
	T102			66.04	69.48

V103	8.927	121.4	61.12	
H104				
E105			59.68	32.91
I106	8.209	120.5	65.91	37.61
L107	8.457	118.0	58.47	42.29
S108	6.889	109.6	60.24	63.56
K109	7.913	118.4	54.82	33.07
L110	7.006	118.4	54.29	43.54
S111	8.592	114.4	57.16	66.01
L112	8.628	124.6	56.00	42.64
E113	8.433	125.8	57.03	30.78
G114	8.304	111.9	45.18	
D115	7.943	126.0	55.94	42.48
P1			62.40	32.08
S2	9.074	119.3	56.85	65.29
Q3	9.577	120.6	59.65	28.20
M4	8.980	119.3	56.42	30.99
E5			59.77	29.62
H6	8.424	118.2	59.58	29.73
A7	8.448	124.4	55.80	18.21
M8	8.500	117.9	60.18	34.96
E9	8.291	120.5	60.51	29.79
T10	8.564	116.2	67.08	68.18
M11	8.117	122.7	61.25	33.69
M12	8.199	117.9	60.16	35.08
F13	9.235	117.0	60.28	37.81
T14				
F15	7.387	119.2	62.88	38.70
H16	7.513	115.6	61.15	31.42
K17	8.360	122.2	59.33	31.94
F18	7.099	114.4	60.59	40.50
A19	8.483	122.3	53.86	18.74
G20	7.465	100.6	44.79	
D21				
K22			57.77	30.81
G23	7.308	103.9	46.68	
Y24	6.918	113.9	55.60	40.19
L25	8.895	117.5	52.88	42.95
T26	9.298	113.4	60.72	71.85
K27	9.163	120.6	60.50	32.32
E28	8.059	117.1	59.46	29.01
D29	7.547	119.7	56.98	42.61
L30	8.618	118.8	57.52	41.46
R31	8.246	119.4	60.58	30.02
V32	7.661	117.5	66.37	31.58
L33	8.111	121.9	59.21	41.83
M34	8.585	117.5	59.51	32.23
E35	8.449	118.3	59.47	29.96
K36	8.043	115.3	57.72	33.42
E37	8.754	115.0	56.36	29.95
F38	8.186	118.0	56.92	39.31
P39				
G40			48.55	

	F41	8.254	121.9	57.72	40.34
	L42	7.849	119.7	57.68	40.36
	E43			59.50	28.89
	N44	7.359	114.9	53.95	39.30
	Q45	7.435	115.7	54.50	26.94
	K46			56.92	31.16
	D47	7.824	118.0	51.00	42.80
	P48			64.21	32.24
	L49	8.546	119.7	53.81	41.05
	A50	7.622	121.9	56.50	18.43
	V51	8.486	114.8	67.02	30.87
	D52	7.724	120.1	57.57	40.33
	K53			57.53	29.31
	I54	7.947	120.9	65.69	38.46
	M55	8.224	116.0	59.32	32.99
	K56	7.295	115.7	58.69	32.24
	D57	7.364	118.0	54.56	42.09
	L58			56.87	40.57
	D59	8.376	117.1	57.54	40.25
	Q60	8.025	119.7	59.78	32.49
	C61	7.647	116.5	58.77	29.29
	R62			63.17	32.27
“b”	D63	8.491	121.9	55.53	42.36
	G64	8.385	109.7	45.48	
	K65	7.468	118.2	55.33	34.38
	V66	9.436	125.3	62.28	32.37
	G67	8.343	114.4	44.33	
	F68	9.173	121.5	63.19	
	Q69			60.58	27.19
	S70	7.992	117.1	61.67	63.56
	F71	8.762	124.1	60.46	39.06
	F72	9.089	121.5	62.58	38.75
	S73			62.31	62.73
	L74	7.288	123.6	57.67	41.19
	I75	7.373	116.6	63.42	36.07
	A76	9.106	125.3	55.25	19.16
	G77	8.444	104.8	48.42	
	L78	7.708	118.8	58.00	42.31
	T79			67.24	67.68
	I80	9.074	123.6	66.42	38.24
	A81	7.380	120.1	55.39	19.93
	C82	7.753	114.0	63.04	19.96
	N83	8.472	121.8	57.94	39.36
	D84	8.093	119.6	57.88	40.21
	Y85				
	F86	8.876	121.3	61.11	40.15
	V87	8.844	117.9	66.41	31.87
	V88	7.550	117.8	65.42	32.30
	H89	7.928	113.9	57.99	31.58
	M90	7.787	117.4	57.40	34.82
	K91	7.609	120.4	58.47	32.56
	Q92	8.188	117.9	56.87	28.91
	E93	7.870	117.9	56.79	29.95

N94	8.061	117.0	53.81	38.42
L95	7.914	120.1	55.26	42.58
Y96	7.848	118.8	57.46	39.06
F97	7.930	120.6	57.72	39.15
Q98	8.226	121.0	55.94	29.51
G99	8.115	110.1	45.64	
D100	8.327	120.6	54.74	41.45
S101	8.305	113.6	58.27	63.84
T102			65.89	69.44
V103	8.864	121.4	61.13	
H104				
E105			59.79	32.15
I106	8.046	120.1	65.70	38.29
L107	8.352	117.9	58.31	41.72
S108	6.938	110.0	60.41	63.48
K109	7.951	119.2	54.84	32.71
L110	7.139	117.9	54.42	44.61
S111	8.975	114.0	57.25	66.01
L112	8.628	124.6	56.00	42.64
E113	8.433	125.8	56.97	30.85
G114	8.366	110.9	45.23	
D115	7.954	126.1	55.92	42.49

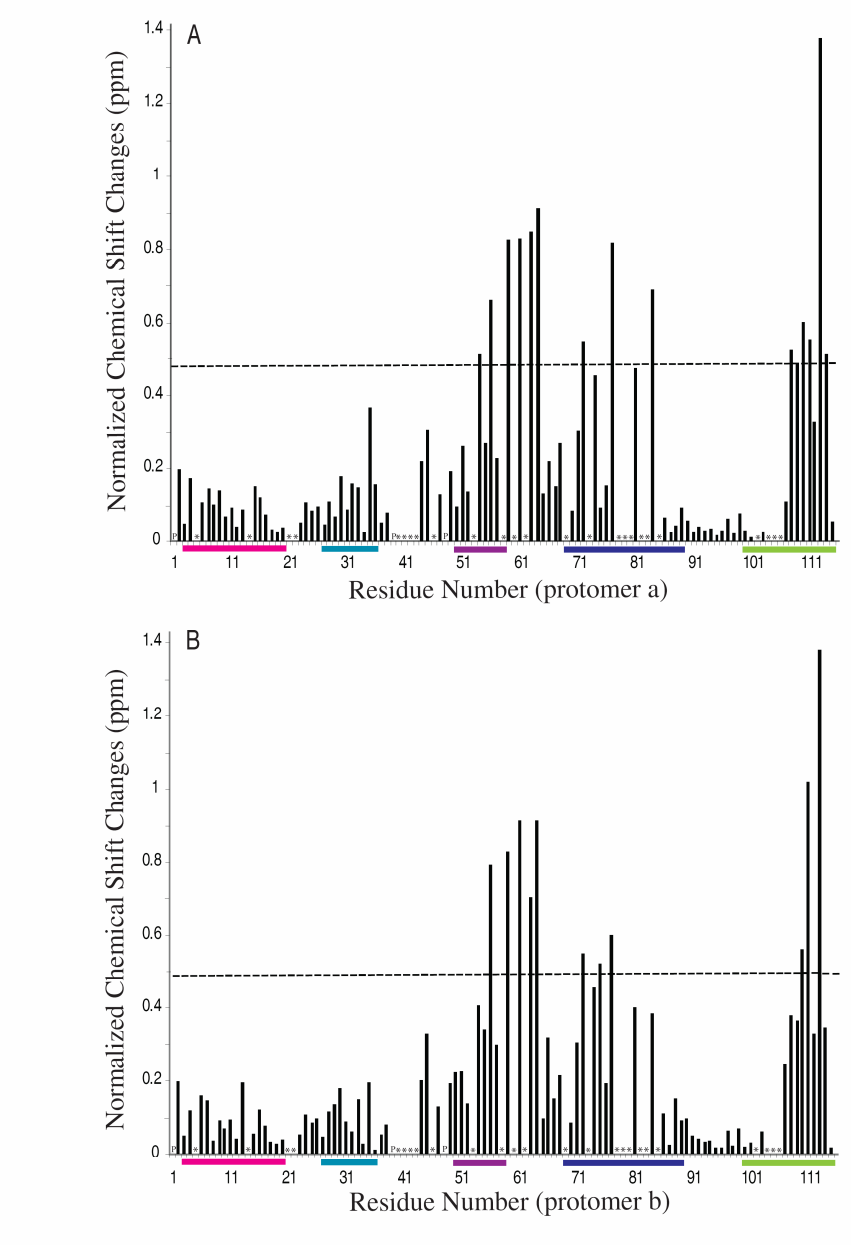

Figure 4.9. Comparison of the changes in chemical shift of the A10A2^{C82S} hybrid protein and AHNAK5-bound A10A2^{C82S} for both protomers a (A) and b (B) in the dimer A10A2^{C82S}.

Chemical shift changes ($\Delta\delta$) were normalized in both ^{1}HN and ^{15}N using the formula $[\{HN^2 + (N/5)^2\}/2]^{1/2}$. The dashed line indicates the average change in chemical shift at 0.48 ppm. Proline residues are shown as "P" and asterisks indicate missing assignments in either or both proteins. Different helices of A10A2^{C82S} (based on the crystal structure of the S100A10-annexin A2 complex) are coloured with helix I in pink, helix II in aqua, helix III in purple, helix IV in blue, and annexin A2 in light green.

residues that were involved in the interaction. The crystal structure of S100A10 in complex with the 12-residue N-terminal peptide of annexin A2 (PDB Code:1BT6) (Rety et al. 1999) was used to map all of the chemical shift changes greater than the average value (0.48 ppm) onto the surface of the A10A2^{C82S} protein (Figure 4.10A). This allowed the interaction surface of the AHNAK5 peptide on the A10A2^{C82S} hybrid protein to be obtained. The length of annexin A2 peptide in the A10A2^{C82S} hybrid construct is 3 residues longer than that in the crystal structure. Thus, residues E113a/b and G114a are not colored in Figure 4.10A. Regardless, the significant change in the chemical shifts for these two residues indicates that E113a/b and G114a are affected by the interaction with the AHNAK5 peptide. Several residues including L58a/b in helix III, Q60a/b and R62a/b in the second calcium binding loop, and S73a/b, L78a/b-I80a/b, and S82a/b-N83a/b in helix IV of the A10A2^{C82S} protomers were lacking chemical shift changes due to missing assignments. Since most of these peaks were assigned in the AHNAK5-bound A10A2^{C82S} (not in the A10A2^{C82S}), the doubling of peaks corresponding to these residues in the complex was considered as a means to identify those affected by the interaction with the AHNAK5 peptide. Among them, only residues Q60a/b, S73a/b and I80a/b appeared as double peaks on the spectrum and thus are inclined to be involved in AHNAK5 binding. In Figure 4.10A, these residues are shaded in a different color to distinguish them from the residues with determined and large chemical shift perturbations. A contiguous surface containing residues E113a-G114a, S108a-S111a, D84a, S82a, I80a, G77a-A76a, S73a, F72a/b, S73b, I75b, A76b-G77b, I80b, L110b-S111b and E113b is formed on the A10A2^{C82S} for the interaction with the AHNAK5. With the current data it is difficult to

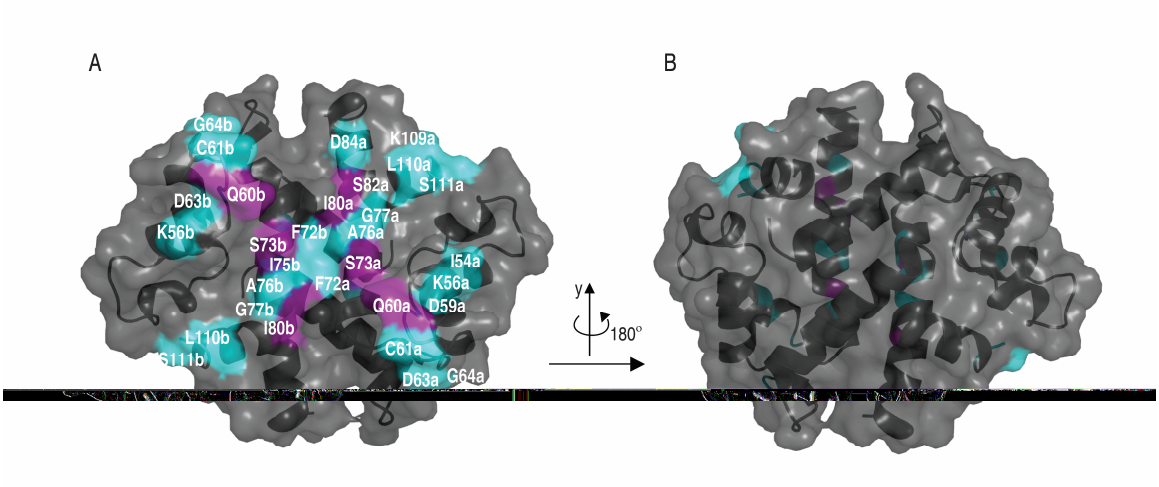

Figure 4.10. The A10A2^{C82S} binding surface for the AHNAK5 peptide.

Surface and ribbon representation of A10A2^{C82S} depicting residues affected by the interaction with the AHNAK5 peptide. **(A)** The surface is coloured according to the chemical shift changes $[\{HN^2 + (N/5)^2\}/2]^{1/2}$ observed in NMR experiments resulting from the interaction with AHNAK5 for both protomers a and b in the dimeric A10A2^{C82S} protein. Residues with chemical shift changes greater than the average chemical shift change of 0.48 ppm are shown in cyan. Residues Q60, S73 and I80 are shaded in purple indicating those that were affected by the binding (doubled peaks in NMR spectrum), even though a chemical shift change could not be determined for them due to the lack of an amide proton or missing assignments in A10A2^{C82S} in the absence of the AHNAK5 peptide. Residues are labeled according to their one-letter amino acid code and residue number. **(B)** The same complex is oriented approximately 180 with respect to (A) to show that the AHNAK5 peptide binds to one side of the A10A2 dimer.

conclude whether residues such as I54a, K56a/b, D59a, Q60a/b, C61a/b, D63a/b and G64a/b are in direct contact with the AHNAK5 peptide or are only affected by the secondary conformational changes resulted from peptide binding. Overall, these data show that the AHNAK5 peptide is bound to only one side of the dimeric A10A2^{C82S} protein, comprised of helices IV and IV' as well as the adjacent C-termini of the annexin A2 peptide region (Figure 4.10A and B).

4.3.4 Crystal Structure of the A10A2-AHNAK5 Complex

4.3.4.1 The Structure of A10A2-AHNAK5 Is Similar to the Non-covalent Complex of S100A10 and Annexin A2

Diffraction quality crystals of the A10A2-AHNAK5 were obtained and the structure of this complex was solved by molecular replacement, using the structure of the S100A10-annexin A2 N-terminal peptide complex (molecules B and D from PDB 1BT6) (Rety et al. 1999) as the search model. The parameters and the statistics of X-ray diffraction data collection and structural model refinement are summarized in Table 4.3. The A10A2-AHNAK5 complex crystallized in the monoclinic space group C2, with two A10A2 molecules (chains a and b) and one AHNAK5 peptide (chain c) in each asymmetric unit. Collected X-ray diffraction data allowed for the computation of electron density maps at a resolution of 2.97Å. Residues Q3a to M90a and Q3b to H89b of the S100A10 regions, T102a to E113a and V103b to E113b of the annexin A2 regions in both protomers of the A10A2 protein, and twelve of the twenty residues of the AHNAK5 were identified. The electron density for some of the residues including C61, I80, A81

Table 4.3. Parameters and statistics of X-ray diffraction data collection and structural model refinement.

A10A2-AHNAK5 Complex	
X-ray Diffraction Data Collection	
Wavelength (Å)	1.100
Resolution limits[a] (Å)	28.96 – 2.97 (3.02 – 2.97)
Space group	C2
Unit-cell constants	
a, b, c (Å)	79.80, 54.99, 62.92
α, β, γ (°)	90, 113.56, 90
Number of unique reflections	5,107 (265)
Redundancy	3.7 (3.7)
Completeness (%)	97.3 (99.3)
R_{sym}[b] (%)	5.1 (45.5)
$I / \sigma(I)$	22.2 (2.9)
Structural Model Refinement	
Resolution range (Å)	28.96 – 2.97
R_{work} / R_{free}[c] (%)	31.43 / 39.72
Number of non-hydrogen atoms per asymmetric unit (average B factors, Å^2)	
Protein	1,483 (175.81)
Solvent	0 (---)
Root-mean-square deviation from ideal geometry	
Bond lengths (Å)	0.006
Bond angles (°)	1.070
Ramachandran statistics	
Most favored (%)	70.8
Additional allowed (%)	25.3
Generously allowed (%)	3.9
Disallowed (%)	0.0

[a] Numbers in the parentheses refer to the highest resolution bins.

[b] $R_{sym} = \sum_{hkl}\sum_i|I_{hkl,i} - \langle I_{hkl}\rangle| / \sum_{hkl}\sum_i I_{hkl,i}$, where $I_{hkl,i}$ and $\langle I_{hkl}\rangle$ are the i-th observed intensity and the average intensity of the reflection hkl, respectively.

[c] $R_{work} = \sum||F_o| - |F_c|| / \sum|F_o|$, where $|F_o|$ and $|F_c|$ are the observed and the calculated structure factor amplitudes of a particular reflection, respectively. The summation is over 95 % of the reflections in the specified resolution range. The remaining 5 % of the reflections were randomly selected before the structure refinement and not included in the structure refinement. R_{free} was calculated over these reflections using the same equation as for R_{work} (Brünger 1992).

and M90 in the S100A10 region of protomer b, K91, G114-D115 in the annexin A2 region as well as the nine residues in the linker connecting the S100A10 to the annexin A2 peptide of both protomers were not visible. The structural model presented here was refined to an R_{work} and an R_{free} values of 31.43 % and 39.72 %, respectively. A high percentage (96.1%) of residues in this structural model lie in the most favored and the additionally allowed regions of the Ramachandran Plot.

The A10A2-AHNAK5 complex contains an A10A2 dimer (Figure 4.11B), whose structure is analogous to that of S100A10 in complex with the N-terminal peptide of annexin A2 (Figure 4.11A). Similarly, helices I, I', IV and IV' of A10A2 comprise the dimer interface. In the A10A2 dimer, helices IV and IV' are roughly antiparallel to each other and form a portion of the dimer interface on one side of the protein as in the other S100 structures. Further, the two annexin A2 peptide regions of the A10A2 dimer bind in nearly the same manner to either side of the S100A10 regions of the dimer such that the C-termini of the annexin A2 peptides are positioned on the same side of the complex as helices IV and IV'. The hydrophobic surface of the annexin A2 peptide region is made up of residues V3a/b, I6a/b, L7a/b and L10a/b. For instance, in protomer a of the A10A2 dimer, V3a of the annexin A2 peptide region interacts with a large number of residues in helix I' (E5', M8', E9', M12'). The residue at position 6a (I) makes contacts with helix IV (C82, Y85, F86, M90). The sidechain of L7a makes numerous contacts with the S100A10 region via residues in the linker sequence (F38, F41), helix IV (L78, C82) and helix I' (E5', M8'). Finally, the residue at position 10a (L) is in close proximity of helix IV (A81, C82, Y85). All of these findings are in perfect agreement with the X-ray

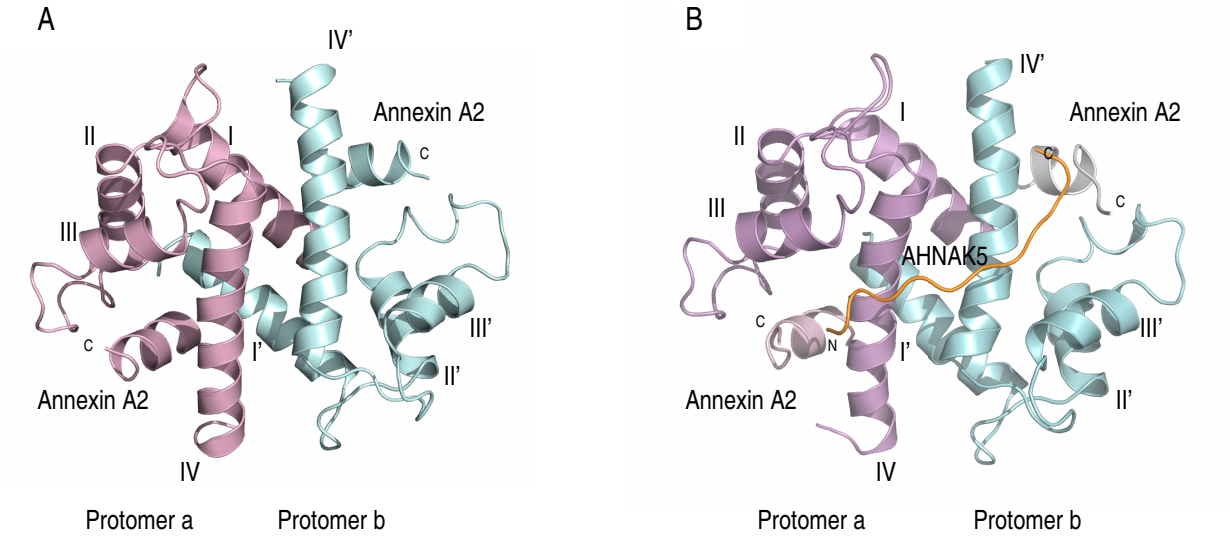

Figure 4.11. Comparison of the S100A10-annexin A2 structures alone and in complex with the AHNAK5 peptide.

Ribbon diagrams of **(A)** S100A10 bound to the N-terminal peptide of annexin A2 (Rety et al. 1999) and **(B)** A10A2 in complex with the AHNAK5 peptide are shown in similar orientations to demonstrate the lack of conformational changes that occur upon binding to the AHNAK5 peptide. In both structures, protomer a (including its associated annexin A2 peptide) is shown in light purple and its helices are numbered I-IV, while protomer b (including its corresponding bound annexin A2 peptide) is presented in light blue and its helices are numbered I'-IV'. The single AHNAK5 peptide is shown as a yellow strand bound to an A10A2 dimer in (B). Superposition of these two structures gives a backbone rmsd value of 0.66 Å.

crystallographic results (Rety et al. 1999) for the S100A10-annexin A2 complex in the absence of AHNAK5. Despite the non-covalent complex of S100A10 and the individual N-terminal peptide of annexin A2 in the X-ray crystallographic structure (Rety et al. 1999), and the covalent linkage between these two proteins in the A10A2-AHNAK5 complex, these two structures are indeed similar to each other with an rmsd of 0.66 Å. This provides further evidence that the linker connecting S100A10 to the N-terminal peptide of annexin A2 in the A10A2 hybrid protein has not perturb the structure.

Comparison between the structures of S100A10 in complex with the individual N-terminal peptide of annexin A2, A10A2 and AHNAK5-bound A10A2 with the S100A10 protein resulted in small rmsd values of 0.91, 1.11, and 1.37 Å, respectively. Once more, these values confirm that the backbone structure of S100A10 does not change significantly in any of the complexes when S100A10 binds to either annexin A2 or both annexin A2 and AHNAK5 peptides.

4.3.4.2 Binding Region of AHNAK5 on A10A2

Following fitting for the S100A10 and annexin A2 portions of the A10A2 structure, outstanding electron densities were clearly observed for the backbone of the AHNAK5 peptide in the electron density maps (Figure 4.12A). This electron density was only sufficient to fit a single AHNAK5 peptide on helix IV side of the A10A2 complex. This stoichiometry of 1:1 for an A10A2(dimer):AHNAK5 complex is in agreement with the fluorescence, NMR and non-denaturing mass spectroscopy experiments presented in Chapter 3. As explained above and shown in Figure 4.11, interaction of the AHNAK5

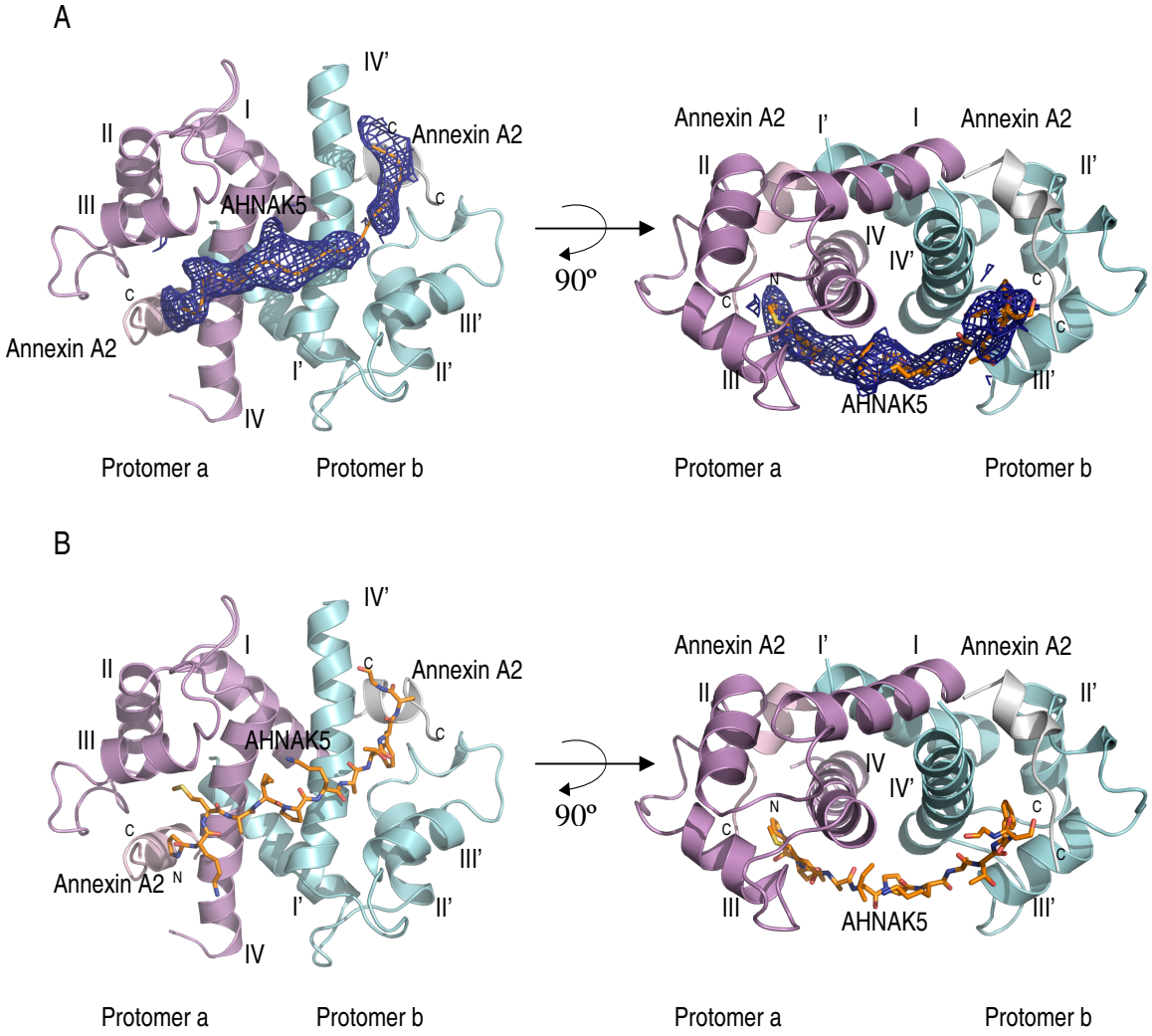

Figure 4.12. Orthogonal views of the A10A2-AHNAK5 complex.

Outstanding electron density of the AHNAK5 peptide are shown in **(A)** and omitted for clarity purposes in **(B)**. In both diagrams, the ribbon representation of the A10A2-AHNAK5 complex is oriented approximately 90º with respect to each other to show the binding region of a single AHNAK5 peptide. Protomer a of the A10A2 dimer is colored in light purple and its helices are numbered I-IV, whereas protomer b is shown in light blue and its helices are numbered I'-IV'. The single AHNAK5 peptide is represented as sticks, with carbon atoms in yellow, nitrogen atoms in blue and oxygen atoms in red.

peptide with the A10A2 dimer does not cause a significant conformational change in the backbone structure of the A10A2 hybrid protein. Adopting a coil conformation, the bound AHNAK5 peptide was located on one face of the dimeric A10A2, comprising helices IV and IV' as well as the adjacent C-termini of the annexin A2 peptide regions (Figure 4.11B and 4.12). In the model shown, residues P6 to G17 of the AHNAK5 peptide (ie. PKMKIPKFTFSG) were modeled in the electron densities. However, the sidechain conformations of K9, and F13 could not be determined (Figure 4.13). The PDB file for the crystal structure was used in the LIGPLOT program (Wallace et al. 1995) to generate schematic 2D representations of the A10A2-AHNAK5 complex, showing intermolecular interactions as well as their strengths including hydrogen bonds, hydrophobic interactions and atom accessibilities (Figure 4.14). Based on this analysis, P6, M8, F15, and S16 of the AHNAK5 peptide are involved in interactions with the A10A2 dimer (Figure 4.13 and 4.14). The residue at position 6 (P) of the AHNAK5 peptide interacts with S111 at the C-terminus of the annexin A2 peptide region of protomer a in the A10A2 dimer. M8 of the AHNAK5 makes contacts with helix III (I54, L58) of the S100A10 region of also protomer a. F15 of the AHNAK5 peptide interacts with L78 of the S100A10 and L112 from the C-terminus of the annexin A2 peptide regions of protomer b in the dimeric A10A2 protein. Lastly, a hydrogen bond exists between the sidechain of S16 of the bound AHNAK5 with S111 at the C-terminus of the annexin A2 peptide region of protomer b in the A10A2 dimer.

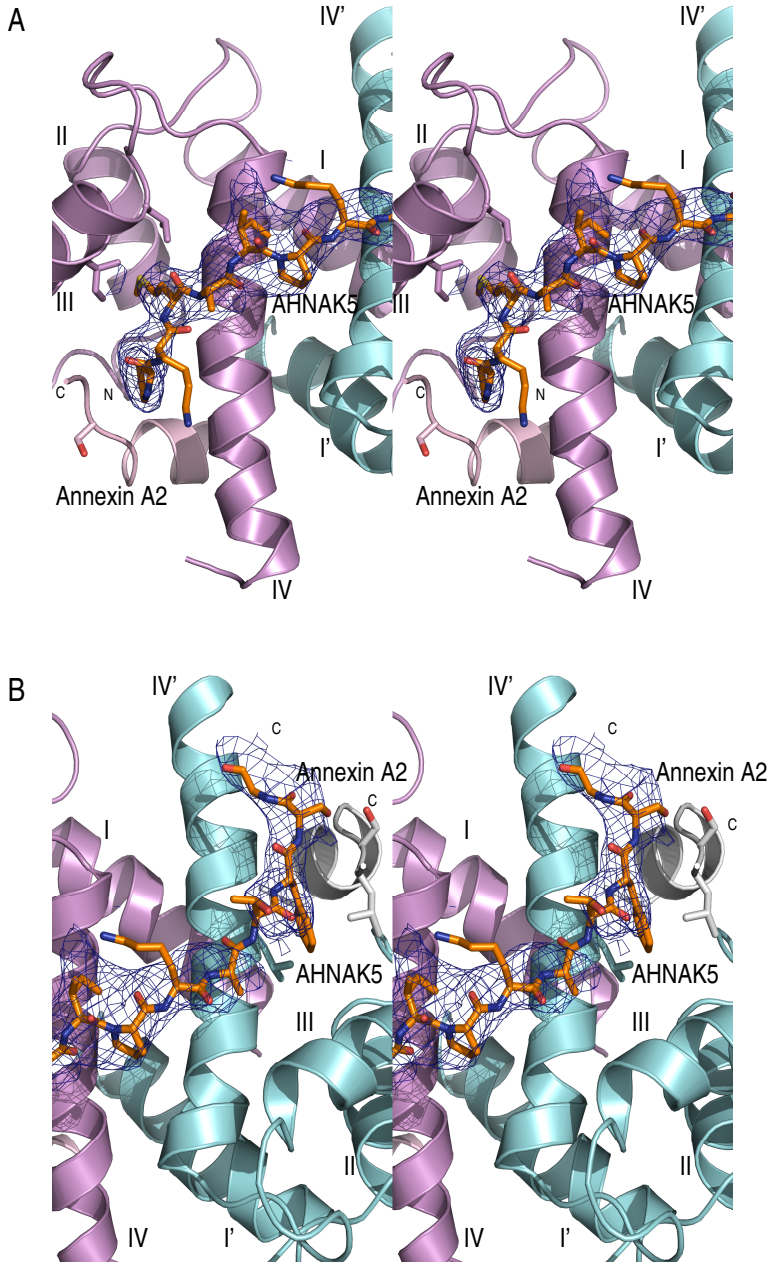

Figure 4.13. AHNAK5-binding site on the A10A2 dimer.

Close-up stereo views of the **(A)** N-terminal half and **(B)** C-terminal half of the bound AHNAK5 peptide on the A10A2 dimer are shown. In both diagrams, the two A10A2 subunits are colored in light purple (protomer a) and light blue (protomer b), and the helices are numbered I-IV and I'-IV' for protomer a and b, respectively. The single AHNAK molecule is represented in orange. Residues of A10A2 interacting with the AHNAK5 peptide are also presented as sticks, with carbon atoms in the original color, nitrogen atoms in blue and oxygen atoms in red.

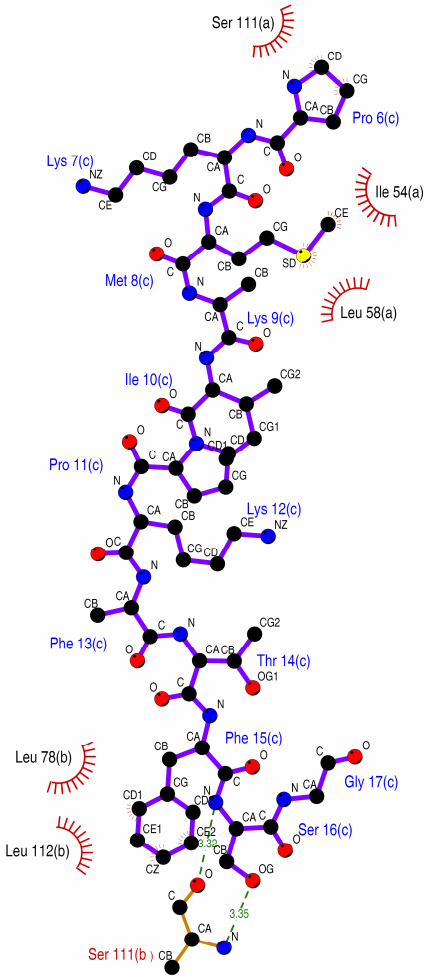

Figure 4.14. Schematic representation of intermolecular interactions in the A10A2-AHNAK5 complex.

The LIGPLOT program was used to generate a 2D schematic for the intermolecular interactions between the residues from the AHNAK5 peptide and A10A2 protein. The hydrogen bonds and their distances are indicated by (3.0). Covalent bonds in the AHNAK5 peptide are shown by ( ), while covalent bonds in the A10A2 dimer are presented by ( ). Residues of the A10A2 dimer (protomers a and b) and specific atoms involved in Van der Waals contacts are indicated by ( ) and ( ), respectively.

4.4 Discussion

4.4.1 Comparison of the Binding Surface of AHNAK5 on A10A2 Determined by X-ray Crystallography and NMR Spectroscopy

In this chapter, the AHNAK5 peptide which had previously shown the strongest interaction with $A10A2^{C82S}$ was utilized to identify the arrangement of the S100A10-annexin A2-AHNAK5 ternary complex. NMR spectroscopy and X-ray crystallography were used to determine which residues of A10A2 protein and AHNAK5 peptide are involved in the interaction. ^{1}H-^{15}N HSQC spectra were collected to monitor the changes made in the $A10A2^{C82S}$ spectra after addition of the AHNAK5 peptide. NMR experiments revealed a significant number of chemical shift changes in the amide cross peaks of the two spectra confirming that an interaction with the AHNAK5 peptide has taken place. Significant changes in chemical shift were observed mainly for residues in helix IV and IV' of protomers a and b of the S100A10 region (D84a, S82a, I80a, G77a-A76a, S73a, F72a/b, S73b, L74b, A76b-G77b, I80b), as well as the residues from the annexin A2 peptide region (E113a-G114a, S108a-S111a, L110b-S111b and E113b) of $A10A2^{C82S}$ protein (Figure 4.10). Overall, these results showed that interaction of a single AHNAK5 peptide with the $A10A2^{C82S}$ protein is consistent with asymmetrical binding to one face of the dimeric protein comprising helices IV and IV' and the adjacent annexin A2 C-termini. A number of significant chemical shift changes also occurred in helix III and III' as well as the second calcium-binding loops of both protomers of $A10A2^{C82S}$ protein (Figure 4.10) either through direct contact with the AHNAK5 peptide or by indirect changes resulting from peptide binding.

Determining resonance assignments for an unlabeled peptide such as AHNAK5 in a protein-peptide complex is difficult by NMR spectroscopy as only proton signals of the unlabeled peptide will be observed in the spectra. Consequently, residues from the AHNAK5 peptide that are directly involved in the interaction could not be determined. X-ray crystallography of the A10A2-AHNAK5 complex was useful in obtaining detailed information on the bound peptide. The backbone structure of A10A2-AHNAK5 complex is similar to that of S100A10 in complex with the N-terminal peptide of annexin A2 (Figure 4.11A and B). The hydrophobic surface of the annexin A2 peptide region of the A10A2 hybrid protein in the A10A2-AHNAK5 complex was also similar to that of the X-ray crystallographic results of the S100A10 bound to individual N-terminal peptide of annexin A2. Even though computation of electron density maps was only possible to a resolution of 2.97Å, it was still clear that only one AHNAK5 peptide is bound to one face of the dimeric A10A2, comprising helices IV and IV' as well as the adjacent C-termini of the annexin A2 peptide regions (Figure 4.11B and 4.12A and B). This is in perfect agreement with the results obtained by NMR spectroscopy. Some of the important residues for this interaction included I54, L58 and S111 of protomer a, and L78, S111 and L112 of protomer b in the A10A2 protein. The X-ray crystallography data explains some of the NMR spectroscopy observations. For instance, the significant chemical shift of I54a is due to interaction of this residue with the methionine sidechain at position 8 of the AHNAK5 peptide. This interaction would explain the large chemical shifts of other residues in helix III and the second calcium-binding loop of protomer a in the dimeric A10A2 protein. Chemical shift changes could not be determined for residue

L58a and L78b of the A10A2 protein by NMR experiments due to the missing assignments or lacking chemical shift changes, respectively. However, chemical shift changes greater than the average chemical shift values for S111 in both protomers a and b was observed. Although, a significant chemical shift for S111a was observed, the change in chemical shift (more than twice the average chemical shift value) was more pronounced for S111 in protomer b. This could be explained by the hydrogen bond formed between the sidechain of S16 of the bound AHNAK5 with S111 at the C-terminus of the annexin A2 peptide region of protomer b in the A10A2 dimer. Residue L112 in protomer b of the dimeric A10A2 protein was identified as one of the residues involved in the interaction with the AHNAK5 peptide by X-ray crystallography, while a chemical shift change below the average change in chemical shift was obtained for this residue by NMR spectroscopy. Further, the fractional accessible surface area for the sidechains of residues of A10A2 in the absence and presence of AHNAK5 peptide were calculated from the three-dimensional X-ray crystallography model using the program VADAR (Willard et al. 2003). This showed that 558 $Å^2$ of the sidechain surface area in A10A2 protein was buried upon binding AHNAK5 in A10A2-AHNAK5 complex. Residues in the A10A2 protein that decreased their sidechain exposure by greater than 40% upon AHNAK5 binding included F41, I54, L58, S73, L74, A76, G77, L78, A81, L110 and L112 of protomer a and I54, L58, S73, L74, G77, L78, D84, L110 and L112 of protomer b of the A10A2 protein. This method allowed identifying additional residues such as F41 and A81 in protomer a, as well as I54 and L58 in protomer b of A10A2 that were buried by the interaction of AHNAK5. Higher quality crystals allowing higher resolution

electron density maps, or complete NMR assignments of A10A2 protein alone and in complex with the AHNAK5 peptide could help finding the answer to some of the discrepancies observed here.

X-ray crystallography results complemented the peptide array experiments in identifying the important residues of AHNAK5 that were involved in A10A2 binding (Chapter 3). Peptide array identified a nine residue consensus sequence for AHNAK, represented as +X+XPKφXφ (X – variable; φ – hydrophobic residue; + – positively charged residue; P – proline; K – lysine) (Figure 3.1). Proline at position 6 of the AHNAK5 peptide that showed interaction with S111 at the C-terminus of the annexin A2 region of protomer a in the A10A2 dimer, is not included in the consensus sequence. However, the binding was abolished as soon as the 3 residues FPK (positions 5-7 of AHNAK5) were eliminated from the peptide sequence on the array. Residue M8 of the AHNAK5 peptide makes contacts with helix III (I54, L58) of the S100A10 region of protomer a. This residue is presented as a variable (X) in the consensus, while peptide array sequence analysis showed that smaller sidechain of methionine at this position enhances the interaction. The consensus sequence does not include residues F15 and S16 of the AHNAK5 peptide that associated with L78, S111 and L112 of protomer b in the A10A2 protein by X-ray crystallography. However; the strongest interaction was observed when these residues became a part of the peptide sequence on the array.

Interestingly, amino acids F41, I54, L58, S73, L74, A76, G77, L78 and A81 in the S100A10 region of A10A2 protein that were the key residues in binding AHNAK5 in the X-ray crystallographic structure, are conserved hydrophobic residues in the S100

family of proteins (Wilder et al. 2006). While, the possibility of a similar complex formed between an S100 dimer, a pair of annexins and a single AHNAK exists, only some of the S100 proteins have shown an interaction with annexin family of proteins. These include Ca^{2+}-S100A1 with annexin A5 (Garbuglia et al. 1998) and annexin A6 (Propper et al. 1999; Arcuri et al. 2002); Ca^{2+}-S100A6 with annexin A11 (Watanabe et al. 1993; Tomas and Moss 2003; Williams et al. 2005), annexin A2 (Zeng et al. 1993; Filipek et al. 1995), annexin A5 (Tokumitsu et al. 1992), and annexin A6 (Zeng et al. 1993); Ca^{2+}-S100A11 with annexin A1 (Rety et al. 2000; Bianchi et al. 2003); Ca^{2+}-S100B with annexin A6 (Garbuglia et al. 1998; Arcuri et al. 2002); apo-S100A4 with annexin A2 (Semov et al. 2005); and apo-S100A10 with annexin A2 (Osborn et al. 1988; Johnsson and Weber 1990; Bianchi et al. 1992; Rety et al. 1999). Closer look at the first fourteen amino acid residues at the N-terminus of annexin A1, A2, A5, A6, and A11 reveals that in fact only annexin A1 and A2 have significant sequence similarity. Thus, formation of a ternary complex involving an AHNAK protein associated with annexin A2-bound apo-S100A10, apo-S100A4 or Ca^{2+}-S100A6; or annexin A1-bound Ca^{2+}-S100A11 could occur in a similar manner, where any one of these complexes could perform a similar function in the appropriate cell type.

4.5 References:

Adams, P.D., Afonine, P.V., Bunkoczi, G., Chen, V.B., Davis, I.W., Echols, N., Headd, J.J., Hung, L.W., Kapral, G.J., Grosse-Kunstleve, R.W., et al. 2010. PHENIX: a comprehensive Python-based system for macromolecular structure solution. *Acta Crystallogr D Biol Crystallogr* **66:** 213-221.

Arcuri, C., Giambanco, I., Bianchi, R., and Donato, R. 2002. Annexin V, annexin VI, S100A1 and S100B in developing and adult avian skeletal muscles. *Neuroscience* **109:** 371-388.

Bianchi, R., Giambanco, I., Arcuri, C., and Donato, R. 2003. Subcellular localization of S100A11 (S100C) in LLC-PK1 renal cells: calcium- and protein kinase C-dependent association of S100A11 with S100B and vimentin intermediate filaments. *Microsc Res Tech.* **60:** 639-651.

Bianchi, R., Pula, G., Ceccarelli, P., Giambanco, I., and Donato, R. 1992. S-100 protein binds to annexin II and p11, the heavy and light chains of calpactin I. *Biochim. Biophys. Acta* **1160:** 67-75.

Bhattacharya, S., Large, E., Heizmann, C. W., Hemmings, B., Chazin, W. J. 2003. Structure of the Ca^{2+}/S100B/NDR kinase peptide complex: insights into S100 target specificity and activation of the kinase. *Biochemistry* **42:** 14416-14426.

Brünger, A. T. 1992. Free R value: a novel statistical quantity for assessing the accuracy of crystal structures. *Nature* **355:** 472 -475.

Charpentier, T.H., Thompson, L.E., Liriano, M.A., Varney, K.M., Wilder, P.T., Pozharski, E., Toth, E.A., and Weber, D.J. 2010. The effects of CapZ peptide (TRTK-12) binding to S100B-Ca2+ as examined by NMR and X-ray crystallography. *J Mol Biol* **396:** 1227-1243.

Delaglio, F., Grzesiek, S., Vuister, G.W., Zhu, G., Pfeifer, J., and Bax, A. 1995. NMRPipe: a multidimensional spectral processing system based on UNIX pipes. *J Biomol NMR* **6:** 277-293.

Emsley, P., Lohkamp, B., Scott, W.G., and Cowtan, K. 2010. Features and development of Coot. *Acta Crystallogr D Biol Crystallogr* **66:** 486-501.

Filipek, A., Wojda, U., and Lesniak, W. 1995. Interaction of calcyclin and its cyanogen bromide fragments with annexin II and glyceraldehyde 3-phosphate dehydrogenase. *Int J Biochem Cell Biol* **27:** 1123-1131.

Garbuglia, M., Verzini, M., and Donato, R. 1998. Annexin VI binds S100A1 and S100B and blocks the ability of S100A1 and S100B to inhibit desmin and GFAP assemblies into intermediate filaments. *Cell Calcium* **24:** 177-191.

Grant, G. 2002. *Synthetic Peptides: A User's Guide*. Oxford University Press, New York.

Grzesiek, S., and Bax, A. 1992. Correlating backbone amide and sidechain resonances in larger proteins by multiple relayed triple resonance NMR. *J. Am. Chem. Soc.* **114:** 6291-6293.

Inman, K.G., Yang, R., Rustandi, R.R., Miller, K.E., Baldisseri, D.M., and Weber, D.J. 2002. Solution NMR structure of S100B bound to the high-affinity target peptide TRTK-12. *J. Mol. Biol.* **324:** 1003-1014.

Johnson, B.A., and Belvins, R.A. 1994. NMRView: A computer program for the visualization and analysis of NMR data. *J Biomol NMR* **4:** 603-614.

Johnsson, N., and Weber, K. 1990. Alkylation of cysteine 82 of p11 abolishes the complex formation with the tyrosine-protein kinase substrate p36 (Annexin 2, Calpactin 1, Lipocortin 2). *J. Biol. Chem.* **265:** 14464-14468.

Kay, L.E., Ikura, M., Tschudin, R., and Bax, A. 1990. Three-dimentional triple-resonance NMR spectroscopy of isotopically enriched proteins. *J. Magn. Reson.* **89:** 496-514.

Laskowski, R.A., MacArthur, M.W., Moss, D.S., and Thornton, J.M. 1993. PROCHECK: a program to check the stereochemical quality of protein structures. *J. Appl. Cryst.* **26:** 283-291.

Lee, Y.T., Dimitrova, Y.N., Schneider, G., Ridenour, W.B., Bhattacharya, S., Soss, S.E., Caprioli, R.M., Filipek, A., and Chazin, W.J. 2008. Structure of the S100A6 complex with a fragment from the C-terminal domain of Siah-1 interacting protein: a novel mode for S100 protein target recognition. *Biochemistry* **47:** 10921-10932.

McClintock, K.A., and Shaw, G.S. 2003. A novel S100 target conformation is revealed by the solution structure of the Ca2+-S100B-TRTK-12 complex. *J Biol Chem* **278:** 6251-6257.

Osborn, M., Johnsson, N., Wehland, J., and Weber, K. 1988. The submembranous location of p11 and its interaction with the p36 substrate of pp60 src kinase in situ. *Exp. Cell Res.* **175:** 81-96.

Otwinowski, Z., and Minor, W. 1997. *Processing of X-ray diffraction data collected in oscillation mode. Methods in Enzymology*. Academic Press, New York, NY, pp. 307-326.

Propper, C., Huang, X., Roth, J., Sorg, C., and Nacken, W. 1999. Analysis of the MRP8-MRP14 protein-protein interaction by the two-hybrid system suggests a prominent role of the C-terminal domain of S100 proteins in dimer formation. *J Biol Chem.* **274:** 183-188.

Rety, S., Osterloh, D., Arie, J.P., Tabaries, S., Seeman, J., Russo-Marie, F., Gerke, V., and Lewit-Bentley, A. 2000. Structural basis of the Ca(2+)-dependent association between S100C (S100A11) and its target, the N-terminal part of annexin I. *Structure Fold Des* **8:** 175-184.

Rety, S., Sopkova, J., Renouard, M., Osterloh, D., Gerke, V., Tabaries, S., Russo-Marie, F., and Lewit-Bentley, A. 1999. The crystal structure of a complex of p11 with the annexin II N-terminal peptide. *Nat Struct Biol* **6:** 89-95.

Rezvanpour, A., Phillips, J.M., and Shaw, G.S. 2009. Design of high-affinity S100-target hybrid proteins. *Protein Sci* **18:** 2528-2536.

Rezvanpour, A., and Shaw, G.S. 2009. Unique S100 target protein interactions. *Gen Physiol Biophys* **28 Spec No Focus:** F39-46.

Rustandi, R.R., Baldisseri, D.M., and Weber, D.J. 2000. Structure of the negative regulatory domain of p53 bound to S100B(ββ). *Nat. Struct. Biol.* **7:** 570-574.

Semov, A., Moreno, M.J., Onichtchenko, A., Abulrob, A., Ball, M., Ekiel, I., Pietrzynski, G., Stanimirovic, D., and Alakhov, V. 2005. Metastasis-associated protein S100A4 induces angiogenesis through interaction with Annexin II and accelerated plasmin formation. *J Biol Chem* **280:** 20833-20841.

Tokumitsu, H., Mizutani, A., Minami, H., Kobayashi, R., and Hidaka, H. 1992. A calcyclin-associated protein is a newly identified member of the Ca2+/phospholipid-binding proteins, annexin family. *J Biol Chem* **267:** 8919-8924.

Tomas, A., and Moss, S.E. 2003. Calcium- and cell cycle-dependent association of annexin 11 with the nuclear envelope. *J Biol Chem* **278:** 20210-20216.

Wallace, A.C., Laskowski, R.A., and Thornton, J.M. 1995. LIGPLOT: a program to generate schematic diagrams of protein-ligand interactions. *Protein Eng* **8:** 127-134.

Watanabe, M., Ando, Y., Tokumitsu, H., and Hidaka, H. 1993. Binding site of annexin XI on the calcyclin molecule. *Biochem Biophys Res Commun* **196:** 1376-1382.

Wilder, P.T., Lin, J., Bair, C.L., Charpentier, T.H., Yang, D., Liriano, M., Varney, K.M., Lee, A., Oppenheim, A.B., Adhya, S., et al. 2006. Recognition of the tumor suppressor protein p53 and other protein targets by the calcium-binding protein S100B. *Biochim Biophys Acta*.

Willard, L., Ranjan, A., Zhang, H., Monzavi, H., Boyko, R.F., Sykes, B.D., and Wishart, D.S. 2003. VADAR: a web server for quantitative evaluation of protein structure quality. *Nucleic Acids Res* **31:** 3316-3319.

Williams, L.H., McClive, P.J., Van Den Bergen, J.A., and Sinclair, A.H. 2005. Annexin XI co-localises with calcyclin in proliferating cells of the embryonic mouse testis. *Dev Dyn* **234:** 432-437.

Wittekind, M., and Mueller, L. 1993. HNCACB, a high-sensitivity 3D NMR experiment to correlate amide-proton and nitrogen resonances with the alpha- and beta-carbon resonances. *J. Magn. Reson. Series B.* **101:** 171-180.

Wright, N.T., Cannon, B.R., Wilder, P.T., Morgan, M.T., Varney, K.M., Zimmer, D.B., and Weber, D.J. 2009. Solution structure of S100A1 bound to the CapZ peptide (TRTK12). *J Mol Biol* **386:** 1265-1277.

Wright, N.T., Prosser, B.L., Varney, K.M., Zimmer, D.B., Schneider, M.F., and Weber, D.J. 2008. S100A1 and calmodulin compete for the same binding site on ryanodine receptor. *J Biol Chem* **283:** 26676-26683.

Zeng, F.Y., Gerke, V., and Gabius, H.J. 1993. Identification of annexin II, annexin VI and glyceraldehyde-3-phosphate dehydrogenase as calcyclin-binding proteins in bovine heart. *Int J Biochem* **25:** 1019-1027.

Chapter 5

SUMMARY

5.1 Introduction

The S100 proteins are a group of proteins comprising at least 25 members in humans including S100B, S100A1, S100A6, S100A10 and S100A11 (Donato 2001; Heizmann et al. 2002). These proteins are dimeric, having two "EF-hand" calcium-binding motifs in each subunit. *In vivo* experiments have shown that both homo- and heterodimeric S100 complexes are formed (Propper et al. 1999; Deloulme et al. 2000; Wang et al. 2005). The S100 proteins act as calcium-signaling molecules by converting changes in cellular calcium levels to a variety of biological responses. In this manner, many of the S100 proteins modulate enzyme activities, oligomerization of cytoskeletal protein components (tubulin, glial fibrillary acidic protein), modulate ubiquitination, control membrane vesicle formation and participate in trafficking of proteins to the inner surface of the plasma membrane (Santamaria-Kisiel et al. 2006).

Most S100 proteins bind calcium ions and undergo a conformational change that allows them to interact with specific target proteins and control a cellular activity (Zimmer et al. 2003; Santamaria-Kisiel et al. 2006; Wilder et al. 2006). Three-dimensional structures of several S100 proteins in the calcium-free (apo) and calcium-bound states show that the major structural change involves the movement of helix III with respect to helix IV. This leads to the exposure of previously buried residues and creates a hydrophobic surface. In one S100 protein, S100A10, substitutions in both its calcium-binding sites have left this protein with the inability to coordinate calcium.

Consequently, S100A10 does not undergo a calcium-induced structural change and instead adopts a structure in its calcium-free state that is very similar to the calcium-bound states of other S100 proteins (Rety et al. 1999; Rety et al. 2000). As a result S100A10 interacts and controls the functions of more than a dozen proteins in a calcium-insensitive manner.

In the last few years, several proteins (AHNAK, TASK-1, dysferlin, NS3) have been found to interact with S100A10 together with annexin A2 as a possible means for trafficking of these proteins to the plasma membrane or assemble multiprotein complexes important in membrane repair processes. Unfortunately, lack of structural information on the arrangement, affinities and structures of these proteins in the complex does not allow understanding the mechanisms they are involved in. In this thesis, the focus was on the complexes of S100A10 with annexin A2, AHNAK, and dysferlin proteins to provide the first structural model of a multi-protein assemblage required for membrane repair.

5.2 Previous Work

Frequent partners for the S100 proteins are members of the annexin protein family. At least 10 different S100-annexin complexes have been characterized (Santamaria-Kisiel et al. 2006). Each annexin protein has a core domain comprised of four (annexins A1-A5, A7- A11, A13) or eight (annexin A6) structurally conserved repeats, each possessing five α-helices and a short 30-reside N-terminal ‘tail’. Calcium binding to the annexins promotes association with phospholipid membranes, which leads to the release of the N-terminal tail for interaction with the S100 proteins.

The first two structures of S100 proteins in complex with the annexins were solved by Rety et al. (Rety et al. 1999; Rety et al. 2000) and comprised apo-S100A10 and Ca^{2+}-S100A11 in complex with the N-terminal peptides of annexin A2 and A1, respectively. Despite the difference in the calcium-bound states of the proteins and that the two annexin peptides are from different protein sources, both structures demonstrate two annexin peptides per S100 dimer, located in near-identical binding sites on either side of the S100 molecule (Figure 1.4). Each peptide makes contacts with both S100 protomers resulting in the bridging of the two monomers by the annexin protein. Gerke and Moss proposed an elegant model in which calcium-binding by an annexin protein promotes its association with a phospholipid membrane and facilitates interaction with either S100A10 or Ca^{2+}-S100A11, allowing two membrane surfaces to be brought within close proximity during a fusion or vesiculation event (Gerke and Moss 2002).

Recently, a multiprotein complex was identified between S100A10, annexin A2 and AHNAK (Figure 1.8B) (Benaud et al. 2004; De Seranno et al. 2006). AHNAK is important for cell membrane differentiation and membrane repair (Kouno et al. 2004), is expressed in epithelial cells and localizes near the plasma membrane. In the absence of annexin A2, a weak interaction between S100A10 and the C-terminal portion of AHNAK exists. However, the strength of this interaction is increased more than 150-fold in the presence of annexin A2. Further, *in vitro* binding assays demonstrated no detectable interactions between annexin A2 and the C-terminus of AHNAK, in the absence of S100A10, or S100A10 with AHNAK in the absence of annexin A2. These observations suggest that S100A10-annexin A2 tetramer formation is likely a prerequisite for the

interaction with AHNAK. Similar to S100A10 and annexin A2, AHNAK protein localizes on the plasma membrane (Kouno et al. 2004), where the interaction between dysferlin and this complex can mediate the docking and fusion of the patch and sealing of the membrane. A high calcium concentration (extracellular, via the wound) causes annexin A1 and A2 association with a dysferlin-containing vesicle and damaged plasma membranes. The key protein in this process, dysferlin (Doherty and McNally 2003; Shao et al. 2006; Glover and Brown 2007), co-localizes and co-immunoprecipitates with annexins A1 and A2 (Lennon et al. 2003). In addition, recent experiments have shown that the C-terminus of AHNAK is responsible for binding to the N-terminal C2A domain of dysferlin. Calcium binding to the dysferlin C2A domain is not required for its interaction with AHNAK. The exact mechanisms whereby AHNAK is recruited for plasma membrane repair are not clear, however, S100A10 and annexin A2 co-localize with AHNAK and dysferlin proteins at the plasma membrane, providing some evidence for the function of this multiprotein complex in membrane repair.

5.3 Design of High-Affinity S100-Target Hybrid Proteins

Due to the presence of multiple proteins in larger complexes, studying the arrangement, affinities and mechanisms used by multi-protein complexes is quite challenging. This task could be achieved by devising a method in which the number or the sizes of the proteins involved in the interactions are reduced. In order to study multi-protein complexes involved in membrane repair, chapter 2 focused on designing a hybrid protein in which the S100A10 was linked in tandem to the N-terminal peptide of annexin

A2 (residues 1-15). A similar hybrid molecule was also generated for S100B and the central region of CapZ (TRTK12; residues 1-12). These two proteins were selected to test this approach for one protein (S100B) that undergoes a calcium-induced conformational change in order to interact with a target, and one protein (S100A10) that is calcium-insensitive. Further advantage of this method was protection of the target peptide from degradation to proteases by the S100 protein, which was used as a carrier.

Analysis of the structures of S100A10 in complex with the N-terminus of annexin A2 (1BT6) (Rety et al. 1999), and Ca^{2+}-S100B complexed to a portion of the CapZ (TRTK12) (1MWN, 1MQ1) (Inman et al. 2002; McClintock and Shaw 2003), allowed determining the length of the linker connecting the S100 protein to the target peptide. In both these structures (Figure 2.6), the C-termini of helix IV in the S100 protein are proximal to the N-terminus of the binding peptide. A nine-residue linker comprised of a TEV protease cleavage site (ENLYFQ/G) was introduced to connect the S100A10 protein to the N-terminal peptide of annexin A2 (A10A2). Similarly, an eleven-residue linker containing a PreScission protease cut site (LFQ/GP) and four glycine residues were used to connect the S100B protein to the TRTK12 peptide (BT12). High yields of isotopically labeled A10A2 and BT12 were purified to prepare the concentrated samples required for the collection of heteronuclear NMR experiments. The resonance assignments for nearly all of the atoms of each one of the hybrid proteins were completed. *In situ* proteolytic cleavage monitored by ^{1}H-^{15}N HSQC spectra showed the linker did not perturb the structures of the S100A10-annexin A2 or S100B-TRTK12 complexes. Overall, these results indicated that the structures and interactions of the S100 proteins

and the peptides in the A10A2 and BT12 hybrid proteins are nearly identical to those obtained for the complexes formed between the individual S100 proteins and synthetic peptides. Furthermore, analysis of the chemical shift assignments (^{1}H, ^{15}N, and ^{13}C) showed that residues T102-S108 of annexin A2 formed a well-defined α-helix in the A10A2 hybrid while the TRTK12 region was unstructured at the N-terminus with a single turn of α-helix from D108-K111 in the BT12 hybrid protein. The two S100 hybrid proteins provide a simple yet extremely efficient method for obtaining high yields of intact S100 target peptides. Since cleavage of the S100 hybrid protein is not necessary for structural characterization, this approach may be useful as a scaffold for larger S100 complexes.

5.4 An Asymmetric Platform for AHNAK Recruitment

The availability of the A10A2 hybrid protein, designed in previous chapter, allowed performing a series of experiments that assisted greatly in understanding the arrangement of the novel multi-protein complex formed between the S100A10, annexin A2 and AHNAK proteins. Peptide array analysis identified eight potential binding regions within the C-terminus of AHNAK for the A10A2 protein. Important amino acids of AHNAK for this interaction were characterized by +X+XPKφXφ consensus sequence, whereby amino acids with smaller sidechains at the second and forth positions of this sequence enhanced the interaction of A10A2. The sequence of AHNAK with the most intense binding (residues 5654-5673, AHNAK5) that was consistent with previous GST-AHNAK pull-down assay (De Seranno et al. 2006), was utilized in NMR titration

experiments. Using both the A10A2^{C82S} hybrid protein and complex of S100A10^{C82S} with an N-terminal peptide of the annexin A2, a single AHNAK5 peptide was found to coordinate in an asymmetric fashion to the S100A10-annexin A2 heterotetramer. Since the annexin A2 portion of A10A2^{C82S} was also ^{15}N-labeled and visible in the spectrum, it was clear that the binding of AHNAK5 affected both the S100A10^{C82S} and annexin A2 regions of the hybrid protein. Significant chemical shift changes occurred mainly for residues in helix IV of the S100A10^{C82S} (Gly^{77}, Ala^{81}), as well as the N-terminus of the annexin A2 (Leu^{112}, G^{114}) peptides. The plot of the change in peak intensities as a function of AHNAK5 and A10A2^{C82S} concentrations showed a stoichiometry of one AHNAK5 peptide to one A10A2^{C82S} dimer. Further, non-denaturing electrospray mass spectrometry results corroborated the NMR titration experiments. The binding affinity between AHNAK5 and A10A2^{C82S} was measure to approximately 3 nM. Repeating similar experiments using AHNAK5 and S100A10^{C82S} showed a much poorer interaction in the absence of annexin A2. Thus, confirming that both S100A10 and annexin A2 are required for strong association with the C-terminal domain of AHNAK.

Consistent with the two-hybrid and co-immunoprecipitation experiments (van de Graaf et al. 2003; Borthwick et al. 2008), possible formation of a ternary complex involving S100A10, annexin A2 proteins and the transient receptor potential cation channel protein, TRPV5 was examined by peptide array analysis. Both, S100A10^{C82S} or A10A2^{C82S} associated to the same regions on multiple sites of the TRPV5 peptide array, indicating that interaction of TRPV5 with S100A10^{C82S} or annexin A2-bound S100A10^{C82S} differs from the complex formed with the AHNAK, where residues from

both S100A10^{C82S} and annexin A2 are required for the strong interaction of the peptide. Regardless, it is important to repeat these experiments at lower protein concentrations in order to reduce the non-specific or weaker interactions.

5.5 Interactions between Other Proteins in the Membrane Repair Complex

With the aim of identifying secondary binding sites on annexin A2 (other than the twelve-residue N-terminal region) by S100A10 protein, peptide array experiments of full length annexin A2 were performed. Due to the sequence similarity of the helices within each repeat unit of annexin A2 (Barton et al. 1991; Jost et al. 1994), different potential binding sites corresponding to all four structural repeats were observed. Some of these repeats are buried in the structure of annexin A2 and clearly are not available to interact with S100A10. Similar to the TRPV5, the peptide array of annexin A2 was also probed at higher protein concentrations and it is important to repeat them using lower amount of protein to eliminate the non-specific or weaker interactions.

Lack of information on the arrangement or assembly of the proteins in the membrane repair complex does not allow understanding the membrane repair mechanism. To shed light into this, the possible interactions between pairs of proteins in the complex were examined. Knowing the backbone assignment of some of these proteins would provide the information on how some residues are affected by the binding to other proteins in the complex. High yields of unlabeled and isotopically labeled S100A10, AHNAK C-terminal domain and dysferlin C2A domain were purified and concentrated samples for the collection of heteronuclear NMR experiments were prepared. The

resonance assignments of S100A10 were determined. However, NMR spectroscopy of S100A10 and dysferlin C2A domain did not indicate a direct interaction between these two proteins in the presence or absence of calcium. This result was contradictory to the interaction observed between S100A13 and synaptotagmin C2A domain (Mohan et al. 2009; Mohan et al. 2010). It will be very interesting to test whether optimizing the experimental conditions such as the salt concentration in the buffer would change the outcome.

Similarly, no interaction was identified between the C-terminus of AHNAK and dysferlin C2A domain in the presence or absence of calcium by NMR spectroscopy, contradicting the previous GST-pull down assay (Huang et al. 2007) and peptide array experiment performed in this thesis. The AHNAK protein used in the NMR experiments was much shorter than the AHNAK fragment used in the GST-pull down assay and it will be exciting to repeat this experiment using a larger AHNAK construct in optimized experimental conditions.

No structural information is available for dysferlin C2A domain to date. Calcium titrations into the sample of dysferlin C2A domain showed sequential binding of six calcium ions to this region. It is important to obtain apo- and calcium-bound structures of dysferlin C2A domain to locate the interaction site formed between this protein and others in the membrane repair complex.

5.6 Structure of S100A10-Annexin A2-AHNAK5 Complex

The last chapter of this thesis was focused on determining the binding region of AHNAK5 on A10A2 protein by NMR spectroscopy and X-ray crystallography methods. The resonance assignments for $A10A2^{C82S}$ alone and in complex with the AHNAK5 peptide were completed. Chemical shift perturbation mapped the binding surface of AHNAK5 on helices IV and IV' of protomers a and b of the S100A10 region (D84a, S82a, I80a, G77a-A76a, S73a, F72a/b, S73b, L74b, A76b-G77b, I80b), as well as some residues from the annexin A2 peptide region (E113a-G114a, S108a-S111a, L110b-S111b and E113b) of the $A10A2^{C82S}$ protein (Figure 4.10).

X-ray crystallography of the A10A2-AHNAK5 complex showed that the backbone structure of A10A2-AHNAK5 complex is similar to that of S100A10 in complex with the N-terminal peptide of annexin A2 (Rety et al. 1999). The symmetric dimer contained four α-helices per subunit (I-IV), with helices I, I', IV and IV' comprising the dimer interface of the A10A2. The hydrophobic surface of the annexin A2 peptide region of the A10A2 hybrid protein in the A10A2-AHNAK5 complex was also similar to that of the X-ray crystallographic structure of the S100A10 bound to individual N-terminal peptide of annexin A2. Some of the important residues for the interaction with the AHNAK5 peptide included I54, L58 and S111 of protomer a, and L78, S111 and L112 of protomer b in the A10A2 protein. From the structure, it was clear that only one AHNAK5 peptide was bound to a dimeric A10A2 protein. This result was in perfect agreement with the results obtained by NMR spectroscopy, however, this mode of interaction for AHNAK5 peptide differs from other interaction in S100-target complexes

observed to date (Figure 5.1). For instance, in the Ca^{2+}-S100B structures with TRTK12 (1MWN, 1MQ1, 3IQO, Figure 5.1A) (Inman et al. 2002; McClintock and Shaw 2003; Charpentier et al. 2010), Ndr kinase (1PSB, Figure 5.1A) (Bhattacharya et al. 2003) and p53 (1DT7) (Rustandi et al. 2000); and the Ca^{2+}-S100A1 structure with TRTK12 (2KBM, Figure 5.1A) (Wright et al. 2009); the interaction occurs between the target peptide and the exposed hydrophobic surface between helices III and IV of the calcium-bound S100 protein. The second mode of interaction used by the S100 proteins is observed in the structures of Ca^{2+}-S100A11 (1QLS, Figure 5.1B) and apo-S100A10 (1BT6) in complexes with the N-terminal peptides from annexins A1 and A2, respectively. In both structures the annexin peptide bridges the two S100 protomers such that its C-terminus interacts with the linker and helix IV of one protomer while the annexin N-terminus has contacts near the N-terminus of helix I' of the partner protomer. The third mode of interaction utilized by the S100 proteins involves the Ca^{2+}-S100A6 and the C-terminal domain from the Siah-1 Interacting Protein (2JTT) (Figure 5.1C). In this structure the SIP peptide forms two distinct α-helices oriented nearly perpendicular to each other. The first helix (Helix A) occupies the hydrophobic groove between helices III and IV, while the second helix in SIP (helix B) lies across helix I' of the adjacent protomer. The binding surface of AHNAK5 on the A10A2 protein is unique, as the peptide binds diagonally across helices IV and IV' of the S100A10 region (Figure 5.1), which is on the opposite face of the molecule with respect to other S100-target complexes. In addition, AHNAK5 makes contacts with residues on the adjacent C-termini of the annexin A2 peptide regions (Figure 5.1D) of the A10A2 hybrid protein.

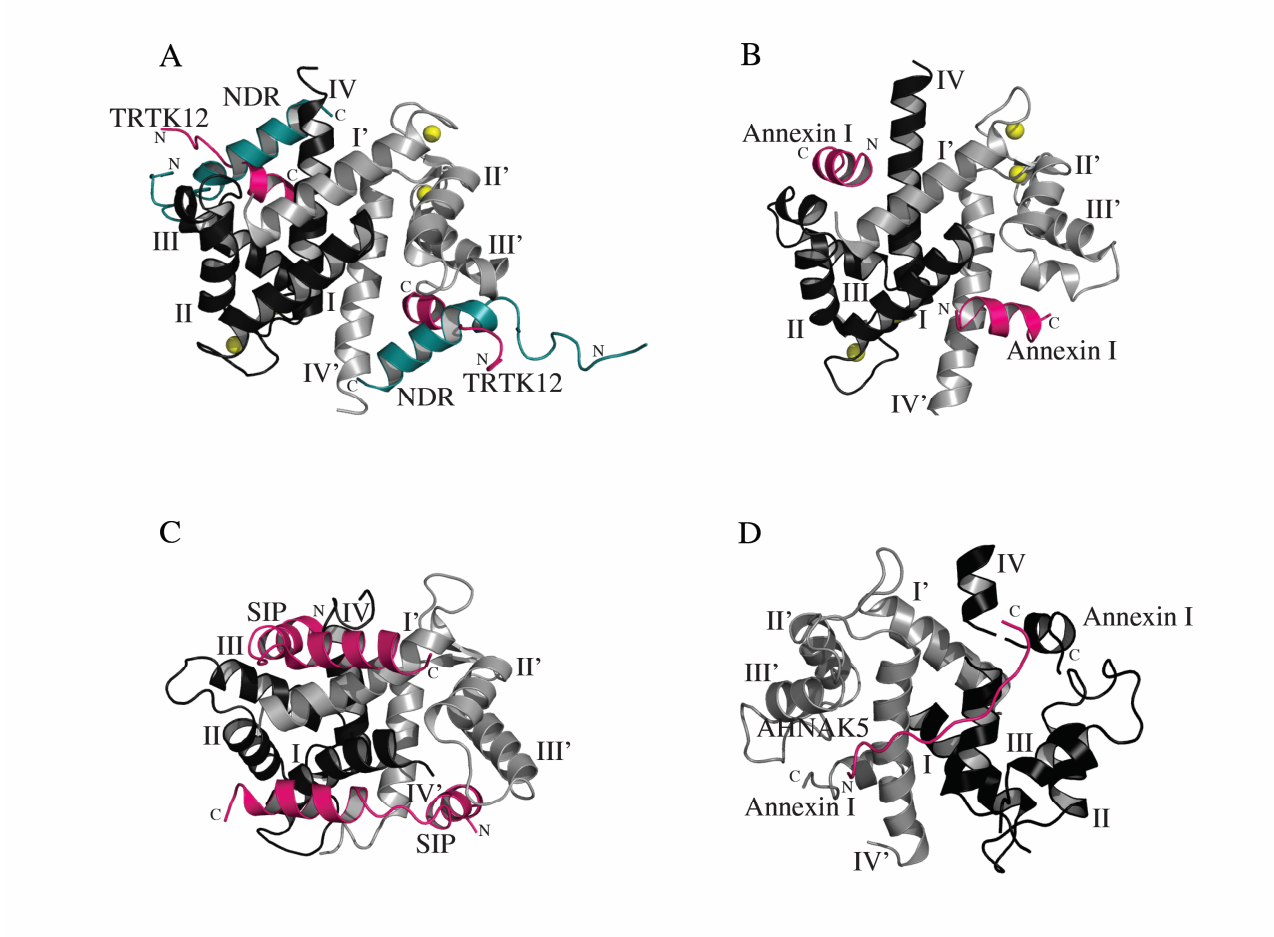

Figure 5.1. Different modes for target protein interaction with S100 proteins.

(A) Binding to the helix III-IV hydrophobic displayed by TRTK12 (pink) bound to Ca2+-S100A1 (2KBM) (Wright et al. 2009) and NDR kinase (cyan) bound to Ca2+-S100B (1PSB) (Bhattacharya et al. 2003). **(B)** Binding near helix I' at the dimer interface displayed by the N-terminal region of annexin A1 (pink) and Ca2+-S100A11 (1QLS) (Rety et al. 2000). **(C)** Two- site surface mode displayed by the C-terminal region of SIP bound to Ca2+-S100A6 (2JTT) (Lee et al. 2008). **(D)** Binding to the helices IV and IV‘ as well as the adjacent C-termini of annexin A2 peptides one face of the A10A2 hybrid protein. The diagram in (D) is rotated by 180 alonge the y-axis with respect to (A-C). Ribbon diagrams of the calcium-saturated S100 or apo-A10A2 proteins are presented with one of the protomers shaded in black (helices labeled as I-IV for the S100 or as I-IV and annexin A2 for the A10A2) and the other protomer shown in light grey (helices labeled as I'-IV' for the S100 or as I'-IV' and annexin A2 for the A10A2). Calcium ions are illustrated in yellow spheres.

5.7 Membrane Repair mechanism

Membrane repair involves a complicated assembly of multiple proteins. Strong *in vivo* evidence suggests that S100A10 is an important regulator of plasma membrane repair and membrane receptor trafficking. One of the central proteins in these functions is the calcium-sensitive annexin A2 protein. Many different experiments including co-immunoprecipitation and two-hybrid assays supporte the formation of a tight complex with the S100A10 protein. The interaction between S100A10 and annexin A2 utilizes the N-terminus of annexin A2 similar to that observed in the S100A10-annexin A2 tetramer crystal structure (Rety et al. 1999) with a K_d of approximately 30 nM. An S100A10 dimer can coordinate a pair of annexin A2 proteins, potentially bridging adjacent phospholipid membranes into close proximity during a membrane fusion event (Gerke and Moss 2002). This allows for the aggregation of vesicles and formation of an endomembrane patch required for membrane repair during calcium flood through the disrupted membrane. The endomembrane patch trafficking is facilitated by affixin. Meanwhile, calpain-3 cleaves cytoskeletal proteins to mediate disassembly of the damaged actin cytoskeleton at the damaged site. The next component involved in membrane repair is the AHNAK protein. In this thesis, it was shown that despite the symmetric structure of dimeric S100A10-annexin A2 complex, only one AHNAK5 peptide was bound asymmetrically to the heterotetramer (Figure 5.1) with a K_d of about 3 nM. Simialr to the yeast triple-hybrid and *in vitro* binding assays (De Seranno et al. 2006), it was also shown that both S100A10 and annexin A2 are required for strong association with the C-terminal domain of AHNAK. This requirement indicates there are two calcium-regulated steps for AHNAK

delivery to the membrane surface both mediated by annexin A2. The first is the extrusion of N-terminus of annexin A2 upon calcium binding to the protein core domain allowing formation of the heterotetramer and subsequent recruitment of AHNAK. The second step is the localization of the entire complex to the phospholipid surface through calcium bridging between annexin A2 and the membrane. Peptide array experiments identified the possibility for eight binding regions in the C-terminus of AHNAK for the S100A10-annexin A2 complex. This is consistent with a scaffolding role for AHNAK where up to eight S100A10-annexin A2 heterotetramers could be assembled on the C-terminus of AHNAK. Since binding of the complex to the phospholipid surface is governed by calcium binding to the annexin moiety, this would allow a highly cooperative association of the complex with the membrane. Stronger association of only one of the sequences in the array could also imply that some or the remaining binding sites are masked by the AHNAK tertiary structure. Regardless of the number of S100A10-annexin A2 complexes that could be recruited by one AHNAK onto the plasma membrane, the AHNAK protein gets located on the plasma membrane (Kouno et al. 2004), where the interaction between dysferlin and this complex can mediate the docking and fusion of the patch and sealing of the membrane.

5.8 Conclusion

The work in this thesis has provided valuable information regarding multi-protein complexes involved in membrane repair. The details on the arrangement of the proteins, stoichiometry and affinity of AHNAK for the S100A10-annexin A2 complex, as

well as structural information on this ternary complex proposed a novel model for a larger protein assembly during the membrane repair.

5.9 Future Work

The data presented in this thesis demonstrate an assembly of at least four proteins involved in membrane repair. Given the essential role of membrane repair in cell survival, it is important to invest on understanding the arrangement, affinities and structural information of the proteins in the complex. Although the structures of S100 proteins bound to the target peptides are informative, they lack the overall architecture of the proteins in the complex. Thus, it is exciting to obtain more structural information on larger protein fragments alone or associated with other proteins in the complex. For instance, the apo- and calcium-bound structures of dysferlin C2A domain must first be solved in order to locate the binding sites of other members of the repair complex (ie. S100A10, annexin A2, and AHNAK). Finally, this structural model and the identified protein-protein interactions must be confirmed by site-directed mutation experiments. The preliminary work on the association of some of the pair complexes (ie. S100A10 or AHNAK with dysferlin) did not indicate an interaction, however, it is important to repeat these experiments under optimized experimental conditions.

These structures could further be used in explaining some of the diseases caused by impaired membrane repair. For example, single V67D point mutation in dysferlin C2A domain is responsible for limb-girdle form of muscular dystrophy. Dysferlin has been shown to co-localize and co-immunoprecipitate with annexins A2 and A1 (Lennon et al.

2003) as well as the C-terminal domain of AHNAK. Therefore, it is quite interesting to study the effect of this mutation on the stability, structure and interactions of dysferlin C2A domain and other proteins in the complex.

5.10 References

Barton, G.J., Newman, R.H., Freemont, P.S., and Crumpton, M.J. 1991. Amino acid sequence analysis of the annexin super-gene family of proteins. *Eur J Biochem* **198:** 749-760.

Benaud, C., Gentil, B.J., Assard, N., Court, M., Garin, J., Delphin, C., and Baudier, J. 2004. AHNAK interaction with the annexin 2/S100A10 complex regulates cell membrane cytoarchitecture. *J Cell Biol* **164:** 133-144.

Bhattacharya, S., Large, E., Heizmann, C.W., Hemmings, B., and Chazin, W.J. 2003. Structure of the Ca2+/S100B/NDR kinase peptide complex: insights into S100 target specificity and activation of the kinase. *Biochemistry* **42:** 14416-14426.

Borthwick, L.A., Neal, A., Hobson, L., Gerke, V., Robson, L., and Muimo, R. 2008. The annexin 2-S100A10 complex and its association with TRPV6 is regulated by cAMP/PKA/CnA in airway and gut epithelia. *Cell Calcium* **44:** 147-157.

Charpentier, T.H., Thompson, L.E., Liriano, M.A., Varney, K.M., Wilder, P.T., Pozharski, E., Toth, E.A., and Weber, D.J. 2010. The effects of CapZ peptide (TRTK-12) binding to S100B-Ca2+ as examined by NMR and X-ray crystallography. *J Mol Biol* **396:** 1227-1243.

De Seranno, S., Benaud, C., Assard, N., Khediri, S., Gerke, V., Baudier, J., and Delphin, C. 2006. Identification of an AHNAK binding motif specific for the Annexin2/S100A10 tetramer. *J Biol Chem* **281:** 35030-35038.

Deloulme, J.C., Assard, N., Mbele, G.O., Mangin, C., Kuwano, R., and Baudier, J. 2000. S100A6 and S100A11 are specific targets of the calcium- and zinc-binding S100B protein in vivo. *J. Biol. Chem.* **275:** 35302-35310.

Doherty, K.R., and McNally, E.M. 2003. Repairing the tears: dysferlin in muscle membrane repair. *Trends Mol Med* **9:** 327-330.

Donato, R. 2001. S100: a multigenic family of calcium-modulated proteins of the EF-hand type with intracellular and extracellular functional roles. *Int. J. Biochem. Cell Biol.* **33:** 637-668.

Gerke, V., and Moss, S.E. 2002. Annexins: from structure to function. *Physiol Rev* **82:** 331-371.

Glover, L., and Brown, R.H., Jr. 2007. Dysferlin in membrane trafficking and patch repair. *Traffic* **8:** 785-794.

Heizmann, C.W., Fritz, G., and Schafer, B.W. 2002. S100 proteins: Structure, functions and pathology. *Front. Biosci.* **7:** d1356-1368.

Huang, Y., Laval, S.H., van Remoortere, A., Baudier, J., Benaud, C., Anderson, L.V., Straub, V., Deelder, A., Frants, R.R., den Dunnen, J.T., et al. 2007. AHNAK, a novel component of the dysferlin protein complex, redistributes to the cytoplasm with dysferlin during skeletal muscle regeneration. *Faseb J* **21:** 732-742.

Inman, K.G., Yang, R., Rustandi, R.R., Miller, K.E., Baldisseri, D.M., and Weber, D.J. 2002. Solution NMR structure of S100B bound to the high-affinity target peptide TRTK-12. *J. Mol. Biol.* **324:** 1003-1014.

Jost, M., Weber, K., and Gerke, V. 1994. Annexin II contains two types of Ca(2+)-binding sites. *Biochem J* **298 Pt 3:** 553-559.

Kouno, M., Kondoh, G., Horie, K., Komazawa, N., Ishii, N., Takahashi, Y., Takeda, J., and Hashimoto, T. 2004. Ahnak/Desmoyokin is dispensable for proliferation, differentiation, and maintenance of integrity in mouse epidermis. *J Invest Dermatol* **123:** 700-707.

Lennon, N.J., Kho, A., Bacskai, B.J., Perlmutter, S.L., Hyman, B.T., and Brown, R.H., Jr. 2003. Dysferlin interacts with annexins A1 and A2 and mediates sarcolemmal wound-healing. *J Biol Chem* **278:** 50466-50473.

McClintock, K.A., and Shaw, G.S. 2003. A novel S100 target conformation is revealed by the solution structure of the Ca2+-S100B-TRTK-12 complex. *J Biol Chem* **278:** 6251-6257.

Mohan, S.K., Rani, S.G., Kumar, S.M., and Yu, C. 2009. S100A13-C2A binary complex structure-a key component in the acidic fibroblast growth factor for the non-classical pathway. *Biochem Biophys Res Commun* **380:** 514-519.

Mohan, S.K., Rani, S.G., and Yu, C. 2010. The heterohexameric complex structure, a component in the non-classical pathway for fibroblast growth factor 1 (FGF1) secretion. *J Biol Chem* **285:** 15464-15475.

Propper, C., Huang, X., Roth, J., Sorg, C., and Nacken, W. 1999. Analysis of the MRP8-MRP14 protein-protein interaction by the two-hybrid system suggests a prominent role of the C-terminal domain of S100 proteins in dimer formation. *J Biol Chem.* **274:** 183-188.

Rety, S., Osterloh, D., Arie, J.P., Tabaries, S., Seeman, J., Russo-Marie, F., Gerke, V., and Lewit-Bentley, A. 2000. Structural basis of the Ca(2+)-dependent

association between S100C (S100A11) and its target, the N-terminal part of annexin I. *Structure Fold Des* **8:** 175-184.

Rety, S., Sopkova, J., Renouard, M., Osterloh, D., Gerke, V., Tabaries, S., Russo-Marie, F., and Lewit-Bentley, A. 1999. The crystal structure of a complex of p11 with the annexin II N-terminal peptide. *Nat Struct Biol* **6:** 89-95.

Rustandi, R.R., Baldisseri, D.M., and Weber, D.J. 2000. Structure of the negative regulatory domain of p53 bound to S100B(bb). *Nat. Struct. Biol.* **7:** 570-574.

Santamaria-Kisiel, L., Rintala-Dempsey, A.C., and Shaw, G.S. 2006. Calcium-dependent and -independent interactions of the S100 protein family. *Biochem J* **396:** 201-214.

Shao, C., Zhang, F., Kemp, M.M., Linhardt, R.J., Waisman, D.M., Head, J.F., and Seaton, B.A. 2006. Crystallographic analysis of calcium-dependent heparin binding to annexin A2. *J Biol Chem* **281:** 31689-31695.

van de Graaf, S.F., Hoenderop, J.G., Gkika, D., Lamers, D., Prenen, J., Rescher, U., Gerke, V., Staub, O., Nilius, B., and Bindels, R.J. 2003. Functional expression of the epithelial Ca(2+) channels (TRPV5 and TRPV6) requires association of the S100A10-annexin 2 complex. *Embo J* **22:** 1478-1487.

Wang, G., Zhang, S., Fernig, D.G., Martin-Fernandez, M., Rudland, P.S., and Barraclough, R. 2005. Mutually antagonistic actions of S100A4 and S100A1 on normal and metastatic phenotypes. *Oncogene* **24:** 1445-1454.

Wilder, P.T., Lin, J., Bair, C.L., Charpentier, T.H., Yang, D., Liriano, M., Varney, K.M., Lee, A., Oppenheim, A.B., Adhya, S., et al. 2006. Recognition of the tumor suppressor protein p53 and other protein targets by the calcium-binding protein S100B. *Biochim Biophys Acta*.

Wright, N.T., Cannon, B.R., Wilder, P.T., Morgan, M.T., Varney, K.M., Zimmer, D.B., and Weber, D.J. 2009. Solution structure of S100A1 bound to the CapZ peptide (TRTK12). *J Mol Biol* **386:** 1265-1277.

Zimmer, D.B., Wright Sadosky, P., and Weber, D.J. 2003. Molecular mechanisms of S100-target protein interactions. *Microsc Res Tech* **60:** 552-559.

CURRICULUM VITAE

Atoosa Rezvanpour

Department of Biochemistry
The University of Western Ontario, London, ON N6A 5C1

Education

2007 – 2011	The University of Western Ontario Ph.D. (Biochemistry)	London, ON
2004 – 2006	The University of Western Ontario Master of Science (Biochemistry)	London, ON
1999 – 2003	McMaster University B.Sc. Honours (Biochemistry)	Hamilton, ON

Awards Received

1. Province of Ontario,
   Ontario Graduate Scholarship (OGS), 2010-11
2. Department of Biochemistry, University of Western Ontario,
   Western Graduate Research Scholarship, 2009-10
3. Department of Biochemistry, University of Western Ontario,
   USC Teaching Honour Roll (Excellence in Teaching in Biochemistry), 2008-09
4. Department of Biochemistry, University of Western Ontario,
   Western Graduate Research Scholarship, 2008-09
5. Department of Biochemistry, University of Western Ontario,
   Western Graduate Research Scholarship, 2007-08
6. Department of Biochemistry, University of Western Ontario,
   Schulich Graduate Scholarship, 2007-08
7. Department of Biochemistry, University of Western Ontario,
   Schulich Scholarship for Medical Research, 2007-08
8. Department of Biochemistry, University of Western Ontario,
   Western Graduate Research Scholarship, 2006-07
9. Department of Biochemistry, University of Western Ontario,
   Western Graduate Research Scholarship in Science and Technology, 2006-07
10. Department of Biochemistry, University of Western Ontario,
    Western Graduate Research Scholarship, 2009-1011.
11. Department of Biochemistry, McMaster University,
    McMaster University Travel Award, 2002-03

12. Department of Biochemistry, McMaster University,
McMaster University Entrance Scholarship, 1998-1999
13. York University,
Entrance Scholarship of Distinction, 1998-1999 (Declined)
14. Ministry of Education, Toronto, Canada
Ontario Chemistry Award, 1998-99
15. Ministry of Education, Toronto, Canada
Ontario Scholar Award, 1998-99

Academic and Research Work Experience

Jan. 2007 – Present — University of Western Ontario
Graduate Student / Research Assistant

Sept. 2007 – Aug. 2010 — University of Western Ontario
Undergraduate Training Co-supervisor

Sept. 2004 – April 2010 — University of Western Ontario
Teaching Assistant

Sept. 2004 – Sept. 2006 — University of Western Ontario
Graduate Student / Research Assistant

May 2003 – Aug. 2003 — McMaster University
Summer Undergraduate Research Assistant

Sept. 2002 – Apr. 2003 — McMaster University
Undergraduate Research Assistant

May 2002 – Sept. 2002 — McMaster University
Summer Undergraduate Research Assistant

Publications

Articles Published in Refereed Journals:

1. Stocks, B. B.**, Rezvanpour, A.**, Shaw, G. S., Konermann, L. (2011). Temporal Development of Protein Structure during S100A11 Folding and Dimerization Probed by Oxidative Labeling and Mass Spectrometry. *J. Mol. Biol.* **409:** 669-679.
2. Ma, X., Stead, B. E., **Rezvanpour, A.**, and Davey, M. J. (2010) The Effect of Oligomerization on *Saccharomyces cerevisiae* Mcm4/6/7 Function. *BMC Biochem.* **11:** 37-52.
3. **Rezvanpour, A.**, Phillips, J. M., and Shaw, G. S. (2009) Design of High-Affinity S100-Target Hybrid Proteins. *Protein Science*. **18:** 2528-2536.
4. **Rezvanpour, A.**, and Shaw, G. S. (2009) Unique S100 Target Protein Interactions. *General Physiology and Biophysics* **28:** F39-F46.

5. Rintala-Dempsey, A. C., **Rezvanpour, A.**, and Shaw, G. S. (2008) S100-Annexin Complexes-Structural Insights. *FEBS J.* **275:** 4956-4966.

Articles Submitted to Refereed Journals:

1. **Rezvanpour, A.**, and Shaw, G. S. (Jan. 2011) The S100A10-Annexin A2 Complex Provides a Novel Asymmetric Platform for AHNAK Recruitment. *J. Biol. Chem*.

Conference Presentations

1. **Rezvanpour, A.**, Shaw, G. (2011) Structural Role of S100 Proteins in Membrane Repair. Oral presentation. Department of Biochemistry Seminar Series, University of Western Ontario.
2. **Rezvanpour, A.**, Shaw, G. (2010) Structural Role of S100 Proteins in Membrane Repair. Poster. Department of Biochemistry Seminar Series, University of Western Ontario.
3. **Rezvanpour, A.**, Shaw, G. (2009) A Novel Technique Allows for Structural Characterization of High-Affinity S100-Peptide Interactions. Poster. European Calcium Society Workshop. Smolenice, Slovakia.
4. **Rezvanpour, A.**, Shaw, G. (2008) Characterization of Interactions for S100-Binding Peptides and S100 Family of Proteins by NMR Spectroscopy. Poster. 22nd Annual Symposium of the Protein Society. San Diego, CA, USA.
5. **Rezvanpour, A.**, Shaw, G. (2008) Characterization of Interactions for S100-Binding Peptides and S100 Family of Proteins by NMR Spectroscopy. Oral presentation. Department of Biochemistry Seminar Series, University of Western Ontario.
6. **Rezvanpour, A.**, Shaw, G. (2008) Characterization of Interactions for High-Affinity S100-Binding Peptide Hybrid Molecules by NMR Spectroscopy. Poster. 50 Years of NMR at McMaster University.
7. **Rezvanpour, A.**, Shaw, G. (2006) Characterization of Interactions for S100-Binding Peptides and S100 Family of Proteins by NMR Spectroscopy. Poster. Department of Biochemistry Seminar Series, University of Western Ontario.
8. **Rezvanpour, A.**, Davey, M. J. (2005) The Mechanisms of the Mcm4/6/7 Complex. Oral presentation. Department of Biochemistry Seminar Series, University of Western Ontario.
9. **Rezvanpour, A.**, Davey, M. J. (2004) The Mechanisms of the Mcm4/6/7 Complex. Oral presentation. Department of Biochemistry Seminar Series, University of Western Ontario.

Extracurricular Activities

Jun 2008 – Jun 2011 University of Western Ontario
Graduate Representative of the Area, Equipment and Safety committee

Jun 2006 – Jun 2008 University of Western Ontario
Social Coordinator for the Biochemistry Graduate Student Society